



Plan- β : a bioengineering approach against type 1 diabetes

Mijke Buitinga

Plan- β : a bioengineering approach against type 1 diabetes

Mijke Buitinga
2015

Members of the Graduation Committee

Chairman:

Prof. Dr. ir. J.W.M. Hilgenkamp University of Twente

Promotores:

Prof. Dr. H.B.J. Karperien University of Twente
Prof. Dr. C.A. van Blitterswijk Maastricht University

Co-promotor:

Dr. A.A. van Apeldoorn University of Twente

Members:

Prof. Dr. E.J.P. de Koning Leiden University Medical Center/ Hubrecht Institute
Prof. Dr. M. Gotthardt Radboud University Medical Center
Prof. Dr. P. de Vos University Medical Center Groningen
Prof. Dr. ir. P. Jonkheijm University of Twente
Dr. R. Truckenmüller Maastricht University
Dr. S. Manohar University of Twente

Plan-β: a bioengineering approach against type 1 diabetes
2015, Mijke Buitinga

All rights are reserved. No part of this publication may be reproduced, stored, or transmitted in any form or by any means, without permission of the copyright owners.

ISBN: 978-94-6233-062-7

Layout and printed by Gildeprint – Enschede

Illustrations by Laurien Buitinga

The research described in this thesis was supported by the Dutch Diabetes Cell Therapy Initiative (DCTI), and the Dutch Diabetes Research Foundation.

The printing of this thesis was kindly supported by the Netherlands Society of Biomaterials and Tissue Engineering.

PLAN- β : A BIOENGINEERING APPROACH AGAINST TYPE 1 DIABETES

DISSERTATION

To obtain
the degree of doctor at the University of Twente,
on the authority of the rector magnificus,
Prof. Dr. H. Brinksma,
on account of the decision of the graduation committee,
to be publicly defended on Friday, October 30th 2015 at 12:45 hours

By

Mijke Buitinga
born on March 9th, 1985
in Hengelo, The Netherlands

This dissertation has been approved by:

Prof. Dr. H.B.J. Karperien (Promotor)

Prof. Dr. C.A. van Blitterswijk (Promotor)

Dr. A.A. van Apeldoorn (Co-promotor)

Contents

Chapter 1	Barriers in clinical islet transplantation: current limitations and future prospects	7
Chapter 2	Microwell scaffolds for the extrahepatic transplantation of islets of Langerhans	61
Chapter 3	Microwell scaffolds with a defined porosity: a potential platform for extrahepatic islet transplantation	83
Chapter 4	Composite human islets with proangiogenic support cells to improve islet revascularization at the subcutaneous transplantation site	111
Chapter 5	Non-invasive monitoring of β -cells in a porous microwell scaffold platform by ^{111}In -exendin-3 SPECT imaging: a pilot study	131
Chapter 6	Conclusions and Outlook	145
	Summary	163
	Nederlandse samenvatting	165
	List of publications	167
	Acknowledgements	169
	Curriculum Vitae	171



Chapter 1

Barriers in clinical islet transplantation: current limitations and future prospects

1.1 INTRODUCTION

Given its vast medical, financial and social implications, diabetes mellitus is a huge burden on society (1). With a worldwide prevalence of 382 million people (2), it is one of the most common chronic diseases. And the prevalence of diabetes is still increasing each year (3). In 2013, the global health expenditure on this disease is estimated to be at least 581 billion International Dollars (2).

The American Diabetes Association (ADA) classifies diabetes according to both clinical stages and etiologic types (Figure 1). All patients can be classified according to clinical stage. Considering etiology, three main types can be distinguished: type 1, type 2, and gestational diabetes (4). Type 1 diabetes accounts for only 5-10% of those with diabetes (4). Although the etiology is not completely understood, the general pathological finding is the destruction of pancreatic β -cells, usually in the presence of islet cell autoantibodies, autoantibodies to insulin, autoantibodies to glutamic acid decarboxylase, and/or autoantibodies to the tyrosine phosphatase IA-2 and IA-3 β . Type 1 diabetes has multiple genetic predispositions (5), but the observation that the concordance rate in monozygotic twins is not 100% indicates that beside genetic factors, environmental factors are also involved in the development of the disease (6). This type of diabetes usually affects children or young adults, but it can occur at any age. Some forms of type 1 diabetes do not have known etiologies and these fall under the category idiopathic diabetes. Patients with this type of diabetes usually do not show evidence of islet autoimmunity, but they are prone to episodes of ketoacidosis and show varying degrees of insulin deficiency. Idiopathic diabetes is strongly inherited and there seems to be an ethnic preference since most patients are of African or Asian ancestry (4).

Type 2 diabetes is the most common type of diabetes and accounts for over 90% of the cases globally (7). A combination of relative insulin deficiency, insulin resistance and an inadequate compensatory insulin secretory response characterize this type of diabetes (4). Usually it occurs in adults, but it is also seen in children and young adults. The cause of this type of diabetes is a complex mixture of both genetic and epigenetic predispositions interacting with societal factors that determine behavior and the exposure to risk factors. Some of these risk factors are obesity, dietary factors, physical inactivity, advancing age, family history of diabetes, ethnicity, environmental toxins, gestational diabetes affecting the unborn child (8). In contrast to patients with type 1 diabetes, those with type 2 diabetes usually do not require exogenous insulin therapy to survive.

Gestational diabetes mellitus is diabetes diagnosed during pregnancy that is not clearly overt diabetes (4), but has health consequences for both mother and child and not only in the short term but also in the long term. Achieving glycemic control during pregnancy with lifestyle modifications and/or pharmaceutical intervention reduces or even prevents the risk of adverse pregnancy outcome like fetal overgrowth (9, 10). The remaining group is categorized as

high mortality rates and appalling early outcomes, it was considered a risky undertaking (20). In 1972, the interest for pancreatic islet transplantation was renewed when Lacy and coworkers described a method to isolate and transplant intact islets of Langerhans in rodents (21). Almost 20 years later, in 1990, the first case of insulin independence after allogeneic islet infusion into the portal vein was reported, which lasted for nearly one month (22).

The scope of this chapter is to provide an overview about the current status of clinical islet transplantation and the hurdles the medical field need to address before this therapy can be more widely applied. Promising strategies to overcome these hurdles will be discussed followed by a prospective on experimental strategies that might improve the feasibility of islet transplantation as a treatment option for patients with severe diabetes.

1.2 CURRENT STATUS OF CLINICAL ISLET TRANSPLANTATION

1.2.1 Clinical outcome

The early success of insulin independence after allogeneic islet infusion into the portal vein, has established the liver as the site of choice for islet transplantation in the clinical practice (22). The outcomes of clinical islet transplantation have improved significantly since its introduction, due to improvements in islet procurement, enzyme blends, and the introduction of more effective immunosuppressive regimens. Between 1990 and 1999, less than 10% of the islet recipients achieved insulin independence for longer than 1 year. In 2000, Shapiro *et al.* reported their initial findings in seven patients treated with a new protocol, combining the infusion of an adequate islet mass with a glucocorticoid-free immunosuppressive therapy. All seven recipients remained insulin dependent for an average of 11 months (23). After the success of this new protocol, islet transplant programs expanded.

In the latest update of the Collaborative Islet Transplant Registry (CITR), it was reported that between 1999 and 2010, about 5 times more islet transplantations were performed compared to the preceding decade (24). The CITR registered 1375 allograft infusions in 677 patient (25). Of these patients, ~36% received one infusion, ~44% received two, ~18% received three, 1.3% received four, and less than 1% received six infusions (25). In these 10 years, a significant improvement in insulin independence was achieved; 44% of the patients who received transplants in the 2007-2010 era, were insulin independent after 3 years, compared to 27% of the patients transplanted in the 1999-2002 era (25). However, long-term data remain disappointing; even though more than 70% of the implants retained C-peptide secretion 8 years after transplantation, only 15% of the patients were still insulin independent (26).

A matter of concern is the limited availability of donor organs restricting the extent to which this therapy option can be implemented. In order for islet transplantation to become more widely available, it should ideally achieve insulin independence using islets from a single donor. Another factor supporting single-donor transplantations is the increased risk of recipient sensitization to human leukocyte antigens after receiving islets from multiple donors,

associated with islet graft failure (27). Although the outcome for single-donor transplantations is improving over the years, to date multiple-donor islet transplantations still outperform (25, 28, 29). Recently, Al-Adra *et al.* have identified factors that are associated with the achievement of insulin independence after single-donor islet transplantation, such as preoperative insulin requirements, the use of heparin and insulin during transplantation, and the number of islets transplanted (29). Together with improvements in donor and recipient selection, and refinement of islet isolation techniques and immunosuppressive regimens, these factors might potentially increase single-donor transplantation success in the future.

1.2.2 Indications for islet transplantation

To date, islet transplantation has been restricted to patients with type 1 diabetes and labile glycemic control. These patients exhibit, despite intensive insulin regimens, severe glycemic fluctuations, recurrent hypoglycemia, and hypoglycemic unawareness. Also main causes of glycemic lability, such as lipodystrophy, malabsorption, adrenal insufficiency, autonomic neuropathy, dental infection and excessive alcohol intake (30), should be ruled out to become eligible for islet transplantation. The reasons why this therapy is not widely applied and only patients with labile glycemic control are considered candidates are the shortage of donor organs, the need for life-long immunosuppressive regimens, and the high costs of the isolation procedure and clean-room facilities. Only for patients who already received a donor kidney, the criterion of labile glycemic control is not strictly required, because they already receive immunosuppressant therapy for their kidney graft.

1.2.3 Risks and challenges of intrahepatic islet transplantation

The infusion of islets into the portal vein is not without risks. It has been reported that procedure-related complications occur in about 20% of the infusions (31). The acute risks concerned with this procedure are bleeding, portal vein thrombosis, and puncture of the biliary system (31). Long-term effects of islet infusion are not fully known, but the occurrence of parenchymal hepatic changes has been reported (32). Over the years, the incidence of infusion-related adverse events reduced significantly (24), probably due to an increase in islet transplantation experience, and the measures undertaken to avert the acute risks, like the use of agents that plug the catheter tract, the infusion of heparin during islet transplantation, and limiting packed cell volume <5mL (33).

Acute stress factors – Considering the graft, it is estimated that about 60-80% of the islets can be retrieved from a donor pancreas (34). Figure 2 depicts the survival of islets from organ procurement to islet isolation and transplantation. Many islets die during the isolation, culture, or engraftment period. The first exposure to stressful stimuli already occurs during pancreas cold ischemia time. Cold ischemia is known to stimulate inflammatory pathways and suppresses the repair/cytoprotective pathways (35). It has been demonstrated that a significant negative correlation exists between cold ischemia time of the donor pancreas and the IEQ obtained (36).

During the isolation and purification process also pro-apoptotic intracellular pathways are activated, likely due the mechanical, enzymatic, osmotic, and ischemic stresses the islets are exposed to (37). However, it is estimated that most islets are lost during the immediate post-transplantation period. Once the islets are infused into the liver and come into contact with whole blood, a thrombotic/inflammatory reaction occurs elicited by tissue factor and pro-inflammatory mediators secreted by the islets. This reaction is called the instant blood-mediated inflammatory reaction (IBMIR) and is characterized by activation and rapid binding of platelets to the infused islets, together with the activation of the coagulation and complement systems. Due to this, one hour after infusion, most islets are infiltrated with leukocytes resulting in disruption of islet integrity and ultimately in islet loss (38–41). It has been demonstrated by positron emission tomography (PET) studies with ^{18}F -fluorodeoxyglucose-labeled islets that only ~50% of the administered radioactivity can be detected one hour after islet transplantation in the liver, suggesting that in the immediate post-transplantation period half the transplanted islet cells are damaged to the extent that the ^{18}F -fluorodeoxyglucose they contained is released (42).

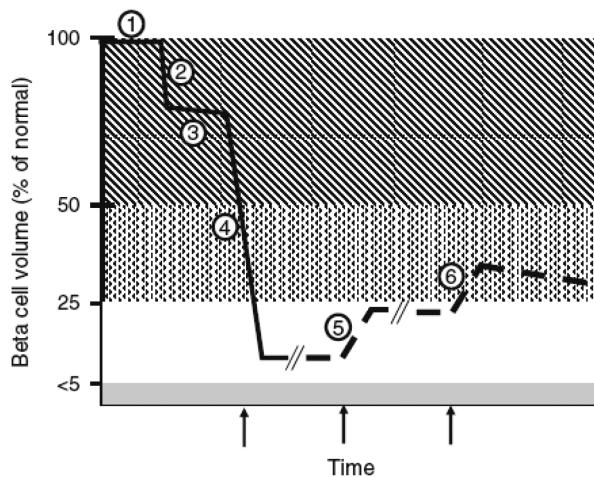


Figure 2. Depiction of the beta cell mass after clinical intrahepatic islet transplantation. The normal beta cell mass in humans is considered to be 100%; if it is reduced to $<50\%$, most patients develop signs of impairment in glucose metabolism (e.g. postprandial hyperglycemia). If further reduced to $<25\%$, exogenous insulin therapy is required. The beta cell mass in a person with long-standing type 1 diabetes is usually 1–5% of that in a healthy individual. Against this background, the tentative islet mass in a donor is illustrated. (1) The islet mass in a donor is assumed to be close to 100%, although the quality of the islets may be influenced by the cause of death and the process of brain death. (2) About 60–80% of the islets can be successfully retrieved in an experienced islet isolation facility. (3) About 10% of the islets are lost during culture while awaiting transplantation. (4) Most islets fail to engraft after intraportal islet transplantation. The estimated islet replacement level is about 10% after each transplantation procedure. (5) If the procedure is repeated (dotted line) once or twice (arrows) (6) the total beta cell mass reaches a level at which insulin can be withdrawn, although most recipients show impaired glucose metabolism (postprandial hyperglycemia). Adapted from (34).

To reduce the impact of cold ischemia time, studies have focused on the development of novel methods to improve organ preservation during transport. Traditional methods of pancreas preservation have been identified as suboptimal due to insufficient oxygenation. The use of pancreas persufflation, or vascular graft perfusion, to preserve pancreata before islet isolation has been shown to facilitate oxygenation of more than 90% of the pancreas tissue (43). Another approach to improve oxygenation is to store pancreata in preoxygenated F6H8S5, a mixture of perfluorohexyloctane (F6H8) and polydimethylsiloxane-5. A significant higher intrapancreatic oxygenation was reported, as well as enhanced transplantation outcomes and diabetes reversal (44).

Several strategies to improve transplantation outcome by inhibiting the IBMIR have been investigated (41). An example of a systemic approach is the administration of low-molecular-weight dextran sulphate (LMW-DS), which has an inhibitory effect on IBMIR and can be used as an alternative for heparin to avoid the risk of bleedings associated with heparin (45, 46). In experimental setting, LMW-DS has been shown to inhibit both complement and coagulation activation. The exact mechanism by which LMW-DS inhibits IBMIR remains unclear. Unlike heparin, LMW-DS does not contain any specific anti-thrombin binding sites. Nevertheless, LMW-DS has been shown to be far more effective in inhibiting IBMIR than heparin (45). In a recent clinical trial, it has been shown that LMW-DS can be safely applied in humans. Their findings in healthy volunteers suggest that platelets are unaffected by short-term treatment with LMW-DS and that there are no signs of increased bleeding risk (46). Currently, LMW-DS is under investigation in two phase-II clinical trials (NCT00789308, NCT00790439) to assess its safety and effectiveness on post-transplant islet function in people with type 1 diabetes.

Other promising strategies to improve the blood compatibility of islets involve localized, targeted approaches, such as *ex vivo* manipulating of the donor tissue surface masking the inherent properties of the cells that support the IBMIR or inhibiting the propagation of the coagulation cascade. The advantage of such a strategy is the local effect without presenting systemic consequences. Surface-modification approaches to abrogate the IBMIR and enhance islet survival include surface heparinization via a biotin/avidin approach (47), PEGylation (48), and encapsulation in an ultra-thin polymer membrane using PEG-conjugated phospholipid bearing maleimide group (49). These approaches show promising results regarding immunoreactive properties both *in vitro* (47, 49) and *in vivo* (47, 48). Currently, heparinized islets are under investigation in a clinical trial (ClinicalTrials.gov Identifier: NCT00678990).

Ischemia and hypoxia – Ischemia and hypoxia are also likely to contribute to early islet loss. Until transplanted islets get revascularized, they depend solely on diffusion for oxygen and nutrient supply (34). However, in humans, the majority of intraportally transplanted islets seem unable to escape the vascular compartment. Even years after transplantation, most islets reside within the portal vein lumen or are incorporated in portal vein walls (50, 51). Revascularization of the islets does occur, even when islets remain in the portal vein lumen (51), but it is unclear how fast and to which extent this process occurs. In the liver, only ~20% of the blood perfusion

is from the hepatic artery, whereas the remaining blood flow is venous and derived from the portal vein. Therefore, the oxygen tension in the liver is low compared to e.g. the pancreas parenchyma (3–8 mmHg vs. ~30 mmHg) (52). Intrahepatic islets, being vascularized by a mixture of portal vein and hepatic artery blood, might suffer from inadequate oxygen supply since the oxygen tension in the portal circulation is only 10–15 mmHg (53). *In vitro* studies have shown that such low oxygen tensions have detrimental effects on islet survival and function, mainly through the stabilization of hypoxia inducible factor (HIF)-1 α and the subsequent activation of its target genes (54), which lead to a cascade of events that result in apoptosis and necrosis (55). In addition, the activation of HIF-1 α has been shown to result in impaired glucose sensing and GSIS (56). Even mild islet hypoxia causes significant functional impairment of glucose-induced insulin release. In comparison with islets cultured in normoxia, insulin secretion is reduced by 50% when islets are cultured at an oxygen tension of 27 mmHg, and by 98% in islets cultured at an oxygen tension of 5 mmHg (57). Therefore, ischemia and hypoxia in islet transplantation represent a major concern.

An attractive approach to limit the detrimental effects of hypoxia is to provide adequate levels of oxygen to the islets using oxygen-releasing biomaterials. For example, fluorinated compounds (58) or peroxides (59) have been incorporated into biomaterials to enable controlled release of oxygen. Pedraza *et al.* have shown that the addition of a PDMS-CaO₂ disk in the culture medium can prevent hypoxia-induced cell death in islets (60). However, to apply such a strategy to intraportal islet transplantation, the oxygen-releasing compounds should be incorporated into an encapsulation matrix. Technically this is possible, as shown by Khattak *et al.* (61), however, the main challenge then remains to obtain sustained release of oxygen over extended periods of time. Another suggested strategy is to pre-culture islets in oxygenated plasma-based matrices using emulsified perfluorodecalin (62). A pre-culturing period of 24 hours prior to islet implantation has been shown to reduce anoikis and hypoxia without inducing viability and functionality. However, when transplanting these pre-cultured islets intrahepatically, enhanced IBMIR is observed, probably due to plasma residues indicating the need for synthetic bio-inert matrixes that can be easily dissolved to recover the islets.

Other strategies focus on the enhancement or acceleration of islet revascularization. One of these approaches is to increase the action of pro-angiogenic agents and/or inhibit the action of anti-angiogenic factors (63–66). The main challenge though, is the requisite to precisely control timing, dose, and duration of these factors' action to obtain optimal formation of mature, fully functional islet vasculature. Another strategy is to directly use pro-angiogenic cells. Johansson *et al.* (67) have shown that coating human islets with endothelial cells initiates the formation of vessel-like structures *in vitro*, without impairing islet functionality. The sprouting capacity of endothelial cell-coated islets was further improved by the addition of mesenchymal stromal cells. Animal studies confirm that co-transplanting islets with mature endothelial cells (68), stromal cells (69–73), or endothelial progenitor cells (74–76) derived from various sources can induce neovascularization *in vivo*, resulting in enhanced intra-islet vascular density and better

function, regardless whether the implantation site was underneath the kidney capsule (68, 69, 71, 72, 74, 76), or in the liver (70, 73, 75). In Table 1 a detailed overview of the outcome of these studies is presented. At the moment, clinical trials are being conducted to evaluate the safety and efficacy of co-transplanting mesenchymal stromal cells and islets in both patients with chronic pancreatitis undergoing autologous islet transplantation (ClinicalTrials.gov Identifier: NCT02384018) and in patients with type 1 diabetes (ClinicalTrials.gov Identifier: NCT00646724).

Allograft rejection and autoimmune recurrence – Other factors influencing islet survival, are allograft rejection and autoimmune disease recurrence. However, immunosuppressive drugs used in the clinic are designed to prevent alloreactivity and graft rejection, rather than inducing or restoring immune tolerance to autoantigens. At the time patients receive islet transplantation, their β -cell mass is believed to be very low. This results in minimal stimulation, keeping the autoreactive T-cell pool in a resting state. Upon islet transplantation, islet-specific epitopes will become available again, which could lead in some cases to reactivation of these resting memory T-cells, leading to recurrent β -cell destruction (77). In addition, several immunosuppressive agents are islet-toxic and interfere with insulin secretion and insulin action, and impair islet engraftment, and neogenesis (78). Also in this context, the liver might not be the preferred transplantation site, since the levels of these agents are about twice as high in the portal vein compared to systemic venous levels (79).

To induce or restore immune tolerance to autoantigens and prevent the induction of allograft reaction, the development of different immunosuppression strategies is needed. Examples of emerging approaches involve T-cell-directed induction, immunodepletion or modulation (with e.g. anti-CD3 antibody Teplizumab), inhibition of B-cells (with e.g. anti-CD20 antibody Rituximab), costimulatory blockade (with e.g. Betalcept), induction of regulatory T-cells (78, 80), and the injection of hematopoietic CD34⁺ stem cells to induce chimerism (81, 82). Other strategies focus on immunoprotection of the islets using encapsulation (83, 84) or coating (85) procedures. The advantage of these strategies is the obviation of immunosuppressive treatment. However, the challenge remains to obtain a physiological endocrine response, because of the barriers the metabolites encounter. For a complete overview of novel immunological strategies for islet transplantation and encapsulation techniques, readers are directed to recent reviews by Tezza *et al.* (86) and de Vos *et al.* (84).

1.3 EXTRAHEPATIC TRANSPLANTATION SITES: (PRE-)CLINICAL ADVANCES

The site-specific drawbacks associated with intrahepatic islet transplantation have initiated the search for alternative transplantation sites. The ideal site should be able to lodge sufficient islets, within close proximity of a robust vascular network that provides (1) adequate oxygen tension to islets to survive in the immediate post-transplant period; and (2) can induce islet revascularization. Moreover, the site should prevent early islet loss caused by host inflammatory

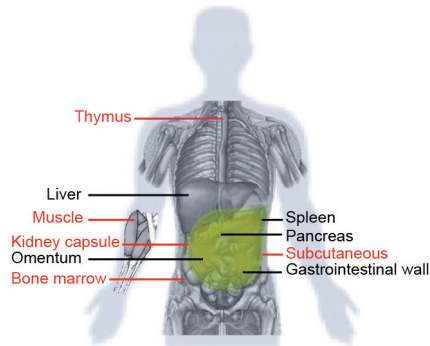


Figure 3. Implantation sites for islet cells. Several implantation sites have been proposed for islet cells, besides the intrahepatic portal system. The sites presented in black have a portal drainage. Adapted from (184) and modified.

reactions. Other important factors to consider are the surgical accessibility of the transplant site with minimal procedural risk and the ability to recover the graft, the last being of utmost importance when insulin producing stem cell therapies are translated into clinical practice. In addition, it would be beneficial if the transplantation site allows monitoring of islets post-transplantation without the need for biopsies. This option would not only provide information about islet survival at the given transplantation site, but also permit longitudinal evaluation of therapeutic strategies targeted towards improving islet engraftment or suppressing inflammatory responses.

In preclinical studies, many different transplantation sites have been explored, each with their (dis)advantages. We categorize the sites according to the route the insulin of the transplanted graft would be drained: portal versus systemic (Figure 3). The normal route for insulin delivery is via the portal vein to the liver, where a fraction of the insulin is extracted. The physiological importance of hepatic portal delivery of insulin is not fully understood, but insulin administration without exposure to the liver is associated with hyperinsulinemia and whole body insulin resistance (87). It has been shown that recipients with pancreas allografts with systemic venous drainage have elevated basal and stimulated insulin levels and that these are primarily due to alterations of first-pass hepatic insulin clearance (88). Whether this is also true when only the islets are transplanted at sites with systemic insulin delivery remains to be evaluated, although preclinical studies in mice strongly suggest it is (89).

1.3.1 Extrahepatic transplantation sites with portal drainage

Evaluated transplantation sites with portal drainage are the pancreas, spleen, omental pouch, and gastrointestinal wall (Figure 3).

Pancreas – Being the native home of islets, the pancreas has been suggested to be the most suitable transplantation site. Indeed, animal studies show its superiority to the intrahepatic site.

Not only fewer islets are required to reverse hyperglycemia (90), also the metabolic activity of islets is higher when recovered from the pancreatic transplantation site compared to the liver (91). These superior results observed with the pancreatic site indicate the importance of both the islets macro- and micro-environment. In clinical practice, however, the pancreas has hardly been considered as an alternative transplantation site, mainly because surgical interventions in the pancreas entail a high risk of complications such as pancreatitis and tissue damage due to the leakage of digestive enzymes from the exocrine pancreas. Furthermore, the presence of preexisting type 1 diabetes may make the pancreas a poor site of choice since pancreatic lymph nodes may be more primed and equipped to promote rejection.

Spleen – Several studies have reported islet transplantation into the spleen by either infusion of islets into a splenic vein tributary (92–95) or by direct injection of islets into the splenic pulp (96–98). The rich vascularization and a parenchymal oxygen tension that is comparable to that of the pancreatic parenchyma (52) make the spleen an interesting site for islet transplantation. Although the results in animal models are promising (92, 96–99), the limited volume that can be injection into the spleen due to high risks of splenic rupture and splenic vein thrombosis (93) hampers clinical application. Also considering the presence of lymphocytes in the spleen, an abnormal alpha cell response after transplantation at this site (95), and the occurrence of the IBMIR when the splenic vein tributary is used for transplantation, this site does not offer an advantage over the liver in clinical practice.

Omentum – The major advantage of the omentum is its virtually unlimited space for islets. By creating a pouch using the omentum and parietal peritoneum, a confined site can be obtained that is relatively well vascularized (100). For islet transplantation, the omentum may not only provide the advantage of being well-vascularized, but also offer some degree of immunoprivilege as suggested by the survival of allogeneic islets transplanted in the omentum of non-immunosuppressed guinea pigs (101). In both rats (102) and dogs (94, 95) it has been shown that islets transplanted in the omentum are able to reverse diabetes. However, a larger number of islets seems to be required compared to the spleen (94). Furthermore, the alpha cell response appears to be absent when islets are transplanted at this transplantation site in mongrel dogs (95), but more extensive and long-term comparison studies in clinically relevant animal models are warranted for this site to progress to clinical use.

Gastrointestinal wall – As the physiological entry site for glucose into the body, the gastrointestinal wall, such as the gastric and intestinal submucosa and subserosa, is considered to be an attractive location for islets to sense glucose. Apart from being highly vascularized, another major advantage of these sites is the possibility of endoscopic or laparoscopic transplantation and follow-up (103–105). The efficacy of these sites has been shown in rats (106), hamsters (107), and pigs (103, 105, 108). Although initial comparison studies with intrahepatic (106) and renal subcapsular (108) transplantations are promising, a full evaluation of islet survival and beta and alpha cell response over time with marginal islet mass is necessary before the gastrointestinal wall can be considered for translation to clinical practice.

1.3.1 Extrahepatic transplantation sites with systemic drainage

Other promising transplantation sites are underneath the kidney capsule, muscle, adipose tissue, subcutaneous tissue, thymus, and bone marrow (Figure 3). Despite their systemic drainage, these sites are still of interest as they are easily accessible, immune-privileged, or they can retain large amounts of islets.

Kidney capsule – The kidney capsule is the preferred site for experimental islet transplantation in rodents, because of the relatively easy surgical procedure with low mortality rates and the ability to retrieve the graft by nephrectomy for both histological evaluation and proof of islet graft function. Although the oxygen tension in the renal capsule is about two to three times lower compared to that of the pancreas parenchyma (52), between 12.5 and 25% of the native endocrine mass is required to maintain normoglycemia in rats (98). Studies comparing the kidney capsule with the intraportal site in mice, indicate that less islets are required for the renal subcapsular site to reverse diabetes (~250 vs. ~800) (109). Unfortunately, the results in clinical practice regarding this site seem less positive. To our knowledge, only one clinical feasibility study has been reported in which islet infusion under the kidney capsule is tested and compared to intraportal islet transplantation. However, due to the limited number of analyzed subjects, hard conclusions cannot be drawn, but this study suggests that in humans the kidney capsule requires a higher islet mass compared to the intraportal site to achieve normoglycemia (110). The difference in performance between both sites in mice and humans is most likely related to species-specific characteristics like the size of the islets and the diameter of the portal vein. Murine islets are larger compared to human islets (111). As a consequence, and due to the smaller diameter of the portal vein, islets embolize earlier in the portal vascular tree in mice than in humans. This results in relatively more hepatic necrosis and reduced oxygen supply which are associated with islet graft failure (112). Additionally, factors as the invasiveness of surgical access to the kidney capsule in humans, the limited available space under the capsule, and the often-existing kidney-related comorbidities like diabetic nephropathy, make this site less suitable for clinical islet transplantation.

Muscle – The advantages of the muscle as a transplantation site are the ease of approach and the possibility to take biopsies or image the islets longitudinally using PET or SPECT techniques (113, 114) to assess islet engraftment and beta cell mass survival with minimal invasion. Striated muscle has been used for islet transplantation in both experimental and clinical settings, but with varied success (115–118). There are indications that this variation in outcome is largely related to the implantation technique. The injection of large islet clusters is associated with substantial early islet death and fibrosis in the center of the graft (116, 117). In contrast, when islets are less densely packed in a pearls-on-a-string fashion, decreased fibrosis and a sustained reversal of diabetes are observed (115). Regarding oxygenation of intramuscular grafts, Svensson *et al.* have reported a six-fold increase compared to renal subcapsular islet grafts in rats, which corresponds to 70% of the oxygen tension measured in native islets (117). However, despite the relatively high oxygen tension in the intramuscular islet grafts, currently

twice the islet mass is required to obtain normoglycemia in rats compared to intraportal islet transplantation (115). Intramuscular islet transplantations in the forearm of diabetic patients have shown promise (118, 119), but further refinement and more detailed studies on the site-specific challenges, such as the effect of intramuscular pressure changes and exercise-mediated glucose consumption, are necessary before this site becomes clinically relevant.

Adipose tissue and subcutaneous space – Other easily accessible sites are adipose tissue and the subcutaneous space. In mice, both the epididymal (120) and mammary (121) fat pad have been subject to islet infusion with promising results. As the mouse epididymal fat pad is well-vascularized (122) and shares many properties similar to that of the greater omentum in humans (120), this site is considered to be a good analogue to the greater omentum in small animal models.

Because of its accessibility, subcutaneous islet transplantation has already been performed in humans as early as 1994 (123). However, unlike the fat pad, the subcutaneous site is poorly vascularized and without prevascularization techniques, the performance of subcutaneous islet grafts is deprived (124, 125). An interesting approach to increase the vascular state of the subcutaneous space is recently published by Pepper *et al.* (126). They report the implantation of a hollow nylon catheter to induce the foreign-body response in a controlled manner so as to induce local neovascularization. After removal of the catheter, a space lined with neovessels is created and they have shown that transplantation of islets into this space enables the reversal of diabetes in mice without the use of growth-factors.

Immune-privileged sites – To date, the thymus and bone marrow are the only immune-privileged sites considered for clinical practice, mainly because of the space, accessibility, applicability, and safety compared to other immune-privileged sites as the testis, anterior eye chamber or the brain. The advantage of such sites is that they may offer complete or partial protection from rejection without the need for concurrent immunosuppressive therapy. The thymus has been studied as a transplant site in both small (127–129) and large (130) animal models with promising results. It is suggested that since T-cell maturation occurs in the thymus, this site would enable negative selection of reactive T-cells toward islet autoantigens by exposing maturing T-cells to the islet graft. This hypothesis is supported by the finding that intrathymic islets of Lewis rats can survive in BioBreeding rats, an autoimmune model of type 1 diabetes (127). However, compared to the kidney capsule a higher number of islets is required to achieve normoglycemia (129), though more extensive comparative studies should be performed to assess the long-term effect of immune-privilege on islet function and survival.

Regarding the bone marrow, a long-term preclinical study in mice has shown the potential of this site being superior to the liver (131). These promising results have led to a successful feasibility study in humans (132) showing sustained C-peptide release for the maximum follow-up of 944 days. How the potential of this site relates to intraportal islet transplantation in humans is currently being assessed in a phase-II clinical trial (ClinicalTrials.gov Identifier: NCT01722682).

1.4 BIOMATERIAL SCAFFOLDS FOR ISLET TRANSPLANTATION

While transplant outcome is largely dependent on inherent characteristics of the transplantation site, bioengineering methods can be applied to further enhance the supporting environment for an improved outcome. To date, a wide variety of biomaterials is available which are either biologically derived or synthetically made, such as fibrin or poly(lactic- co-glycolic acid), respectively. It is well established that microenvironmental cues presented by these biomaterials play a crucial role in modulating the foreign body response. This response does not solely depend on the chemical composition of the applied biomaterial; also physical properties as stiffness, roughness, porosity and pore-size largely influence the body response (133, 134). In some cases, these physical properties can even be tuned in such way that the islet graft is protected from the hosts' immune system. Although an interesting avenue, in this chapter we will mainly focus on hydrogel-based and solid scaffold designs (summarized in Table 2) that can support islet engraftment and revascularization at extrahepatic transplantation sites. For a detailed review about immunoprotective devices, we refer to recent reviews by Robles *et al.* (135), de Vos *et al.* (84), and Vériter *et al.* (136)

1.4.1 Hydrogel-based scaffold designs for islet transplantation

Hydrogels are highly water-swollen cross-linked polymers that can be formed from biocompatible natural or synthetic polymers. These biomaterials can be tailored to have tissue-like elastic properties, which make them excellent mimetics of native tissue. The advantage of a hydrogel based scaffold design is that it allows minimally invasive transplantation by means of simple injection (137).

Examples of natural hydrogels intended for islet transplantation are collagen (138, 139), plasma (140), fibrin (65, 125, 141, 142), and alginate (66). Recently, also promising *in vitro* results have been published incorporating islets in silk hydrogels, though the material properties of this hydrogel as presented in this study are not yet suitable to facilitate physical implantation *in vivo* (143). In general, the merits of these natural polymers are their inherent biological activity, such as the presentation of growth-factor binding sites and susceptibility to cell-triggered proteolytic degradation and remodeling.

Alginate-based hydrogels are most commonly used for immune-isolation of pancreatic islets (144). However, Witkowski *et al.* (66) report the use of low molecular weight alginate in combination with proangiogenic growth factors and RGD peptide as a transplantation matrix that allows vascular ingrowth. These constructs have been used to improve the vascularization of the intramuscular transplantation site prior to islet injection. They show that this prevascularization strategy significantly improves islet survival and function at this transplantation site.

Another natural hydrogel used for islet transplantation is fibrin gel. Initial results obtained with fibrin glue (TISSEEL fibrin sealant, Baxter Healthcare) show the potential of this material for subcutaneous islet transplantation (141). Reduced blood glucose levels were obtained within

days, though a relatively large amount of islets was implanted. In a more thorough study, Kim *et al.* have explored the influence of different fibrin and thrombin concentrations on islet function when transplanted subcutaneously (125). They found that by tuning these concentrations a matrix could be obtained that facilitates islet function at the subcutaneous transplantation site in such an extent that the marginal islet mass for this site is comparable to that of the renal subcapsular site. However, due to the low amounts of fibrinogen and thrombin used for this matrix, an open question remains whether this gel has sufficient mechanical properties to protect the islets from mechanical stress. To acquire more mechanical stability, some approaches combine these natural hydrogels, with solid support matrixes, including polyvinyl alcohol sponges (139) and microporous poly(dimethylsiloxane) (PDMS) scaffolds (65).

Issues associated with mechanical stability, purification, immunogenicity, pathogen transmission, and batch-to-batch variations have spurred the development of synthetic hydrogels. Synthetic hydrogels applied for islet transplantation are mainly based on polyethylene glycol (PEG). The advantage of these PEG hydrogels is their tunable structural properties. By varying the cross-linking density, mechanically stable and even immunoprotective hydrogels can be obtained (145–150). The incorporation of peptide sequences that can be cleaved by matrix metalloproteinases (MMPs) have resulted in the development of PEG-based matrices that allow cellular infiltration *in vivo* (151). For example, Phelps *et al.* (152) have studied the potential of incorporating the fast-degrading peptide, GCRDVPMSMRGGDRCG, in PEG-maleimide hydrogels to obtain a matrix suitable for islet engraftment and revascularization. They show that this gel facilitates a more robust *in vitro* islet survival and function compared to alginate gels. Furthermore, initial *in vivo* implantations onto the small bowel mesentery reveal that this hydrogel platform promotes a promising degree of vascularization. In a follow-up study, they show the potential of these hydrogels to cure diabetes when transplanted onto the surface of the small bowel mesentery of C57Bl/6J mice (153).

Another promising approach, proposed by Brubaker *et al.* (154), is a branched catechol derivatized PEG precursor. By adding sodium periodate solution oxidation of catechol moieties occurs and reactive quinones are formed that react with phenol groups that exist in the hydrogel precursor itself and also with primary amines present in tissue, allowing this precursor to simultaneously form a hydrogel and also act as a bioadhesive. They have shown that this reaction allows the effective immobilization of the islet-containing hydrogels onto the surface of the liver and the epididymal fat pad and enables revascularization and glucose management. However, the mean recovery time to reach normoglycemia is significantly longer for islets immobilized onto the liver surface compared to intrahepatic islet delivery or to immobilized islets onto the fat pad. Possible explanations for this are delayed revascularization at the liver surface or delayed islet engraftment because of partial dissociation of the islet graft due to the convex nature of the liver surface.

1.4.2 Solid scaffold designs for islet transplantation

The advantage of solid scaffolds is their mechanical stability. Basic requirements for solid scaffold platforms intended for islet transplantation include biocompatibility, a high surface area/volume ratio with sufficient mechanical integrity, and a high porosity to support nutrient transport by diffusion and the formation of a vascular network within the islet graft.

Most solid scaffold platforms specifically designed for extrahepatic islet transplantation are porous sponge-like disks fabricated from poly(glycolide-L-lactide) (PLG) (155–162) and poly(dimethylsiloxane) (PDMS) (60, 65). In these platforms porosity is obtained by using fabrication techniques, such as needle-punching (155), gas foaming/particulate leaching (139, 156–162) and solvent casting/particulate leaching (65, 163). The obtained scaffolds are highly porous (>90%), with pore sizes ranging from $150 \pm 60 \mu\text{m}$ for the needle-punched scaffolds (155) and 250–425 μm (60, 65, 139, 156–162) or 425–600 μm (158) for scaffolds fabricated by particulate leaching strategies. Other studies have used the commercially available and medically approved DuraPatch, made from Ethisorb (164, 165), a composite biodegradable polymer consisting of polycyclic acid (Vicryl) and poly-p-dioxanone (PDS). Unfortunately, there is no data available on porosity and pore size of these constructs.

The *in vivo* performance of these scaffolds has been tested at intraperitoneal transplantation sites, such as the epididymal (65, 155–160) and intraperitoneal fat pad (161) in mice, the omental pouch in rats (60), pigs (158), beagle dogs (164) and cynomolgus monkeys (165), and the gastric submucosa (158) in pigs. Regardless whether a PLG, PDMS or Ethisorb scaffold is used, or which transplantation site is selected, the employment of a scaffold does improve graft performance. This finding suggests that a scaffold supports the islet engraftment process at these extrahepatic transplantation sites. However, in most cases the required time to achieve normoglycemia is still longer compared to control groups such as islet transplantation in the liver or under the kidney capsule, indicating that the engraftment process at these extrahepatic transplantation sites remains delayed.

Factors that could contribute to the compromised performance of these constructs compared to intrahepatic or renal subcapsular islet transplantation, are poor islet retention in the scaffold platforms, delayed revascularization, or the cell-biomaterial interactions which can tremendously affect cell function. To ensure islet distribution throughout the scaffold, the majority of the described studies have selected quite large pore size ranges (250–425 μm and 425–600 μm). However, these large pore sizes impede islet retention, since the majority of the islets is smaller than 150 μm (111). Pedraza *et al.* indicate a correlation between islet retention within porous PDMS scaffolds (pore size \sim 250–425 μm) and islet size, with increased islet loss for isolations containing a large portion of islets <100 μm in diameter (60). Therefore, some studies have employed hydrogels, such as matrigel (155), collagen type 1 gel (139), or fibrin gel (65), to ensure islet retention in these porous scaffold platforms. The disadvantage of these hydrogels however, is that they impose an additional barrier to invading vessels potentially delaying islet engraftment. It has been suggested that incorporating proangiogenic factors in these hydrogels,

such as platelet-derived growth factor (PDGF), might partly overcome this barrier. As shown by Brady *et al.*, PDMS scaffolds seeded with an islet suspension in fibrin gel supplemented with PDGF result in a significant decrease in the mean reversal time to normoglycemia compared to scaffolds seeded with islets without the supporting fibrin gel (65). However, it remains to be evaluated whether this improved performance is because of better islet retention in the scaffold platform or due to enhanced islet engraftment.

It has been suggested that large pore sizes not only impede islet retention but also the ingrowth of vascularized tissue which might affect islet engraftment. Sharkawy *et al.* have shown that the vascular density around PVA sponges with a pore size of 700 μm , is decreased compared to sponges with a pore size of 60 μm (166). This is later confirmed using highly controlled porous template scaffolds (PTs) demonstrating that constructs with 30-40 μm pores achieve maximal vascularization and minimal fibrous encapsulation compared to constructs with smaller or larger pores (167). The only study that describes the effect of pore size on islet function, compares pore size ranges of 250-425 μm and 425-600 μm (158). Although vascular density is not determined in these islet grafts, the observation that the curing rate is not significantly different between both constructs might implicate that within this order of magnitude pore size does not affect islet engraftment. However, more thorough studies are necessary to determine the effect of pore size on early islet engraftment.

Another factor that might influence graft performance is the material used for scaffold fabrication. In an attempt to identify the best substrate for islets, high-throughput approaches have been developed. Both Williams *et al.* (168) and Mei *et al.* (169) studied the interaction of dispersed rat islet cells on a wide variety of polymer films. They observed that only a few polymers with distinct characteristics supported islet cell attachment. However, it remains to be evaluated which of these polymers support islet function and survival, though these high-throughput systems would offer an elegant approach to study this. Also for *in vivo* studies, no direct comparison has been performed in terms of islet function and engraftment in scaffolds with similar design characteristics, such as porosity and pore size, but fabricated from different polymer materials. In two separate studies, Gibly *et al.* (158) and Brady *et al.* (65) do describe the transplantation of porous scaffold platforms with comparable dimensions and pore size range, fabricated from either PLG or PDMS, in the epididymal fat pad of STZ-induced diabetic C57Bl6 mice. Interestingly, for PLG scaffolds fewer islets are required to obtain normoglycemia compared to PDMS scaffold (75 vs 250 islets) and the reported time to achieve normoglycemia is much shorter (12 vs 45 days). However these scaffold designs do differ slightly from each other, which hamper a fair comparison. Direct comparative studies have been performed to assess the effect of different extracellular matrix-coatings, such as collagen IV, fibronectin, and laminin-332 on islet function in porous PLG scaffolds (159, 160, 170). These studies describe that restoration of islet cell-ECM contacts, in particular collagen type IV, results in decreased islet cell apoptosis, and enhanced islet viability, metabolism and glucose-stimulated insulin secretion *in vitro* and that *in vivo* these coatings result in a pronounced decrease in time to reach euglycemia and an

increase in intra-islet vascular density. These findings highlight the importance and strength of direct comparative studies in order to identify the microenvironment that is most supportive for islet function and engraftment.

A strategy to enhance islet engraftment in porous scaffolds is *in vitro* or *in vivo* prevascularization. Juang *et al.* (171) have explored the effect of one week *in vivo* prevascularization prior to islet transplantation on subcutaneous islet engraftment in both polyvinyl alcohol disks and PGA sheets. However, they did not observe a significant improvement compared to non-prevascularized constructs. At the same transplantation site, Pileggi *et al.* (172) have used an *in vivo* prevascularization period of 40 days. Their design comprised of a 2cm-long cylindrical stainless-steel mesh with polytetrafluoroethylene stoppers at both sites. In order to prevent complete occlusion of the lumen during the prevascularization period, a PTFE plunger was inserted in the graft. Forty days after implantation, the plunger was removed and islets were injected. These constructs were able to reverse diabetes in seven out of eight recipients and showed metabolic function comparable to the control group who received the same islet mass in the liver. Histological examination showed well-preserved and vascularized islet structures as early as 10 days after transplantation, implying that a long prevascularization period might be crucial for islet revascularization and survival at the subcutaneous transplantation site. Another approach is to perform a prevascularization period *in vitro* using endothelial cells. Kaufman *et al.* have reported improved glucose regulation in porous PLGA/PLLA scaffolds transplanted subcutaneously, using a prevascularization period of 5 days with HUVECs and human foreskin fibroblast cells (173).

1.5 CLINICAL ISLET TRANSPLANTATION: WHERE SHOULD WE GO?

Pancreatic islet transplantation has come a long way since the first successful clinical case study in 1990 describing insulin independence after intraportal islet infusion (22). Progress in islet transplantation has improved glycemic control protecting patients from severe hypoglycemic reactions. However, if success is defined as long-term insulin independence, then outcomes remain disappointing. In this chapter, several barriers that restrict the success of pancreatic islet transplantation into the liver have been identified. Suggested solutions to some of these problems have been described and we have shed some light on recent advances in this field aiming to improve long-term survival and function of pancreatic islet transplants. But what direction should we go?

As outlined in this chapter, the general consensus is that the liver does not provide an optimal transplantation environment for islets of Langerhans and that extrahepatic sites might improve long-term islet survival and function. Extrahepatic sites that are extravascular and spacious enough to enable the transplantation of sufficient amount of islets, is narrowed down to the omentum and gastrointestinal wall with portal drainage and the muscle, adipose tissue, subcutaneous site, thymus and bone marrow with systemic drainage. However, in order for

extrahepatic islet transplantation to be implemented within the clinical setting, its performance must not only be effective, but also surpass that of islets transplanted intrahepatically. To date, the engraftment process at these sites is delayed compared to intrahepatic controls. It has been shown that islet function and engraftment at these sites can be improved using biomaterial scaffolds, but despite these measures, the engraftment process remains delayed. Therefore, advancements in this field should focus on promoting transplant efficiency and stimulating islet engraftment at these extrahepatic transplantation sites. Strategies one can think of are modifications of the islet microenvironment with stimulating cues, in the form of growth factors, ECM molecules, or the provision of immunomodulatory or proangiogenic cell sources. One should also not overlook the importance of scaffold design regarding islet distribution and retention, and by this, transplant efficiency. In addition, a growing body of evidence suggests that scaffold design parameters such as pore size and surface topography can largely influence fibrous and vascular tissue formation in and around an implant (166, 167, 174–179).

Looking beyond the development of an ideal islet transplant environment, whereby islets optimally engraft and exhibit superior long-term function, a significant obstacle remains the requirement for systemic immunosuppressive drugs. Given the serious disadvantages of these drugs, such as increased susceptibility to infection and cancer and their negative effects on islet revascularization and function (78), the treatment option of islet transplantation and systemic immunosuppression would still be restricted to only severely diabetic patients, even if the designed scaffold environment would perform far superior compared to intrahepatic islet transplantation. Therefore, we believe that the ultimate islet transplantation strategy will require a combinatorial approach involving both immunomodulatory regimens to induce tolerance towards the islet graft and “smart scaffolds”, specifically designed to stimulate the regeneration process and islet engraftment.

1.6 OUTLINE OF THIS THESIS

The perspective above provides the context for the scaffold platform developed in this thesis, where we specifically focus on precise and systematic control over structural design to ensure islet retention and facilitate vascularized tissue ingrowth. The proposed scaffold design comprises of a microwell scaffold platform with a high degree of controllability over porosity and pore-size. The advantages of the proposed design are that it (1) prevents islet attachment, spreading, and aggregation by the confinement of individual islets in separate microwells preserving the rounded islet morphology; (2) is mechanically stable to protect islets against physical stresses; and (3) has an open structure permitting fast vascular ingrowth. In **Chapter 2** the concept of the microwell design is introduced using thin films and electrospun meshes and its potential to support islet survival, function and morphology is tested *in vitro*. **Chapter 3** explores the use of three different fabrication methods to obtain porous microwell scaffolds with well-defined pores with a diameter < 40 μm to ensure islet retention and

facilitate vascularized tissue ingrowth. Transplantation studies in the epididymal fat elucidate the potential of this porous scaffold platform to restore blood glucose levels and islet engraftment in a diabetic mouse model. **Chapter 4** describes a cell-based strategy to further improve islet engraftment after transplantation. Composite islets with different supporting cells are fabricated and the angiogenic potential of these composites is explored in *in vitro* and *in vivo* angiogenesis assays. **Chapter 5** explores the feasibility of SPECT imaging to monitor beta cell survival in intraperitoneally transplanted porous microwell scaffolds using ^{111}In -labelled exendin. A collective overview summarizes how the results obtained in this thesis advance the field of extrahepatic islet transplantation and bring closer the realization of a long-term functional bio-artificial pancreas for the treatment of type 1 diabetes (**Chapter 6**).

Table 1 Co-transplantation of islets with proangiogenic cells

Origin cell source	Study and publication date	Cell type	Definition cell type	Transplantation site and experimental groups
Bone marrow	Figliuzzi <i>et al.</i> (69), 2009	BM-MSCs	Rat BM-mononuclear cells cultured in α -MEM supplemented with 20% FCS and 1mU/mL pen/strep	Kidney capsule Groups: 1. BM-MSC + islets 2. Islets alone
	Solari <i>et al.</i> (180), 2009	BM-MSCs	Rat BM-mononuclear cells seeded (density 20×10^6 cells/75cm ²) in RPMI-1640 supplemented with 10% FBS, 2 mM L-glutamine, 0.1 M non-essential amino acids, 1 mM sodium pyruvate, 100 U/ml penicillin, 100 μ g/ml streptomycin, and 55 μ M 2-ME. Cells were expanded until p.4-8.	Omental pouch Groups: Syngeneic: 1. Lewis islets alone (600) (n=8) 2. Lewis islets (600)+ Lewis BM-MSCs (n=10) Allogeneic: 1. Wistar Furth islets (600-800) + cyclosporine A (n=8) 2. Wistar Furth islets (600-800) + lewis BM-MSCs + cyclosporine A (n=10) 3. Wistar Furth islets (600-800) + Wistar Furth BM-MSC+cyclosporine A (n=5) 4. Wistar Furth islets (600-800) + cyclosporine A + anti-lymphocyte serum (n=5) 5. Wistar Furth islets (600-800) + Lewis BM-MSC+cyclosporine A + anti-lymphocyte serum (n=7)

Transplantation model	Number of transplanted islets and proangiogenic cells/factors	Achieved normoglycemia	Improved islet function and revascularization
Syngeneic, lewis rats STZ induced diabetes: 65 mg/kg Co-infusion of islets and BM-MSCs	2000 islets 1*10 ⁶ BM-MSCs	<ol style="list-style-type: none"> Group 1: yes, exact number of cured animals not mentioned Group2: glucose levels decreased but mice did not revert to normoglycemia in observed time (36 days) 	<p>Function: IPGTT not performed, but glycemic control seems better indicated by blood glucose measurements when BM-MSCs are added</p> <p>Revascularization: (Based on RECA-1 staining) Significant increase in vessel density between group 1 and 2 30 days after transplantation</p>
Syngeneic and allogeneic Lewis or Wistar Furth islets/BM-MSCs in Lewis rats STZ induced diabetes: 40/50 mg.kg i.v. Co-infusion of islets and BM-MSCs	600-800 islets 3*10 ⁶ BM-MSCs	<p>Expressed as graft survival in days</p> <p>Syngeneic:</p> <ol style="list-style-type: none"> Group 1 (n=8): 2, 2, 2, 2, 12, 15, 15, >21 Group 2 (n=10): 7, >21 x 9 <p>Allogeneic:</p> <ol style="list-style-type: none"> Group 1 (n=8): 2, 2, 5, 8, 8, 8, 12, 12 Group 2 (n=10): 5, 8, 15, 21, 21, 35, >103 x4 Group 3 (n=5): 5, 12, 12, 15, 15 Group 4 (n=5): 2,2,2,8, 15 Group 5 (n=10): 5, 5, 12, 15, 19, 21, 25, >60, >78 x2 	<p>Function: IPGTT not performed, but BM-MSCs promoted islet graft survival and function in syngeneic and allogeneic transplantation model.</p> <p>Revascularization: Not studied</p> <p>NOTE: T cells from recipients transplanted with allogeneic islets + BM-MSC produced low levels of IFN-γ and TNF-α upon <i>ex-vivo</i> activation, and this transplantation protocol promoted the generation of IL-10-secreting CD4⁺ T cells</p>

Table 1 (Continued)

Origin cell source	Study and publication date	Cell type	Definition cell type	Transplantation site and experimental groups
Bone marrow	Ito <i>et al.</i> (70), 2010	BM-MSCs	Rat BM-mononuclear cells (10^7 cells/well of six-wells plate) cultured in Iscove's modified D-medium, L-glutamine, antibiotics, insulin-transferrin-selenium, linoleic acid-albumin, 10^{-4} M ascorbic acid, 10^{-9} M dexamethasone, 10 ng/mL of epidermal growth factor, 10 ng/mL of platelet-derived growth factor-BB, 10 ng/mL leukemia inhibitory factor, and 20% FBS for 1 week	Intrahepatic Groups: 1. BM-MSC + islets 2. Islets alone
	Sakata <i>et al.</i> (71), 2010	BM-cells	Freshly isolated murine BM-cells	Kidney capsule Groups: 1. BM-cells + islets (n=13) 2. Islets alone (n=12) 3. BM-cells alone (n=11)
	Wu <i>et al.</i> (181), 2013	BM-MSCs	Expanded human BM-mononuclear cells	Kidney capsule Groups: 1. Islets + BM-MSCs 1:50 (n=10) 2. Islets + BM-MSCs 1:100 (n=12) 3. Islets + BM-MSCs 1:200 (n=11) 4. Islets alone (n=11)

Transplantation model	Number of transplanted islets and proangiogenic cells/factors	Achieved normoglycemia	Improved islet function and revascularization
Syngeneic, Lewis rats STZ induced diabetes: 65 mg/kg i.v Co-infusion of islets and BM-MSCs	300/500 islets 1*10 ⁶ BM-MSCs	300 islets: 1. Group 1: 5/9 2. Group 2: 1/10 500 islets: 1. Group 1: 8/8 2. Group 2: 3/10	Function: Glucose tolerance test is not performed, but glucose clearance is significantly faster for group 1 compared to group 2. Revascularization: (Based on vWF staining) Significant increase in the number of capillary segments per β -cell between group 1 and 2 6 days after transplantation
Syngeneic, BALB/c mice STZ induced diabetes: 200 mg/kg i.p Co-infusion of islets and BM-cells	200 islets 1-5*10 ⁶ BM-cells	1. Group 1: 6/13 2. Group 2: 3/12 3. Group 3: 0/11	Function: glucose tolerance appeared better in BM-cells + islets compared to other groups at d.14 and d.28, but no significant difference in AUC between groups at d.84 Revascularization: (Based on vWF staining) Vessel density significantly increased in group 3 compared to group 2 at d.3, and in group 1 and 3 compared to group 2 at d.7. Not at d.14, d.28 and d.84. NOTE: Significant increase in VEGF expression observed based on IHC in BMC-group at d.14 and d.28.
Xenogeneic, humanized NSG mice → intraperitoneal injection of mature human peripheral blood mononuclear (hPBM) cells four weeks after renal subcapsular islet implantation STZ induced diabetes: low-dose 70 mg/kg i.p., 2 injections in 3 weeks. Co-infusion of islets and BM-MSCs	500 human islets islets: BM-MSC ratio: 1:50 1:100 1:200	After i.p. injection of hPBMCs 1. Group 1: 2/10 2. Group 2: 6/12 3. Group 3: 10/11 4. Group 4: 0/11	Function: IPGTT only performed for group 3 and 4 two weeks after i.p. injection of hPBMCs. Group 3 showed faster and better response to the stimulatory glucose compared to group 4. Revascularization: Not determined NOTE: BM-MSCs prevented the cytokine-induced loss-of-function of human islets.

Table 1 (Continued)

Origin cell source	Study and publication date	Cell type	Definition cell type	Transplantation site and experimental groups
Bone marrow	Oh <i>et al.</i> (74), 2013	BM-EPCs	Mouse BM-mononuclear cells cultured in EGM-2 medium for 1 week.	Kidney capsule Groups: 1. CD34 ⁺ /CD14 ⁻ BM cells (non EPCs) + islets (n=14) 2. CD34 ⁺ /CD14 ⁺ BM cells (fresh-EPCs) + islets (n=14) 3. Cultured EPCs + islets (n=17) 4. Islets alone (n=13)
	Quaranta <i>et al.</i> (75), 2014	BM-EPCs	Rat BM-mononuclear cells (25*10 ⁶ cells/well of six-well plate) cultured on gelatin-coated plates in EGM-2 medium for 1 week.	Intrahepatic Groups: 1. Islets + BM-EPCs (n=11) 2. Islets alone (n=6) 3. BM-EPCs alone (n=4)
	Penko <i>et al.</i> (182), 2015	BM-EPCs	Murine BM-mononuclear cells, cultured on fibronectin (50 µl/ml) in M199 medium supplemented with 20% FCS, endothelial cell growth supplement (15µg/mL containing VEGF, FGF, endothelial cell growth factors α and β) and heparin (15µg/mL)	Kidney capsule Groups: 1. Islets + BM-EPCs (n=12) 2. Islets only (n=10)

Transplantation model	Number of transplanted islets and proangiogenic cells/factors	Achieved normoglycemia	Improved islet function and revascularization
Syngeneic, male GFP-Tg and wild-type C57BL/6J mice	200 islets 1*10 ⁶ BM-EPCs	<ol style="list-style-type: none"> Group 1: 5/14 Group 2: 9/14 Group 3: 14/17 Group 4: 5/13 	<p>Function: for group 2 and 3 the AUC (IPGTT d28) was significantly reduced to that of group 1 and group 4</p> <p>Revascularization: (Based on CD31 staining) Significant increase in vessel density between group 3 and 4, 14 and 28 days after tx, other groups not determined. EPC co-localization with CD31 observed</p>
STZ induced diabetes: 180 mg/kg i.p.			
Co-infusion of islets and BM-EPCs			
Syngeneic, lewis rats	700 IEQ 5*10 ⁵ EBM-EPCs	<ol style="list-style-type: none"> Group 1: yes, exact number of cured animals not mentioned Group 2: yes, exact number of cured animals not mentioned, but after day 15 mice became hyperglycemic again Group 3: 0/4 	<p>Function: AUC (IPGTT d15) not determined. Co-transplantation of 700 syn-IE+500,000 EPCs induced a faster decrease of blood glucose levels than the other treatments.</p> <p>Revascularization: (Based on CD31 staining) Significant increase in vessel density between group 1 and 2 30, 120, and 180 days after transplantation (not 15 days) EPC co-localization with CD31 observed</p>
STZ induced diabetes: 65 mg/kg i.p.			
Co-infusion of islets and BM-EPCs			
Syngeneic, C57Bl/6 mice	200 islets 1*10 ⁶ BM-EPCs	<ol style="list-style-type: none"> Group 1: 83% Group 2: 20% 	<p>Function: IPGTT only performed on functional grafts, no significant differences found, but there was a significantly improved cure rate in group 1.</p> <p>Revascularization: not determined.</p>
STZ-induced diabetes: 180–200 mg/kg i.p.			
Co-infusion of islets and BM-EPCs			

Table 1 (Continued)

Origin cell source	Study and publication date	Cell type	Definition cell type	Transplantation site and experimental groups
Umbilical cord blood	Kang <i>et al.</i> (76), 2012	UC-hEPCs	Human mononuclear cells isolated from umbilical cord blood, cultured in EGM-2 medium for 2 weeks for colony formation, then colony was reseeded to gelatin-coated plates for expansion up to p.3	Kidney capsule Groups: 1. Islets + UC-hEPCs (n=9) 2. Islets alone (n=5)
	Jung <i>et al.</i> (183), 2014	UC-hEPCs	Human mononuclear cells isolated from umbilical cord blood, cultured on 2% gelatin coated plates in EGM-2 medium and expanded up to p.10	Intrahepatic Groups: 1. Islets + UC-hEPCs (n=9) 2. Islets alone (n=10)
Kidney Adipose tissue	Rackham <i>et al.</i> (72), 2011	K-MSCs	Murine kidney-derived MSCs, cultured in DMEM supplemented with 1% pen/strep, and 10% FCS for two weeks	Kidney capsule Groups: 1. Islets + K-MSCs (n=13) 2. Islets alone (n=13)

Transplantation model	Number of transplanted islets and proangiogenic cells/factors	Achieved normoglycemia	Improved islet function and revascularization
Xenogeneic, BALB/c nude mice STZ induced diabetes: 180 mg/kg i.p. Co-infusion of islets and UC-EPCs	7000 IEQ (porcine islets) 5*10 ⁵ UC-hEPCs	1. Group 1: yes, exact number not mentioned, after 11 days 2. Group2: glucose levels decreased but mice did not revert to normoglycemia in observed time (35 days)	Function: IPGTT not performed, but glyemic control seems better indicated by blood glucose measurements Revascularization: (Based on BS-1 lectin perfusion, CD31, BS-1 staining) Significant increase in vessel density between group 1 and 2, 2 and 3 weeks after implantation, not after 35 days. NOTE: decreased intensity of Hypoxyprobe was observed in group 1 compared to group 2 suggesting earlier recovery from hypoxia. Furthermore significant increase in proliferating beta cells was observed, only at d14, not at d3 and d35. Based on IHC and qPCR after implantation (d.10) an increased signal intensity in VEGF-A was observed in insulin positive areas between groups.
Xenogeneic, BALB/c nude mice STZ induced diabetes: 200 mg/kg i.p. Composite islets	10.000 IEQ Porcine islets Composite islets were formed co-culturing 6*10 ⁶ UC-hEPCs/ 10.000 IEQ islets for two hours (exact number of attached cells unknown)	1. Group 1: 4/9 2. Group 2: 2/10 but normoglycemia was not maintained	Function: IPGTT not performed, animals not cured, but the blood glucose values for the coated islets are significantly lower compared to uncoated control. Revascularization: not determined NOTE: decrease in markers of IBMIR when islets were coated with UC-hEPCs
Syngeneic, C57Bl/6 mice STZ-induced diabetes: 180 mg/kg i.p. Co-infusion of islets and K-MSCs	150 islets 25*10 ⁴ K-MSCs	1. Group 1: 58% 2. Group 2: 8%	Function: AUC not determined, but IPGTT of performing grafts was comparable between groups Revascularization: (Based on CD34 staining) Significant increase in vascular density between groups at d. 28

Table 1 (Continued)

Origin cell source	Study and publication date	Cell type	Definition cell type	Transplantation site and experimental groups
Kidney Adipose tissue	Cavallari <i>et al.</i> (73), 2012	hASCs	Human adipose tissue-derived stem cells, cultured in DMEM-low glucose, supplemented with 1% pen/strep, 2mM L-glutamine, and 20% FBS and used at p.3-5.	Intrahepatic (caudate lobe) Groups: 1. Composite islets with hASCs (n=7) 2. Composite islets with preconditioned hASCs in a mixture of hyaluronic (HA), butyric (BU), and retinoic (RA) acids (n=7)
	Bhang <i>et al.</i> (142), 2013	hASCs	Human adipose tissue-derived stem cells, cultured in α MEM supplemented with 100 U/mL penicillin, 100 μ g/mL streptomycin, and 10% FBS.	Subcutaneous in 0.2 mL fibrin gel Groups: 1. Islets + hASCs (n=8) 2. Islets + hASCs +FGF2 (n=8) 3. Islets alone (n=8)
Aorta	Li <i>et al.</i> (68), 2013	ECs	Rat aorta-derived ECs, cultured in RPMI-1640, supplemented with 10% FBS.	Kidney capsule Groups: 1. Islets alone (n=10) 2. EC-islets (n=10) 3. Sertolli cell injection + islets (n=10) 4. Sertolli cell injection + EC-Islets (n=10)

Transplantation model	Number of transplanted islets and proangiogenic cells/factors	Achieved normoglycemia	Improved islet function and revascularization
Syngeneic, Lewis rats	500 islets	1. Group 1: 0/7 2. Group 2: 2/7	Function: AUC not determined, but IPGTT at d.15 showed improvement in blood glucose control in preconditioned group. Revascularization: (Based on BS-1 staining) Significant increase in vascular density observed in preconditioned group at d.15.
STZ-induced diabetes: 70 mg/kg i.p.	Composite islets were formed with cell/islet ratio of 5,000/100 in two hours (exact number of attached cells unknown)		
Composite islets			
Xenogeneic, athymic mice	800 Lewis rat islets 8*10 ⁵ hAHCs	1. Group 1: no (reduced blood glucose) 2. Group 2: yes (significant reduction of blood glucose) 3. Group 3: no	Function: significant reduction of blood glucose levels in group 2 compared to other groups. Vascularization: not directly determined, but expression of human (VEGF, not α -SMA and vWF) in mouse (α -SMA, vWF, NG2, ICAM, VCAM) endothelial factors enhanced when hASCs are added. NOTE: viability of islets was improved by the addition of FGF2 supplement. Apoptotic activity of islets reduced when hASCs were added. Apoptotic activity of hASCs reduced when FGF2 supplement was added.
STZ-induced diabetes: 200mg/kg	25 μ g FGF2		
Co-transplantation in fibrin plug			
Allogeneic, Sprague-Dawley cells in Wistar rats.	1000 islets Composite islets were formed	Expressed as graft survival in days (n=10 per group)	Function: not determined by IPGTT, but presented as graft survival. ECs and sertolli cells promoted islet graft survival and function in allogeneic transplantation model.
STZ-induced diabetes: 220 mg/kg i.p.	co-culturing 3*10 ⁶ ECs/ 1000 IEQ islets for two hours (exact number of attached cells unknown)	1. Group 1: 6,5,4,7,5, 4,5,7,4,5 2. Group 2: 9,13,30, 25,14,11,10,12,9,19 3. Group 3: 28,33,39, 27,31,25,29,30,30, 26 4. Group 4: 47,55, 68,81,40,50,70,49, 56,60	Revascularization: (Based on vWF staining) Significant increase in vascular density when ECs are used at d3, d7, d14. NOTE: Sertoli cells infusion inhibits lymphocyte activation and inflammatory factor of recipient by islet and ECs (more lymphocyte activation when ECs are added).
Composite islets with infusion of sertolli cells (prior to tx)			

Table 2 Scaffold designs for extrahepatic islet transplantation

Category	Transplantation site	Material	Study	Scaffold design
Hydrogel scaffold	Subcutaneous	Collagen type 1	Hiscox <i>et al.</i> (138), 2008	Three layers of collagen type-I gel: two outer layers with microvessel fragments, the inner layer with islets
		Plasma-fibroblast gel	Perez-Basterrechea <i>et al.</i> (140), 2009	Bulk hydrogel (prefabricated)
		Fibrin gel	Kim <i>et al.</i> (125), 2012	<ul style="list-style-type: none"> • Patch like hydrogel (prefabricated) • <i>In situ</i> formation of hydrogel
			Andrades <i>et al.</i> (141), 2007	Bulk hydrogel (prefabricated)
			Bhang <i>et al.</i> (142), 2013	Bulk hydrogel (prefabricated)

Animal model	Number of transplanted islets	Observed time period	Achieved normoglycemia	Comments
Xenogeneic transplantation (islets and microvessel fragments from male Sprague-Dawley rats) in non-diabetic female SCID mice (CB-17/ICR background)	Not specified	1 month	N.A.	<i>In vitro</i> prevascularization period of 7 days of outer layers containing microvessel fragments
Xenogeneic transplantation (islets from male Wistar rats) in STZ induced diabetic male SPF Swiss nu/nu mice Dose: i.p. injection of 225mg/kg STZ	3000 IEQ	2 months	Kidney capsule control: 7 out of 7 (mean: 1.29±0.18d) SC control (islets only): 0 out of 7 (died/sacrificed; too diabetic) SC construct: 7 out of 7 (mean: 3.86±1.16d)	Addition of skin fibroblasts to construct
Xenogeneic transplantation (human islets) in STZ induced diabetic NOD/SCID mice Dose: two i.p. injections of 125 mg/kg STZ for two consecutive days	500, 1000, 2000, 3000, 5000 IEQ Marginal islet mass: 1000-2000 IEQ	70 days	(for 5000 IEQ) SC patch: 8 out of 8 (3.4 days) SC hydrogel: 5 out of 5 (22.5 days) (for 2000 IEQ) Kidney capsule control: 9 out 11 SC hydrogel: 5 out of 5	Addition of fibrinogen
Syngeneic transplantation in STZ induced C3H mice Dose: not mentioned	800 IEQ	1 month	Kidney capsule control: blood glucose levels reduced, curing not mentioned SC construct: blood glucose levels reduced, curing not mentioned	
Xenogeneic transplantation model (islets from male Lewis rates) in STZ induced athymic female mice Dose: i.p. injection of 200mg/kg STZ	800 islets 8*10 ⁵ hADSCs	21 days	SC gel + islets: 0 out of 8 SC gel + islets + hADCS: 0 out of 8 (but improved) SC gel + islets + hADCS +FGF2: cured, <5 days but exact number not mentioned)	Addition of hADSCs and FGF2

Table 2 (Continued)

Category	Transplantation site	Material	Study	Scaffold design
Hydrogel scaffold	Intramuscular (abdominal muscle (AM))	Alginate	Witkowsky <i>et al.</i> (66), 2009	Alginate scaffold with cyclic arginine-glycine-aspartic acid RGD peptide (+VEGF/PDGF)
	Intra-peritoneally (Epididymal fat pad (EFP))	Catechol-derivatized poly(ethylene glycol) hydrogel	Brubaker <i>et al.</i> (154), 2010	<i>In situ</i> formation of hydrogel (tissue adhesive)
	Intra-peritoneally (Intestinal mesentery (IM))	PEG-maleimide hydrogels	Phelps <i>et al.</i> (152), 2013	<i>In situ</i> formation of hydrogel, hydrogel contains RGD peptide (+VEGF)
			Phelps <i>et al.</i> (153), 2013	<i>In situ</i> formation of hydrogel, hydrogel contains RGD peptide (+VEGF)

Animal model	Number of transplanted islets	Observed time period	Achieved normoglycemia	Comments
Syngeneic transplantation in STZ induced diabetic male Lewis rats Dose: 50 mg/kg STZ injected in penile vein	2400 islets	60 days	AM islets only: 2 out of 6 (within 5 days) AM construct –VEGF/PDGF: 3 out of 6 (within 5 days) AM construct + VEGF/PDGF: 6 out of 6 (within 5 days)	<i>In vivo</i> prevascularization of construct two weeks prior to islet injection in non-diabetic rat. Four days prior to islet transplantation, diabetes was induced by STZ injection
Syngeneic transplantation in STZ induced diabetic male C57Bl/6 mice Dose: i.p. injection of 220mg/kg STZ	150 islets	112 days	Liver control: 7 out of 7 (7.6±1.1 days) Liver surface + construct: 8 out of 9 (50.8±8.5 days) EFP islets only: 7 out of 7 (5.1±1.3 days) EFP construct : 8 out of 8 (11.5±2.2 days)	
Syngeneic transplantation in Lewis rats	1500 islets	1 month	-	Incorporation of RGD peptide and VEGF
Syngeneic transplantation in STZ induced diabetic male C57Bl/6J mice Dose: 5 successive daily i.p. injection of 30mg/kg STZ	400 islets	1 month	Liver control: 0 IM construct: blood glucose was just above the target range of 250 mg/dL IM construct + VEGF: cured <10 days (faster to respond to the glucose challenge compared to group without VEGF) Exact numbers not mentioned	Incorporation of RGD peptide and VEGF

Table 2 (Continued)

Category	Transplantation site	Material	Study	Scaffold design
Solid scaffold	Subcutaneous	polyvinyl alcohol (PVA) and polyglycolic acid (PGA)	Juang <i>et al.</i> (171), 1996	Polyvinyl alcohol (PVA) disks (0.6 x 0.6 x 0.25 cm) and polyglycolic acid (PGA) sheets (1 x 1 x 0.1 cm) soft fibrous polymer mats, porosity and pore size not mentioned
		Stainless-steel	Pileggi <i>et al.</i> (172), 2006	Cylindrical mesh with two polytetrafluoroethylene stoppers at both sides (2cm long, diameter 0.6cm); pore-size: 450µm
		1:1 blend poly (lactide-co-glycolide) (PLGA) and poly-L-lactic acid (PLLA)	Kaufman <i>et al.</i> (173), 2014	Porous sponge fabricated by salt leaching (5x4x1mm) Pore-size: 300 – 600 µm, 93% porosity In vitro prevascularization (5 days) with Human foreskin fibroblast cells (HFFs) and Human umbilical vein endothelial cells (HUVECs)
	Intra-peritoneally (Epididymal fat pad (EFP))	Poly(glycolide-L-lactide)	Dufour <i>et al.</i> (155), 2005	Fibrous scaffolds (diameter 8mm, thickness 2mm, pore-size: 150±60µm) loaded with Matrigel

Animal model	Number of transplanted islets	Observed time period	Achieved normoglycemia	Comments
Syngeneic transplantation in STZ induced diabetic male inbred B6AF1 mice Dose: i.p. injection of 160mg/kg	400 islets	3 months	PVA + islets PVA + prevascularization + islets PGA + islets PGA + prevascularization + islets Only a few mice were cured, not mentioned which group, there was no effect of prevascularization	<i>In vivo</i> prevascularization of 1 week
Syngeneic transplantation in STZ induced diabetic male Lewis rats Dose: two IV injections of 60 mg/kg STZ two-three days apart	3000 IEQ	80 days and 170 days	Liver control: 4 out of 4 (median: 1d) SC construct: 7 out of 8 (median: 6d)	<i>In vivo</i> prevascularization period of 40 days
Syngeneic transplantation in STZ induced diabetic DM nude mice Dose: dose not mentioned	50 islets 5*10 ⁴ HUVECs + 3*10 ⁴ HFFs per islet	14 days	SC construct: 0/4 SC construct+HFF+HUVEC: lower blood glucose levels, curing not mentioned (n=6)	<i>In vitro</i> prevascularization period of 5 days with HUVECs and HFFs
Syngeneic transplantation in STZ induced diabetic male BALB/c mice Dose: i.p. injection of 275mg/kg STZ	500, 1000 islets	101 days	(for 500 islets) Kidney capsule control: 7 out of 7 (6 out of 7 within 3 days) EFP Matrigel control: 7 out of 11 (few died) (2 out of 11 within 3 days) EFP islets only: 3 out of 11 (few died) (2 out of 11 within 3 days) EFP Construct: 11 out of 11 (few died) (11 out of 11 within 3 days)	Addition of Matrigel

Table 2 (Continued)

Category	Transplantation site	Material	Study	Scaffold design
Solid scaffold	Intra-peritoneally (Epididymal fat pad (EFP))	Poly(glycolide-L-lactide)	Salvay <i>et al.</i> (170), 2008	<p>Porous scaffolds fabricated by gas foaming/particulate leaching; treated with collagen IV, fibronectin, laminin-332, or serum proteins.</p> <p>Pore size not assessed</p>
			Kheradmand <i>et al.</i> (157), 2011	<p>Porous scaffolds fabricated by gas foaming/particulate leaching (diameter 5mm, pore-size 250-425μm)</p>
			Gibly <i>et al.</i> (158), 2011	<p>Porous poly(glycolide-L-lactide) scaffolds fabricated by gas foaming/particulate leaching (diameter 5mm/13mm, height 2mm, pore-size 250-425μm and 425-600μm)</p>

Animal model	Number of transplanted islets	Observed time period	Achieved normoglycemia	Comments
Syngeneic transplantation in STZ induced diabetic male C57Bl/6 mice Dose: i.p. injection of 220mg/kg STZ	125 islets	297 days	EFP construct + serum proteins (control): 6 out of 8 (36.0±18.1 days) EFP construct + collagen IV: 7 out of 7 (4.4±1.0 days) EFP construct + fibronectin: 8 out of 8 (26.9±4.6 days) EFP construct + laminin-332: 8 out of 8 (26.8±6.8 days)	Protein adsorption with collagen IV, fibronectin, laminin-332.
Allogeneic transplantation (islets from BALB/c mice) in STZ induced diabetic male C57Bl/6 (Foxp3-GFP knock-in) mice Dose: 190mg/kg STZ	500 islets	150 days	Kidney capsule control (+TOL): 3 out of 3 (immediately cured, no graft rejection) Liver control (+TOL): 7 out of 7 (immediately cured, but 5 graft were rejected within 70 days) Liver control(-TOL): 8 out of 8 (immediately cured, but all grafts were rejected within 20 days) EFP construct (+TOL): 5 out of 5 (immediately cured, but 1 graft was rejected within 20 days) EFP construct (-TOL): 6 out of 6 (immediately cured, but all grafts were rejected within 20 days)	Tolerance to allograft was induced by i.v. injections (Tx-7d and Tx+1d) of ethylcarbodiimide-treated donor splenocytes
Syngeneic transplantation in STZ induced diabetic male C57Bl/6 mice Dose: i.p. injection of 220mg/kg STZ	Mice: 75, 125 islets Pigs: 1000, 4000, 10000 IEQ	Mice: 44 days Pigs: 14 days	Mice: EFP construct 125 islets: 19 out of 19 (1.95±0.68 days) EFP construct 75 islets: 10 out of 10 (12.1±4.1 days)	Pigs received immunosuppression (CTLA4-Ig and Sirolimus)
Syngeneic transplantation in pigs (transplantation sites: gastric submucosa and omentum)				

Table 2 (Continued)

Category	Transplantation site	Material	Study	Scaffold design
Solid scaffold	Intra-peritoneally (Epididymal fat pad (EFP))	Poly(glycolide-L-lactide)	Yap <i>et al.</i> (160), 2013	Porous scaffolds fabricated by gas foaming/particulate leaching (diameter 5mm, height 2mm, pore-size 250-425µm), treated with collagen IV, fibronectin (only for in vitro analysis), or laminin-332(only for in vitro analysis)
			Gibly <i>et al.</i> (159), 2013	Porous scaffolds fabricated by gas foaming/particulate leaching (diameter 5mm, height 1mm, pore-size 250-425µm) treated with human collagen IV, or ECM mixture
			Hlavati <i>et al.</i> (162), 2014	Layered scaffold, with protein-loaded (exendin-4 and insulin-like growth factor-1) center sandwiched between two porous outer layers fabricated by gas foaming/particulate leaching (diameter 5mm, height 3mm, pore-size 250-425µm)

Animal model	Number of transplanted islets	Observed time period	Achieved normoglycemia	Comments
Syngeneic transplantation in STZ induced diabetic male C57Bl/6 mice Dose: i.p. injection of 220mg/kg STZ	100 islets	113 days	EFP construct (medium control): 6 out of 6 (17.7–2.7 days) EFP construct + collagen IV: 6 out of 6 (3.0±1.8 days)	Protein adsorption with collagen IV (<i>in vitro</i> and <i>in vivo</i>), fibronectin (<i>in vitro</i>), and laminin-332 (<i>in vitro</i>)
Xenogeneic transplantation (human islets) in STZ induced diabetic male NOD-scid IL-2Ry ^{null} mice Dose: i.p. injection of 130mg/kg STZ	500, 1000, 1200, 1500, 2000 IEQ	140 days	(for 2000 IEQ) Kidney capsule control: 5 out of 5 (within days) EFP construct: 5 out of 5 (within days)	Protein adsorption with collagen IV, and ECM mixture
			Transplantation of sub-minimal islet mass (~1500 IEQ), no curing, but collagen IV treated scaffolds significantly improved degree of graft function over	
Xenogeneic transplantation (human islets) In STZ induced male diabetic NOD-scid IL2Rgamma ^{null} Dose: i.p. injection of 130mg/kg STZ	1500-2000 30 days IEQ		EFP construct: 0 out of 8 EFP construct + Ex4: 0 out of 8 (but improved compared to control) EFP construct +IGF-1: 0 out of 8	Addition of IGF-1 and exendin-4

Table 2 (Continued)

Category	Transplantation site	Material	Study	Scaffold design
Solid scaffold	Intra-peritoneally (Epididymal fat pad (EFP))	poly(dimethyl-siloxane)	Brady <i>et al.</i> (65), 2013	Porous scaffolds fabricated by solvent casting and particulate leaching (diameter 10mm, height 2 mm, pore-size 250-425 μ m), treated with fibronectin and islets are loaded in fibrin-fibronectin-PDGF-BB gel
		For one condition islets are loaded in fibrin-fibronectin-PDGF-BB gel		
		Polyvinyl alcohol sponge disks	Vernon <i>et al.</i> (139), 2012	Polyvinyl alcohol sponge disks (Meroce/ Medtronic, Inc., diameter 6mm, thickness 2mm, average pore-size: 500 μ m), with a central hole of 1.5mm diameter (loaded with VEGF-Alginate macrosphere) and with eight peripheral holes of 1mm diameter (for islets suspended in a type 1 collagen hydrogel)
		Islets loaded in collagen type 1 gel		
	Intraperitoneally (Intraperitoneal fat pad (IFP))	poly(glycolide-L-lactide)	Blomeier <i>et al.</i> (161), 2006	Porous scaffolds fabricated by gas foaming/particulate leaching (diameter 5mm, height 5mm, pore-size 250-400 μ m)

Animal model	Number of transplanted islets	Observed time period	Achieved normoglycemia	Comments
Syngeneic transplantation in STZ induced diabetic male C57Bl/6 mice Dose: i.v. injection of 200mg/kg STZ	250, 500 IEQ	150 days	(for 500 IEQ) EFP islets only: 6 out of 6 (mean 19.5 days (7–74 days)) EFP construct – (fibrin-fibronectin-PDGF-BB gel): 9 out of 9 (mean 11 days (1–34 days)) EFP construct + (fibrin-fibronectin-PDGF-BB gel): 9 out of 9 (mean 11 days (1–43 days)) (for 250 IEQ) EFP islets only: 6 out of 7 (mean 48 days (16–56 days)) EFP construct – (fibrin-fibronectin-PDGF-BB gel): 8 out of 8 (mean 45 days (9–98 days)) EFP construct + (fibrin-fibronectin-PDGF-BB gel): 8 out of 8 (mean 19 days (8–25 days))	Addition of fibrin-fibronectin-PDGF-BB gel
Syngeneic transplantation in STZ induced diabetic C57Bl/6 mice Dose: i.p. injection of 200mg/kg STZ	450-500 islets	54 days	IM Construct –VEGF: 5 out of 8 (10.4 ± 2.1 days) IM Construct +VEGF: 8 out of 7 (13.3 ± 3.4 days)	Addition of VEGF
Syngeneic transplantation in STZ induced diabetic male C57Bl/6 or male FVB/N mice Dose: i.p. injection of 220mg/kg STZ	125, 175, 280 islets	100 days	(for 175 islets) Kidney capsule control: 7 out of 7 (2.3±1.3 days) IFP islets only: 8 out of 8 (11.5±5.1 days) IFP construct: 8 out of 8 (3.9±2.2 days) (for 125 islets) IFP islets only: 5 out of 8 (37.0±13.0 days) IFP construct: 8 out of 8 (20.0±7.0 days)	

Category	Transplantation site	Material	Study	Scaffold design
Solid scaffold	Intraperitoneally (omental pouch (OMP))	Ethisorb	Kin <i>et al.</i> (164), 2008	Ethisorb Dura Patch (composed of VICRYL and Poly-p-dioxanone)
			Berman <i>et al.</i> (165), 2009	Ethisorb Dura Patch (composed of VICRYL and Poly-p-dioxanone)
		poly(dimethylsiloxane)	Pedraza <i>et al.</i> (60), 2013	Porous scaffolds fabricated by solvent casting and particulate leaching (diameter 10mm, height 2 mm, pore-size 250-425µm)

Animal model	Number of transplanted islets	Observed time period	Achieved normoglycemia	Comments
Autologous transplantation in male beagle dogs	2233-5775 IEQ/kg	Variable (dependent on duration of insulin independence)	OMP islets only: 0 out of 2 OMP construct: 4 out of 4	Note: transplanted islet mass was variable
Syngeneic transplantation in STZ induced diabetic cynomolgus monkeys Dose: i.v. injection of 1250 mg/m ² STZ	4200-14544 IEQ/kg	Variable > 100 days	All animals required low dose of insulin. 4 out of 5 recipients experienced gradual decline in endogenous insulin requirement associated with increasing C-peptide levels	
Syngeneic transplantation in STZ induced diabetic male Lewis rats Dose: two i.v. injections (2-3 days apart) of 60mg/kg STZ	1800 IEQ	110/170 days	Kidney capsule control: 2 out of 2 (0 and 2 days) OMP islets only: 5 out of 6 (5±5.61 days) OMP construct: 5 out of 6 (1.8±1.3 days)	

1.7 REFERENCES

1. Economic costs of diabetes in the U.S. in 2012. (2013) *Diabetes Care* 36:1033–46.
2. IDF diabetes atlas sixth edition (2013) 1–160. Available at: http://www.idf.org/sites/default/files/EN_6E_Atlas_Full_0.pdf.
3. Narayan KMV, Boyle JP, Geiss LS, Saaddine JB, Thompson TJ (2006) Impact of recent increase in incidence on future diabetes burden: U.S., 2005-2050. *Diabetes Care* 29:2114–6.
4. American Diabetes Association (2013) Diagnosis and classification of diabetes mellitus. *Diabetes Care* 36 Suppl 1:S67–74.
5. van Belle T, Coppieters K, von Herrath MG (2011) Type 1 Diabetes: Etiology, Immunology, and Therapeutic Strategies. 79–118.
6. Redondo MJ et al. (2001) Heterogeneity of Type I diabetes: Analysis of monozygotic twins in Great Britain and the United States. *Diabetologia* 44:354–362.
7. Zimmet P, Alberti KGMM, Shaw J (2010) Global and societal implications of the diabetes epidemic. 414.
8. Chen L, Magliano DJ, Zimmet PZ (2012) The worldwide epidemiology of type 2 diabetes mellitus--present and future perspectives. *Nat Rev Endocrinol* 8:228–36.
9. Crowther CA et al. (2005) Effect of Treatment of Gestational Diabetes Mellitus on Pregnancy Outcomes Caroline. *N Engl J Med* 352:2477–2486.
10. Landon MB et al. (2009) A multicenter, randomized trial of treatment for mild gestational diabetes. *N Engl J Med* 361:1339–48.
11. Kitabchi AE, Umpierrez GE, Miles JM, Fisher JN (2009) Hyperglycemic crises in adult patients with diabetes. *Diabetes Care* 32:1335–43.
12. Rask-Madsen C, King GL (2013) Vascular complications of diabetes: mechanisms of injury and protective factors. *Cell Metab* 17:20–33.
13. Forbes JM, Cooper ME (2013) Mechanisms of diabetic complications. *Physiol Rev* 93:137–88.
14. Nouwen A et al. (2011) Prevalence of depression in individuals with impaired glucose metabolism or undiagnosed diabetes: a systematic review and meta-analysis of the European Depression in Diabetes (EDID) Research Consortium. *Diabetes Care* 34:752–62.
15. McCrimmon RJ, Ryan CM, Frier BM (2012) Diabetes and cognitive dysfunction. *Lancet* 379:2291–9.
16. Jackson G (2004) Sexual dysfunction and diabetes. *Int J Clin Pract* 58:358–62.
17. David M. Nathan, MD, Bernard Zinman, MD, Patricia A. Cleary, MS, Jye-Yu C. Backlund, MS, Saul Genuth, MD, Rachel Miller, MS, Trevor J. Orchard, MD and DC and CT of DI and C (DCCT/ ERG (2009) Modern-Day Clinical Course of Type 1 Diabetes Mellitus After 30 Years' Duration: The Diabetes Control and Complications Trial/Epidemiology of Diabetes Interventions and Complications and Pittsburgh Epidemiology of Diabetes Complications Experience (1983-2. *Arch Intern Med* 169:1307–1316.
18. Cryer PE (2002) Hypoglycaemia: the limiting factor in the glycaemic management of Type I and Type II diabetes. *Diabetologia* 45:937–48.
19. Williams P.W. (1894) Notes on diabetes treated with extract and by grafts of sheep's pancreas. *Br Med J* 2:1303–1304.
20. Lillehei RC et al. (1969) Transplantation of the intestine and pancreas. *Transplant Proc* 1:230–238.
21. Ballinger WF, Lacy PE (1972) Transplantation of intact pancreatic islets in rats. *Surgery* 72:175–186.
22. Scharp DW et al. (1990) Rapid Publications Insulin Independence After Islet Transplantation Into Type I Diabetic Patient. 39:515–518.
23. Shapiro, A.M.J., Lakey, J.R.T., Ryan, E.A, Korbitt, G.S., Toth, E., Warnock, G.L., Kneteman, N.M., Rajotte RV (2000) Islet transplantation in seven patients with type 1 diabetes mellitus using a glucocorticoid-free immunosuppressive regimen. *N Engl J Med* 343:230–238.

24. The CITR Coordinating Center Investigators (2011) The Collaborative Islet Transplant Registry (CITR) 2011 Seventh Annual Report. *US Dep Heal Hum Serv Bethesda, MA, USA*.
25. Barton FB et al. (2012) Improvement in outcomes of clinical islet transplantation: 1999-2010. *Diabetes Care* 35:1436-45.
26. McCall M, Shapiro a MJ (2012) Update on islet transplantation. *Cold Spring Harb Perspect Med* 2:a007823.
27. Naziruddin B et al. (2012) HLA class I sensitization in islet transplant recipients: report from the Collaborative Islet Transplant Registry. *Cell Transplant* 21:901-8.
28. Ryan EA et al. (2005) Five-year follow-up after clinical islet transplantation. *Diabetes* 54:2060-2069.
29. Al-Adra DP et al. (2014) Single-Donor Islet Transplantation and Long-term Insulin Independence in Select Patients With Type 1 Diabetes Mellitus. *Transplantation* 00:1-6.
30. Vantuyghem M-C et al. (2014) Treating diabetes with islet transplantation: Lessons from the past decade in Lille. *Diabetes Metab* 40:108-119.
31. Owen RJT et al. (2003) Vascular and Interventional Radiology Radiology Pancreatic Islet Cell Transplantation in Type 1 Diabetes Mellitus : Radiologic. 1973:165-170.
32. Maffi P et al. (2005) Minimal focal steatosis of liver after islet transplantation in humans: a long-term study. *Cell Transplant* 14:727-733.
33. Kawahara T et al. (2011) Portal vein thrombosis is a potentially preventable complication in clinical islet transplantation. *Am J Transplant* 11:2700-7.
34. Korsgren O et al. (2008) Optimising islet engraftment is critical for successful clinical islet transplantation. *Diabetologia* 51:227-232.
35. Pileggi A et al. (2009) Impact of pancreatic cold preservation on rat islet recovery and function. *Transplantation* 87:1442-50.
36. D'Aleo V et al. (2010) Functional and survival analysis of isolated human islets. *Transplant Proc* 42:2250-2251.
37. Abdelli S et al. During Human Islet Preparation and Following Acute Cytokine Exposure. 2815-2823.
38. Moberg L et al. (2002) Production of tissue factor by pancreatic islet cells as a trigger of detrimental thrombotic reactions in clinical islet transplantation. 360:11-13.
39. Johansson H et al. (2005) Tissue factor produced by the endocrine cells of the islets of Langerhans is associated with a negative outcome of clinical islet transplantation. *Diabetes* 54:1755-62.
40. Bennet W et al. (1999) Incompatibility between human blood and isolated islets of Langerhans: a finding with implications for clinical intraportal islet transplantation? *Diabetes* 48:1907-1914.
41. Citro A, Cantarelli E, Piemonti L (2013) Anti-inflammatory strategies to enhance islet engraftment and survival. *Curr Diab Rep* 13:733-44.
42. Eich, Torsten, Eriksson O (2007) Visualization of Early Engraftment in Clinical Islet Transplantation by Positron-Emission Tomography. *N Engl J Med* 356:2754-2755.
43. Scott WE et al. (2010) Pancreas oxygen persufflation increases ATP levels as shown by nuclear magnetic resonance. *Transplant Proc* 42:2011-2015.
44. Brandhorst H et al. (2010) A new oxygen carrier for improved long-term storage of human pancreata before islet isolation. *Transplantation* 89:155-160.
45. Johansson H et al. (2006) Low molecular weight dextran sulfate: a strong candidate drug to block IBMIR in clinical islet transplantation. *Am J Transplant* 6:305-12.
46. Schmidt P, Magnusson C, Lundgren T, Korsgren O, Nilsson B (2008) Low molecular weight dextran sulfate is well tolerated in humans and increases endogenous expression of islet protective hepatocyte growth factor. *Transplantation* 86:1523-30.

47. Cabric S et al. (2007) Islet surface heparinization prevents the instant blood-mediated inflammatory reaction in islet transplantation. *Diabetes* 56:2008–15.
48. Teramura Y, Iwata H (2009) Surface Modification of Islets With PEG-Lipid for Improvement of Graft Survival in Intraportal Transplantation. *Transplantation* 88.
49. Teramura Y, Oommen OP, Olerud J, Hilborn J, Nilsson B (2013) Microencapsulation of cells, including islets, within stable ultra-thin membranes of maleimide-conjugated PEG-lipid with multifunctional crosslinkers. *Biomaterials* 34:2683–93.
50. Davalli a M et al. (2000) Insights from a successful case of intrahepatic islet transplantation into a type 1 diabetic patient. *J Clin Endocrinol Metab* 85:3847–52.
51. Molnár Cet al. (2013) Islet engraftment and revascularization in clinical and experimental transplantation. *Cell Transplant* 22:243–51.
52. Carlsson P, Palm F, Andersson A, Liss P (2001) Markedly Decreased Oxygen Tension in Transplanted Site sure of oxygen (P O 2) levels of these transplanted islets. 50.
53. Sezai S et al. (1993) content and extraction in liver cirrhosis. 31–35.
54. Moritz W et al. (2002) Apoptosis in hypoxic human pancreatic islets correlates with HIF-1 α expression. *FASEB J* 16:745–747.
55. Giuliani M et al. (2005) Central necrosis in isolated hypoxic human pancreatic islets: evidence for postisolation ischemia. *Cell Transplant* 14:67–76.
56. Cantley J, Grey ST, Maxwell PH, Withers DJ (2010) The hypoxia response pathway and β -cell function. 12:159–167.
57. Dionne KE, Colton CK, Yarmush ML (1993) Effect of hypoxia on insulin secretion by isolated rat and canine islets of Langerhans. *Diabetes* 42:12–21.
58. Seifu DG, Isimjan TT, Mequanint K (2011) Tissue engineering scaffolds containing embedded fluorinated-zeolite oxygen vectors. *Acta Biomater* 7:3670–8.
59. Camci-Unal G, Alemdar N, Annabi N, Khademhosseini A (2013) Oxygen Releasing Biomaterials for Tissue Engineering. *Polym Int* 62:843–848.
60. Pedraza E et al. (2013) Macroporous Three-Dimensional PDMS Scaffolds for Extrahepatic Islet Transplantation. *Cell Transplant* 22:1123–1135.
61. Khattak SF, Chin K, Bhatia SR, Roberts SC (2007) Enhancing oxygen tension and cellular function in alginate cell encapsulation devices through the use of perfluorocarbons. *Biotechnol Bioeng* 96:156–66.
62. Schaschkow a. et al. (2015) Impact of an autologous oxygenating matrix culture system on rat islet transplantation outcome. *Biomaterials* 52:180–188.
63. Stendahl JC, Wang L, Chow LW, Kaufman DB, Stupp I (2008) Growth factor delivery from self-assembling nanofibers to facilitate islet transplantation. *Transplantation* 86:478–481.
64. Chow LW, Wang L, Kaufman DB, Stupp SI (2010) Self-assembling nanostructures to deliver angiogenic factors to pancreatic islets. *Biomaterials* 31:6154–61.
65. Brady A-C et al. (2013) Proangiogenic Hydrogels Within Macroporous Scaffolds Enhance Islet Engraftment in an Extrahepatic Site. 19:2544–2552.
66. Witkowski P et al. (2009) Islet grafting and imaging in a bioengineered intramuscular space. *Transplantation* 88:1065–74.
67. Johansson U et al. (2008) Formation of composite endothelial cell-mesenchymal stem cell islets: a novel approach to promote islet revascularization. *Diabetes* 57:2393–401.
68. Li Y et al. (2013) Combined Strategy of Endothelial Cells Coating, Sertoli Cells Coculture and Infusion Improves Vascularization and Rejection Protection of Islet Graft. *PLoS One* 8.

69. Figliuzzi M et al. (2009) Bone marrow-derived mesenchymal stem cells improve islet graft function in diabetic rats. *Transplant Proc* 41:1797–800.
70. Ito T et al. (2010) Mesenchymal Stem Cell and Islet Co-Transplantation Promotes Graft Revascularization and Function. *Transplantation* 89:1438–1445.
71. Sakata N, Chan NK, Chrisler J, Obenaus A, Hathout E (2010) Bone marrow cell cotransplantation with islets improves their vascularization and function. *Transplantation* 89:686–93.
72. Rackham CL et al. (2011) Co-transplantation of mesenchymal stem cells maintains islet organisation and morphology in mice. *Diabetologia* 54:1127–1135.
73. Cavallari G et al. (2012) Mesenchymal Stem Cells and Islet Transplantation in Diabetic Rats: Improved Islet Graft Revascularization and Function By Human Adipose Tissue-Derived Stem Cells Preconditioned With Natural Molecules. *Cell Transplant* 21:2771–2781.
74. Oh BJ et al. (2013) Co-transplantation of bone marrow-derived endothelial progenitor cells improves revascularization and organization in islet grafts. *Am J Transplant* 13:1429–40.
75. Quaranta P et al. (2014) Co-transplantation of endothelial progenitor cells and pancreatic islets to induce long-lasting normoglycemia in streptozotocin-treated diabetic rats. *PLoS One* 9:e94783.
76. Kang S et al. (2012) Endothelial progenitor cell cotransplantation enhances islet engraftment by rapid revascularization. *Diabetes* 61:866–76.
77. Abreu JRF, Roep BO (2013) Immune monitoring of islet and pancreas transplant recipients. *Curr Diab Rep* 13:704–12.
78. Shapiro a MJ (2011) State of the art of clinical islet transplantation and novel protocols of immunosuppression. *Curr Diab Rep* 11:345–54.
79. Desai NM et al. (2003) Elevated portal vein drug levels of sirolimus and tacrolimus in islet transplant recipients: local immunosuppression or islet toxicity? *Transplantation* 76:1623–5.
80. Gala-Lopez B, Pepper AR, Shapiro a MJ (2013) Biologic agents in islet transplantation. *Curr Diab Rep* 13:713–22.
81. Guo Z et al. (2003) A substantial level of donor hematopoietic chimerism is required to protect donor-specific islet grafts in diabetic NOD mice. *Transplantation* 75:909–915.
82. Fiorina P et al. (2011) Targeting the CXCR4-CXCL12 axis mobilizes autologous hematopoietic stem cells and prolongs islet allograft survival via programmed death ligand 1. *J Immunol* 186:121–131.
83. O’Sullivan ES, Vegas A, Anderson DG, Weir GC (2011) Islets transplanted in immunoisolation devices: a review of the progress and the challenges that remain. *Endocr Rev* 32:827–44.
84. De Vos P, Lazarjani HA, Poncelet D, Faas MM (2014) Polymers in cell encapsulation from an enveloped cell perspective. *Adv Drug Deliv Rev* 67-68:15–34.
85. Tomei A a et al. (2014) Device design and materials optimization of conformal coating for islets of Langerhans. *Proc Natl Acad Sci U S A* 111:10514–9.
86. Tezza S et al. (2014) Novel immunological strategies for islet transplantation. *Pharmacol Res*:1–7.
87. Murphy ED (2014) Insulin : Appropriate Placement in the Portal Vein. *Advances in Diabetes and Metabolism* 2:1–3.
88. Diem P, Abid M, Redmon JB, Sutherland DER, Robertson RP (1990) Systemic Venous Drainage of Pancreas Al log rafts as Independent Cause of Hyperinsulinemia in Type I Diabetic Recipients. 39:534–540.
89. Guan J et al. (1997) Insulin resistance prevented by portal delivery of insulin in rats with renal subcapsular islet grafts. *Diabetes* 46:372–8.
90. Stagner JI, Rilo HL, White KK (2007) The pancreas as an islet transplantation site. Confirmation in a syngeneic rodent and canine autotransplant model. *JOP* 8:628–36.

91. Lau J, Carlsson C, Nyqvist D, Ko M, Berggren P (2007) Implantation Site–Dependent Dysfunction of Transplanted Pancreatic Islets.
92. Kaufman DB, Morel P, Field JM, Munn SR, Sutherland DER (1990) Purified canine islet autograft. *Transplantation*:385–391.
93. White S a et al. (1999) Splenic infarction after total pancreatectomy and autologous islet transplantation into the spleen. *Pancreas* 18:419–21.
94. Ao Z, Matayoshi K, Lakey JRT, Rajotte R V, Warnock GL (1993) Survival and function of purified islets in the omental pouch site of outbred dogs. *Transplantation* 56:524–529.
95. Gustavson SM et al. (2005) Islet auto-transplantation into an omental or splenic site results in a normal beta cell but abnormal alpha cell response to mild non-insulin-induced hypoglycemia. *Am J Transplant* 5:2368–77.
96. Finch DRA, Wise PH, Morris PJ (1977) Successful Intra-Splenic Transplantation of Syngeneic and Aliogeneic Isolated Pancreatic Islets. *Diabetologia* 199:195–199.
97. Korsgren O, Jansson L, Andersson A, Sundler F (1993) Reinnervation of transplanted pancreatic islets. *Transplantation*:138–143.
98. Van Suylichem PT., Strubbe JH, Houwing H, Wolters GHJ, van Schilfgaarde R (1994) Rat islet isograft function. *Transplantation* 57:1010–1017.
99. Gray DW (1990) Islet isolation and transplantation techniques in the primate. *Surg Gynecol Obstet* 170:225–232.
100. Yasunami Y, Lacy PE, Finke EH (1983) A new site for islet transplantation- a peritoneal- omental pouch. *Transplantation* 36:181–182.
101. Ferguson J, Scothorne RJ, Johnston ID (1973) Proceedings: the survival of transplanted isolated pancreatic islets in the omentum and testis. *Br J Surg* 60:907.
102. Kin T, Korbitt GS, Rajotte R V (2003) Survival and metabolic function of syngeneic rat islet grafts transplanted in the omental pouch. *Am J Transplant* 3:281–5.
103. Echeverri GJ et al. (2009) Endoscopic gastric submucosal transplantation of islets (ENDO-STI): technique and initial results in diabetic pigs. *Am J Transplant* 9:2485–96.
104. Fujita M et al. (2013) Technique of endoscopic biopsy of islet allografts transplanted into the gastric submucosal space in pigs. *Cell Transplant* 22:2335–44.
105. Wszola M et al. (2009) TransEndoscopic Gastric SubMucosa Islet Transplantation (eGSM-ITx) in pigs with streptozotocine induced diabetes – technical aspects of the procedure –preliminary report. *Ann Transplant* 14:45–50.
106. Sageshima J et al. (2001) Small bowel subserosal space as a site for islet transplantation and local drug delivery. *Transplant Proc* 33:1710.
107. Tchervenivanov N, Yuan S, Lipsett M, Agapitos D, Rosenberg L (2002) Morphological and functional studies on submucosal islet transplants in normal and diabetic hamsters. *Cell Transplant* 11:529–37.
108. Caiazzo R et al. (2007) Evaluation of alternative sites for islet transplantation in the minipig: interest and limits of the gastric submucosa. *Transplant Proc* 39:2620–3.
109. Sakata N et al. (2010) ITSC08 Efficacy Comparison between Intraportal and Subcapsular Islet Transplants in a Murine Diabetic Model. *Transplant Proc* 41:346–349.
110. Jindal RM, Sidner RA, Mcdaniel HB, Johnson MS, Fineberg SE (1998) Intraportal vs kidney subcapsular site for human pancreatic islet transplantation. *Transplant Proc* 1345:398–399.
111. Kim A, Miller K, Jo J, Kilimnik G, Wojcik P (2009) Islet architecture: A comparative study. *Islets* 1:129–136.
112. Yin D et al. (2006) Liver ischemia contributes to early islet failure following intraportal transplantation: benefits of liver ischemic-preconditioning. *Am J Transplant* 6:60–8.

113. Brom M et al. (2014) Non-invasive quantification of the beta cell mass by SPECT with (111)In-labelled exendin. *Diabetologia* 57: 950-959.
114. Pattou F, Kerr-Conte J, Wild D (2010) GLP-1-receptor scanning for imaging of human beta cells transplanted in muscle. *N Engl J Med* 363:1289–90.
115. Lund T, Korsgren O, Aursnes I a, Scholz H, Foss A (2010) Sustained reversal of diabetes following islet transplantation to striated musculature in the rat. *J Surg Res* 160:145–54.
116. Christoffersson G et al. (2010) Clinical and experimental pancreatic islet transplantation to striated muscle: establishment of a vascular system similar to that in native islets. *Diabetes* 59:2569–78.
117. Svensson J, Lau J, Sandberg M, Carlsson P-O (2011) High vascular density and oxygenation of pancreatic islets transplanted in clusters into striated muscle. *Cell Transplant* 20:783–8.
118. Rafael E et al. (2008) Intramuscular autotransplantation of pancreatic islets in a 7-year-old child: a 2-year follow-up. *Am J Transpl* 8:458–462.
119. Stegall MD (1997) Monitoring human islet allografts using a forearm biopsy site. *Ann Transplant* 2:8–11.
120. Chen X et al. (2007) The epididymal fat pad as a transplant site for minimal islet mass. *Transplantation* 84:122–5.
121. Outzen HC, Leiter EH (1981) Transplantation of pancreatic islets into cleared mammary fat pads. *Transplantation* 32:101–105.
122. Chubb C, Desjardins C (1982) Vasculature of the mouse, rat, and rabbit testis-epididymis. *Am J Anat* 165:357–72.
123. Scharp DW et al. (1994) Protection of encapsulated human islets implanted without immunosuppression in patients with type I or type II diabetes and in nondiabetic control subjects. *Diabetes* 43:1167–70.
124. Fumimoto Y et al. (2009) Creation of a rich subcutaneous vascular network with implanted adipose tissue-derived stromal cells and adipose tissue enhances subcutaneous grafting of islets in diabetic mice. *Tissue Eng Part C Methods* 15:437–44.
125. Kim J-S et al. (2012) In situ application of hydrogel-type fibrin-islet composite optimized for rapid glycemic control by subcutaneous xenogeneic porcine islet transplantation. *J Control Release* 162:382–90.
126. Pepper AR et al. (2015) A prevascularized subcutaneous device-less site for islet and cellular transplantation. 33.
127. Posselt AM et al. (1990) Induction of donor-specific unresponsiveness by intrathymic islet transplantation. *Science* 249:1293–5.
128. Gerling IC, Serreze D V, Christianson SW, Leiter EH (1992) Intrathymic islet cell transplantation reduces beta-cell autoimmunity and prevents diabetes in NOD/Lt mice. *Diabetes* 41:1672–6.
129. Rayat GR, Korbitt GS, Elliott JF, Rajotte R V (1997) Survival and function of syngeneic rat islet grafts placed within the thymus versus under the kidney capsule. *Cell Transplant* 6:597–602.
130. Watt PC et al. (1994) Successful engraftment of autologous and allogeneic islets into the porcine thymus. *J Surg Res* 56:367–371.
131. Cantarelli E et al. (2009) Bone marrow as an alternative site for islet transplantation. *Blood* 114:4566–74.
132. Maffi P et al. (2013) Autologous pancreatic islet transplantation in human bone marrow. *Diabetes* 62:3523–31.
133. Bryers JD, Giachelli CM, Ratner BD (2013) Engineering Biomaterials to Integrate and Heal: The Biocompatibility Paradigm Shifts. 109:1898–1911.
134. Sridharan R, Cameron AR, Kelly DJ, Kearney CJ, O'Brien FJ (2015) Biomaterial based modulation of macrophage polarization: a review and suggested design principles. *Mater Today* 00.

135. Robles L, Storrs R, Lamb M, Alexander M, Lakey JR (2013) Current Status of Islet Encapsulation. *Cell Transplant* 23:1321–1348.
136. V eriter S, Gianello P, Dufrane D (2013) Bioengineered sites for islet cell transplantation. *Curr Diab Rep* 13:745–55.
137. Lee KYMDJ (2001) Hydrogels for Tissue Engineering Applications. *Chem Rev* 101:1869–1880.
138. Hiscox AM, Stone AL, Limesand S, Hoying JB, Williams SK (2008) An islet-stabilizing implant constructed using a preformed vasculature. *Tissue Eng Part A* 14:433–440.
139. Robert B. Vernon, Anton Preisinger, Michel D. Gooden, Leonard A. D’Amico, Betty B. Yue, Paul L. Bollyky, Christian S. Kuhr, Thomas R. Hefty, Gerald T. Nepom and J. Gebe A (2012) Reversal of Diabetes in Mice With a Bioengineered Islet Implant Incorporating a Type I Collagen Hydrogel and Sustained Release of Vascular Endothelial Growth Factor. *Cell Transplant* 21:1–21.
140. Perez-Basterrechea M et al. (2009) Plasma-fibroblast gel as scaffold for islet transplantation. *Tissue Eng Part A* 15:569–577.
141. Andrades P et al. (2007) Subcutaneous Pancreatic Islet Transplantation Using Fibrin Glue as a Carrier. *Transplant Proc* 39:191–192.
142. Bhang SH et al. (2013) Mutual effect of subcutaneously transplanted human adipose-derived stem cells and pancreatic islets within fibrin gel. *Biomaterials* 34:7247–56.
143. Davis NE et al. (2012) Enhanced function of pancreatic islets co-encapsulated with ECM proteins and mesenchymal stromal cells in a silk hydrogel. *Biomaterials* 33:6691–7.
144. De Vos P, Faas MM, Strand B, Calafiore R (2006) Alginate-based microcapsules for immunoisolation of pancreatic islets. *Biomaterials* 27:5603–5617.
145. Cruise GM, Hegre OD, Scharp DS, Hubbell J a. (1998) A sensitivity study of the key parameters in the interfacial photopolymerization of poly(ethylene glycol) diacrylate upon porcine islets. *Biotechnol Bioeng* 57:655–665.
146. Weber LM, He J, Bradley B, Haskins K, Anseth KS (2006) PEG-based hydrogels as an in vitro encapsulation platform for testing controlled ??-cell microenvironments. *Acta Biomater* 2:1–8.
147. Weber LM, Hayda KN, Haskins K, Anseth KS (2007) The effects of cell-matrix interactions on encapsulated ??-cell function within hydrogels functionalized with matrix-derived adhesive peptides. *Biomaterials* 28:3004–3011.
148. Weber LM, Hayda KN, Anseth KS (2008) Cell-matrix interactions improve beta-cell survival and insulin secretion in three-dimensional culture. *Tissue Eng Part A* 14:1959–1968.
149. Weber LM, Anseth KS (2008) Hydrogel encapsulation environments functionalized with extracellular matrix interactions increase islet insulin secretion. *Matrix Biol* 27:667–673.
150. Weber LM, Lopez CG, Anseth KS (2009) The effects of PEG hydrogel crosslinking density on protein diffusion and encapsulated islet survival and function. *J Biomed Mater Res* 90:720–729.
151. Patterson J, Hubbell J a. (2010) Enhanced proteolytic degradation of molecularly engineered PEG hydrogels in response to MMP-1 and MMP-2. *Biomaterials* 31:7836–7845.
152. Phelps E a., Templeman KL, Thul e PM, Garc a AJ (2013) Engineered VEGF-releasing PEG–MAL hydrogel for pancreatic islet vascularization. *Drug Deliv Transl Res*:125–136.
153. Phelps E a., Headen DM, Taylor WR, Thul e PM, Garc a AJ (2013) Vasculogenic bio-synthetic hydrogel for enhancement of pancreatic islet engraftment and function in type 1 diabetes. *Biomaterials* 34:4602–4611.
154. Brubaker CE, Kissler H, Wang L-J, Kaufman DB, Messersmith PB (2010) Biological performance of mussel-inspired adhesive in extrahepatic islet transplantation. *Biomaterials* 31:420–7.

155. Dufour JM et al. (2005) Development of an ectopic site for islet transplantation, using biodegradable scaffolds. *Tissue Eng* 11:1323–1331.
156. Salvay DM et al. (2009) Extracellular Matrix Protein-Coated Scaffolds Promote the Reversal of Diabetes After Extrahepatic Islet Transplantation. *Transplantation* 85:1456–1464.
157. Kheradmand T et al. (2011) Permanent protection of PLG scaffold transplanted allogeneic islet grafts in diabetic mice treated with ECDI-fixed donor splenocyte infusions. *Biomaterials* 32:4517–24.
158. Gibly RF et al. (2011) Extrahepatic islet transplantation with microporous polymer scaffolds in syngeneic mouse and allogeneic porcine models. *Biomaterials* 32:9677–84.
159. Gibly RF, Zhang X, Lowe WL, Shea LD (2013) Porous scaffolds support extrahepatic human islet transplantation, engraftment, and function in mice. *Cell Transplant* 22:811–9.
160. Yap WT et al. (2013) Collagen IV-Modified Scaffolds Improve Islet Survival and Function and Reduce Time to Euglycemia. 19.
161. Blomeier H et al. (2006) Polymer scaffolds as synthetic microenvironments for extrahepatic islet transplantation. *Transplantation* 82:452–459.
162. Hlavaty K a et al. (2014) Enhancing human islet transplantation by localized release of trophic factors from PLG scaffolds. *Am J Transplant* 14:1523–32.
163. Pedraza E, Coronel MM, Fraker C a, Ricordi C, Stabler CL (2012) Preventing hypoxia-induced cell death in beta cells and islets via hydrolytically activated, oxygen-generating biomaterials. *Proc Natl Acad Sci U S A* 109:4245–50.
164. Kin T et al. (2008) The use of an approved biodegradable polymer scaffold as a solid support system for improvement of islet engraftment. *Artif Organs* 32:990–993.
165. Berman DM et al. (2009) Long-term survival of nonhuman primate islets implanted in an omental pouch on a biodegradable scaffold. *Am J Transpl* 9:91–104.
166. Sharkawy a a, Klitzman B, Truskey G a, Reichert WM (1998) Engineering the tissue which encapsulates subcutaneous implants. II. Plasma-tissue exchange properties. *J Biomed Mater Res* 40:586–97.
167. Madden LR et al. (2010) Proangiogenic scaffolds as functional templates for cardiac tissue engineering. *Proc Natl Acad Sci U S A* 107:15211–6.
168. Williams, S.J., Wang, Q., MacGregor, R.R., Siahaan, T.J., Stehno-Bittel, L, Berkland C (2012) Adhesion of Pancreatic Beta Cells to Biopolymer Films. *Biopolymers* 91:676–685.
169. Mei, Y., Hollister-Lock, J., Bogatyrev, S.R., Cho, S., Weir, G.C., Langer, R., Anderson DG (2012) A High Throughput Microarray System of Polymer Surfaces for the Manipulation of Primary Pancreatic Islet Cells. *Biomaterials* 31:8989–8995.
170. Salvay DM et al. (2008) Extracellular matrix protein-coated scaffolds promote the reversal of diabetes after extrahepatic islet transplantation. *Transplantation* 85:1456–1464.
171. Juang JH, Bonner-Weir S, Ogawa Y, Vacanti JP, Weir GC (1996) Outcome of subcutaneous islet transplantation improved by polymer device. *Transplantation* 61:1557–1561.
172. Pileggi A et al. (2006) Reversal of diabetes by pancreatic islet transplantation into a subcutaneous, neovascularized device. *Transplantation* 81:1318–24.
173. Kaufman-Francis K, Koffler J, Weinberg N, Dor Y, Levenberg S (2012) Engineered vascular beds provide key signals to pancreatic hormone-producing cells. *PLoS One* 7:e40741.
174. Sharkawy a a, Klitzman B, Truskey G a, Reichert WM (1997) Engineering the tissue which encapsulates subcutaneous implants. I. Diffusion properties. *J Biomed Mater Res* 37:401–12.
175. Sharkawy a a, Klitzman B, Truskey G a, Reichert WM (1998) Engineering the tissue which encapsulates subcutaneous implants. III. Effective tissue response times. *J Biomed Mater Res* 40:598–605.

176. Williams SK, Berman SS, Kleinert LB (1997) Differential healing and neovascularization of ePTFE implants in subcutaneous versus adipose tissue. *J Biomed Mater Res* 35:473–81.
177. Brauker JH et al. (1995) Neovascularization of synthetic membranes directed by membrane microarchitecture. *J Biomed Mater Res* 29:1517–24.
178. Salzman DL, Kleinert LB, Berman SS, Williams SK (1997) The effects of porosity on endothelialization of ePTFE implanted in subcutaneous and adipose tissue. *J Biomed Mater Res* 34:463–76.
179. Saino E et al. (2011) Effect of electrospun fiber diameter and alignment on macrophage activation and secretion of proinflammatory cytokines and chemokines. *Biomacromolecules* 12:1900–1911.
180. Solari MG et al. (2009) Marginal mass islet transplantation with autologous mesenchymal stem cells promotes long-term islet allograft survival and sustained normoglycemia. *J Autoimmun* 32:116–124.
181. Wu H, Wen D, Mahato RI (2013) Third-party Mesenchymal Stem Cells Improved Human Islet Transplantation in a Humanized Diabetic Mouse Model. *Mol Ther* 21:1778–1786.
182. Penko D et al. (2015) Endothelial progenitor cells enhance islet engraftment, influence beta cell function and modulate islet connexin 36 expression. *Cell Transplant* 61:1–29.
183. Jung HS et al. (2014) The potential of endothelial colony-forming cells to improve early graft loss after intraportal islet transplantation. *Cell Transplant* 23:273–283.
184. Fotino N, Fotino C, Pileggi A (2015) Re-engineering islet cell transplantation. *Pharmacol Res*:1–10.

Chapter 2

Microwell scaffolds for the extrahepatic transplantation of islets of Langerhans



*Mijke Buitinga¹, Roman Truckenmüller², Marten A. Engelse³,
Lorenzo Moroni², Hetty W.M. ten Hoopen⁴, Clemens A. van Blitterswijk²,
Eelco J.P. de Koning^{3,5,6}, Aart A. van Apeldoorn¹, Marcel Karperien¹*

¹ *Department of Developmental BioEngineering, University of Twente, Enschede, The Netherlands*

² *Department of Tissue Regeneration, University of Twente, Enschede, The Netherlands*

³ *Department of Nephrology, Leiden University Medical Center, Leiden, The Netherlands*

⁴ *Department of BioMedical Chemistry, University of Twente, Enschede, The Netherlands*

⁵ *Department of Endocrinology, Leiden University Medical Center, Leiden, The Netherlands*

⁶ *Hubrecht Institute, Utrecht, The Netherlands*

ABSTRACT

Allogeneic islet transplantation into the liver has the potential to restore normoglycemia in patients with type 1 diabetes. However, the suboptimal microenvironment for islets in the liver is likely to be involved in the progressive islet dysfunction that is often observed post-transplantation. This study validates a novel microwell scaffold platform to be used for the extrahepatic transplantation of islet of Langerhans. Scaffolds were fabricated from either a thin polymer film or an electrospun mesh of poly(ethylene oxide terephthalate)-poly(butylene terephthalate) (PEOT/PBT) block copolymer (composition: 4000PEOT30PBT70) and were imprinted with microwells, $\sim 400\ \mu\text{m}$ in diameter and $\sim 350\ \mu\text{m}$ in depth. The water contact angle and water uptake were $39 \pm 2^\circ$ and $52.1 \pm 4.0\ \text{wt}\%$, respectively. The glucose flux through electrospun scaffolds was three times higher than for thin film scaffolds, indicating enhanced nutrient diffusion. Human islets cultured in microwell scaffolds for seven days showed insulin release and insulin content comparable to those of free-floating control islets. Islet morphology and insulin and glucagon expression were maintained during culture in the microwell scaffolds. Our results indicate that the microwell scaffold platform prevents islet aggregation by confinement of individual islets in separate microwells, preserves the islet's native rounded morphology, and provides a protective environment without impairing islet functionality, making it a promising platform for use in extrahepatic islet transplantation.

INTRODUCTION

Type 1 diabetes is characterized by the autoimmune-mediated destruction of insulin producing β -cells, resulting in absolute insulin deficiency. It is estimated that almost 100,000 children under 15 years of age develop this type of diabetes annually worldwide (1). Although intensive glucose monitoring combined with exogenous insulin administration can effectively control blood glucose levels, long-term micro- and macrovascular complications, such as nephropathy, retinopathy, neuropathy, and accelerated atherosclerosis, affect many patients (2).

During the last decade, allogeneic islet transplantation in the liver via the infusion of islets into the portal vein has been explored as a potential therapy for patients with type 1 diabetes. Although clinical results for islet transplantation are promising, especially with regard to reducing or eliminating hypoglycemic episodes (3–5), widespread application is hindered by the necessity of immunosuppressive agents and by a lack of donor organs. Typically, pancreata from at least two donors are required to achieve normoglycemia in a single patient and insulin independence lasts for only a few years, due to progressive islet loss in the post-transplantation period (3, 4, 6). It has been estimated that the β -cell volume in islet recipients is only 20–40% that of a healthy person, even when islets are obtained from two to four donors (7). The islet loss is likely related to the consequences of their injection directly into the portal vein, where they are exposed to several stress factors such as high levels of immunosuppressive drugs, the instant blood-mediated inflammatory reaction (IBMIR), hyperglycemia, and low oxygen tension (7, 8).

These significant disadvantages surrounding intraportal islet transplantation have stimulated the search for extrahepatic, extravascular transplantation sites (8, 9), such as the omental pouch (9), muscle fibers (10), and bioartificial transplantation sites using biomaterials. The advantage of the latter is that the microenvironment can be tailored in order to provide optimal spatial and functional support for the islets, which could ultimately lead to enhanced survival. It has been shown that the efficacy of islet transplantation into adipose tissue can be improved using polymer scaffolds (11, 12). Furthermore, polymer scaffolds immobilize the islets permitting easy transplantation, monitoring of the islet graft after transplantation, and explantation in the case of complications or graft failure. Various scaffold designs, from microporous scaffolds (11–18) to hydrogel-based scaffolds (19–21), have been assessed both *in vitro* (16, 20) and *in vivo* (11–15, 17–19, 21) for extrahepatic islet transplantation. However, there remain limitations regarding suitability due to pore geometry and interconnectivity, diffusion rate, stability, and islet fusion.

An interesting class of biocompatible biomaterials for islet transplantation are the poly(ethylene oxide terephthalate) and poly(butylenes terephthalate) (PEOT/PBT) block copolymers. The advantage of these copolymers is that their physical properties and degradation behavior can be tailored by changing the copolymer composition (22–27). Different compositions

of these copolymers have been used for *in vivo* skin, bone, and cartilage regeneration and are clinically used as cement stoppers, bone fillers, (28) and as dermal substitutes (29).

The aim of this study is to develop a novel non cell-adhesive, PEOT/PBT microwell scaffold platform to be used for extrahepatic islet transplantation. The advantages of the proposed microwell platform over previously mentioned scaffold designs are that it (1) prevents islet attachment, spreading, and aggregation by the confinement of individual islets in separate microwells preserving the rounded islet morphology; (2) is mechanically stable to protect against physical stresses; and (3) has an open structure permitting fast vascular ingrowth. Polymer thin films and porous meshes, prepared by solvent casting and electrospinning, respectively, were used to fabricate microwell scaffolds by micro back molding. Scaffolds were characterized for their wettability, water uptake, nutrient diffusion, and cytotoxicity. Subsequent *in vitro* experiments demonstrated that human islets cultured in the microwell scaffolds retained their native morphology and their insulin secretion was comparable to that of free-floating control islets indicating that this novel scaffold platform does not hamper islet functionality. Our data therefore indicate that the PEOT/PBT microwell scaffold is a potential carrier for extrahepatic islet transplantation.

MATERIALS AND METHODS

PEOT/PBT thin film fabrication

The chemical composition of PEOT/PBT polymer is indicated as aPEOTbPBTC, in which 'a' is the molecular weight of the starting poly(ethylene glycol) PEG segments used in the polymerization process, while 'b' and 'c' refer to the weight percentage of PEOT and PBT blocks, respectively. The composition 4000PEOT30PBT70 was selected for its slow degradation rate and its limited cell-adhesive properties. The thin film microwell scaffolds were prepared from ~50 μm thick 4000PEOT30PBT70 block copolymer films (IsoTis Integra Orhobiologics S.A., Irvine, USA). These polymer films were fabricated by solvent casting. A 10% (w/w) polymer solution was prepared in 20% (w/w) 1,1,1,3,3,3-hexafluoro-2-isopropanol (Biosolve, Valkenswaard, The Netherlands) and 80% (w/w) chloroform (Merck, Darmstadt, Germany) and casted on a silicon wafer at ambient temperature ($23 \pm 3^\circ\text{C}$). The films were placed under nitrogen-flow for 12 hours to form dense films, incubated in ethanol overnight to remove solvent residue, and dried in a vacuum oven (Heraeus, Hanau, Germany) at 30°C for 3 days.

PEOT/PBT electrospun mesh fabrication

Electrospun microwell scaffolds were fabricated from 150 μm thick electrospun 4000PEOT30PBT70 block copolymer meshes. The meshes were fabricated from a 10% (w/w) polymer solution in 20% (w/w) 1,1,1,3,3,3-hexafluoro-2-isopropanol and 80% (w/w) chloroform using an electrospinning apparatus as previously described (30). Electrospinning was performed at 12 kV constant voltage, with a 1.2 mm diameter needle, a 10 cm distance between the syringe

and the collector, and a flow rate of 2 ml/h. Electrospun meshes were dried in a vacuum oven (Heraeus, Hanau, Germany) at 30°C for 3 days.

Microwell scaffold fabrication

Microwell scaffolds were fabricated from the PEOT/PBT thin films and electrospun meshes by micro back molding (31), a variant of microthermoforming, which involves shaping a heated polymer film by three-dimensional stretching into a negative mold using a backing material (Figure S1) (32–35). The negative mold was produced by Lightmotif BV (Enschede, The Netherlands) out of a 350 μm thick stainless steel (AISI 304) foil. Approximately 500 circular holes with a diameter of 400 μm were ablated by a titanium-sapphire laser (800 nm wavelength, circular polarized, 50 kHz pulse repetition rate, 5 μJ energy, and 200 fs pulse duration). A 25 μm laser spot was achieved by a 100 mm focal length lens. The laser bundle was scanned over the foil by a two-mirror galvanometer (Scanlab Scangine 14). After machining, the mold was cleaned in an ultrasonic bath. Molding temperature and pressure for thin film scaffolds were 85°C and 25 kN, respectively and for the electrospun microwell scaffolds they were 17°C and 3 kN, respectively. Scaffold geometry and architecture were characterized by scanning electron microscopy (SEM) on a Philips XL 30 ESEM-FEG. Scaffolds were gold sputter coated (Cressington, UK) prior to SEM analysis. The dimensions of the microwells ($n=10$) were measured in three different samples per type of scaffold using ImageJ software (<http://rsb.info.nih.gov/ij/>).

PEOT/PBT wettability and water uptake

To assess the effect of micro back molding on polymer wettability and water uptake, 4000PEOT30PBT70 block copolymer films were heat-treated (85°C) to simulate the scaffold fabrication cycle. The wettability was determined by static water contact angle measurements using the captive bubble method before and after heat-treatment. Measurements were performed using a video-based optical contact angle meter OCA 15 (DataPhysics Instruments GmbH, Filderstadt, Germany). The polymer films were mounted onto Scaffold CellCrown inserts (Tampere, Finland) and incubated for three days in ultrapure Milli-Q water at 37°C. For measurements, the samples were placed with the flat polymer surface downward in an optical cuvette filled with ultrapure Milli-Q water. Water contact angle was determined by applying an air bubble ($\sim 10 \mu\text{L}$) on the film using an electronically regulated Hamilton syringe containing a curved needle. The contact angle was calculated using SCA20 software (DataPhysics Instruments GmbH, Filderstadt, Germany). The equilibrium water-uptake in ultrapure Milli-Q water was defined as the percentage weight gain of the polymer film after incubation at 37°C for 7 days. The swollen weight was measured after blotting the films with filter paper to remove surface water using a high-precision balance with an accuracy of $\pm 0.01 \text{ mg}$ (Sartorius BP210D, Göttingen, Germany).

PEOT/PBT cytotoxicity

Heat-treated (85°C) 4000PEOT30PBT70 block copolymer films were tested for cytotoxicity using a minimum essential medium (MEM) extract test (adapted from ISO 10993/EN 30993 standard). Small pieces of the polymer films (total surface of 36 cm²) were sterilized in 70% (v/v) ethanol overnight and dried for at least 12 hours. For extraction, the films were incubated in medium (α -MEM (Invitrogen, Carlsbad, USA) supplemented with 2 mM l-glutamine, 1 mM sodium pyruvate, 10% FBS, 100 U/ml penicillin and 10 μ g/ml streptomycin) for 72 hours in a shaking water bath (37°C, 60 rpm). Natural rubber (Gelria Packing BV, Enschede, The Netherlands), polylactic acid films (PLA; Plastic Suppliers/Sidaplast, EarthFirst Packaging Film, Gentbrugge, Belgium), and polypropylene films (Walothen O 25 E, Germany) were extracted identically and used as a positive control, a reference, and a negative control for cytotoxicity, respectively. The extracts were added to a subconfluent monolayer of MC3T3-E1 cells (mouse pre-osteoblasts) and cultured for 72 hours. After 24, 48 and 72 hours the cells were evaluated under light microscopy and scored in a single-blinded manner three times for confluency, degree of floating cells, and change of cell morphology related to the negative control. After 72 hours, the cells were trypsinized and counted (Beckman Coulter, Miami, USA). Based on these results, the cytotoxic response index was scored according to ISO 10993/EN 30993 standard

Nutrient diffusion through microwell scaffolds

As an indicator for nutrient transport through thin film and electrospun scaffolds, glucose diffusion was assessed as previously described (36). Briefly, the setup consisted of two double-walled compartments: a donor compartment filled with RPMI-1640 (Gibco) containing 11.1 mM d-glucose, and an acceptor compartment containing RPMI-1640 without d-glucose (both compartments were supplemented with 100 U/ml penicillin and 10 μ g/ml streptomycin). The scaffolds were pre-wetted for several hours with an ethanol to medium (without d-glucose) gradient and placed between the two compartments which were maintained at 37°C with circulating water. At the indicated time intervals, 80 μ l samples were obtained from both compartments and analyzed for glucose concentration using a Vitros DT60 II chemistry system (Ortho-Clinical Diagnostics, Raritan, USA). The glucose flux, the amount of glucose that passes through a certain surface in time, was calculated using the equation:

$$\text{Flux (gm}^{-2} \text{ s}^{-1}\text{)} = \frac{C_{\text{acceptor}} (\text{gm}^{-3}) \times V_{\text{acceptor}} (\text{m}^3) / S (\text{m}^2)}{\text{time (s)}}$$

where C_{acceptor} is the glucose concentration in the acceptor compartment, V_{acceptor} is the volume of the acceptor compartment, and S , the surface area of the construct.

Islet isolation and seeding in microwell scaffolds

Human islets of Langerhans from pancreata of organ donors (n=4) were obtained from the Human Islet Isolation Laboratory at the Leiden University Medical Center (Leiden, The Netherlands), which has permission from the Dutch government to isolate human islets for clinical purposes. Human islets of four different donor organs that were not eligible for clinical transplantation were used in these experiments, in accordance with Dutch law and institutional requirements.

Microwell scaffolds were sterilized in 70% (v/v) ethanol overnight and washed in PBS. Before islet seeding, scaffolds were centrifuged in islet culture medium (CMRL-1066 (Mediatech, Cellgro, Herndon, USA) containing 5.5 mM d-glucose, and supplemented with 0.02 mg/ml ciproxin, 0.05 mg/ml gentamicin, 2 mM l-glutamine, 0.25 µg/ml fungizone, 10 mM HEPES, 1.2 mg/ml nicotinamide and 10% (v/v) human serum) at 3500 rpm for 5 minutes to remove air bubbles and were mounted between two Teflon rings. Islets were handpicked and seeded drop-wise onto scaffolds. After 5 minutes of incubation, 8 ml of culture medium was added. Medium was changed every other day. As a reference, islets were also cultured free-floating in ultra-low attachment petri-dishes (Corning, New York, USA).

Islet morphology and function in microwell scaffolds

To assess morphology and viability, human islets were cultured in thin film and electrospun microwell scaffolds for 7 days. To assess islet morphology, samples were fixed in 4% (w/v) paraformaldehyde for 2 hours at ambient temperature ($23 \pm 3^\circ\text{C}$), permeabilized with 0.1% Triton-X for 4 minutes and stained with alexa-488-phalloidin for 30 minutes in the dark to visualize actin in islet cells. Samples were imaged using a Zeiss LSM510 confocal Microscope. Additionally, islet morphology was assessed using SEM. As a reference for islet attachment, islets were cultured for 7 days on tissue culture plastic (NUNC). Prior to SEM analysis, samples were fixed in 4% (w/v) paraformaldehyde for 2 hours at ambient temperature ($23 \pm 3^\circ\text{C}$), dehydrated in graded ethanol series, critical-point dried, and gold sputter coated.

To assess islet function, two measures of islet response to glucose were made: insulin secretion and total insulin content were assessed at day 1 and day 7. Scaffolds containing islets or free-floating islets were transferred to ultra-low attachment 24-well plates (Corning, New York, USA). Each well contained approximately 25 islets. The islets were incubated in pre-warmed KRBH buffer (115 mM NaCl, 5 mM KCl, 24 mM NaHCO_3 and 2.2 mM CaCl_2 , pH 7.4), supplemented with 20 mM HEPES, 2 mg/ml human serum albumin and 1.7 mM d-glucose for a 90 minutes at 37°C and 5% CO_2 . The buffer was replaced by KRBH buffer containing either 1.7 mM or 16.7 mM glucose and the islets were incubated for 60 minutes. Experiments were performed in triplicate for each condition. The supernatant was removed and frozen for future analysis. Islets were harvested, washed in PBS and disrupted by sonication in distilled water (Braun, Melsungen, Germany). Samples from the homogenate were extracted overnight at 4°C in acidic ethanol (0.18 M HCl in 95% (v/v) ethanol). The supernatants and islet homogenate were assayed for insulin using an ELISA immunoassay (Mercodia, Uppsala, Sweden) according

to the manufacturer's instructions. For normalization, total DNA content was quantified using a Quant-iT PicoGreen dsDNA kit (Molecular Probes, Eugene, USA) according to the manufacturer's instructions.

Histological analysis

To identify α and β cells and assess morphology, histology was performed. Islets cultured in either microwell scaffolds or under free-floating conditions were washed in PBS and fixed in 4% (w/v) paraformaldehyde for 2 hours at ambient temperature ($23 \pm 3^\circ\text{C}$). Subsequently, the samples were embedded in 2% (w/v) agarose and prepared for paraffin embedding. The samples were sectioned at $4 \mu\text{m}$, deparaffinized in buthylene, and rehydrated through graded ethanol series to distilled water. Sections were blocked with an avidin-biotin blocking kit (Vector Laboratories, Burlingame, USA) and normal donkey serum (1:50 (in PBS containing 1% lamb serum), Jackson ImmunoResearch, West Grove, USA, 1 hour at room temperature). Primary and secondary antibodies were diluted in PBS containing 1% lamb serum. The following primary antibodies, dilutions, and incubation times were used: guinea pig anti-insulin (1:200, Linco Research, St Charles, USA, 1.5 hours at room temperature) and rabbit anti-glucagon (1:100, Vector Laboratories, Burlingame, USA, overnight at 4°C). The secondary antibodies were donkey anti-guinea pig-TRITC (1:400, Jackson ImmunoResearch, West Grove, USA, 1 hour at room temperature) and biotinylated donkey anti-rabbit (1:200, Jackson ImmunoResearch, West Grove, USA, 1 hour at room temperature) followed by streptavidin-Alexa Fluor488 (1:200 Jackson ImmunoResearch, West Grove, USA, 1 hour at room temperature). Sections were mounted with mounting medium containing DAPI to stain the nuclei (VectaShield, Vector Laboratories, Burlingame, USA) prior to imaging on a confocal microscope (Carl Zeiss, Sliedrecht, the Netherlands).

Statistical analysis

Results are presented as the mean \pm standard deviation. Statistical analyses were performed using an unpaired, two-tailed, Student's t-test, or analysis of variance (ANOVA) with a Bonferroni post-test using SPSS statistics software (Chicago, USA). Statistical significance was considered at $p < 0.05$.

RESULTS

Polymer film characterization and cytotoxicity

We first determined the effects of our processing conditions on the 4000PEOT30PBT70 block copolymer. Water uptake and contact angle of the unprocessed polymer was $52.1 \pm 4.0\%$ (w/w) and $39 \pm 2^\circ$, respectively. After heating the polymer to 85°C , the temperature used for scaffold fabrication, water uptake was significantly decreased to $38.3 \pm 3.4\%$ (w/w), whereas no change in water contact angle was observed (Figure 1). We then sought to ensure the processing conditions did not affect the biocompatibility. To evaluate the cytotoxicity of heat-treated

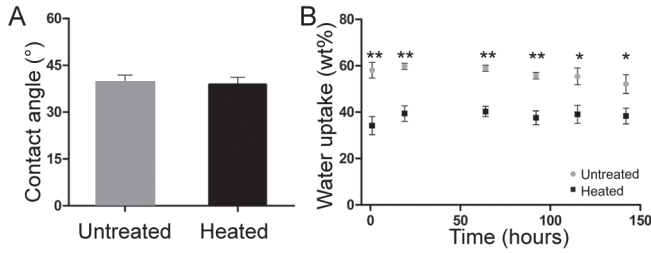


Figure 1. PEOT/PBT wettability and water uptake. (A) Contact angle measurements of non heat-treated and heat-treated 4000PEOT30PBT70 block copolymer films using the captive bubble method. Data represents mean \pm SD of 20 measurements ($N=3$ per condition). (B) Water uptake of non-treated and heat-treated 4000PEOT30PBT70 block copolymer films. Data represents mean \pm SD, ($N=3$ per condition), * $p < 0.05$, ** $p < 0.01$.

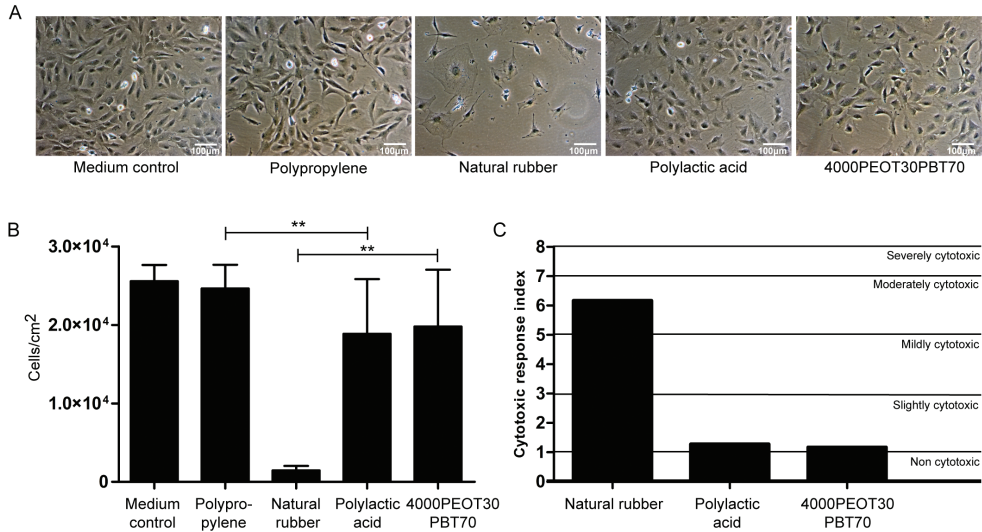


Figure 2. PEOT/PBT cytotoxicity. Cytotoxicity test after 72 hours of incubation. Growth and morphology of MC3T3E-1 cells were analyzed in the presence of extracts of polypropylene films (negative control), natural rubber (positive control), polyactic acid and heated 4000PEOT30PBT70 films. (A) Light microscopy images of MC3T3E-1 cells cultured in standard and in the presence of the different material extracts, (B) Total amount of cells after 72 hours of incubation. Data represent mean \pm SD, ($n=6$), ** $p < 0.01$, (C) The cytotoxic response index based on growth and morphological changes, scored in a single-blinded manner.

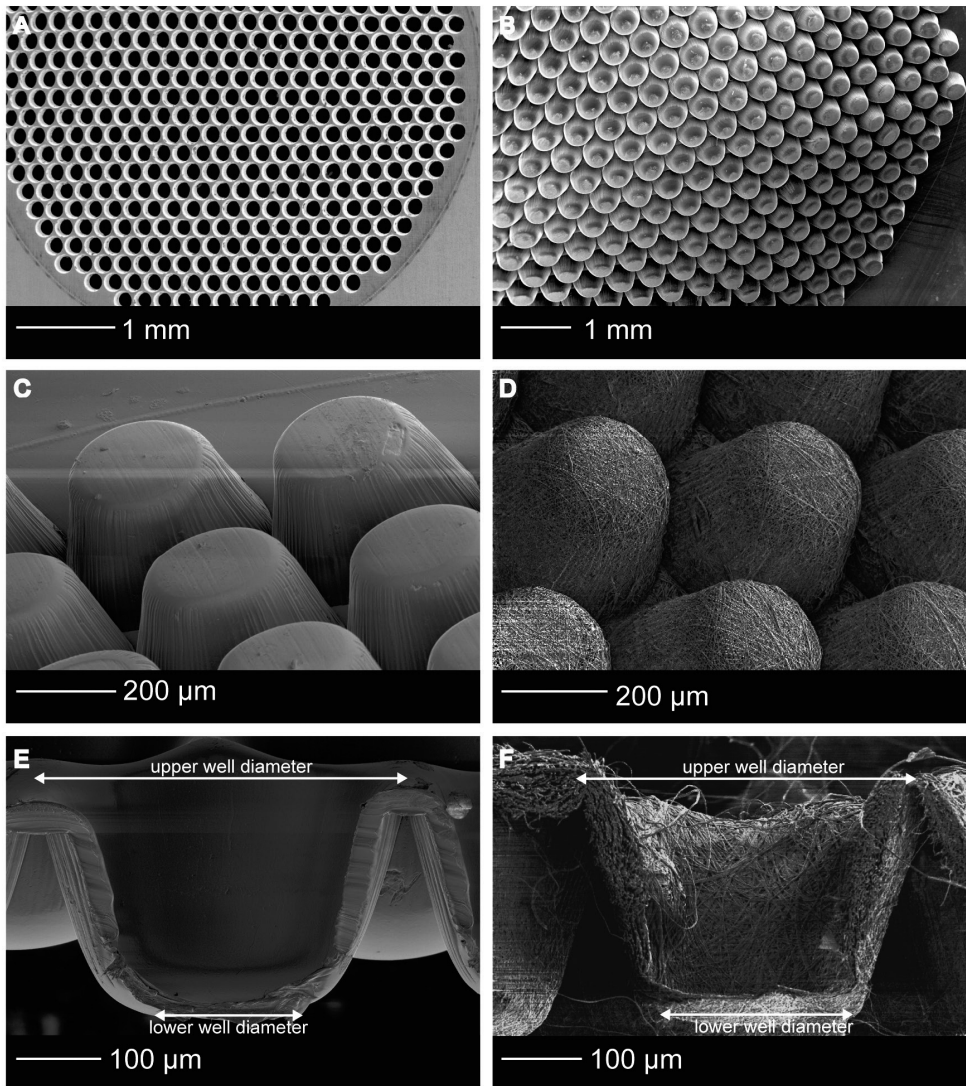


Figure 3. Microwell scaffold morphology. SEM images of (A) the stainless steel mould, (B) the scaffold area, (C) thin film microwell scaffold, (D) electrospun microwell scaffold, (E) cross-section of a thin film microwell showing the tapered shape and the smooth polymer surface, (F) cross-section of a electrospun microwell showing the fibrous network

4000PEOT30PBT70 block copolymer films, extracts of these materials were tested for their effects on growth and morphology of MC3T3-E1 cells. In contrast to exposure to extracts of natural rubber, which served as the positive control for cytotoxicity, nearly confluent monolayers were observed after exposure to extracts of polypropylene (negative control), PLA, and 4000PEOT30PBT70 films (Figure 2 A-B). No significant effect on cell morphology was observed for cells cultured in 4000PEOT30PBT70 extracts compared to PLA or polypropylene, indicating the polymer is biocompatible.

Microwell scaffold morphology

SEM analysis demonstrated homogeneously shaped microwells throughout the entire scaffold area (Figure 3 B), resembling the tapered shape of the mold, (Figure 3 A) and indicating successful demolding. The microwells were stable upon handling, due to the sufficiently high ratios of the thicknesses of the walls to the dimensions of the volumes enclosed by the walls. Per scaffold type, the upper and lower well diameters (Figure 3 E-F) of 10 microwells in three different samples were measured using ImageJ software (<http://rsb.info.nih.gov/ij/>). The upper well diameter of the thin film scaffolds was $377 \pm 5 \mu\text{m}$ and the lower well diameter $251 \pm 9 \mu\text{m}$. For the electrospun microwells the upper diameter was $355 \pm 20 \mu\text{m}$ and the lower diameter was $217 \pm 36 \mu\text{m}$. The fiber-diameter of the electrospun meshes was $1.71 \pm 0.42 \mu\text{m}$. The height of the scaffold corresponded to the height of the mold ($350 \mu\text{m}$) (Figure 3 C-F).

Nutrient diffusion through microwell scaffolds

As glucose is an important nutrient for islets, the diffusion of glucose through thin film and electrospun microwell scaffolds was assessed. Figure 4 A shows typical results of glucose

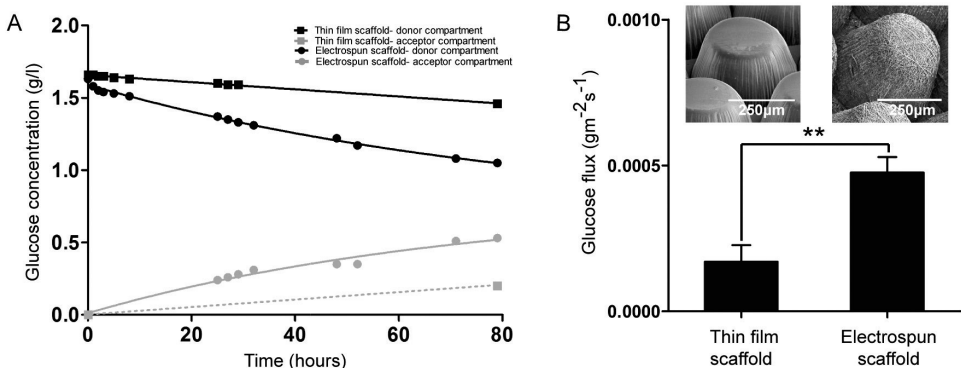


Figure 4. Glucose diffusion through microwell scaffolds. (A) Typical glucose diffusion graphs for thin film and electrospun microwell scaffolds. For the thin film microwell scaffold, the concentration of glucose in the acceptor compartment is represented as a dashed line, because only the last time-point was within analytical range of the Vitros DT60 II chemistry system. (B) Maximum glucose flux through dense and electrospun microwell scaffolds. Data represents mean \pm SD ($n=3$), $** p < 0.01$.

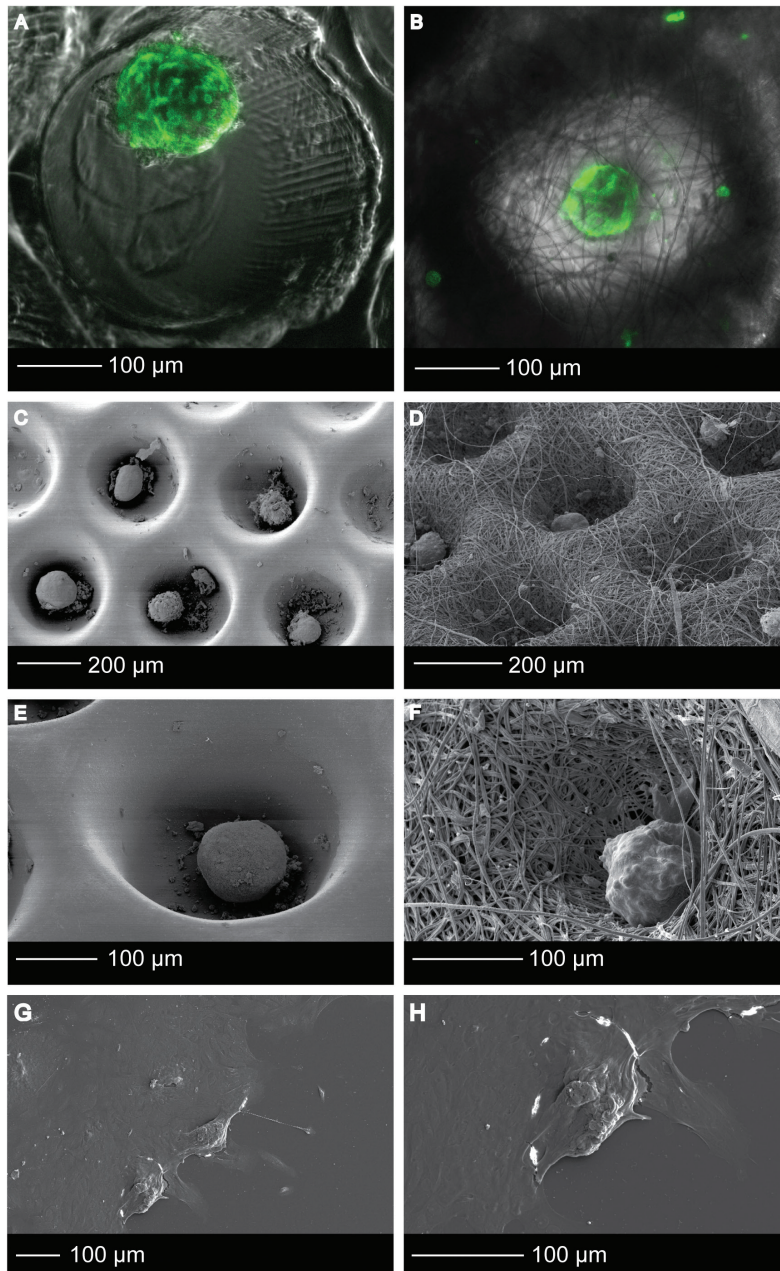


Figure 5. Islet morphology. (A, B) Confocal fluorescence microscopy images of Phalloidin-TRITC stained human islets that were cultured in thin film (A) and electrospun (B) microwell scaffolds. (C-H) High resolution SEM images of islets in the thin film (C,E) and electrospun (D,F) microwell scaffolds, and tissue culture plastic (G,H).

diffusion in time through a thin film and an electrospun scaffold. No adsorption of glucose to the scaffolds was observed, since the difference between the initial concentration of glucose in the donor compartment and the concentration in the donor compartment in time equals the glucose concentration in the acceptor compartment. Due to the water uptake of this polymer composition, some glucose diffusion was observed through thin film microwell scaffolds (Figure 4 A), but the maximum glucose flux was significantly higher for the electrospun scaffolds: $4.76 \pm 0.53 \text{E}10^{-4} \text{ gm}^{-2}\text{s}^{-1}$ compared to $1.70 \pm 0.58 \text{E}10^{-4} \text{ gm}^{-2}\text{s}^{-1}$ for the thin film scaffolds ($p < 0.01$) (Figure 4 B).

Islet morphology in microwell scaffolds

Islets were seeded into the scaffolds by sedimentation. It is known that islets aggregate when they are cultured at high density. In rare cases, multiple islets were observed in one microwell. After prolonged culture, these islets start to fuse, but the final size of the fused islets remained within the dimensions of the microwell ($\sim 350 \mu\text{m}$), comparable to the upper size limit of human islets (37). After 7 days of culture, the cells did not spread out and islets maintained their rounded shape (Figure 5 A-F) in both thin film and electrospun mesh microwell scaffolds. This in contrast to islets that were cultured on adherent tissue culture plastic used as an islet adhesion control (Figure 5 G-H). Some attached cells could be observed at the surface of the scaffold, but the degree of cell attachment was limited.

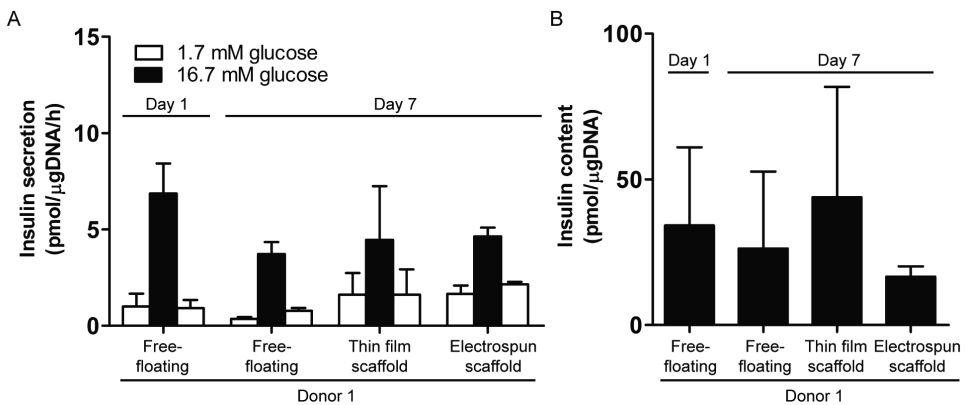


Figure 6. Islet function in microwell scaffolds. (A) Insulin secretory response to glucose stimulation of human islets cultured for 7 days in thin film and electrospun microwell scaffolds. Free-floating islets served as a control. Data represent mean \pm SD ($n = 3$ per condition). (B) Insulin content of human islets cultured in thin film and electrospun microwell scaffold or under free-floating conditions. Data represent mean \pm SD ($n = 3$ per condition).

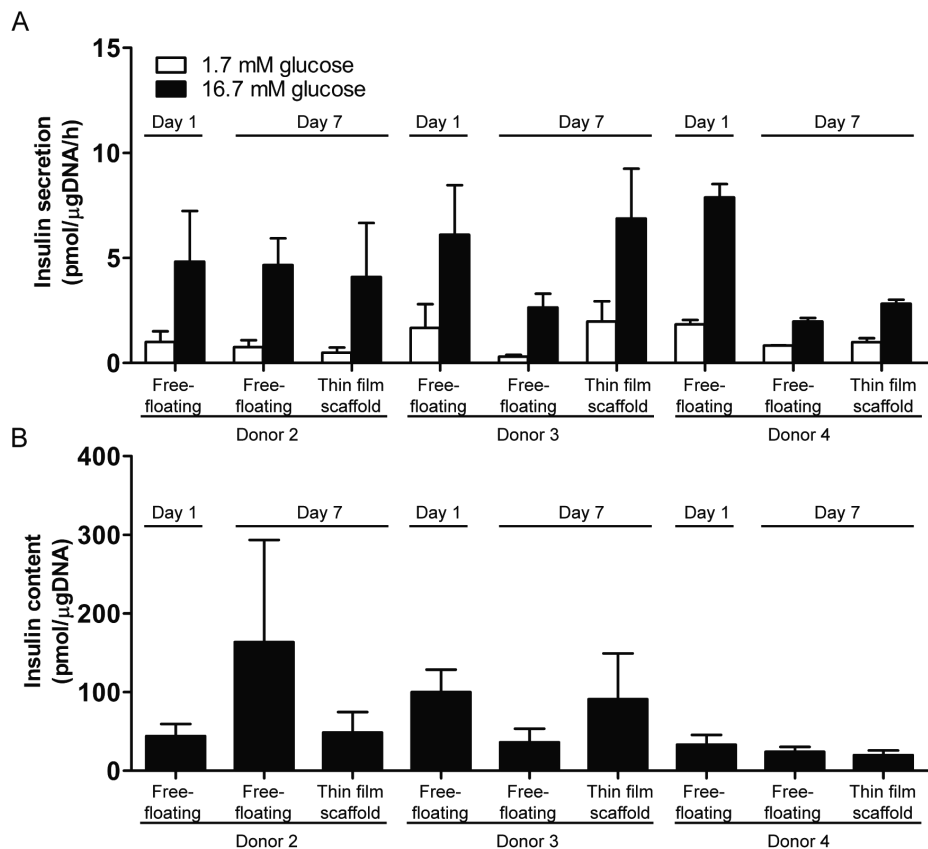


Figure 7. Islet function of multiple donors in thin film microwell scaffolds. (A) Insulin secretory response and, (B) insulin content of islets cultured in thin film scaffolds or under free-floating conditions of three different human donors. Data represent mean \pm SD ($n = 3$ per condition).

Islet response to glucose challenge

To assess whether the microwell scaffolds affect islets functionality, human islets were cultured for 7 days in both thin film and electrospun microwell scaffolds and subjected to a glucose-stimulated insulin secretion (GSIS) test. This test involves exposing islets to low (1.7 mM), high (16.7 mM), and then low glucose concentration and measuring insulin secretion by ELISA. After 7 days of culture, the increase in insulin release upon stimulation, compared to basal insulin release levels, did not significantly differ between islets seeded in either scaffold design (3.9 ± 2.9 and 3.6 ± 1.6 pmol/μgDNA/h for thin film and electrospun microwell scaffolds, respectively) and free-floating control islets (3.6 ± 0.7 pmol/μgDNA/h, $p > 0.05$). Following high glucose stimulation, insulin release levels returned to basal levels when incubated in low glucose buffer, indicating normal responsiveness (Figure 6 A). Total insulin content was also measured

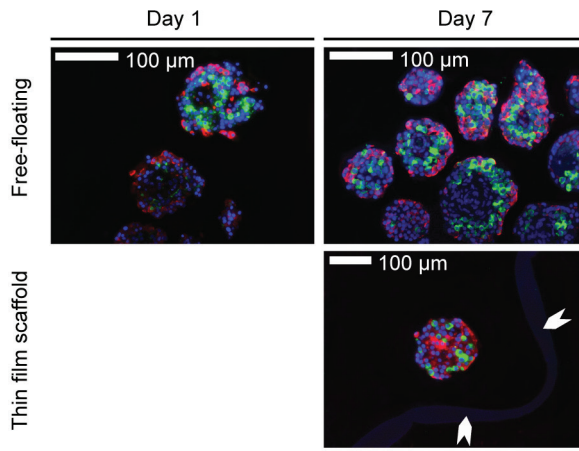


Figure 8. Histology of free-floating control islets and of islets cultured in thin film microwell scaffolds. Insulin (red) and glucagon (green) positive cells can be observed throughout the islets. The microwell scaffold is indicated by the white arrows. All data were obtained after 7 days of culturing.

and did not differ between islets in the microwells or free-floating control islets (Figure 6 B). With no significant differences in insulin secretion between islets cultured in either the thin film or the electrospun mesh microwells, we sought to further demonstrate that donor variability was not influencing our results. We therefore compared insulin secretion and total insulin content in islets derived from three donors either in thin film microwells and free-floating islets and found no statistically significant differences (Figure 7 A-B) indicating that the microwell scaffold platform does not hamper islet functionality in terms of islet's glucose-induced insulin secretion.

Histological analysis

Having found that both the thin film and the electrospun microwell scaffolds supported islet insulin response equally, we performed histology of islets seeded in the thin film scaffold and compared this to free-floating islets. Islet morphology was unaffected by culture in the thin film microwell scaffolds after 7 days of culture (Figure 8). In both groups, glucagon and insulin expressing cells were typically present throughout the islets, further indicating that the microwell scaffolds did not negatively affect islet morphology nor function.

DISCUSSION

Biomaterial scaffolds have recently been proposed as a carrier for islets of Langerhans to improve long-term islet survival and function *in vivo*. They avoid triggering the instant blood-mediated inflammatory reaction (IBMIR) and may provide a better microenvironment for islet transplantation than transplantation in the suboptimal microenvironment of the liver vasculature (38). This study represents the first use of a microwell scaffold platform designed for future islet of Langerhans transplantation. This microwell design permitted easy entrapment of individual islets through sedimentation and the dimensions covered the full size range of the islets (37). In other scaffolds, filling materials such as matrigel (12) and type I collagen gels (16) were used to prevent islet loss during seeding but the microwell scaffold design presented here entraps the islets without the need for additional filling materials even after multiple media changes. The open structure of the microwell scaffold may be advantageous for nutrient diffusion and infiltration of host cells, such as endothelial cells, which are important for islet survival, function and engraftment. This addresses a common problem post-transplantation, where nutrients can only be supplied to the islets through diffusion until the islets are revascularized, which can take up to 14 days. Even then, the vascular density and oxygen tension in these transplanted islets are reduced compared to native islets (39). SEM analysis further revealed that the natural rounded morphology of islets was preserved in the scaffolds, regardless of whether they were seeded in thin films or electrospun meshes.

For this study, a PEOT/PBT block copolymer was used, since its material properties, such as wettability (24), swelling (23, 25, 27), protein adsorption (26), degradation rate (27), and mechanical properties (27) can be tailored for specific applications by changing the copolymer composition (27). The composition 4000PEOT30PBT70 was selected for its slow degradation rate, allowing long-term monitoring after transplantation, and its limited cell-adhesive properties (24) due to the high molecular weight of the initial PEG segments (40). Importantly, our fabrication process did not affect the polymer film wettability, but the water uptake was significantly diminished. The temperature during scaffold fabrication (85°C) was above the PEOT-domain melting temperature (32-47°C (27)), but below the melting temperature of the PBT-domain (173-223°C (27)). Atomic force microscopy showed the distribution of the two different blocks was more organized after heating, indicative of greater phase separation (Figure S2), potentially explaining the diminished water uptake.

Considering that pH is important for islet function and survival (41) and that long-term exposure to non-physiological pH has been demonstrated to result in a loss of islets when below 7.0 and loss of the insulin releasing capacity when above 7.4 (41), it is important that the PEOT/PBT copolymer does not affect the local pH upon degradation. Previous *in vitro* and *in vivo* work has demonstrated that non-enzymatic PEOT/PBT degradation, which is primarily through hydrolysis, is unlikely to affect the pH of the local environment. This is a significant advantage over polymers such as poly(glycolic acid) (PGA) (31, 32) and poly(lactic-co-glycolic

acid) (PLGA) (27–29), which are often used in scaffolds for islet transplantation in which acidic degradation products are formed.

The microwell design confined individual islets in separate microwells, overcoming a major disadvantage of previous scaffold designs in which islets were able to fuse. Islet fusion negatively affects native islet structure, and results in islet aggregates which suffer from diffusion-limited nutrient deprivation (37). This results in central core necrosis and impaired islet function. Furthermore, our design preserved the native islet morphology during 7 days of culture. The rounded islet morphology is thought to be crucial for islet function, as a higher ratio between the basal and glucose-stimulated insulin release is obtained when islets are cultured free-floating compared to islets that are attached to the bottom of a petri-dish (42). Functional tests revealed that the insulin secretory response to glucose stimulation of human islets cultured in the microwell scaffolds was comparable to free-floating control islets. Also the insulin content of scaffold-seeded islets was preserved indicating that there is no change in insulin release and pro-insulin biosynthesis.

The translation of the microwell system to a clinical setting raises some additional challenges; for example, Shapiro *et al.* (5) have shown that a mean of $11,547 \pm 1604$ islet equivalents (IEQ) per kilo bodyweight is needed to obtain insulin independency in patients. Therefore, to be able to transplant the required islet mass to treat a patient of 75 kilograms using a single microwell, the scaffold diameter would have to increase to 40 cm. Even though the height of the scaffold is only 350 μm , it would not be clinically feasible to transplant a scaffold with such dimensions. Thus, before translation of this work to clinically relevant sized implants, we will study methods to scale up the scaffold platform to accommodate a sufficient amount of islets for human islet transplantation. We calculated that multi-layer stacking of microwell scaffolds into a three-dimensional scaffold will already drastically reduce the construct's dimensions: stacking up to 15 scaffold layers will result in a three-dimensional construct with a diameter of 10 cm and a height of 5 mm. When stacking multiple scaffold layers, one should consider diminished mass transport of nutrients and hormones. Therefore, our future studies will focus on introducing micro-porosity into the microwell scaffolds, which will benefit the three-dimensional microwell scaffold design two-fold. First, the enhanced nutrient diffusion will improve islet survival immediately after transplantation, while secondly, the micro-pores allow vascular ingrowth into three-dimensional construct to revascularize the islets rapidly.

CONCLUSIONS

This study is the first to report on a microwell scaffold platform as a potential transplantation device for pancreatic islets. Reproducible microwell scaffolds were prepared from PEOT/PBT thin films and electrospun meshes. The morphology of human islets was preserved in the microwell scaffolds and remained stable during 7 days of culture and the islets showed an insulin release and total insulin content comparable to free-floating control islets. Glucagon

and insulin immunostaining were also comparable between these groups. Together, these data indicate that the microwell scaffold platform does not hamper islet functionality and is a promising platform for use in extrahepatic islet transplantation.

ACKNOWLEDGEMENTS

The authors thank Kim Sweers and Kees van der Werf from the department of Nano Biophysics for their technical assistance in Atomic Force Microscopy imaging, Janneke Hilderink from the department of Developmental BioEngineering for her contribution to the SEM images of attached islets on tissue culture plastic, and Tom Groothuis from the department of Tissue Regeneration for his assistance in confocal fluorescence microscopy.

SUPPLEMENTAL MATERIAL

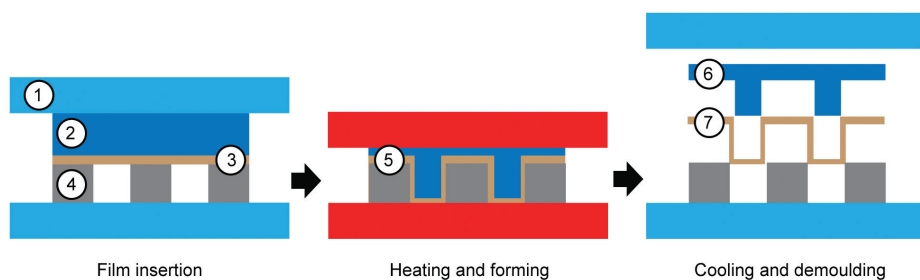


Figure S1. Schematic representation of scaffold fabrication process using micro back molding. (1) press, (2) backing material, (3) thin polymer film or electrospun mesh of 4000PEOT30PBT70 block copolymer, (4) mold, (5) formed thin polymer film or electrospun mesh, (6) solidified backing, (7) microthermoformed microwell scaffold

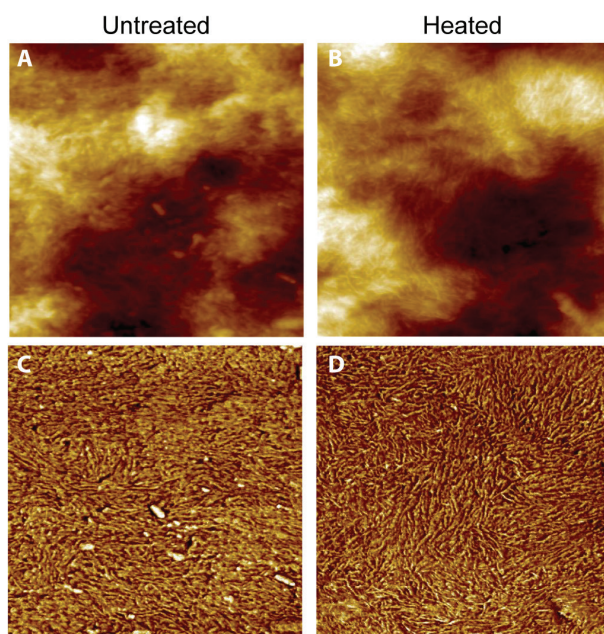


Figure S2. Height and corresponding phase contrast images obtained by tapping mode Atomic Force Microscopy (AFM). (A-C) untreated 4000PEOT30PBT70 block copolymer films; (B-D) heated 4000PEOT30PBT70 block copolymer films. Phase contrast images (C-D) show the PEOT/PBT domains for both samples. Tapping mode imaging was performed on a Multimode with a Nanoscope IV controller (Bruker, Santa Barbara CA, USA) with TESP cantilevers (spring constant is 20-80 N/m, Bruker, Santa Barbara CA, USA) in ambient air with moderate force settings (65% of the free amplitude). Image size is 1x1 μm with 512 pixels.

REFERENCES

1. Soltesz G (2003) Diabetes in the young: a paediatric and epidemiological perspective. *Diabetologia* 46:447–454.
2. Nathan DM (1993) Long-term complications of diabetes mellitus. *N Engl J Med* 328:1676–1685.
3. Shapiro a MJ et al. (2006) International trial of the Edmonton protocol for islet transplantation. *N Engl J Med* 355:1318–30.
4. Ryan EA et al. (2005) Five-year follow-up after clinical islet transplantation. *Diabetes* 54:2060–2069.
5. Shapiro AM et al. (2000) Islet transplantation in seven patients with type 1 diabetes mellitus using a glucocorticoid-free immunosuppressive regimen. *N Engl J Med* 343:230–238.
6. Vantyghem MC et al. (2009) Primary graft function, metabolic control, and graft survival after islet transplantation. *Diabetes Care* 32:1473–1478.
7. Korsgren O et al. (2008) Optimising islet engraftment is critical for successful clinical islet transplantation. *Diabetologia* 51:227–232.
8. Carlsson P-OO (2011) Influence of microenvironment on engraftment of transplanted beta-cells. *Ups J Med Sci* 116:1–7.
9. Merani S, Toso C, Emamaullee J, Shapiro AM (2008) Optimal implantation site for pancreatic islet transplantation. *Br J Surg* 95:1449–1461.
10. Rafael E et al. (2008) Intramuscular autotransplantation of pancreatic islets in a 7-year-old child: a 2-year follow-up. *Am J Transpl* 8:458–462.
11. Blomeier H et al. (2006) Polymer scaffolds as synthetic microenvironments for extrahepatic islet transplantation. *Transplantation* 82:452–459.
12. Dufour JM et al. (2005) Development of an ectopic site for islet transplantation, using biodegradable scaffolds. *Tissue Eng* 11:1323–1331.
13. Salvay DM et al. (2008) Extracellular matrix protein-coated scaffolds promote the reversal of diabetes after extrahepatic islet transplantation. *Transplantation* 85:1456–1464.
14. Juang JH, Bonner-Weir S, Ogawa Y, Vacanti JP, Weir GC (1996) Outcome of subcutaneous islet transplantation improved by polymer device. *Transplantation* 61:1557–1561.
15. Song C et al. (2009) Polyglycolic Acid-islet grafts improve blood glucose and insulin concentrations in rats with induced diabetes. *Transpl Proc* 41:1789–1793.
16. Daoud JT et al. (2011) Long-term in vitro human pancreatic islet culture using three-dimensional microfabricated scaffolds. *Biomaterials* 32:1536–1542.
17. Berman DM et al. (2009) Long-term survival of nonhuman primate islets implanted in an omental pouch on a biodegradable scaffold. *Am J Transpl* 9:91–104.
18. Kin T et al. (2008) The use of an approved biodegradable polymer scaffold as a solid support system for improvement of islet engraftment. *Artif Organs* 32:990–993.
19. Perez-Basterrechea M et al. (2009) Plasma-fibroblast gel as scaffold for islet transplantation. *Tissue Eng Part A* 15:569–577.
20. Zhao M et al. (2010) The three-dimensional nanofiber scaffold culture condition improves viability and function of islets. *J Biomed Mater Res A* 94:667–672.
21. Hiscox AM, Stone AL, Limesand S, Hoying JB, Williams SK (2008) An islet-stabilizing implant constructed using a preformed vasculature. *Tissue Eng Part A* 14:433–440.
22. Van Dijkhuizen-Radersma R et al. (2002) Control of vitamin B12 release from poly(ethylene glycol)/poly(butylene terephthalate) multiblock copolymers. *Biomaterials* 23:1527–1536.

23. Bezemer JM, Grijpma DW, Dijkstra PJ, van Blitterswijk CA, Feijen J (1999) A controlled release system for proteins based on poly(ether ester) block-copolymers: polymer network characterization. *J Control Release* 62:393–405.
24. Olde Riekerink MB, Claase MB, Engbers GH, Grijpma DW, Feijen J (2003) Gas plasma etching of PEO/PBT segmented block copolymer films. *J Biomed Mater Res A* 65:417–428.
25. Van Dijkhuizen-Radersma R, Hesseling SC, Kaim PE, de Groot K, Bezemer JM (2002) Biocompatibility and degradation of poly(ether-ester) microspheres: in vitro and in vivo evaluation. *Biomaterials* 23:4719–4729.
26. Mahmood TA, de Jong R, Riesle J, Langer R, van Blitterswijk CA (2004) Adhesion-mediated signal transduction in human articular chondrocytes: the influence of biomaterial chemistry and tenascin-C. *Exp Cell Res* 301:179–188.
27. Deschamps AA et al. (2002) Design of segmented poly(ether ester) materials and structures for the tissue engineering of bone. *J Control Release* 78:175–186.
28. Bulstra SK et al. (1996) Femoral canal occlusion in total hip replacement using a resorbable and flexible cement restrictor. *J Bone Jt Surg Br* 78:892–898.
29. Mensik I, Lamme EN, Riesle J, Brychta P (2002) Effectiveness and Safety of the PEGT/PBT Copolymer Scaffold as Dermal Substitute in Scar Reconstruction Wounds (Feasibility Trial). *Cell Tissue Bank* 3:245–253.
30. Moroni L, de Wijn JR, van Blitterswijk CA (2006) 3D fiber-deposited scaffolds for tissue engineering: influence of pores geometry and architecture on dynamic mechanical properties. *Biomaterials* 27:974–985.
31. Truckenmüller R et al. (2011) Thermoforming of film-based biomedical microdevices. *Adv Mater* 23:1311–29.
32. Truckenmüller R, Giselbrecht S (2004) Microthermoforming of flexible, not-buried hollow microstructures for chip-based life sciences applications. *IEE Proc Nanobiotechnol* 151:163–166.
33. Gottwald E et al. (2007) A chip-based platform for the in vitro generation of tissues in three-dimensional organization. *Lab Chip* 7:777–785.
34. Truckenmüller R et al. (2008) Flexible fluidic microchips based on thermoformed and locally modified thin polymer films. *Lab Chip* 8:1570–1579.
35. Giselbrecht S et al. (2006) 3D tissue culture substrates produced by microthermoforming of pre-processed polymer films. *Biomed Microdevices* 8:191–9.
36. Papenburg BJ et al. (2007) One-step fabrication of porous micropatterned scaffolds to control cell behavior. *Biomaterials* 28:1998–2009.
37. Lehmann R et al. (2007) Superiority of small islets in human islet transplantation. *Diabetes* 56:594–603.
38. Kort H De et al. (2011) Islet transplantation in type 1 diabetes. *BMJ* 342:d217.
39. Mattsson G, Jansson L, Carlsson PO (2002) Decreased vascular density in mouse pancreatic islets after transplantation. *Diabetes* 51:1362–1366.
40. Gombotz WR, Wang GH, Horbett TA, Hoffman AS (1991) Protein adsorption to poly(ethylene oxide) surfaces. *J Biomed Mater Res* 25:1547–1562.
41. Brunstedt J, Nielsen JH (1978) Long-term effect of pH on B-cell function in isolated islets of Langerhans in tissue culture. *Diabetologia* 15:181–185.
42. Andersson A (1978) Isolated mouse pancreatic islets in culture: effects of serum and different culture media on the insulin production of the islets. *Diabetologia* 14:397–404.

Chapter 3

Microwell scaffolds with a defined porosity: a potential platform for extrahepatic islet transplantation

Mijke Buitinga¹, Frank Assen¹, Maaïke Hanegraaf², Paul Wieringa³, Janneke Hilderink¹, Lorenzo Moroni³, Roman Truckenmüller³, Clemens van Blitterswijk³, Gert-Willem Römer⁴, Françoise Carlotti², Eelco de Koning^{2,5,6}, Marcel Karperien¹, Aart van Apeldoorn¹



¹ Department of Developmental BioEngineering, University of Twente, Enschede, The Netherlands

² Department of Nephrology, Leiden University Medical Center, Leiden, The Netherlands

³ Complex Tissue Regeneration Department, Maastricht University, Maastricht, The Netherlands

⁴ Department of Applied Laser Technology, University of Twente, Enschede, The Netherlands

⁵ Department of Endocrinology, Leiden University Medical Center, Leiden, The Netherlands

⁶ Hubrecht Institute, Utrecht, The Netherlands

ABSTRACT

Despite the clinical success of intrahepatic islet transplantation in treating type 1 diabetes, factors specific to this transplantation site hinder long-term insulin independence. The adoption of alternative, extravascular sites likely improve islet survival and function, but few locations are able to sufficiently confine islets in order to facilitate engraftment. This work describes a porous microwell scaffold with a well-defined pore size and spacing designed to guarantee islet retention at an extrahepatic transplantation site and stimulate islet revascularization. Three modification techniques were characterized for their ability to introduce pores with a maximum diameter of 40 μm into the microwell scaffold platform: particulate leaching; solvent casting on pillared wafers; and laser drilling, of which the laser drilling method best matched our design criteria. Transplantation studies in the epididymal fat elucidated the potential of this porous scaffold platform to restore blood glucose levels in a diabetic mouse model and facilitate islet engraftment. Six out of eight mice reverted to stable normoglycemia, with a mean time to remission of 6.2 ± 3.2 days, which was comparable to that of the gold standard of renal subcapsular islet grafts. In contrast, when islets were transplanted in the epididymal fat pad without a microwell scaffold, only two out of seven mice reverted to stable normoglycemia. Detailed histological evaluation four weeks after transplantation found that scaffold-implanted islets maintained their native morphology and size. The vascular density of both scaffold-seeded islets and renal subcapsular islets was similar to that of native pancreatic islets. Our data indicates that the microwell scaffold efficiently confines islets and improves islet function when islets are transplanted in the epididymal fat pad. Furthermore, we demonstrated that the microwell scaffold platform facilitates detailed analysis at a subcellular level, such as vascular and cellular distribution patterns, to substantiate functional physiological observations.

INTRODUCTION

The transplantation of islets of Langerhans from donor pancreata into the liver has become an established therapeutic option for a small subpopulation of patients with type 1 diabetes and labile glycemic control (1). Although the clinical outcome of this islet transplantation approach has improved over the last decade, progressive islet loss in the post-transplantation period often prevents long-term insulin independence to only a subset of patients (2). One advantage of the intrahepatic site has been the ease of islet delivery, achieved by islet infusion into the portal vein. However, this exposes islets directly to blood and elicits the instant blood-mediated inflammatory reaction (IBMIR). This has been shown to cause islet destruction and islet loss (3, 4). In addition, the hepatic environment imposes additional challenges and stress to islet engraftment and survival, such as the exposure to reduced oxygen tension (5, 6) and high concentrations of immunosuppressants (7).

While these limitations can be partly overcome by employing extrahepatic extravascular transplantation sites, such as the subcutaneous tissue or the omentum, these sites are typically challenged by limited space to transplant sufficient amount of islets, the inability to restrict islet migration, or poor vascularization (8). These challenges have driven the field towards engineering efficient and tailored transplant microenvironments using biomaterials that ensure optimal islet spatial distribution and promote revascularization (9–11).

Pancreatic islets are highly vascularized by a dense network of capillaries. This capillary network is not only crucial for an adequate nutrient supply, but it is also critical for glucose sensing and the rapid secretion of islet hormones into the blood stream (12); islets with vascular defects do not regulate blood glucose levels properly (12, 13). These requirements dictate that an islet tissue engineered construct should allow for high mass transport and good vascularization, implying the creation of a porous implantable construct that permits blood vessel infiltration. However, recent findings report that it is a narrow range of pore size, 30–40 μm , that maximizes vascularization (14), suggesting that having precise control over pore size would greatly facilitate revascularization of an implantable scaffold.

Recently, we have developed a novel polymer film-based microwell scaffold platform for islet transplantation that provides a mechanically protective environment while maintaining islet morphology and islet functionality *in vitro* (15). In the current study, we sought to further optimize this scaffold platform to promote islet engraftment *in vivo* by facilitating vascular tissue ingrowth via introduction of well-defined pores with a maximum diameter of 40 μm . Therefore, we have evaluated the feasibility of three process sequences based on substrate modification and replication by (micro)thermoforming (SMART) (16) in conjunction with the following methods to introduce pores with controlled dimensions and spacing in polymer films: 1) particulate leaching using salt crystals; 2) solvent casting on patterned silicon wafers; and 3) laser drilling using an ultra-short pulsed laser source, of which laser drilling best matched our design criteria. As a first step in identifying the *in vivo* potential of this porous microwell

scaffold for extrahepatic islet transplantation, we have investigated whether this highly flexible and tunable platform can support islet function and engraftment in a diabetic mouse model.

MATERIALS AND METHODS

PEOT/PBT thin film fabrication

Scaffolds were fabricated from a poly(ethylene oxide terephthalate)/poly(butylene terephthalate) block copolymer with composition 4000PEOT30PBT70 (PolayActive™, IsoTis Orthobiologics S.A., Irvine, USA) as previously described (15). A 15% (w/w) polymer solution was prepared in 35% (w/w) 1,1,1,3,3,3-hexafluoro-2-isopropanol (Biosolve, Valkenswaard, The Netherlands) and 65% (w/w) chloroform (Merck, Darmstadt, Germany). The polymer solution was cast on silicon wafers at a height of 200 μm, finally resulting in ~15 μm thick films. The films were placed under nitrogen-flow for 12 hours, incubated in ethanol overnight to remove solvent residue, and dried in a vacuum oven (Heraeus, Hanau, Germany) at 30°C for 3 days.

Microwell scaffold fabrication and characterization

Microwell scaffolds consisted of a thin PEOT/PBT polymer film patterned with microwells and a porous lid with ~40 μm pores. Microthermoforming (17) was employed to create the microwell structure into PEOT/PBT thin polymer films as described previously (15). In short, a heated polymer film was pressed into a stainless steel mold (produced by Lightmotif BV, Enschede, The Netherlands) using polyethylene films as backing material. Molding temperature and pressure were 85°C and 45 kN, respectively. Pore geometry and architecture were characterized by scanning electron microscopy (SEM, Philips XL 30 ESEM-FEG, Eindhoven, The Netherlands). Scaffolds were gold sputter coated (Cressington, UK) prior to SEM analysis. Pore dimensions were measured in three different samples per type of scaffold at the side, rim and bottom of the microwells using ImageJ software (<http://rsb.info.nih.gov/ij/>).

Particulate leaching

To fabricate porous microwell scaffolds by particulate leaching, sodium chloride crystals were added to the polymer solution just before solvent casting. The crystals were manually grinded and sieved on an automatic shaker (sieve range 38-63 μm). Three different salt-to-polymer ratios were tested: 1:2, 1:1.5, and 1:1. After scaffold fabrication by microthermoforming, the scaffolds were leached in demi-water at 50 °C for 4 days. To assess whether residual sodium chloride crystals were present, C and O (the polymer) and Na and Cl atoms were mapped using a SEM integrated energy dispersive spectrometer (EDS, EDAX, AMETEK Materials Analysis Division, Mahwah, USA).

Pillared wafer

To fabricate porous microwell scaffolds using microfabrication techniques, silicon wafers patterned with micropillars were produced. For this purpose, a chromium-glass mask was designed for patterning photoresist on the wafers. The photomask design contained circular features to produce a grid pattern of pillars with a diameter of ~ 20 , 30 , and $40 \mu\text{m}$, spaced at $200 \mu\text{m}$. Process flow design, lithography and etching were done by ThermoFisher (ThermoFisher Scientific Inc., Enschede, The Netherlands). Briefly, single side-polished wafers (100 mm diameter, $525 \mu\text{m}$ thick) were oxidized to a thickness of $1 \mu\text{m}$. Photoresist OiR 907-17 was patterned using the abovementioned mask using an EVG[®]620 Automated Mask Alignment System (EV Group, St. Florian am Inn, Austria). The oxide masking layer was etched by a reactive ion etching (RIE) step. To form pillars of a height of $75 \mu\text{m}$, a deep RIE (DRIE) step was performed. The photoresist and passivation layer were stripped and the wafer was cleaned in a Piranha solution ($\text{H}_2\text{SO}_4 : \text{H}_2\text{O}_2 = 3:1$ (v/v)). To improve demolding of the thin PEOT/PBT films, pillared wafers were coated with trichloro(1H, 1H, 2H, 2H-perfluorooctyl)silane (Sigma Aldrich, USA). The polymer solution was cast at a height of $90 \mu\text{m}$, $15 \mu\text{m}$ above the pillars, to ensure perforation of the film during solvent evaporation and subsequent thinning of the polymer film. The porous polymer films were used for microwell scaffold fabrication.

Laser drilling

To produce porous microwell scaffolds by laser drilling, an Yb:YAG laser source (TruMicro 5050, Trumpf GmbH, Germany) with a fixed pulse duration of about 7 ps , a maximum pulse frequency of 400 kHz , and a central wavelength of 1030 nm (IR) was used. A third harmonic generation (THG) unit was applied to convert the central wavelength to 343 nm (UV), since in polymer films the absorption of laser energy at this wavelength is considerably higher than at 1030 nm and, for a lens with a given focal length, the focal spot diameter is smaller at 343 nm than at 1030 nm . The beam showed a nearly Gaussian power density profile (beam quality $M^2 < 1.3$). The radiation was linearly polarized. To manipulate the beam over the sample, a two-mirror Galvano-scanner system (Intelliscan 14, Scanlab GmbH, Germany) was used. The beam was focused to a diameter of about $10 \mu\text{m}$ by a telecentric fq-lens (Ronar, Linos GmbH, Germany) with a focal length of 100 mm . All experiments were performed in a cleanroom facility. The $\sim 15 \mu\text{m}$ thick thin polymer films were stretched on a custom-made Teflon sample holder to ensure a flat surface for laser processing. Holes with various diameters ($10 \mu\text{m}$, $20 \mu\text{m}$, $30 \mu\text{m}$, and $40 \mu\text{m}$) and spacings ($50 \mu\text{m}$, $100 \mu\text{m}$, and $200 \mu\text{m}$) were introduced into the polymer films by either percussion drilling or trepanning. A diameter of $10 \mu\text{m}$ was obtained by percussion drilling using a pulse energy (E_p) of $1 \mu\text{J}$ and 150 pulses at a pulse-repetition frequency (F_{pr}) of 10 kHz . Trepanning with a pulse energy of $1 \mu\text{J}$, a pulse-repetition frequency of 10 kHz , 2 iterations, and a beam velocity of 15 mm/s was used to cut holes with larger diameters.

Raman spectroscopy

Raman spectroscopy was used to identify whether the laser processing induced chemical modifications of the polymer. For this, a laser processed film was mounted on a CaF₂ slide (Crystran Ltd., Dorset, UK), immersed in Millipore water and covered with a cover slip. Raman measurements were performed using a custom-built confocal Raman spectrometer as described previously (18). Briefly, a krypton ion laser (Inova 90-K; Coherent, Inc) emitting at 647.1 nm at a power of 15 mW under the objective was used as an excitation source. Raman spectra of the circumference of the holes were acquired in spectral scanning mode using a 40x/0.75 NA objective (Olympus UPFLN). Raman imaging was performed by raster-scanning the laser beam over an area of 20x20 μm with a step size of 1.25 μm and an accumulation time of 0.5 s/step, while collecting a single spectrum at each step. All data manipulations were performed in routines written in MATLAB 7.6 (The MathWorks).

***In vitro* cellular migration assay**

To demonstrate the potential of the porous construct for cell infiltration, an *in vitro* cell migration assay was performed with iMSCs, an immortalized human mesenchymal stromal cell line (19). For this, HRE-GFP iMSCs (20) were seeded in a density of 3*10⁴ cells per cm² on a layer of growth factor-reduced Matrigel (diluted 1:1 in medium; BD Biosciences, The Netherlands). After cell attachment, a porous microwell scaffold, fabricated by laser-drilling (pore spacing 200 μm), was placed on the cell layer and filled with growth factor-reduced Matrigel. After 48 hours of culture, the sample was carefully washed with PBS and immersed in 4% paraformaldehyde in PBS for 30 minutes. Fixation was followed by two washing steps in PBS and a 30 minutes permeabilization step in 0.3% Triton-X 100/PBS. The sample was stained for F-Actin filaments with alexa-647-phalloidin (Invitrogen, Carlsbad, USA, 1:40, 30 min) and counterstained with DAPI (Invitrogen, USA, 1:100, 30 min). Imaging was performed using an EVOS® FL Imaging System (Invitrogen, USA).

Nutrient diffusion through microwell scaffolds

As an indicator for nutrient transport, the glucose diffusion through the porous microwell scaffolds was assessed as described previously (15, 21, 22). Briefly, the setup consisted of two double-walled compartments: a donor compartment filled with RPMI-1640 (Invitrogen, USA) containing 11.1 mM d-glucose, and an acceptor compartment containing RPMI-1640 without d-glucose (both compartments were supplemented with 100 U/ml penicillin and 10 μg/ml streptomycin (Invitrogen, USA)). The scaffolds were pre-wetted for several hours in RPMI-1640 (without d-glucose) and positioned between the two compartments. The temperature in the setup was maintained at 37°C with circulating water. At various time intervals, 80 μl samples were obtained from both compartments and analyzed for glucose concentration using a Vitros DT60 II chemistry system (Ortho-Clinical Diagnostics, USA). The diffusion coefficient D across

the scaffold can be calculated using the following equation, derived from Fick's first law of diffusion:

$$D = \frac{V_1 V_2}{V_1 + V_2} \cdot \frac{L}{A} \cdot \frac{1}{t} \cdot \ln \frac{(C_1)_0}{(C_1)_t - (C_2)_t}$$

Here, $(C_1)_0$ and $(C_1)_t$ are the initial and intermediary concentrations (at time t) of the solute in the donor compartment, respectively; $(C_2)_t$ is the intermediary concentration (at time t) of the solution in the acceptor compartment; V_1 and V_2 are the volumes in the donor and acceptor compartments, respectively; L is the thickness of the scaffold; and A is the diffusion area of the scaffold.

Animals and induction of diabetes

Fasted male BALB/c mice, 6 weeks old (Charles River Laboratories, Wilmington, MA, USA), were rendered diabetic with an intraperitoneal injection of 225mg/kg streptozotocin (Sigma Aldrich, USA), freshly dissolved in citrate buffer (pH 4.5). Blood glucose levels were measured in whole blood obtained from the tail vein using a glucose meter (Accu-Chek, Roche Diagnostics, Switzerland). Only those mice exhibiting non-fasting blood glucose levels >20 mM for two consecutive days were considered diabetic and used as transplant recipients. Animal experiments were approved by the institutional ethical committee on animal care and experimentation at the Leiden University Medical Center.

Islet isolation and scaffold seeding

Islets were isolated from male BALB/c mice weighing >28 g. Donor mice were anesthetized with isoflurane. After a midline abdominal incision, the common bile duct was cannulated and perfused with 3mL of 3mg/mL collagenase type V (Sigma Aldrich, USA) in RPMI-1640 medium (Invitrogen, USA), supplemented with 2 μ g/mL DNase I (Pulmozyme, Roche, Switzerland). The pancreas was dissected and digested at 37°C for 15 minutes. Islets were handpicked and cultured overnight in islet medium (RPMI-1640 medium (Invitrogen, USA), supplemented with 10% (v/v) heat-inactivated FCS (Bodinco, The Netherlands), penicillin/streptomycin (100 U/mL and 10 μ g/mL, respectively, Invitrogen, USA), and 2 μ g/mL DNase I (Pulmozyme, Roche, Switzerland). An islet mass of 300 islets was seeded onto the porous microwell scaffolds in islet medium. After islet seeding, scaffolds were covered with a porous 400PEOT30PBT70 polymer film containing an array of 40 μ m holes, with a 200 μ m spacing. The porous cover was attached to the scaffold with three 6-0 silk sutures (Ethicon, UK).

Islet transplantation

Prior to isoflurane anesthetics, mice were given 0.1 mg/kg buprenorfin (Temgesic, Schering-Plough, Belgium). For the scaffold and the non-scaffold control group, the epididymal fat was identified with a midline lower abdominal incision. Microwell scaffolds were inserted between

the epididymal fat and peritoneum, with the lid of the construct facing the epididymal fat. For the non-scaffold group, the marginal islet mass of 300 islets was delivered in the epididymal fat using a Hamilton syringe (Hamilton, USA) and siliconized polyethylene tubing (PE50, Becton Dickinson, USA) with Sigmacote (Sigma Aldrich, Germany). A second control group included animals, according to the gold standard, receiving 300 islets underneath the kidney capsule. For this, a small incision was made in the flank of the mouse which gave access to the kidney. Islets were injected underneath the kidney capsule using the Hamilton syringe and siliconized polyethylene tubing as described elsewhere (23). After transplantation, the peritoneum and skin were closed and the animals were allowed to recover under a warm lamp. Blood glucose levels were measured in whole blood from the tail vein three times a week. Mice were considered normoglycemic when blood glucose levels were consistently less than 12 mM. Four weeks after transplantation, the mice were sacrificed and the grafts were retrieved for histological analysis. Two animals that received grafts underneath the kidney capsule underwent nephrectomy to confirm that normoglycemia after transplantation was graft dependent.

Intraperitoneal glucose tolerance testing

For metabolic assessment, intraperitoneal glucose tolerance tests (IPGTTs) were performed two and four weeks after transplantation. In overnight-fasted mice, blood glucose levels were measured before and 15, 30, 60, and 120 minutes after intraperitoneal injection of 2g/kg glucose solution.

Tissue collection and immunohistochemistry

Histological analyses were performed to compare the morphology and architecture of the transplanted islets compared to those of islets within pancreata from healthy mice. Grafts or pancreata from healthy control mice were immersed in 4% paraformaldehyde in PBS overnight at 4°C and prepared for paraffin embedding. Each graft or pancreas was completely sectioned in eight-micrometer slices. To identify islet-containing regions, sections spaced 160 µm apart were stained for insulin combined with a Masson-Goldner trichrome staining (Merck Chemicals, Darmstadt, Germany). Sections were immunostained with rabbit anti-insulin IgG (Santa Cruz Biotechnology, Santa Cruz, CA, USA, 1:400) for 1 hour followed by an HRP-conjugated secondary antibody (DAKO, Glostrup, Denmark, 1:100) for 1 hour. Sections were developed with DAB liquid chromogen system (DAKO, Belgium) and counterstained with hematoxylin and Masson-Goldner trichrome staining according to manufacturer's protocol. Slides were imaged using a Nanozoomer slide scanner 2.0 RS (Hamamatsu, Hamamatsu City, Japan).

Consecutive slides from two to three levels were randomly selected from islet-containing regions and immunostained for either insulin and glucagon, or insulin and CD31, to determine cellular composition and distribution, as well as the vascular density within the islets. Per islet transplant and control pancreas at least 30 islets were analyzed. Prior to staining, heat-mediated antigen retrieval (pressure cooker, 80°C, 30 min) was performed in sodium citrate buffer (pH 6.0). For blocking normal goat serum, normal donkey serum, and a biotin/avidin blocking kit

(Vector, USA) were applied. Primary antibodies used were guinea pig-anti-insulin (Abcam, Cambridge, MA, USA, 1:200, 1.5h), rabbit-anti-glucagon (Vector Laboratories, Burlingame, CA, 1:100, o/n) and rabbit-anti-CD31 (Abcam, Cambridge, MA, USA, 1:20, o/n) were used. Secondary antibodies were Alexa-647-anti-guinea pig (Invitrogen Life Technologies, Paisley, UK, 1:500, 2h), biotin-SP-conjugated anti-rabbit (Jackson ImmunoResearch, West Grove, USA, 1:200, 1h), and Alexa-488-SA (Invitrogen Life Technologies, Paisley, UK, 1:200, 1h). DAPI (Invitrogen Life Technologies, Paisley, UK) was applied as nuclear counterstaining. Sections were examined using a BD Pathway 435 system (BD BioSciences, San Jose, CA, USA) with a custom designed macro (ImageJ software (<http://rsb.info.nih.gov/ij/>)).

Morphometric analysis

Custom-written ImageJ/Fiji (<http://rsb.info.nih.gov/ij/>) macros were used for morphometric analysis of histological parameters. To determine the vascular density per islet area, images were pre-processed by subtracting background signal and enhancing local contrast and converted to 8-bit images. The outline of the islets and vessels were semi-automatically delineated using several thresholding algorithms. The position of the blood vessel within the islets was determined by normalizing the distance between the center of the islet and the center of the blood vessel to the distance between the center of the islet and the boundary of the islet along the same radial vector. Thus, the position of the blood vessel was expressed as a value between 0 and 1 with 0 representing the center of the islet and 1 the boundary of the islet. Also for the characterization of cellular composition, images were pre-processed by subtracting background signal and enhancing local contrast and converted to 8-bit images. The insulin and glucagon positive regions were semi-automatically delineated based on the individual images using several thresholding algorithms, whereas the outline of the islet was determined based on a merged image of both stainings. The DAPI image was segmented using Adjustable Watershed to obtain masks for individual cells. The insulin and glucagon selections were used to determine whether the cells were negative or positive for the hormones. As for the blood vessels, the position of the individual cells was represented by normalizing the distance between the center of the islet and the nuclei to the distance between the center of the islet and the boundary of the islet. Data were processed and analyzed using R (24), GraphPad Prism (La Jolla, CA, USA), and SPSS version 22 (SPSS, Chicago, IL, USA).

Statistics

Statistical analyses were performed using SPSS version 22 (SPSS, Chicago, IL, USA). The results were presented as mean \pm standard error of the mean (SEM). Time to remission, defined as the number of days required to re-establish blood glucose levels consistently lower than 12 mM, was evaluated by Kaplan-Meier survival analysis with the log-rank test comparison. The Kruskal-Wallis test was used for multiple group comparisons ($p < 0.05$, corrected for multiple comparisons) and paired comparisons by means of the Mann-Whitney U test were performed as post-hoc test in case the Kruskal-Wallis test indicated significant differences.

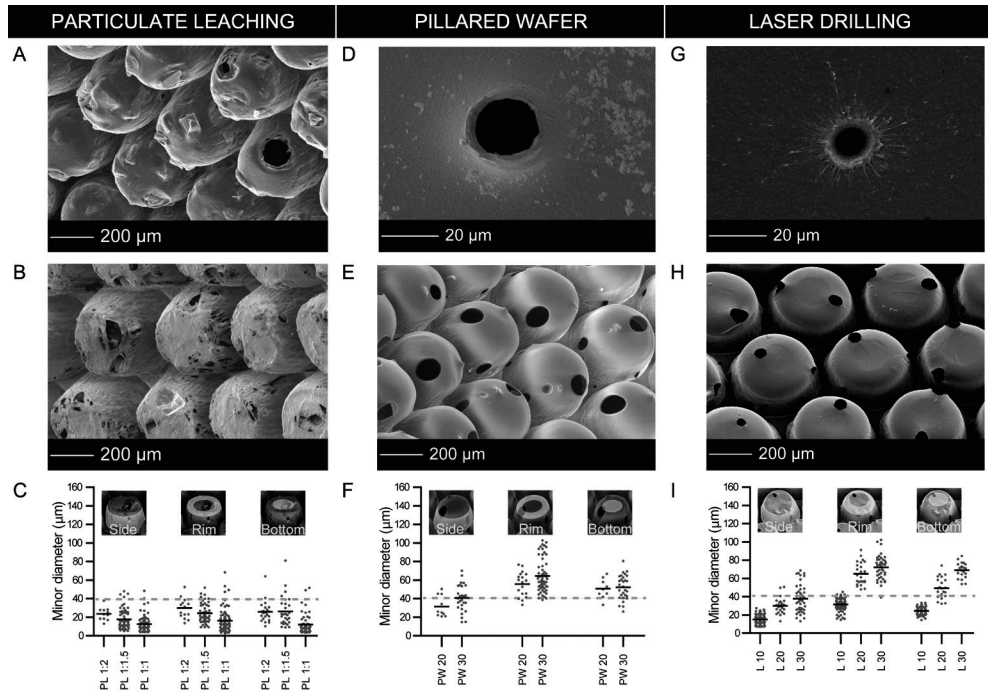


Figure 1. Characterization of pore formation in microwell scaffolds. (A-B) SEM images of microwell scaffolds fabricated by a combination of solvent casting of particulate-loaded polymer films, microthermoforming of the casted films and particulate leaching before (A) and after (B) leaching. C) Pore-size measurements at the side, rim and bottom of the microwells with pores introduced by particulate leaching. Three different concentrations are analyzed (sodium chloride : polymer ratios of 1:2, 1:1.5, and 1:1). D) Representative SEM image of a pore with a diameter of 20 μm fabricated by solvent casting of a film over a wafer with micropillar arrays. E) SEM image of a microwell scaffold fabricated by a combination of solvent casting of a film over a wafer with 20 μm diameter pillars, and microthermoforming of the porous film. F) Pore-size measurements at the side, rim and bottom of the microwells with pores introduced by solvent casting over wafers with pillars having a diameter of 20 and 30 μm . G) Representative SEM image of a pore with a diameter of 10 μm fabricated by laser drilling into a film. H) SEM image of a microwell scaffold fabricated by a combination of laser drilling of 10 μm diameter holes into a film, and microthermoforming of the porous film. I) Pore-size measurements at the side, rim and bottom of the microwells with pores introduced by laser drilling of holes with diameters of 10, 20, and 30 μm .

RESULTS

Comparison of different fabrication methods for porous microwell scaffolds

Three different fabrication methods were compared to obtain both porous microwell scaffolds and porous lids with a maximum pore diameter of 40 μm . Methods were evaluated for pore size and geometry, reproducibility and flexibility, and the form and stability of the final construct. The first method consists of a solvent-casting and particulate leaching technique (Supplemental

Figure 1). After microthermoforming, sodium chloride crystals could clearly be observed distributed throughout the microwell scaffold in a random manner (Figure 1A). Crystals were efficiently removed (Figure 1B) by dissolution as confirmed by EDX analysis (Supplemental Figure 2), which resulted in porous constructs. The porosity could be controlled by increasing the salt-to-polymer ratio, resulting in a concomitant increase in the diffusion coefficient (Table 1). Although high porosities were obtained using this method, the average pore diameter was small (18.3 μm) (Figure 1C), and control over pore size and distribution was limited, as reflected by the large pore size distribution range (5–65 μm). Furthermore, the shape of the microwells was irregular and rough, with a large variation throughout the entire construct.

The second technique used involved casting of the PEOT/PBT polymer solution on a patterned silicon wafer comprising small pillars (Supplemental Figure 1, Supplemental Figure 3). The method was optimized by varying the pillar diameter with a constant pillar spacing of 200 μm (Supplemental Figure 3). A minimum film thickness of 15 μm was needed for stable microwell thermoforming, requiring a pillar height of 75 μm to ensure this film was perforated during solvent evaporation. To achieve this height, the minimum pillar diameter that had sufficient mechanical properties was found to be 20 μm . This resulted in final pore sizes ranging from 20 μm at the side of the microwells to 85 μm at the rim, exceeding our stated upper limit of 40 μm (Figure 1F). Compared to particulate leaching, the pore geometry and spatial distribution

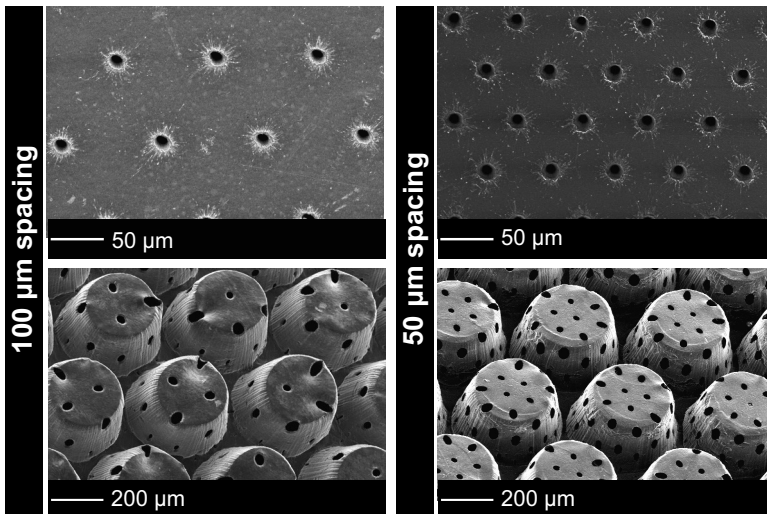


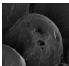
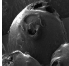

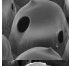
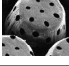
Figure 2. Increased pore density in laser-drilled microwell scaffolds. Representative SEM images of porous polymer films and microwell scaffolds with a pore diameter of 10 μm and a distance of 100 μm (left panel) and 50 μm (right panel) fabricated by a combination of laser drilling and microthermoforming.

were found to be very uniform (Figure 1D-E). However, material properties of the mold and the associated pillar strength limited the minimum pore dimension that could be obtained.

The third method we investigated was laser drilling using an ultra-short pulsed laser source (Supplemental Figure 1). The main advantage of this technique is its flexibility compared to the other techniques; the pore size can be easily adapted in a highly reproducible and controllable manner, resulting in a very defined pore size distribution. After laser drilling, a small heat affected zone (HAZ) was observed around each pore (Figure 1G-H). Spectroscopic analysis of the HAZ using a confocal Raman microscope found no significant differences between Raman spectra of the HAZ and unprocessed polymer film, indicating that the molecular composition of the polymer was not changed (Supplemental Figure 4D). The smallest pore diameter that could be obtained with this technique was 10 μm , which resulted after microthermoforming in an average pore size below 40 μm , varying between 10 μm at the side of the microwells and 40 μm at the rim (Figure 1I). By reducing the pore spacing, we found that the highest feasible pore density that did not adversely affect microwell morphology was an orthogonally stacked pore pattern with a spacing of 50 μm (Figure 2). This porosity resulted in a glucose diffusion coefficient of $20.0 \cdot 10^{-7} \pm 2.4 \cdot 10^{-7} \text{ cm}^2/\text{s}$, a four-fold increase compared to the glucose diffusion coefficient of pillared-wafer scaffolds and approaching the coefficient that could be obtained with the particulate leaching technique (Table 1).

Light-microscopy and SEM analysis of scaffold-seeded islets confirmed the laser pores were small enough to entrap islets in the microwells (Supplemental Figure 5A-C). To analyse whether the porous structures allow cell infiltration, an *in vitro* migration assay was performed. For this, laser-drilled scaffolds were filled with Matrigel and placed on a layer of iMSCs seeded on Matrigel. Upon culturing hMSCs successfully penetrated and bridged the pores indicating its potential for cell infiltration (Supplemental Figure 5D-E).

Table 1. Diffusion coefficients of glucose through porous microwell scaffolds in medium at 37°C.

Condition		Diffusion coefficient ($10^{-7} \text{ cm}^2/\text{s}$)
Particulate-leaching 1:2		5.5 \pm 0.4
Particulate-leaching 1:1.5		11.8 \pm 1.5
Particulate-leaching 1:1		32.4 \pm 7.2
PW \varnothing 20 μm \leftrightarrow 200 μm		4.8 \pm 0.2
Laser \varnothing 10 μm \leftrightarrow 50 μm		20.0 \pm 2.4

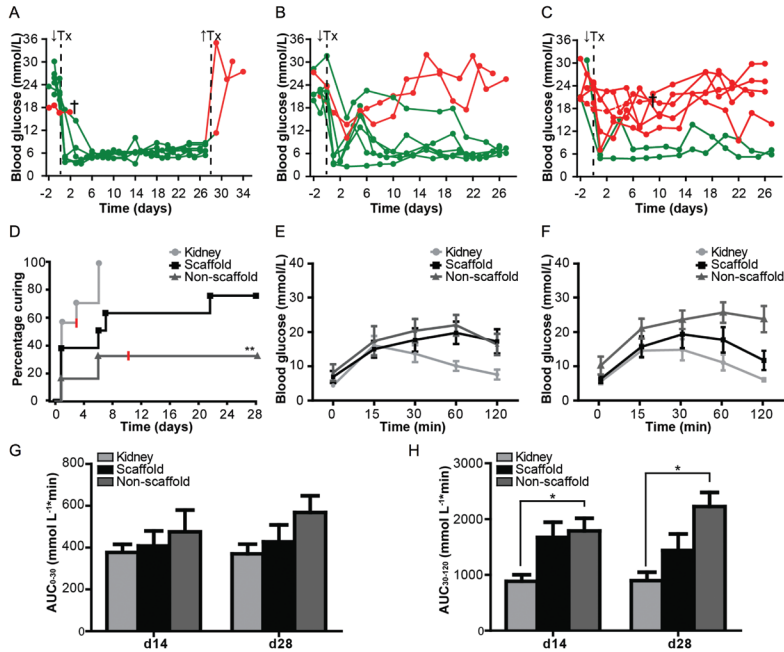


Figure 3. Blood glucose levels and glucose tolerance tests after islet transplantation. (A-C) Non-fasting blood glucose levels of diabetic male BALB/C mice that were transplanted at d0 with 300 islets underneath the kidney capsule ($n=7$) (A), in the scaffold in the epididymal fat pad ($n=8$) (B), or in the epididymal fat pad without a scaffold ($n=8$) (C). Green lines represent animals that were cured during the observed period (stable blood glucose values < 12 mmol/L). Two mice died from diabetes complications. In two mice with renal subcapsular islet transplants, a nephrectomy was performed. Both mice reverted to a state of hyperglycemia after graft removal, indicating that the islet grafts were responsible for sustaining normoglycemia. D) Kaplan–Meier analysis of animals receiving transplants of 300 islets underneath the kidney capsule, in the scaffold in the epididymal fat pad, or in the epididymal fat pad without a scaffold. Percentage of curing was determined by the percentage of animals with stable blood glucose levels of < 12 mmol/L. The two mice that died are represented in red. ** $P < 0.01$ non-scaffold group vs. renal subcapsular control. At day 14 (E) and day 28 (F) posttransplant, an intraperitoneal glucose tolerance test (IPGTT) was performed for grafts underneath the kidney capsule ($n=6$), in the scaffold ($n=8$), and in the epididymal fat pad without a scaffold ($n=7$). The early (G) and late (H) phase response of the grafts was analyzed by determining the area under the curve (AUC) at 0–30 minutes and 30–120 minutes. The response of islet grafts in the epididymal fat pad was delayed when no scaffold was employed. * < 0.05 by Mann-Whitney U test.

Porous microwell scaffolds support extrahepatic islet transplantation

To further assess the potential of the laser-drilled porous microwell scaffold platform to assist extrahepatic islet engraftment, constructs were seeded with islets, covered with a flat porous thin-film lid with $40 \mu\text{m}$ pores and transplanted into a diabetic mouse model for 28 days. When islets were transplanted in the scaffold, six out of eight animals (75%) reverted to stable normoglycemia, with a mean time to remission of 6.2 ± 3.2 days (Figure 3A-B).

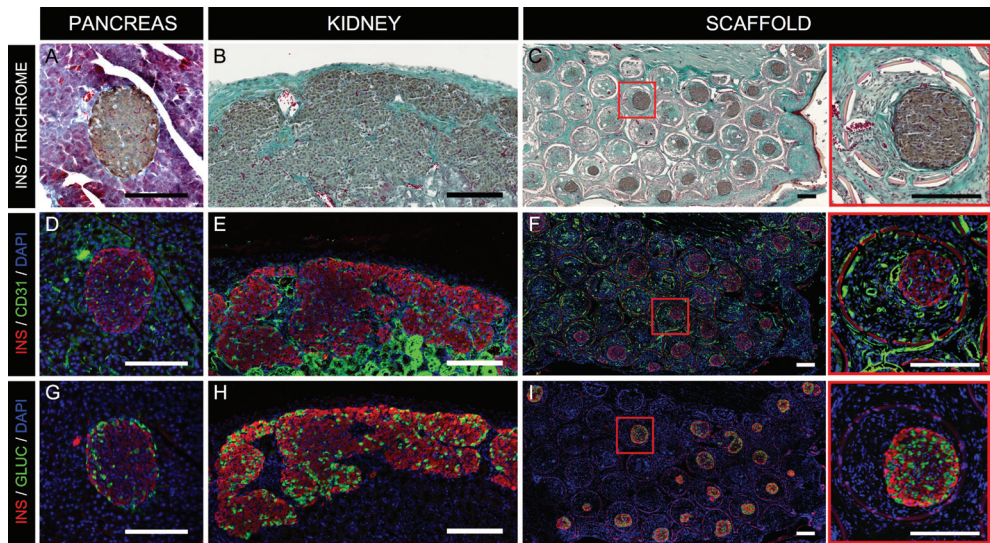


Figure 4. Histological evaluation of islet transplants compared to native pancreatic islets. (A-C) Representative Masson's trichrome stainings combined with an immunostaining for insulin of native pancreatic islets (A), islets transplanted underneath the kidney capsule (B), and islet transplanted in the microwell scaffold (C). Graft revascularization and hormone expression were assessed with CD31 (D-F), insulin, and glucagon (G-I) immunofluorescent stainings. When islets were implanted in the epididymal fat without a microwell scaffold, islet grafts could not be retrieved successfully, likely due to islet migration or loss. Scale bars are 200 μm .

Although reversal time in the scaffold group was longer compared to the kidney control (2.2 ± 0.83 days) (Figure 3A-B), pairwise comparisons of the Kaplan-Meier curves indicated no significant difference between the two groups ($p=0.093$) (Figure 3D). In marked contrast, in the non-scaffold group 71% of the mice failed to restore blood glucose levels to normal values. The time to normoglycemia for the non-scaffold group was significantly longer compared to the kidney capsule control ($p<0.01$) (Figure 3A,C-D). Pairwise comparison with the scaffold group did not reveal a significant difference ($p=0.068$) (Figure 3B-D). The body weight of all recipients increased following islet transplantation, indicating an overall improvement in the metabolic state (data not shown). In two mice with an islet transplant underneath the kidney capsule, a nephrectomy was performed. Both mice reverted to a state of hyperglycemia after graft removal, indicating that the islet grafts were responsible for sustaining normoglycemia (Figure 3A). The function of the islet grafts was examined further with intraperitoneal glucose tolerance tests (IPGTTs) two and four weeks post-transplantation (Figure 3E-F). Two weeks after transplantation, baseline fasting glucose levels were similar between the groups. When islets were transplanted in the epididymal fat, either with or without a scaffold, glucose levels were elevated during IPGTT, with a peak at 60 minutes compared to 15 minutes for renal subcapsular controls. Four weeks after implantation, the response of scaffold-implanted islets was improved

reaching a peak at 30 minutes, which was comparable to renal subcapsular islet grafts. However, when islets were implanted in the epididymal fat without a scaffold, glucose levels remained elevated following exogenous glucose administration, with a peak-value at 60 minutes. Analysis of early ($AUC_{(0-30\text{min})}$) and late-phase ($AUC_{(30-120\text{min})}$) response showed a significant delay in late-phase response at both time points when islets were implanted in the epididymal fat without a scaffold compared to subcapsular control islets, this in contrast to scaffold-implanted islet grafts (Figure 3 G-H).

Porous microwell scaffolds allow vascular ingrowth

Histological assessment showed viable islets within porous microwell scaffolds four weeks after transplantation (Figure 4). Scaffolds were filled with granulation tissue and perfused vascular structures infiltrated the islet graft through the porous structure, indicating the formation of a functional vascular network within the islets (Figure 4C). Unfortunately, we were unable to locate islet grafts for histological evaluation when islets were implanted in the epididymal fat without a scaffold. To assess vascular density and distribution, CD31 positive structures were identified within the islet grafts (Figure 4D-F, Figure 5). Vascular density within renal subcapsular and scaffold-implanted islets was similar and comparable to native pancreatic islets (Figure 5D). The distribution of vessels within scaffold-implanted islets was found to be anisotropic, with a higher vascular density in the outer shell compared to the inner core (1830 ± 68 vessels/ mm^2 vs. 924 ± 87 vessels/ mm^2) (Figure 5F). This is in contrast to subcapsular islet grafts that show a homogeneous vessel distribution within the islets; a pattern similar to native pancreatic islets (Figure 5F).

Islet area and cellular composition

To address whether islet area and composition changed after transplantation, the islet area and the density of both beta- and alpha-cells were determined (Figure 6A-D). Islets transplanted in the microwell scaffold maintained their rounded morphology and islet size did not significantly differ from native islets (Figure 6E and Supplemental Figure 6). In contrast, islets transplanted underneath the kidney capsule showed some degree of aggregation and fusion increasing the islet size compared to pancreatic islets ($p < 0.01$) (Figure 6E, Supplemental Figure 6). Although the morphology of scaffold-implanted islets was maintained, cellular density within the islets was significantly decreased compared to native islets (pancreas 10251.5 ± 328.0 cells/ mm^2 vs. scaffold 8630.5 ± 211.9 cells/ mm^2 , $p < 0.01$), with the most pronounced decrease in the core of the islets (Figure 6F). This decrease was mainly attributed to a reduction in beta-cells (pancreas 6531.4 ± 87.5 cells/ mm^2 vs. scaffold 4107.2 ± 116.5 cells/ mm^2 , $p < 0.01$), whereas the alpha-cell density slightly, but not significantly, increased (pancreas 979.1 ± 157.1 cells/ mm^2 vs. scaffold 1382.4 ± 101.9 cells/ mm^2 , $p = 0.073$) (Figure 6G). Although renal subcapsular islet grafts exhibited a higher beta-cell density compared to scaffold-implanted islets (kidney capsule 5324.6 ± 365.6

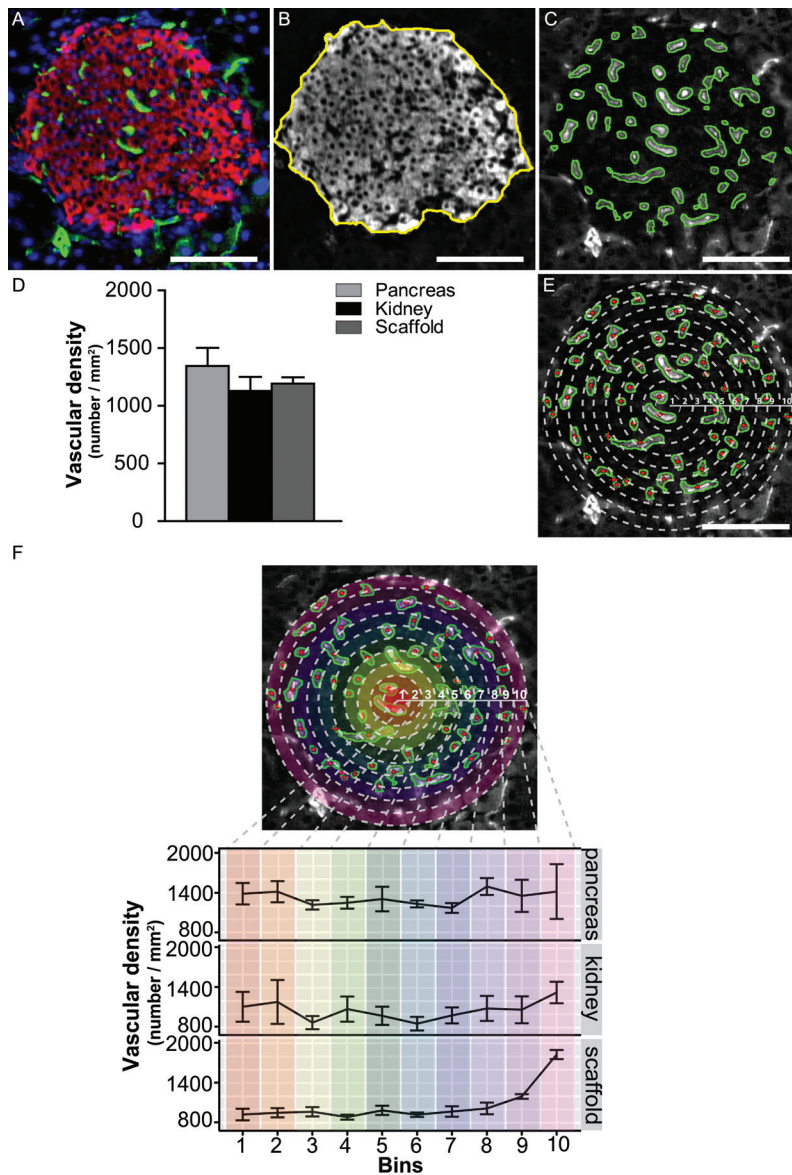


Figure 5. Quantitative analysis of islet vascular density and spatial distribution. Vascular density (D) was assessed by quantifying segmented blood vessels (C) within the insulin positive area (B). The center of mass of the blood vessels was determined (E) and their position relative to the center of the islet was calculated (F) to provide the vascular spatial distribution within the islet. Scale bars are 100 μ m.

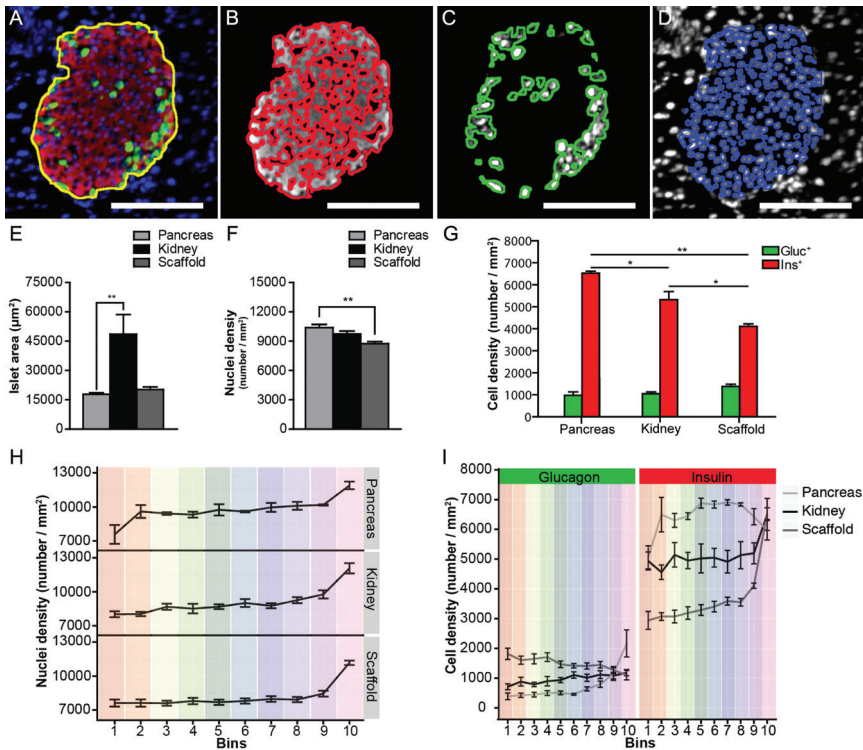


Figure 6. Endocrine cell mass and islet architecture. The islet area (F) was determined based on the composite image of insulin and glucagon (A). For quantitative assessment of the cellular density (G) and the endocrine cell mass (H), insulin- and/or glucagon-positive, and insulin/glucagon-negative cells (E) were determined by segmenting the insulin (B), glucagon (C), and DAPI (D) images. The islet architecture was further assessed by analyzing the position of the nuclei (I) and the different cell types (J) within the islets. Scale bars are 100 μm . * $<0,05$ and ** $<0,01$ by Mann-Whitney U test

vs. scaffold 1382.4 ± 101.9 , $p < 0.05$), this density was significantly lower compared to native islets (pancreas 6531.4 ± 87.5 cells/ mm^2 vs. kidney capsule 5324.6 ± 365.6 cells/ mm^2 , $p < 0.05$).

A distinct core-mantle structure was found in native islets, reflected by a higher alpha-cell density in the islet's outer shell compared to the central core (shell 2168.0 ± 454.6 cells/ mm^2 vs. core 319.3 ± 108.5 cells/ mm^2) (Figure 6H); characteristic for rodent islets (25). Remarkably, this core-mantle structure was disrupted in both the scaffold-implanted and renal subcapsular islet grafts, presenting a more homogeneous distribution of alpha-cells throughout the islets and a reduction in the beta-cell density (Figure 6H-I).

DISCUSSION

This study shows that with our microwell scaffold platform extrahepatic islet transplantation becomes a viable option. In a diabetic mouse model, we achieved glycemic control that approaches the gold standard of renal subcapsular islet grafts. The microwell structure prevents islet aggregation, ensuring maintenance of the native rounded morphology and islet size. Meanwhile, the highly controlled pore size and pore distribution not only guarantees islet retention in the construct, but also allows mass transfer of metabolites and ingrowth of blood vessels, resulting in an intra-islet vascular density that is comparable to native islets.

Creating microwells with an appropriate size and distribution allows us to sequester and retain islets while limiting islet aggregation and fusion. When islets are cultured or transplanted in high density without physical separation, islets fuse in large clusters (26); this is observed for islets implanted underneath the kidney capsule (Figure 5B). As an increase in islet size is associated with more abundant apoptosis and necrosis (27–29) and with compromised *in vivo* performance (28, 29), this is desirable to avoid. Previously reported porous sponges designed for islet transplantation can prevent mass fusion to some degree, but these constructs have poor control over islet spacing, distribution and density (30–38) and can still enable islets to aggregate and coalesce. The unique aspect of microthermoforming is that it enables the reproducible creation of microwell structures with a designed shape, size, and distribution that not only limit islet aggregation, but also recreate the islet density found in human pancreatic tissue (39, 40).

The renal subcapsular site, as the gold standard for islet transplantation in pre-clinical mouse models, offers the advantage of a confined environment for islet retention and engraftment. Many clinically relevant sites currently considered, such as the omentum (38, 41) and the intraperitoneal fat (36), are unable to appropriately confine islets. At these sites, better glycemic control can be achieved in diabetic animals when scaffolds are used to spatially stabilize the islets. Success of these implants, however, largely depends on the degree of islet retention and the efficiency of islet revascularization (42). Previous scaffold designs attempted to achieve high rates of vascularization by providing large pores, varying from ~250–600 μm , open for tissue infiltration. However, since islet themselves have diameters ranging from ~50 to 400 μm (43), these scaffolds are intrinsically prone to islet loss; this has been specifically reported for islets smaller than 100 μm in diameter (38), a typical size for human islet preparations (43). To improve islet retention, hydrogels have been used as a seeding matrix in concert with large-pored solid scaffolds (30, 37, 44). Although hydrogels are able to sustain islet retention and prevent islet aggregation, vessel invasion is often limited by the rate of cell-mediated degradation due to the small mesh size of the crosslinked network (45, 46).

Our islet carrier platform is the first to employ a pore size that ranges from 10 to 40 μm , stimulating nutrient diffusion and vascular ingrowth through these well-defined pores while still providing high retention of islets. Not only has pore dimension been shown to promote

vascularization by passively permitting cell infiltration, but it can also play an active role in the stimulation of vascularized tissue formation (14). Interestingly, implants with 30–40 μm pores elicit a response with minimal fibrous encapsulation and maximal vascularization compared to constructs with smaller or larger pores (14). Although the exact mechanisms, which underlie this observed response, remain largely unknown, it is hypothesized that pore size influences macrophage polarity initiating the transition from M1 to M2 phenotype and, by this, promotes constructive tissue remodeling (47). Specific to our platform, the laser drilling method for pore fabrication is amenable to further optimization of pore size and distribution and holds great potential for developing a construct that can tune the host tissue response to maximize vascularization and subsequent islet engraftment.

In this study, we demonstrate that the microwell scaffold makes the epididymal fat a viable option for islet transplantation, with performance that is approaching the gold standard and in contrast to the poor outcome transplanting islet in the epididymal fat without the scaffold platform. Consistent with previous studies (30, 31, 33), the epididymal fat pad was selected as the site of implantation due to its surgical accessibility, vascularization, and structural similarity to the greater omentum, a potential extrahepatic transplantation site in humans (48). Furthermore, we obtain similar functional results using significantly fewer islets in comparison to the only other report on scaffold-aided islet transplantation in the epididymal fat of BALB/C mice (30), further highlighting the effectiveness of our strategy.

To the best of our knowledge, we are the first to directly compare the intra-islet vascular and cellular density and distribution of native pancreatic islets to both scaffold-engrafted islets and renal subcapsular-transplanted islets. We have shown that islets in our scaffold achieve a vascular density similar to subcapsular grafts and native pancreatic islets, although we observe differences in vascular distribution. Blood vessels in scaffold-implanted islets are preferentially located in the islet periphery while a homogeneous distribution is observed in both renal-transplanted and native islets. Corresponding to this vascularization pattern, we observe a decrease in cellular density in the islet core, possibly indicating hypoxia-induced cell death. We have shown that the diffusion coefficient of the scaffold ($20.0 \times 10^{-7} \pm 2.4 \times 10^{-7} \text{ cm}^2/\text{s}$) is comparable to that of fibrous tissue such as dura mater ($\sim 25.9 \times 10^{-7} \text{ cm}^2/\text{s}$) (49) and human sclera ($\sim 34.5 \times 10^{-7} \text{ cm}^2/\text{s}$) (50), but the scaffold likely imposes an additional barrier for vascular ingrowth which would expose islets to an avascular, hypoxic environment for a longer period of time. Although hypoxia enhances VEGF expression and secretion from islet cells (51), thereby inducing revascularization, prolonged hypoxic exposure has been shown to result in central core necrosis (27). This cell loss would translate to a decrease in VEGF production in the islet core, reinforcing a superficial revascularization pattern. Supporting this hypothesis is a report on similar changes in vascularization observed in Rip-Cre;VEGF^{fl/fl} islets, where VEGF-A expression occurs only in the islet perimeter (52). Therefore, we speculate that the observed change in vascularization pattern is a result of oxygen-gradient dependent cell death and a concomitant reduction in expression of proangiogenic factors, such as VEGF, due to delayed engraftment.

Islets transplanted within our scaffold platform are able to maintain a viable beta-cell population and, as a result, restore systemic glycemic control. However, we do observe a significant decrease in the beta-cell population after islet transplantation. The finding of a preferential decrease in beta-cell density compared to alpha-cell density might be attributed to a combination of the core-mantle structure of rodent islets, with beta-cells in the core and alpha-cells in the periphery (53), and the higher susceptibility of beta-cells to hypoxia compared to alpha-cells (54). Interestingly, we also detect more glucagon positive cells within the core of transplanted islets compared to native pancreatic islets. Possible explanations for this observation could be cellular rearrangement after cell death in the inner core or a reduced expression of cell adhesion molecules, such as N-CAM; heterozygote and null mutant mice for NCAM show infiltrating alpha-cells into the islet core (55). Alternatively, the conversion of beta-cells into alpha-cells could explain the increased presence of alpha cells in the islet core. Beta-cell to alpha-cell conversion has recently been shown to occur after beta-cell degranulation (56) and is associated with hyperglycemic and oxidative stress (57, 58). Further research is necessary to identify the underlying cause of this observation and the implications it has for islet functionality.

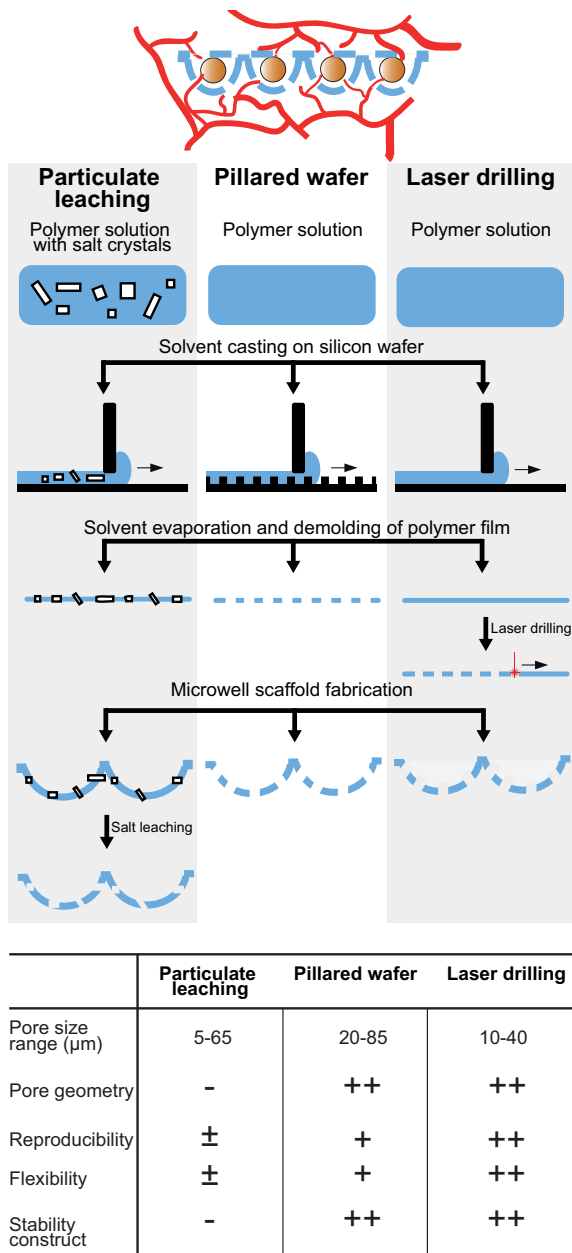
The current study presents a microwell scaffold as a suitable carrier for islets at extrahepatic sites, providing a promising alternative to intrahepatic transplantation. The approach of thermoformed microwells fabrication combined with laser-drilled micropores results in a highly flexibly and tunable platform. Possible avenues for further optimization should focus on approaches which allay hypoxia during the early engraftment period, such as the use of oxygen-generating biomaterials (59) or the incorporation of ECM molecules (34, 35, 60) or growth factors (37, 44) within the scaffold to expedite vascularization. A simple means of optimization, intrinsic to this system, is the further tuning of micropore size and distribution so as to elicit a predominant M2 macrophage phenotype. Not only will this result in an optimal loose fibrous capsule for fast and effective vessel infiltration (14), but also promote beta-cell regeneration (61). As the current study has shown, the microwell scaffold platform facilitates detailed analysis at a subcellular level to substantiate functional physiological observations. This makes the microwell scaffold not only a potential platform for extrahepatic islet transplantation, but also a suitable candidate to thoroughly study the effect of different strategies on islet function and survival during the early engraftment period.

ACKNOWLEDGEMENTS

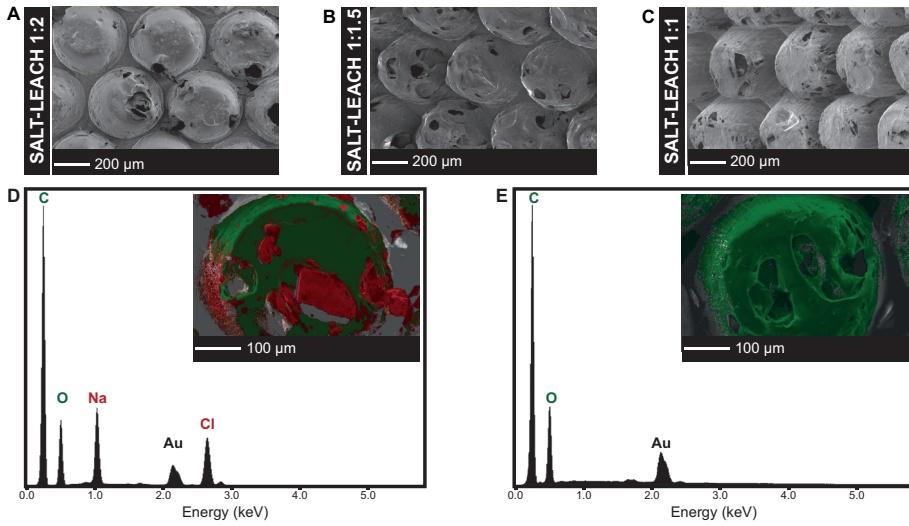
This project was financially supported by the Diabetes Cell Therapy Initiative (DCTI) including the Dutch Diabetes Research Foundation (DF). The authors thank H.A.M Töns and dr. J.H. Ellenbroek from the department of Nephrology (Leiden University Medical Center, Leiden, The Netherlands) for their assistance in islet isolation and handpicking, Ing. G.H.P. Eberink from the department of Mechanical Automation (University of Twente, Enschede, The Netherlands)

for his technical assistance in laser drilling, Z. Tahmasebi Birgani from the department of Tissue Regeneration (University of Twente, Enschede, The Netherlands) for her technical support with the EDAX analysis, Prof.dr. D. Stamatialis, department of Biomaterials Science and Technology (University of Twente, Enschede, The Netherlands) for his scientific support regarding the glucose diffusion experiments, and Prof.dr. J. van der Palen, Department of Research Methodology, Measurement and Data Analysis, Faculty of Behavioral Science (University of Twente, Enschede, The Netherlands) for his assistance regarding the statistical analysis of the data.

SUPPLEMENTAL MATERIAL

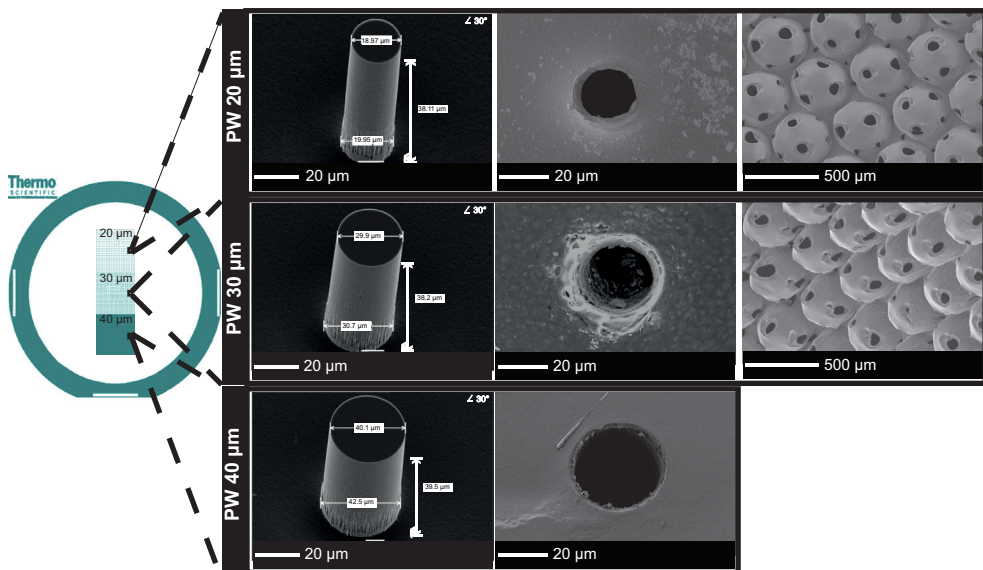


Supplemental figure 1. Schematic representation of the three process sequences based on substrate modification and replication by (micro)thermoforming (SMART) in conjunction with 1) particulate leaching using salt crystals; 2) solvent casting on patterned silicon wafers; and 3) laser drilling using an ultra-short pulsed laser source.

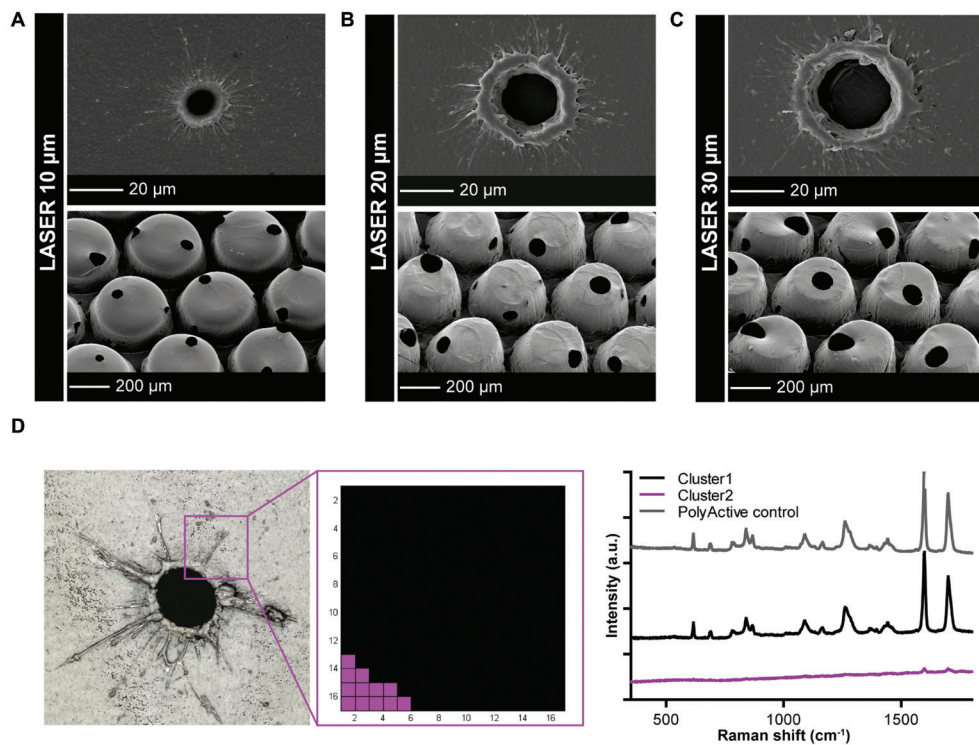


3

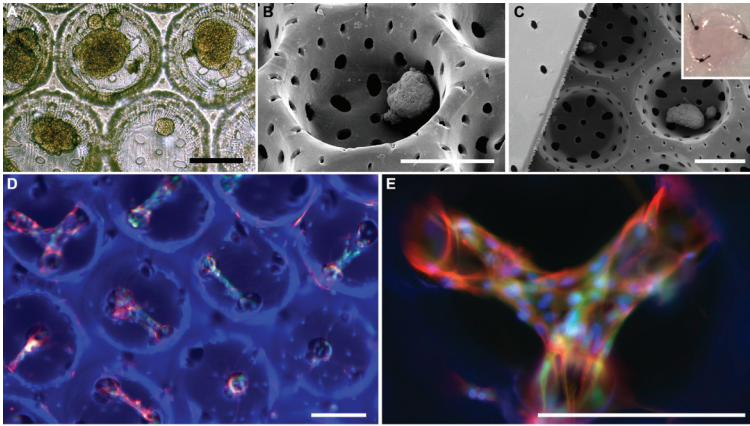
Supplemental figure 2. Porous microwell scaffolds fabricated by a combination of microthermoforming and particulate leaching. (A-C) Representative SEM images of microwell scaffolds fabricated using different polymer-to-sodium-chloride ratios (1:2, 1:1.5, and 1:1). EDX analysis was performed to analyze the presence of sodium chloride particles before (D) and after (E) leaching.



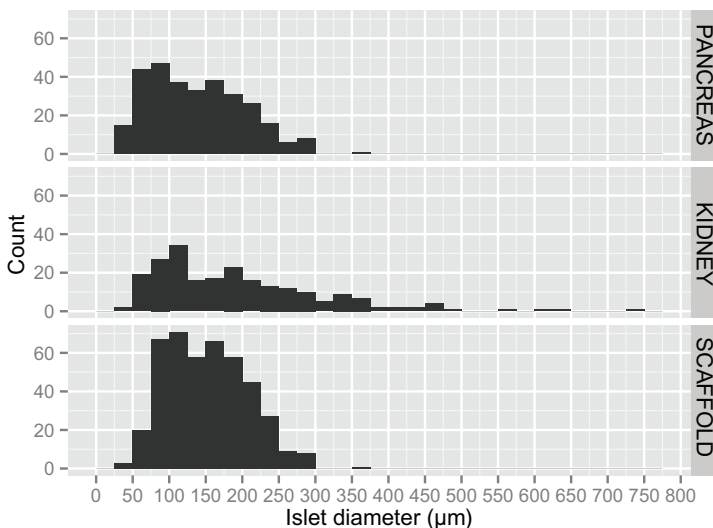
Supplemental figure 3. Porous microwell scaffolds fabricated by a combination of solvent casting on wafers with micropillars, and microthermoforming. Three different pillar diameters were assessed: 20, 30 and 40 μm . The obtained height of the pillars was $\sim 76 \mu\text{m}$ (correcting for the angle). The latter diameter was assessed to determine whether it would be possible to use this technique to obtain porous polymer films for the lid of the construct.



Supplemental figure 4. Porous microwell scaffolds fabricated by laser drilling. A-C Representative SEM images of porous films and microwell scaffolds with different pore dimensions (10, 20, 30 μm). To analyze whether the polymer composition changed due to laser processing, the head affected zone around the hole was analyzed with confocal RAMAN spectroscopy and compared to unprocessed polymer film. There were no shifts in the RAMAN spectrum observed, which would be indicative for a change in chemical composition of the polymer.



Supplemental figure 5. Light-microscopy (A) and SEM (B-C) images of islets seeded in the porous microwell scaffold fabricated by a combination of laser drilling and microthermoforming. The insert in (C) demonstrates the construct with the porous lid with 40 μm pores sutured to the patterned scaffold. D-E Representative images of the migration assay through porous microwell scaffolds fabricated by laser drilling. A porous scaffold with a pore spacing of 200 μm was placed on a monolayer of HRE-GFP iMSCs on Matrigel and filled with a layer of Matrigel. Migration of the iMSCs was clearly observed after 48h (D). Immunofluorescent analysis of F-actin filaments (red) (D-E) shows the formation of cellular ingrowth into the microwells through the pores. Scale bars are 200 μm .



Supplemental figure 6. Size-frequency distribution of islets in the native pancreas and transplanted underneath the kidney capsule and in the microwell scaffold.

REFERENCES

1. Shapiro AM et al. (2006) International trial of the Edmonton protocol for islet transplantation. *N Engl J Med* 355:1318–1330.
2. Barton FB et al. (2012) Improvement in outcomes of clinical islet transplantation: 1999–2010. *Diabetes Care* 35:1436–45.
3. Moberg L et al. (2002) Production of tissue factor by pancreatic islet cells as a trigger of detrimental thrombotic reactions in clinical islet transplantation. 360:11–13.
4. Nilsson B, Ekdahl KN, Korsgren O (2011) Control of instant blood-mediated inflammatory reaction to improve islets of Langerhans engraftment. *Curr Opin Organ Transplant* 16:620–6.
5. Carlsson P, Palm F, Andersson A, Liss P (2001) Markedly Decreased Oxygen Tension in Transplanted Site sure of oxygen (P O 2) levels of these transplanted islets. 50.
6. Olsson R, Olerud J, Pettersson U, Carlsson P-O (2011) Increased numbers of low-oxygenated pancreatic islets after intraportal islet transplantation. *Diabetes* 60:2350–3.
7. Desai NM et al. (2003) Elevated portal vein drug levels of sirolimus and tacrolimus in islet transplant recipients: local immunosuppression or islet toxicity? *Transplantation* 76:1623–5.
8. Cantarelli E, Piemonti L (2011) Alternative transplantation sites for pancreatic islet grafts. *Curr Diab Rep* 11:364–74.
9. Borg DJ, Bonifacio E (2011) The use of biomaterials in islet transplantation. *Curr Diab Rep* 11:434–44.
10. Amer LD, Mahoney MJ, Bryant SJ (2014) Tissue Engineering Approaches to Cell-Based Type 1 Diabetes Therapy 1,2. 20:1–13.
11. Salvatori M et al. (2014) Extracellular Matrix Scaffold Technology for Bioartificial Pancreas Engineering: State of the Art and Future Challenges. *J Diabetes Sci Technol* 8:159–169.
12. Richards OC, Raines SM, Attie AD (2010) The role of blood vessels, endothelial cells, and vascular pericytes in insulin secretion and peripheral insulin action. *Endocr Rev* 31:343–63.
13. Lammert E et al. (2003) Role of VEGF-A in Vascularization of Pancreatic Islets. *Curr Biol* 13:1070–1074.
14. Madden LR et al. (2010) Proangiogenic scaffolds as functional templates for cardiac tissue engineering. *Proc Natl Acad Sci U S A* 107:15211–6.
15. Buitinga M et al. (2013) *Microwell scaffolds for the extrahepatic transplantation of islets of langerhans.*
16. Giselbrecht S et al. (2006) 3D tissue culture substrates produced by microthermoforming of pre-processed polymer films. *Biomed Microdevices* 8:191–9.
17. Truckenmuller R et al. (2011) Thermoforming of film-based biomedical microdevices. *Adv Mater* 23:1311–1329.
18. Hilderink J et al. (2013) Label-free detection of insulin and glucagon within human islets of Langerhans using Raman spectroscopy. *PLoS One* 8:e78148.
19. Skårn M et al. (2014) Generation and Characterization of an Immortalized Human Mesenchymal Stromal Cell Line. *Stem Cells Dev* 00:1–13.
20. Doorn J et al. (2013) A small molecule approach to engineering vascularized tissue. *Biomaterials* 34:3053–3063.
21. Papenburg BJ et al. (2007) One-step fabrication of porous micropatterned scaffolds to control cell behavior. *Biomaterials* 28:1998–2009.
22. Chu L-Y, Niitsuma T, Yamaguchi T, Nakao S (2003) Thermoresponsive transport through porous membranes with grafted PNIPAM gates. *AIChE J* 49:896–909.
23. Zot GL, Koudria P, Bluestone J a (2007) Transplantation of pancreatic islets into the kidney capsule of diabetic mice. *J Vis Exp*:404.

24. R Core Team (2013) R: A language and environment for statistical computing. R Foundation for Statistical Computing.
25. Brissova M et al. (2005) Assessment of human pancreatic islet architecture and composition by laser scanning confocal microscopy. *J Histochem Cytochem* 53:1087–97.
26. Davalli AM et al. (1996) Vulnerability of Islets in the Immediate Posttransplantation Period. 19:1161–1167.
27. Giuliani M et al. (2005) Central necrosis in isolated hypoxic human pancreatic islets: evidence for postisolation ischemia. *Cell Transplant* 14:67–76.
28. Lehmann R et al. (2007) Superiority of small islets in human islet transplantation. *Diabetes* 56:594–603.
29. Macgregor RR, Williams SJ, Tong PY, Kover K, Moore W V (2006) Small rat islets are superior to large islets in in vitro function and in transplantation outcomes. 66160:771–779.
30. Dufour JM et al. (2005) Development of an ectopic site for islet transplantation, using biodegradable scaffolds. *Tissue Eng* 11:1323–1331.
31. Salvay DM et al. (2009) Extracellular Matrix Protein-Coated Scaffolds Promote the Reversal of Diabetes After Extrahepatic Islet Transplantation David. *Transplantation* 85:1456–1464.
32. Kheradmand T et al. (2011) Permanent protection of PLG scaffold transplanted allogeneic islet grafts in diabetic mice treated with ECDI-fixed donor splenocyte infusions. *Biomaterials* 32:4517–24.
33. Gibly RF et al. (2011) Extrahepatic islet transplantation with microporous polymer scaffolds in syngeneic mouse and allogeneic porcine models. *Biomaterials* 32:9677–84.
34. Gibly RF, Zhang X, Lowe WL, Shea LD (2013) Porous scaffolds support extrahepatic human islet transplantation, engraftment, and function in mice. *Cell Transplant* 22:811–9.
35. Yap WT et al. (2013) Collagen IV-Modified Scaffolds Improve Islet Survival and Function and Reduce Time to Euglycemia. 19.
36. Blomeier H et al. (2006) Polymer scaffolds as synthetic microenvironments for extrahepatic islet transplantation. *Transplantation* 82:452–459.
37. Brady A-C et al. (2013) Proangiogenic Hydrogels Within Macroporous Scaffolds Enhance Islet Engraftment in an Extrahepatic Site. 19:2544–2552.
38. Pedraza E et al. (2013) Macroporous Three-Dimensional PDMS Scaffolds for Extrahepatic Islet Transplantation. *Cell Transplant* 22:1123–1135.
39. Meier JJ et al. (2008) Beta-Cell Replication Is the Primary Mechanism Subservicing the Postnatal Expansion of beta-Cell Mass in Humans. *Diabetes* 57:1584–1594.
40. Butler A E et al. (2010) Adaptive changes in pancreatic beta cell fractional area and beta cell turnover in human pregnancy. *Diabetologia* 53:2167–2176.
41. Kin T et al. (2008) The use of an approved biodegradable polymer scaffold as a solid support system for improvement of islet engraftment. *Artif Organs* 32:990–993.
42. Pepper AR, Gala-Lopez B, Ziff O, Shapiro a MJ (2013) Revascularization of transplanted pancreatic islets and role of the transplantation site. *Clin Dev Immunol* 2013:352315.
43. Buchwald P et al. (2009) Quantitative assessment of islet cell products: estimating the accuracy of the existing protocol and accounting for islet size distribution. *Cell Transplant* 18:1223–35.
44. Robert B. Vernon, Anton Preisinger, Michel D. Gooden, Leonard A. D’Amico, Betty B. Yue, Paul L. Bollyky, Christian S. Kuhr, Thomas R. Hefty, Gerald T. Nepom and J, Gebe A (2012) Reversal of Diabetes in Mice With a Bioengineered Islet Implant Incorporating a Type I Collagen Hydrogel and Sustained Release of Vascular Endothelial Growth Factor. *Cell Transplant* 21:1–21.
45. Sokic S, Christenson M, Larson J, Papavasiliou G (2014) In situ generation of cell-laden porous MMP-sensitive PEGDA hydrogels by gelatin leaching. *Macromol Biosci* 14:731–739.

46. Canal T, Peppas N a (1989) Correlation between mesh size and equilibrium degree of swelling of polymeric networks. *J Biomed Mater Res* 23:1183–1193.
47. Brown BN, Ratner BD, Goodman SB, Amar S, Badylak SF (2012) Macrophage polarization: An opportunity for improved outcomes in biomaterials and regenerative medicine. *Biomaterials* 33:3792–3802.
48. Chen X et al. (2007) The epididymal fat pad as a transplant site for minimal islet mass. *Transplantation* 84:122–5.
49. Bashkatov AN et al. (2003) Glucose and mannitol diffusion in human dura mater. *Biophys J* 85:3310–8.
50. Bashkatov AN et al. (2000) Estimation of glucose diffusion coefficient in scleral tissue. *4001:345–355*.
51. Vasir B et al. (1998) Hypoxia induces vascular endothelial growth factor gene and protein expression in cultured rat islet cells. *Diabetes* 47:1894–1903.
52. Brissova M et al. (2006) Pancreatic islet production of vascular endothelial growth factor-A is essential for islet vascularization, revascularization, and function. *Diabetes* 55:2974–85.
53. Orci L, Unger RH (1975) Functional subdivision of islets of Langerhans and possible role of D cells. *Lancet* 306:1243–1244.
54. Bloch K, Vennäng J, Lazard D, Vardi P (2012) Different susceptibility of rat pancreatic alpha and beta cells to hypoxia. *Histochem Cell Biol* 137:801–810.
55. Esni F et al. (1999) Neural cell adhesion molecule (N-CAM) is required for cell type segregation and normal ultrastructure in pancreatic islets. *J Cell Biol* 144:325–337.
56. Spijker HS et al. (2013) Conversion of mature human β -cells into glucagon-producing α -cells. *Diabetes* 62:2471–80.
57. Talchai C, Xuan S, Lin H V, Sussel L, Accili D (2012) Pancreatic β cell dedifferentiation as a mechanism of diabetic β cell failure. *Cell* 150:1223–34.
58. Valdez IA, Teo AKK, Kulkarni RN (2015) Cellular stress drives pancreatic plasticity. *7*.
59. Pedraza E, Coronel MM, Fraker C a, Ricordi C, Stabler CL (2012) Preventing hypoxia-induced cell death in beta cells and islets via hydrolytically activated, oxygen-generating biomaterials. *Proc Natl Acad Sci U S A* 109:4245–50.
60. Salvay DM et al. (2008) Extracellular matrix protein-coated scaffolds promote the reversal of diabetes after extrahepatic islet transplantation. *Transplantation* 85:1456–1464.
61. Xiao X et al. (2014) M2 macrophages promote beta-cell proliferation by up-regulation of SMAD7. *Proc Natl Acad Sci U S A* 111:E1211–20.
62. LI KKN (1982) The Glucose Distribution in 9L Rat Brain Multicell Tumor Spheroids and its Effect on Cell Necrosis. *Cancer* 50:2066–2073.

Chapter 4

Composite human islets with proangiogenic support cells to improve islet revascularization at the subcutaneous transplantation site

Mijke Buitinga^{1}, Karolina Janeczek Portalska^{2*}, Dirk-Jan Cornelissen¹, Jacqueline Plass¹, Maaïke Hanegraaf³, Françoise Carlotti³, Eelco de Koning^{3,4,5}, Marten Engelse³, Clemens van Blitterswijk⁶, Marcel Karperien¹, Aart van Apeldoorn¹, and Jan de Boer⁷*



¹ Department of Developmental BioEngineering, University of Twente, Enschede, The Netherlands

² Department of Tissue Regeneration, University of Twente, Enschede, The Netherlands

³ Department of Nephrology, Leiden University Medical Center, Leiden, The Netherlands

⁴ Department of Endocrinology, Leiden University Medical Center, Leiden, The Netherlands

⁵ Hubrecht Institute, Utrecht, The Netherlands

⁶ Complex Tissue Regeneration Department, Maastricht University, Maastricht, The Netherlands

⁷ Laboratory for Cell Biology-inspired Tissue Engineering, Maastricht, The Netherlands

* Authors contributed equally

ABSTRACT

While subcutaneous tissue has been proposed as a clinically relevant site for pancreatic islet transplantation, a major issue of concern remains its poor vascular state. In an effort to overcome this limitation, we present an efficient and reproducible method to form human composite islets (CIs) with proangiogenic cell types in a controlled manner using non-adherent agarose microwell templates. In this study, we assessed the three dimensional structure, function and angiogenic potential of composite human islets with human mesenchymal stromal cells (hMSCs), with or without human umbilical vein endothelial cells (HUVECs), and pre-conditioned hMSCs in EGM-2 medium under shear-stress (PC-hMSCs). Distinct cellular rearrangements could be observed in composite islets, but islet functionality was maintained. *In vitro* angiogenesis assays found significantly enhanced sprout formation in case of composite islets. In particular, the number of sprouts emanating from composite islets with PC-hMSCs was significantly increased compared to other conditions. Subsequent *in vivo* assessment confirmed the proangiogenic potential of composite islets. However, in contrast to our *in vitro* angiogenesis assays, composite islets with hMSCs and HUVECs exhibited a higher *in vivo* angiogenic potential compared to control islets or islets combined with hMSCs or PC-hMSCs. These findings highlight the importance and necessity of verifying *in vitro* studies with *in vivo* models to reliably predict, in this case, revascularization outcomes. Regardless, we demonstrate here the therapeutic potential of composite islets with pro-angiogenic support cells to enhance islet revascularization at a clinically relevant, though poorly vascularized transplantation site.

INTRODUCTION

Clinical trials have demonstrated the ability of allogeneic islet transplants to regulate blood glucose levels in patients with type 1 diabetes and labile glycemic control (1–3). The main benefit of this procedure compared to whole organ transplantation is the significant reduction of glycemic fluctuations while having reduced postoperative trauma and complication rates. In clinical practice, the transplantation site of choice is the liver. However, the long-term insulin independence rate at this site is disappointing due to substantial islet loss, necessitating the use of at least two donor organs to cure one patient (1, 3). There is strong evidence that site-specific factors contribute to this islet loss in the liver, such as the exposure to high concentrations of immunosuppressants (4) and the instant blood-mediated inflammatory reaction (IBMIR) (5, 6). This has led to the search for alternative transplantation sites.

The subcutaneous space is a relevant candidate for islet transplantation because the transplant and biopsy procedures for this site are simple with minimal invasion. Furthermore, this site holds the capacity to transplant a sufficient amount of islets. However, a major challenge of this site is its poor vascularization state (7). Since the vascular network is important to maintain the islets' oxygen-dependent metabolism and their ability to quickly secrete insulin in response to changes in blood glucose levels, a reduced vascularization will affect both islet survival and function. Therefore, the vascular connections need to be re-established as fast as possible after transplantation.

Hence, various attempts have been made to improve vascularization of islets after transplantation. One of these attempts is to increase the action of pro-angiogenic factors in order to stimulate the proliferation, migration, and maturation of endothelial cells (8). Precise control over timing, dose delivery and effect duration of these factors remains a major challenge to obtain mature, functional blood vessels within islets. An alternative approach is to directly use endothelial cells, endothelial progenitor cells, or MSCs. Johansson *et al.* (9) have shown that coating human islets with endothelial cells initiates the formation of vessel-like structures *in vitro*, without impairing islet functionality. The sprouting capacity of endothelial cell-coated islets was further improved by the addition of MSCs. Other studies have shown that co-transplanting islets with mature endothelial cells (10), stromal cells (11–15), or endothelial progenitor cells (16–18) derived from various sources can induce neovascularization, resulting in enhanced islet revascularization and better function, regardless whether the implantation site was underneath the kidney capsule (10, 11, 14, 16, 18, 19), or the liver (12, 15, 17). However, a comparison of islet revascularization at the subcutaneous transplantation site when using different support cell types has not been performed.

In the current study we report an efficient and reproducible method to form human islet composites with proangiogenic cell types in a controlled manner using non-adherent agarose microwell templates. Recently, we have shown that incorporation of hMSCs in Dex-g-HA gels, either naïve or pre-conditioned in EGM-2 medium under shear stress, significantly improves

the vascularization of the gels after subcutaneous implantation (20). Therefore, in this study, we directly compare the angiogenic potential of CIs formed with either a mixture of hMSCs and HUVECs, hMSCs, or PC-hMSCs, to that of control islets at the subcutaneous transplantation site.

MATERIALS AND METHODS

Islets of Langerhans isolation and culture

Human islets of Langerhans were obtained from donors with written informed consent (Human Islet Isolation Laboratory, Leiden University Medical Center, Leiden, The Netherlands). Islets were cultured in islet culture medium (CMRL-1066 (Cellgro, Mediatech, VA, USA), supplemented with 10% FBS (Lonza, Verviers, Belgium), 100 U/ml penicillin (GIBCO, Bleiswijk, The Netherlands), and 10 mg/ml streptomycin (GIBCO, Bleiswijk, The Netherlands).

hMSC isolation and culture

Bone marrow aspirates were obtained from donors with written informed consent (Medisch Spectrum Twente hospital, Enschede, The Netherlands), and hMSCs were isolated and proliferated as described previously (20). Briefly, aspirates were resuspended using a 20G needle and plated at a density of 0.5 million mono-nucleated cells per cm². Cells were grown in MSC proliferation medium (alfa-MEM (GIBCO, Bleiswijk, The Netherlands), supplemented with 10% FBS (Lonza, Verviers, Belgium), 100 U/ml penicillin (GIBCO, Bleiswijk, The Netherlands), 10 mg/ml streptomycin (GIBCO, Bleiswijk, The Netherlands), 2 mM L-glutamin (GIBCO, Bleiswijk, The Netherlands), 0.2 mM L-ascorbic acid 2-phosphate magnesium salt (Sigma-Aldrich, Diegem, Belgium) and 1ng/ml bFGF (Fisher Scientific, Waltham, USA) at 37°C in a humid atmosphere with 5% CO₂. Cells were expanded up to passage 2. For further experiments hMSCs from different donors and one immortalized clone (iMSCs, courtesy of Prof. Ola Myklebost, University of Oslo, Norway) (21) were cultured in basic medium (alfa-MEM supplemented with 10% FBS, 100 U/ml penicillin, 10 mg/ml streptomycin, 2 mM L-glutamin and 0.2 mM ASAp). HUVECs (Lonza, Verviers, Belgium) were cultured in endothelial growth medium (EGM-2 medium, Lonza, Verviers, Belgium).

Preconditioning of hMSCs

For pre-conditioning, iMSCs (passage 25, for *in vitro* sprouting assay) and hMSCs from different donors (passage 1-2) were seeded at a density of 3,000 cells per cm² on tissue culture plastic in EGM-2 medium and cultured for 10 days. After one day in static culture, shear force was applied using an orbital shaker (20 rpm). Cells that were cultured according to this protocol will be referred to as PC-hMSCs.

Cell labelling

When indicated, hMSCs (both naïve and pre-conditioned) and HUVECs were labelled using Dil (red) or DiO (green), according to the manufacturer's protocol (Life Technologies, Bleiswijk, The Netherlands). When indicated, hMSCs (both naïve and pre-conditioned) and HUVECs were labelled using Dil (red) or DiO (green), according to the manufacturer's protocol (Life Technologies, Bleiswijk, The Netherlands).

Formation of composite islets

Non-adherent agarose microwell chips were prepared by replica moulding as described previously (22, 23). Briefly, negative replicates of patterned poly-dimethylsiloxane (PDMS, Sylgard 184, Dow Corning, Midland, USA) stamps, each containing 130 pillars with a diameter of 400 µm and a height of 200 µm, were prepared using 3% agarose solution (Ultra-pure agarose, Invitrogen, Bleiswijk, The Netherlands). Prior to cell seeding, the agarose chips were incubated in EGM-2 medium for 8 hours. To produce composite islets (CIs) with proangiogenic cells, islets were homogeneously seeded in the microwells, after which either a cell suspension of hMSCs (1250 cells/islet), a mixture of hMSCs (625 cells/islet) and HUVECs (1250 cells/islet), or PC-hMSCs (1250 cells/islet), was added. Subsequently, the agarose microwell chips were shortly centrifuged at 150G to settle the cells with the islets in the microwells. Cells attached to the surface of the islets within eight hours of culture in EGM-2 medium. These cell aggregates will be referred to as composite islets (CIs). Medium was refreshed every day with a 1:1 mixture of EGM-2 and islet culture medium.

Immunohistochemistry on wholemount islets

At day 1 and 5, CIs and control islets were flushed out of the agarose chips, re-suspended in serum-depleted culture medium, and transferred to Cell-Tak-coated (30s at 42°C, BD Biosciences, Breda, The Netherlands) Ibidi microscopy culture chambers (IBIDI, Planegg, Germany). After attachment, islets were fixed in 4% phosphate-buffered paraformaldehyde for 25 min at room temperature. Fixation was followed by three 30 min washes in PBS and a 3-hr permeabilization in 0.3% Triton-X 100/PBS. Blocking was performed by o/n incubation in 10% NGS/0.15% Triton-X 100/PBS at 4°C. Islets were washed three times for 30 minutes with antibody diluent buffer (1% BSA/0.2 Triton-x 100) prior to incubation with primary antibodies (guinea pig anti Insulin (Abcam, Cambridge, UK) 1:100 and Rabbit anti Glucagon (Vector, Peterborough, UK) 1:100, 48 hours at 4°C), secondary antibodies (Alexa 647-conjugated goat anti guinea pig (Life Technologies, Bleiswijk, The Netherlands) and Alexa 488-conjugated goat anti rabbit (Invitrogen, Bleiswijk, The Netherlands), both 1:200, 48 hours at 4°C) and DAPI (Invitrogen, Bleiswijk, The Netherlands (5mg/ml), 1:100, 20 minutes at room temperature). Samples were subjected to optical sectioning at 0.23 µm increments in axial (z) dimension using Nikon A1 confocal microscope (Nikon BV, Amsterdam, The Netherlands).

Glucose-induced insulin secretion test

To assess islet functionality, a glucose-induced insulin secretion test was performed at day 1 and day 5 after CI formation. Per condition per islet donor, 100 islets were used. As a control, uncoated islets were cultured in agarose chips. CI formation was performed in EGM-2 medium, after which the islets were cultured for 5 days in islet medium, with a medium change every day. For the glucose-induced insulin secretion test, 30 islets per condition (in triplicate) were incubated for 90 minutes in a modified Krebs Ringer Bicarbonate (KRBH) buffer (115 mM NaCl, 5 mM KCl, 24 mM NaHCO₃ and 2.2 mM CaCl₂, pH 7.4), supplemented with 20 mM HEPES, and 2 mg/ml human serum albumin (Sanquin, Amsterdam, The Netherlands). Islets were successively incubated for 1 hour in KRBH buffer with 1.7 mM and 16.7 mM D-glucose at 37°C. Insulin concentration was determined in the supernatants by ELISA (MercoDia, Uppsala, Sweden). The experiment was performed for three islet donors, each time coated with hMSCs from different donors.

Sprouting assays on Matrigel and fibrin gel

For the sprouting assays, control islets, hMSC-, HUVEC/hMSC-, and PC-hMSC-CIs were placed between 2 layers of growth factor-reduced Matrigel (diluted 1:1 in EGM-2 medium; BD Biosciences, Breda, The Netherlands) or fibrin gel (2.5 mg/ml fibrinogen and 2 µg/ml thrombin; Sigma-Aldrich). For each gel layer 1 ml of gel was used. After polymerization, islets were cultured for 96 hours in EGM-2 medium. Islet sprouting was observed over time using an inverted microscope (Nikon Eclipse TE300). Light microscopy pictures were taken at different time points (24, 48 and 96 hours) using a Nikon DS-L2 camera. The Matrigel sprouting assay was performed with islets obtained from 5 different human islet donors, and the fibrin sprouting assay with islets from 2 different donors. Furthermore, hMSCs from 5 different donors, and one clone of iMSCs were used in this study (21). Sprout formation was manually quantified by a single person (blinded to the conditions) in minimally 10 islets per condition, per time point.

Subcutaneous Matrigel plug angiogenesis assay

To test the angiogenic potential of CIs *in vivo*, control islets and hMSC-, HUVEC/hMSC-, and PC-hMSC-CIs were transplanted subcutaneously in Matrigel plugs in the back of 8 weeks old male NMRI-nu mice (Harlan). For this, CIs were formed for 8 hours in the agarose microwells as described before. Subsequently, islets were flushed out, washed in EGM-2 medium (without supplemented growth-factors) and re-suspended in 100 µL growth factor-reduced Matrigel (BD Biosciences, Breda, The Netherlands). The plugs were allowed to solidify at 37°C in a round-bottom 96-wells plate to obtain uniform plugs. After solidification, the Matrigel plugs were recovered from the plate and cultured for 8 hours in islet culture medium. Per condition, 9 plugs were implanted containing each 200 islets. Of these plugs, 3 plugs were prepared using dil pre-labeled cells as described before. Prior to isoflurane anesthetics, mice were given 0.1 mg/kg buprenorfin (Temgesic, Schering-Plough, Belgium). Four small subcutaneous pockets were

created at each quadrant of the back of the mouse. In each mouse, all four conditions were transplanted, but the position of the different conditions was randomized per animal.

Histochemistry and morphometric analysis

Two weeks after implantation, mice were sacrificed and Matrigel plugs were recovered for histological analysis. Grafts were fixed overnight with 4% (w/v) paraformaldehyde at 4°C, embedded in paraffin blocks and sliced into 5 µm sections.

For each Matrigel plug, sections spaced 100 µm apart were stained for insulin combined with a Masson's-Goldner trichrome staining (Merck Chemicals, Darmstadt, Germany) to determine the amount of perfused blood vessels in and around the islets. For this, primary antibody rabbit anti-insulin (Santa Cruz Biotechnology, Heidelberg, Germany, 1:400) was applied for 1 hour followed by an HRP- conjugated goat-anti-rabbit antibody (DAKO, Heverlee, Belgium, 1:100) for 1 hour. Sections were developed with DAB liquid chromogen system (DAKO, Heverlee, Belgium) and counterstained with hematoxylin and Masson's-Goldner trichrome staining according to manufacturer's protocol (Merck Chemicals, Darmstadt, German). Stained sections were imaged with a Nanozoomer slide scanner 2.0 RS (Hamamatsu, SZK, Japan). These sections were used to quantify the amount of perfused blood vessels in and around the islets (within 200 µm) using ImageJ software (<http://rsb.info.nih.gov/ij/>).

To assess the expression of insulin, glucagon and the endothelial marker CD31, immunohistochemistry was performed on consecutive sections of islet-containing regions. For this, heat-mediated antigen retrieval (pressure cooker, 80°C, 30 min) was performed in sodium citrate buffer (pH 6.0). Sections were blocked with normal goat serum and biotin/avidin blocking kit (Vector, Peterborough, UK). Primary antibodies against insulin (Abcam, Cambridge, UK, 1:200, 1.5h), glucagon (Vector, Peterborough, UK, 1:100, o/n) and CD31 (Abcam, Cambridge, UK, 1:20, o/n) were used. Secondary antibodies were Alexa-647 goat-anti-guinea pig (Invitrogen, Bleiswijk, The Netherlands, 1:500, 2h), biotin-SP-conjugated anti-rabbit (Jackson ImmunoResearch, Suffolk, UK, 1:200, 1h), and Alexa-488-SA (Invitrogen, Bleiswijk, The Netherlands). DAPI (Invitrogen, Bleiswijk, The Netherlands) was applied as nuclear counterstaining. Sections were imaged with a Nikon A1 confocal microscope (Nikon BV, Amsterdam, The Netherlands).

Statistics

Results were presented as mean ± standard error of the mean (SEM). Statistical analyses were performed using SPSS version 22 (SPSS, Chicago, USA). Kruskal-Wallis test was used for multiple group comparisons ($p < 0.05$, corrected for multiple comparisons) and paired comparisons by means of Mann-Whitney U test were performed as post-hoc test when Kruskal-Wallis test indicated significant differences.

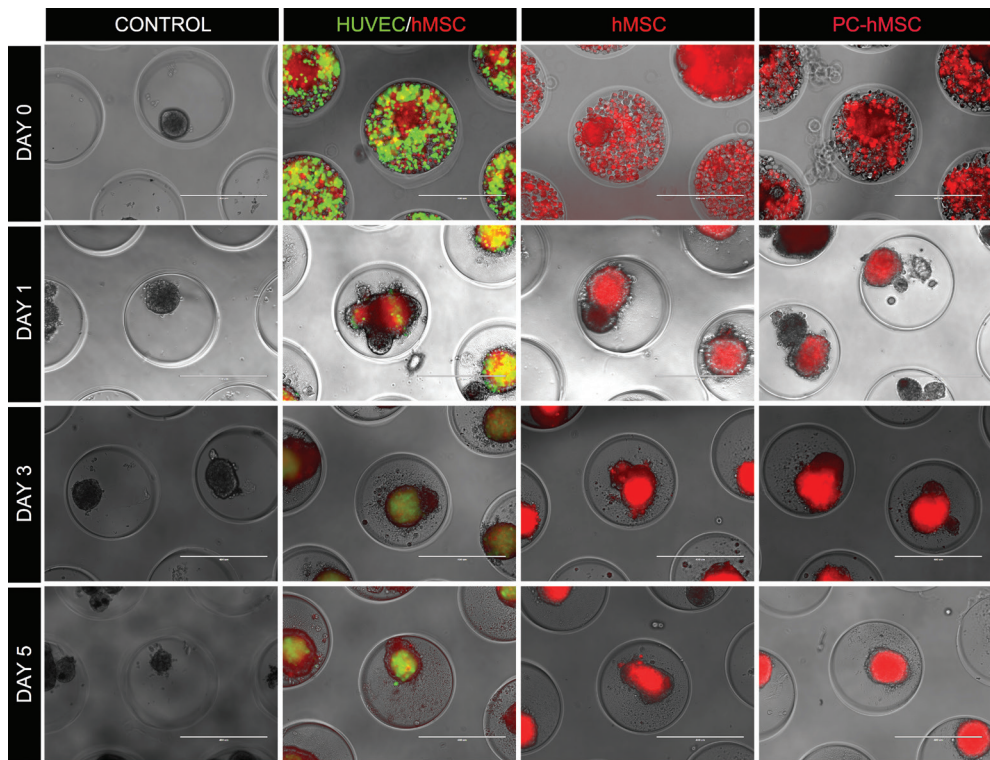


Figure 1. Islet composite formation with different types of support cells in non-adherent agarose microwell templates. Scalebars: 400 μm .

RESULTS

Controlled formation of composite islets

To fabricate the CIs, we used a non-adherent agarose microwell culture platform which has been developed in our group for controlled cell aggregation (22). The microwells were seeded with single islets prior to seeding with fluorescently labelled single cell suspensions of HUVECs, hMSCs, or PC-hMSCs. One day after cell seeding, all single cells present in the microwells were attached to the islet. Upon culturing, the fluorescently labelled support cells became more uniformly distributed over the islets (Figure 1). More detailed analysis of CI formation over time using 3D optical sectioning on wholemount islets revealed that 24 hours after CI formation, the cells attached to the islets as one, or more cell-clusters (Figure 2 A-D). During prolonged cell culture, these cell clusters migrated inwards (Figure 2 E-H). Five days after initial cell seeding, all conditions, regardless of the support cell type, exhibited a core of hMSCs, HUVECs and hMSCs or PC-hMSCs, surrounded by a mantle of insulin and glucagon positive islet cells (Figure 2 E-H).

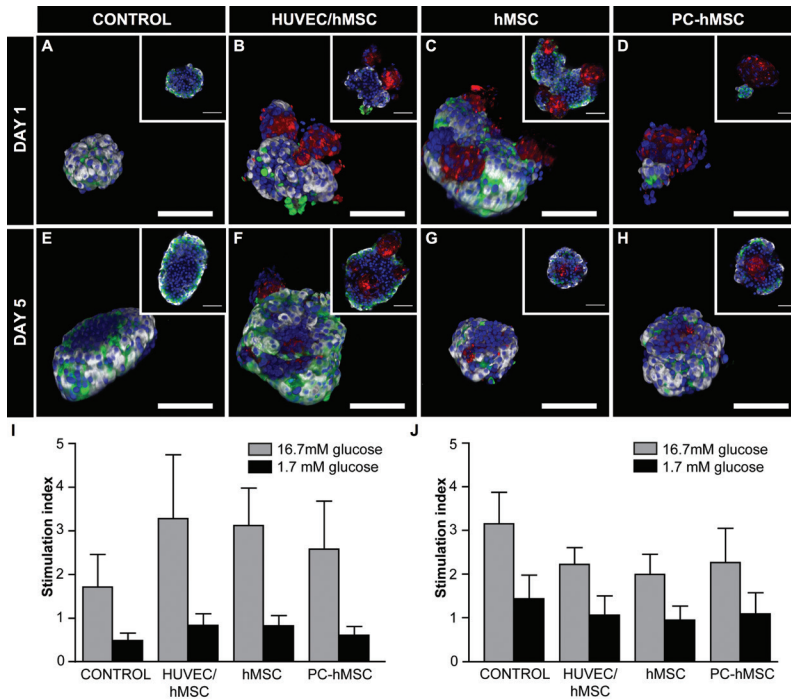


Figure 2. Morphometric appearance and function of control islets and CIs. A-H. Representative 3D reconstructions of optically sectioned control islets and CIs at day 1 (A-D) and day 5 (E-H) after CI formation, with dil labeled support cells in red, beta-cells in white and alpha-cells in green. The inserts represent an optical section through the middle of the islet. I-J. Stimulation index of high glucose (16.7 mM) and subsequently low glucose (1.7 mM) compared to basal insulin secretion levels at 1.7mM glucose for control islets and CIs at day 1 (I) and day 5 (J) after CI formation. Results are presented as mean±SEM of three independent experiments. Scalebars: 100 μm.

Composite islets maintain function *in vitro*

To assess whether the formation of CIs with different proangiogenic cell populations affects islet functionality, the insulin secretory response of the islets to a glucose challenge was measured. For all conditions we found that stimulation with 16.7 mM glucose buffer increased the insulin secretion two to threefold compared to basal insulin secretion at 1.7mM glucose (Figure 2 E-F). At day 1 (Figure 2E) and 5 (Figure 2F) after CI formation, no significant differences in relative insulin secretion levels could be observed between CIs and control islets. In addition, a proper return to basal insulin secretion levels was observed in all conditions, when the islets were exposed to a low, 1.7 mM, glucose buffer following the 16.7 mM glucose challenge. These results imply that CI formation does not alter the islets' insulin secretory capacity.

Composite islets show increased sprout formation *in vitro*

In vitro angiogenesis assays were performed to assess the sprouting potential of CIs and control islets. For this, 8 hours after CI formation, CIs and control islets were flushed out of the microwells and embedded in Matrigel (5 different islet donors) or fibrin gel (2 different islet donors) (Figure 3). Sprouts emanating radially outwards from the islets could be observed in both sprouting matrices (Figure 3 A-D, Figure 4 A-D). Dil and DiO labelling of the different cell types in case of HUVEC/hMSC-CIs revealed that hMSCs and HUVECs are in close contact and that both cell types contribute to sprout formation (Figure 3 E). Quantification of sprout formation in Matrigel revealed significantly more sprouts in the CI conditions compared to control islets (Figure 3 F). In particular, the number of sprouts emanating from PC-hMSC-CIs was significantly increased compared to the other conditions. This difference remained prevalent during the entire culture period, suggesting a persistent advantage of PC-hMSCs over the other observed other cell types. Substituting half of the hMSCs by HUVECs did not seem to further improve sprout formation compared to hMSC-CIs. A similar trend could be observed in fibrin gel (Figure 4 E), though in contrast to Matrigel, control islets did sprout in this gel.

Composite islets stimulate revascularization after subcutaneous transplantation

The proangiogenic effect of CIs compared to control islets was subsequently validated using an *in vivo* Matrigel plug model. For this assay, CIs and control islets were flushed out of the microwells 8 hours after cell seeding, embedded in 100 μ L of growth factor-reduced Matrigel and implanted subcutaneously in the back of NMRI-nu mice.

Two weeks after implantation, grafts were retrieved and prepared for histological analysis. Of the 36 implanted Matrigel plugs (9 per condition), 5 Matrigel plugs could not be recovered; 2 of the control group, 2 of the HUVEC-hMSC-CI group, and 1 of the PC-hMSC-CI group.

Insulin-Trichrome staining showed directed invasion of perfused vessels towards the islet grafts in case of CIs, whereas this was limited for the control islets (Figure 5 A-D). Insulin/glucagon immunostaining of CI-containing plugs showed scattered expression patterns of both hormones throughout the islets (Figure 4 E-H), a cyto-architecture typical for human islets (24). In contrast to *in vitro* observations, Dil labelling of CI support cells did not reveal a core/mantel structure of support cells and islet cells, respectively, when implanted *in vivo*. Further immunostaining for CD31 was performed to assess whether the dil-positive support cells expressed this endothelial marker (Figure 5 I-L). Occasionally, double positive cells for Dil and CD31 were found (Figure 5 J-L inserts), though the majority of Dil positive cells were CD31-negative.

Quantitative evaluation of vascularization in and around the islets (within 200 μ m from the islet) (Figure 6A) confirmed the observation that vascularization was increased in case of CIs compared to control islets (Figure 6 B). Only 7% of the islets in the control group were vascularized (Figure 6 C), whereas this was 32%, 19%, and 36% for HUVEC-hMSC-CIs, hMSC-CIs, and PC-hMSC-CIs, respectively (Figure 6C). In particular, composite formation with either HUVECs combined with hMSCs or PC-hMSCs resulted in a similar increase in vascularization

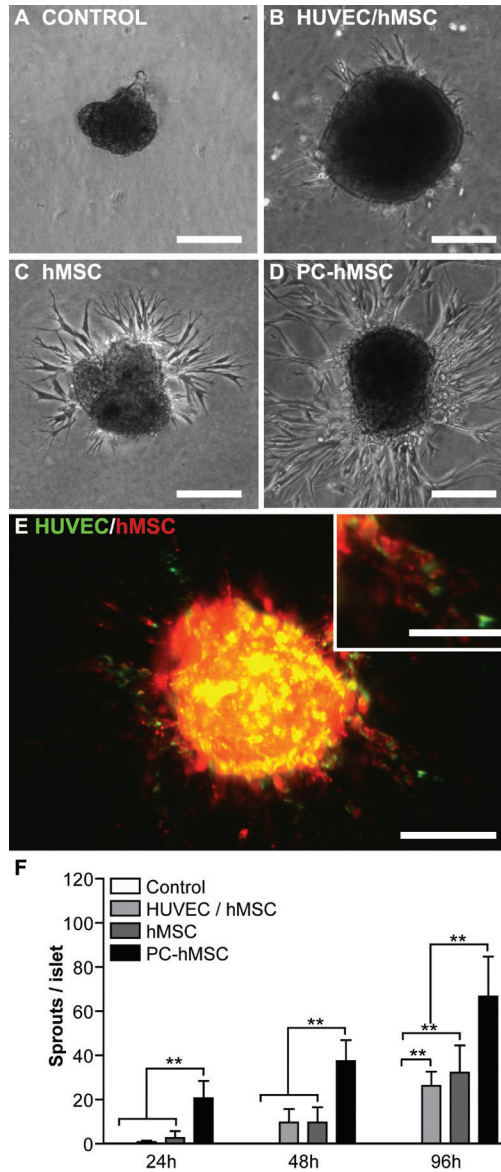


Figure 3. Sprout formation in Matrigel. A-D. Representative phase-contrast microscope images of control islets (A) and CIs (B-D) taken 48 hours after Matrigel embedding. E. Representative fluorescent image of HUVEC/hMSC-Cl 48 hours after Matrigel embedding with HUVECs labeled with DiO (green) and hMSCs with Dil (red). Both HUVECs and hMSCs contribute to sprout formation (insert; scalebar: 50 μ m). F. Quantification of sprout formation 24, 48 and 96 hours after Matrigel embedding. Results are presented as mean \pm SEM of five independent experiments. ** < 0.01 by Mann-Whitney U test. Scalebars: 100 μ m.

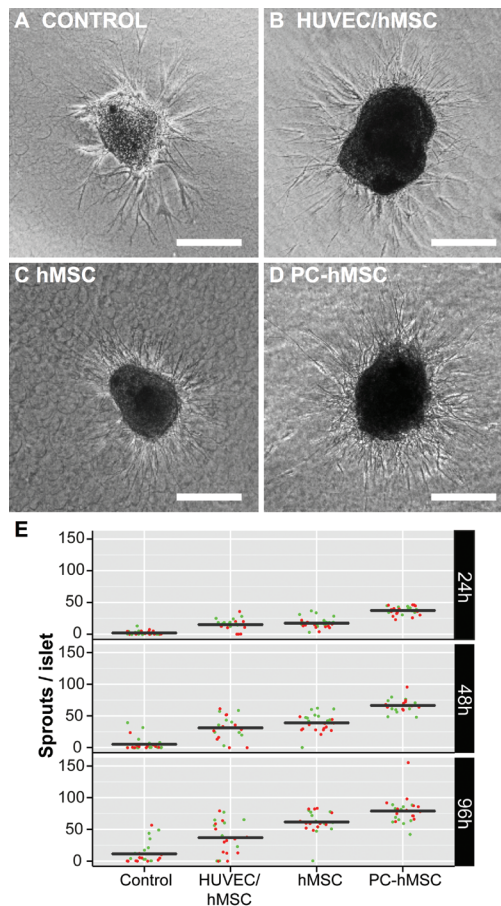


Figure 4. Sprout formation in fibrin gel. A-D. Representative phase-contrast microscope images of control islets (A) and CIs (B-D) taken 48 hours after fibrin gel embedding. E. Quantification of sprout formation 24, 48 and 96 hours after fibrin gel embedding. Results are presented as the mean of two independent experiments. Scalebars: 100 μ m.

frequency of the islets (Figure 6C). More detailed examination of vascular position in and around the vascularized islets (Figure 6D) revealed a general increase in the number of vessels when HUVECs were added to the composite.

DISCUSSION

In the current study, we present a facile and reproducible method to fabricate composite islets with proangiogenic cells as a strategy to improve islet vascularization after subcutaneous islet implantation. Most transplantation sites that can harbour a sufficient amount of islets,

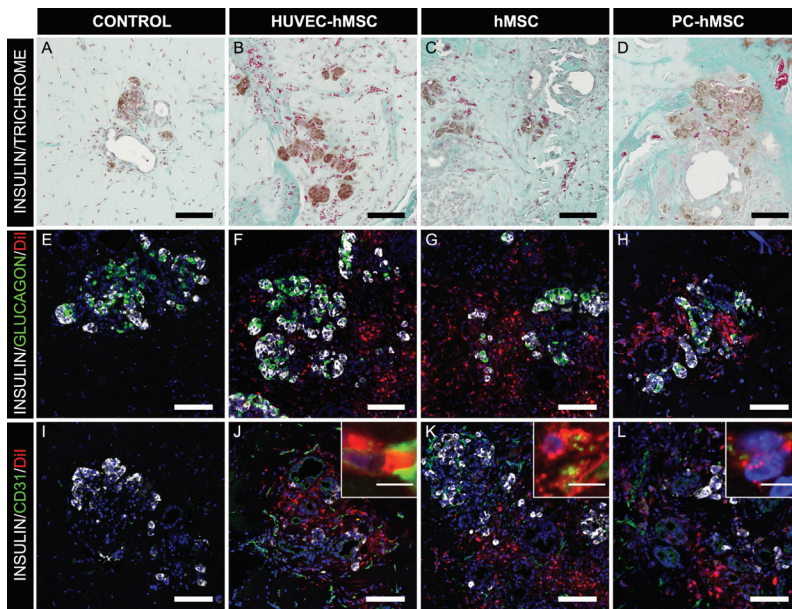


Figure 5. Microvasculature formation and islet composition after *in vivo* subcutaneous Matrigel plug assay. A-D. Representative images stained for insulin and Masson's trichrome indicating perfused vessel formation in islet and CI grafts. E-L. Representative confocal microscopy images of islets and CIs with dil labeled support cells, stained for insulin (white) and glucagon (green) (E-H) and for insulin (white) and CD31 (green) (I-L). Scalebars: 100 μm . Inserts represent CD31-positive Dil labeled support cells. Scalebars: 10 μm

like the subcutaneous tissue, are challenged by poor vascularization (25). To improve the vascularization state of these sites, the possibility of creating microvascular networks using mature endothelial cells derived from vascular tissue has been suggested (26, 27). However, the limited proliferative ability of these mature endothelial cells hampers their clinical applicability. Previous studies have shown that co-transplantation of islets with either MSCs or endothelial progenitor cells can also induce neovascularization (10–18). These cells are easier to harvest compared to mature endothelial cells and harbor greater expansion potential (28), though a direct comparison between different support cell types for islet revascularization at a clinically relevant transplantation site has not been performed. Therefore, the study presented here directly compares the angiogenic potential of different cell types for islet revascularization in an *in vitro* and *in vivo* sprouting assay at a clinically relevant transplantation site using growth factor-reduced Matrigel as a support transplantation matrix.

Previously, we have shown that hMSCs can enhance angiogenesis in Dex-g-HA gels after subcutaneous implantation. The angiogenic potential of hMSCs could be further increased by pre-conditioning them in EGM-2 medium (20). Therefore, in this study we evaluate the effect

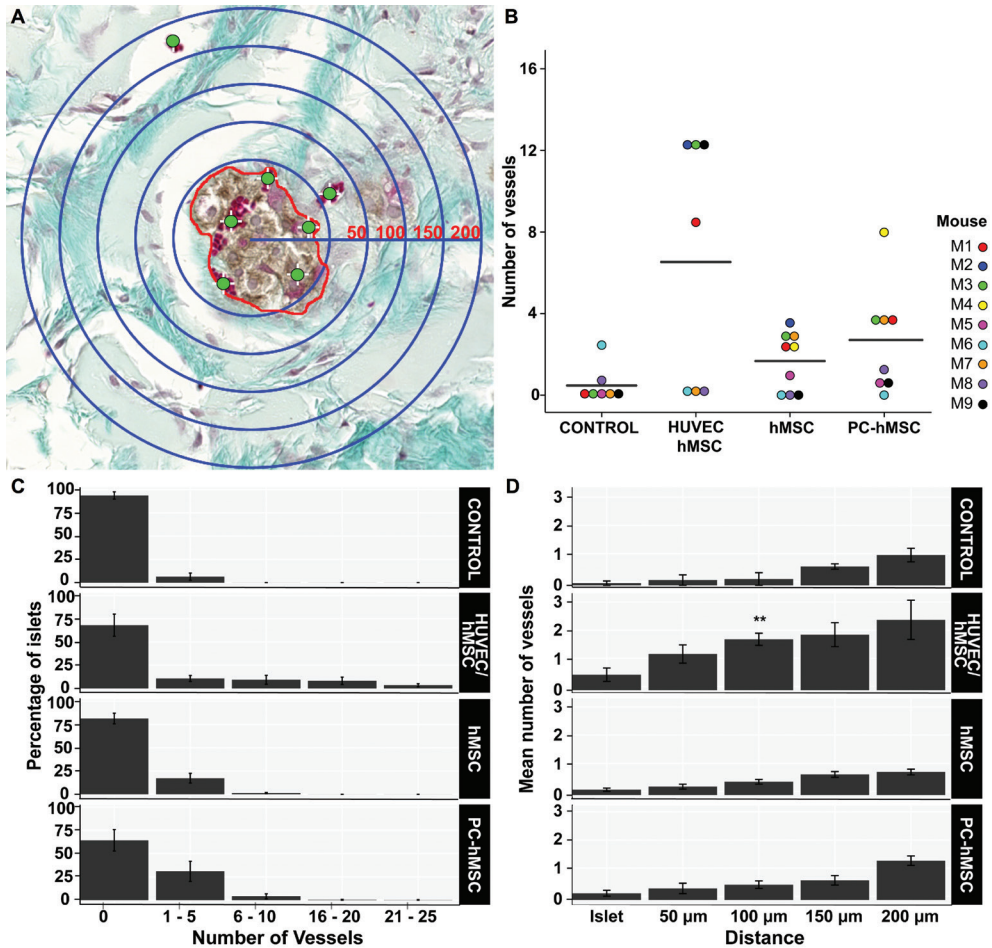


Figure 6. Vascular morphometry of control islets and CIs. A. Image segmentation to determine the number of blood vessels in the insulin positive islet area (in red) and within a radius of 200 μm (divided in 50 μm sections as represented in blue). B. Number of blood vessels per islet for uncoated control islets and CIs. C. Frequency plot for vascularization of control islets and CIs. D. Mean number of vessels within vascularized islets. Results are presented as mean±SEM, ** <0.01 by Mann-Whitney U test. Scalebars: 100 μm.

of hMSCs and PC-hMSCs on islet revascularization and compare their angiogenic potential with mature endothelial cells (HUVECs) supported with hMSCs, a combination shown to enhance the vascularization in subcutaneously transplanted fibrin plugs (29).

Outlined in this study is a novel method for CI formation using a non-adherent agarose microwell platform, which allows for controlled seeding of support cells and islets in individually separated microwells. In contrast to composite formation in suspension culture, the method presented here ensures that all initially seeded cells are incorporated into the CI. In line with

previous findings (9, 30, 31), we observe that CI formation, regardless of the applied support cell type, does not affect the glucose stimulated insulin secretion capacity of the islets. However, the cellular organization of CIs is dramatically changed during *in vitro* culture when no supporting matrix, such as Matrigel, is employed. We show that the support cells preferentially aggregate before adhering to the islets, an observation in line with previous reports (9, 31). These aggregates are engulfed over time by the islet cell mass, corroborating earlier observations by Johansson *et al.* who describes similar internalization of endothelial cells upon culturing (9). Such phenomena can be explained by the “differential adhesion hypothesis”; this postulates that a population of motile, mutually adhesive cells will spontaneously reorganize to substitute weaker intercellular adhesions for stronger ones until a configuration is found that maximizes adhesive bonding (32). This results in a core of cells with strong cohesive interactions surrounded by a shell of cells exhibiting lower affinity. Our observation that the islet cells envelop the support cells suggests that islet cells are less cohesive compared to the support cells. This may be partly attributed to the enzymatic procedure for islet isolation, which destroys the islets’ basement membrane and alters the cellular integrin expression (33). However, we observe an opposite pattern when CIs are embedded in Matrigel or fibrin gel after 8 hours of CI formation, with extensive sprouting of the support cells radially outward to form an outer CI layer penetrating the surrounding gel. Also after *in vivo* implantation of CIs in supporting Matrigel plugs, intact islet cell clusters are observed surrounded by outwardly migrating support cells. These observations suggest that sufficient cell-matrix interactions can counteract the cell-cell based differential adhesion phenomenon observed when no matrix is employed.

Established *in vitro* models of angiogenesis involve the monitoring of capillary-like structure formation in three-dimensional gels mimicking the extracellular matrix, such as Matrigel (34), fibrin gel (9, 35) or collagen gel (36). By using two of these model systems, Matrigel and fibrin gel, we demonstrate the induction of sprout formation of CIs over time. The observation that control islets sprout in fibrin gel is in line with previous reports (9, 37). To our knowledge, no studies have monitored sprouting of control islets in Matrigel. The improved performance in sprouting capacity of uncoated islets in fibrin compared to Matrigel could either be explained by the difference in matrix composition or stiffness, shown to influence sprout formation of mature endothelial cells both *in vitro* (36, 38–41) and *in vivo* (29), or the expression of a specific set of fibrinolytic enzymes in intra-islet endothelial cells specifically enabling successful remodeling of the fibrin matrix (41–43). Our results further indicate that hMSCs, either naïve or pre-conditioned, significantly enhance sprout formation *in vitro* compared to HUVEC-hMSC-CIs or control islets. Cellular invasion and migration in Matrigel, which primarily consists of laminin, collagen IV and enactin, is mainly regulated by MMP activity (44). It has been shown that bone marrow-derived hMSCs express higher levels of MMPs, such as MT1-MMP and MMP-2, compared to HUVECs (35). The two-fold reduction of hMSCs in the HUVEC-hMSC-CI group compared to the hMSC- and PC-hMSC-CI group likely results in a lower expression of proteolytic enzymes, accounting for the observed reduction in *in vitro* sprout formation.

Analysis of *in vivo* implanted Matrigel plugs reveals the highest number of perfused lumen-containing structures in and around the islets when islets are co-implanted with a mixture of HUVECs and hMSCs. Though contrary to our *in vitro* findings, this observation is in line with a previous report where subcutaneously transplanted fibrin plugs containing a mixture of hMSCs and HUVECs exhibited an increased number of perfused vessels compared to constructs containing either hMSCs or HUVECs alone (41). The exact mechanisms by which the hMSC/HUVEC combination results in improved neogenesis remain unclear. However, hMSCs and HUVECs both secrete numerous soluble factors, such as VEGF and bFGF (45), and ECM remodelling enzymes, such as MMPs (46). All of these factors contribute to endothelial cell survival, tip cell migration, proliferation, endothelial tubulogenesis and/or vascular maturation (46–48), and many of them have been shown to have increased expression in HUVEC/hMSC co-cultures (35). Others suggest that hMSCs are able to differentiate into a pericyte or smooth muscle like cell and stabilize newly formed vessels (49), but further studies are warranted.

Although an increasing trend is observed in the percentage of vascularized islets when hMSCs or PC-hMSCs are used compared to control islets, we do not observe a significant difference in perfused vessel density. This is in contrast to previous studies reporting a significant improvement in revascularization rate when islets are co-transplanted with bone marrow-derived MSCs underneath the renal capsule (11, 13) or intrahepatically (12). The reason for this discrepancy is likely multifactorial. First of all, since the subcutaneous site is poorly vascularized compared to the renal subcapsular and intrahepatic transplantation sites, the proangiogenic effect of hMSCs might be unable to induce islet revascularization at this transplantation site within the observed period. Furthermore, growth factor-reduced Matrigel as a supporting matrix imposes an additional barrier for both the diffusion of soluble proangiogenic factors and the infiltration of blood vessels. Another factor that could have influenced the revascularization process is the distribution of the support cells within the hydrogel. In the current study, the support cells are confined around the islets. However, we have previously shown that when hMSCs and PC-hMSCs are homogeneously distributed throughout DEX-g-HA gels, these cells can significantly improve the vascularization in these gels (20). Although DEX-g-HA was used in lieu of Matrigel, possibly accounting for the difference in outcome, we hypothesise that the uniform cellular distribution created a more suitable environment for recruitment and infiltration of blood vessels because of a more homogeneous presentation of angiogenic and proteolytic factors.

Comparing the *in vitro* and *in vivo* results, we observe a discrepancy in angiogenesis. *In vivo*, the highest number of perfused lumen in and around the islets is observed when islets are co-implanted with a mixture of HUVECs and hMSCs, whereas *in vitro* sprout formation is highest for the PC-hMSC-CIs. As mentioned before, *in vitro* tube formation is largely influenced by the invasive capacity of the cells by proteolytic enzyme-mediated ECM degradation. Although ECM degradation is an important component for *in vivo* angiogenesis, the process of de novo blood vessel formation involves a complex interplay between multiple cell types from host and donor,

growth factors, enzymes and extracellular matrix molecules; a level of complexity not mimicked during *in vitro* assays and therefore precludes an accurate prediction of *in vivo* outcome. Our findings highlight the importance and necessity of verifying *in vitro* studies with *in vivo* models to reliably predict, in this case, revascularization outcomes.

In conclusion, this study presents a controlled method to fabricate composite islets to study the angiogenic potential of different support cells. Using a subcutaneous Matrigel plug assay, we demonstrate that composite islets with hMSCs and HUVECs exhibit a higher angiogenic potential compared to control islets or islets combined with hMSCs or PC-hMSCs. However, for this method to be clinically applicable, further efforts are required to identify a clinically relevant pro-angiogenic cell source. Regardless, we show here the therapeutic potential of composite islets with pro-angiogenic support cells to enhance islet revascularization at a clinically relevant, though poorly vascularized transplantation site.

ACKNOWLEDGEMENTS

This project was financially supported by the Diabetes Cell Therapy Initiative (DCTI) including the Dutch Diabetes Research Foundation (DF). The authors thank Janneke Hilderink from the department of Developmental BioEngineering (University of Twente, The Netherlands) for her assistance in islet handpicking.

REFERENCES

1. Ryan EA et al. (2005) Five-year follow-up after clinical islet transplantation. *Diabetes* 54:2060–2069.
2. Shapiro AM et al. (2000) Islet transplantation in seven patients with type 1 diabetes mellitus using a glucocorticoid-free immunosuppressive regimen. *N Engl J Med* 343:230–238.
3. Barton FB et al. (2012) Improvement in outcomes of clinical islet transplantation: 1999–2010. *Diabetes Care* 35:1436–45.
4. Desai NM et al. (2003) Elevated portal vein drug levels of sirolimus and tacrolimus in islet transplant recipients: local immunosuppression or islet toxicity? *Transplantation* 76:1623–5.
5. Moberg L et al. (2002) Production of tissue factor by pancreatic islet cells as a trigger of detrimental thrombotic reactions in clinical islet transplantation. 360:11–13.
6. Johansson H et al. (2005) Tissue factor produced by the endocrine cells of the islets of Langerhans is associated with a negative outcome of clinical islet transplantation. *Diabetes* 54:1755–62.
7. Sakata N (2014) Strategy for clinical setting in intramuscular and subcutaneous islet transplantation. 2009:1–10.
8. Martino MM et al. (2015) Tissue Engineering and Regenerative Medicine Extracellular matrix and growth factor engineering for controlled angiogenesis in regenerative medicine Article type. *Front Bioeng Biotechnol.* 2015; 3: 45.
9. Johansson U et al. (2008) Formation of composite endothelial cell-mesenchymal stem cell islets: a novel approach to promote islet revascularization. *Diabetes* 57:2393–401.
10. Li Y et al. (2013) Combined Strategy of Endothelial Cells Coating, Sertoli Cells Coculture and Infusion Improves Vascularization and Rejection Protection of Islet Graft. *PLoS One* 8.
11. Figliuzzi M et al. (2009) Bone marrow-derived mesenchymal stem cells improve islet graft function in diabetic rats. *Transplant Proc* 41:1797–800.
12. Ito T et al. (2010) Mesenchymal Stem Cell and Islet Co-Transplantation Promotes Graft Revascularization and Function. *Transplantation* 89:1438–1445.
13. Sakata N, Chan NK, Chrisler J, Obenaus A, Hathout E (2010) Bone marrow cell cotransplantation with islets improves their vascularization and function. *Transplantation* 89:686–93.
14. Rackham CL et al. (2011) Co-transplantation of mesenchymal stem cells maintains islet organisation and morphology in mice. *Diabetologia* 54:1127–1135.
15. Cavallari G et al. (2012) Mesenchymal Stem Cells and Islet Co-transplantation in Diabetic Rats: Improved Islet Graft Revascularization and Function By Human Adipose Tissue-Derived Stem Cells Preconditioned With Natural Molecules. *Cell Transplant* 21:2771–2781.
16. Oh BJ et al. (2013) Co-transplantation of bone marrow-derived endothelial progenitor cells improves revascularization and organization in islet grafts. *Am J Transplant* 13:1429–40.
17. Quaranta P et al. (2014) Co-transplantation of endothelial progenitor cells and pancreatic islets to induce long-lasting normoglycemia in streptozotocin-treated diabetic rats. *PLoS One* 9:e94783.
18. Kang S et al. (2012) Endothelial progenitor cell cotransplantation enhances islet engraftment by rapid revascularization. *Diabetes* 61:866–76.
19. Sakata N et al. (2010) ITSC08 Efficacy Comparison between Intraportal and Subcapsular Islet Transplants in a Murine Diabetic Model. *Transplant Proc* 41:346–349.
20. Portalska KJ et al. (2013) Boosting Angiogenesis and Functional Vascularization in Injectable Dextran–Hyaluronic Acid Hydrogels by Endothelial-Like Mesenchymal Stromal Cells. *Tissue Eng Part A* 20:131112094536009.

21. Skårn M et al. (2014) Generation and Characterization of an Immortalized Human Mesenchymal Stromal Cell Line. *Stem Cells Dev* 00:1–13.
22. Rivron NC et al. (2012) Tissue deformation spatially modulates VEGF signaling and angiogenesis. *Proc Natl Acad Sci* 109:6886–6891.
23. Hilderink J et al. (2015) Controlled aggregation of primary human pancreatic islet cells leads to glucose-responsive pseudoislets comparable to native islets. *J Cell Mol Med* XX:1–11.
24. Cabrera O et al. (2006) The unique cytoarchitecture of human pancreatic islets has implications for islet cell function.
25. Kemp CB, Knight MJ, Scharp DW, Ballinger WF, Lacy PE (1973) Effect of transplantation site on the results of pancreatic islet isografts in diabetic rats. *Diabetologia* 9:486–491.
26. Schechner JS et al. (2000) In vivo formation of complex microvessels lined by human endothelial cells in an immunodeficient mouse. *Proc Natl Acad Sci U S A* 97:9191–9196.
27. Nör JE et al. (2001) Engineering and characterization of functional human microvessels in immunodeficient mice. *Lab Invest* 81:453–463.
28. Bara JJ, Richards RG, Alini M, Stoddart MJ (2014) Concise review: bone marrow-derived mesenchymal stem cells change phenotype following in vitro culture: implications for basic research and the clinic. *Stem Cells* 32:1713–23.
29. Kniazeva E, Kachgal S, Putnam AJ (2011) Effects of extracellular matrix density and mesenchymal stem cells on neovascularization in vivo. *Tissue Eng Part A* 17:905–914.
30. Rackham CL et al. (2013) Pre-culturing islets with mesenchymal stromal cells using a direct contact configuration is beneficial for transplantation outcome in diabetic mice. *Cytotherapy* 15:449–459.
31. Jung HS et al. (2014) The potential of endothelial colony-forming cells to improve early graft loss after intraportal islet transplantation. *Cell Transplant* 23:273–283.
32. Foty R a., Steinberg MS (2005) The differential adhesion hypothesis: A direct evaluation. *Dev Biol* 278:255–263.
33. Wang RN, Paraskevas S, Rosenberg L (1999) Characterization of integrin expression in islets isolated from hamster, canine, porcine, and human pancreas. *J Histochem Cytochem* 47:499–506.
34. Donovan D, Brown NJ, Bishop ET, Lewis CE (2001) Comparison of three in vitro human “angiogenesis” assays with capillaries formed in vivo. *Angiogenesis* 4:113–121.
35. Ghajar CM et al. (2010) Mesenchymal cells stimulate capillary morphogenesis via distinct proteolytic mechanisms. *Exp Cell Res* 316:813–825.
36. Abbey C a., Bayless KJ (2014) Matrix density alters zyxin phosphorylation, which limits peripheral process formation and extension in endothelial cells invading 3D collagen matrices. *Matrix Biol* 38:36–47.
37. Linn T et al. (2003) Angiogenic capacity of endothelial cells in islets of Langerhans. *FASEB J* 17:881–883.
38. Sieminski a. L, Hebbel RP, Gooch KJ (2004) The relative magnitudes of endothelial force generation and matrix stiffness modulate capillary morphogenesis in vitro. *Exp Cell Res* 297:574–584.
39. Sieminski a. L, Was a. S, Kim G, Gong H, Kamm RD (2007) The stiffness of three-dimensional ionic self-assembling peptide gels affects the extent of capillary-like network formation. *Cell Biochem Biophys* 49:73–83.
40. Ghajar CM et al. (2008) The effect of matrix density on the regulation of 3-D capillary morphogenesis. *Biophys J* 94:1930–1941.
41. Kniazeva E, Putnam AJ (2009) Endothelial cell traction and ECM density influence both capillary morphogenesis and maintenance in 3-D. *Am J Physiol Cell Physiol* 297:C179–C187.

42. Hiraoka N, Allen E, Apel IJ, Gyetko MR, Weiss SJ (1998) Matrix metalloproteinases regulate neovascularization by acting as pericellular fibrinolysins. *Cell* 95:365–377.
43. Kim I et al. (2000) Angiopoietin-1 induces endothelial cell sprouting through the activation of focal adhesion kinase and plasmin secretion. *Circ Res* 86:952–959.
44. Tarabozetti G et al. (2002) Shedding of the matrix metalloproteinases MMP-2, MMP-9, and MT1-MMP as membrane vesicle-associated components by endothelial cells. *Am J Pathol* 160:673–680.
45. Da Silva Meirelles L, Fontes AM, Covas DT, Caplan AI (2009) Mechanisms involved in the therapeutic properties of mesenchymal stem cells. *Cytokine Growth Factor Rev* 20:419–427.
46. Chen Q et al. (2013) Matrix metalloproteinases: Inflammatory regulators of cell behaviors in vascular formation and remodeling. *Mediators Inflamm* 2013.
47. Carmeliet P (2000) Mechanisms of angiogenesis and arteriogenesis. *Nat Med* 6:389–395.
48. Cross MJ, Claesson-Welsh L (2001) FGF and VEGF function in angiogenesis: Signalling pathways, biological responses and therapeutic inhibition. *Trends Pharmacol Sci* 22:201–207.
49. Grainger SJ, Carrion B, Ceccarelli J, Putnam AJ (2013) Stromal cell identity influences the in vivo functionality of engineered capillary networks formed by co-delivery of endothelial cells and stromal cells. *Tissue Eng Part A* 19:1209–22.

Chapter 5

Non-invasive monitoring of β -cells in a porous microwell scaffold platform by ¹¹¹In-exendin-3 SPECT imaging: a pilot study

Mijke Buitinga^{1}, Inge van der Kroon^{2*}, Maarten Brom²,
Roman Truckenmüller³, Clemens van Blitterswijk³, Gert-Willem Römer⁴,
Marcel Karperien¹, Martin Gotthardt², Aart van Apeldoorn¹*



¹ Department of Developmental BioEngineering, University of Twente, Enschede, The Netherlands

² Department of Radiology and Nuclear Medicine, Radboud University Medical Center, Nijmegen, The Netherlands

³ Complex Tissue Regeneration Department, Maastricht University, Maastricht, The Netherlands

⁴ Department of Applied Laser Technology, University of Twente, Enschede, The Netherlands

* Authors contributed equally

ABSTRACT

A reliable method for *in vivo* quantification of beta cell mass (BCM) could assist in the identification of a transplantation environment that is most beneficial for islet engraftment and long-term islet survival and function. In this pilot study, we investigated the potential of a GLP-1 analogue exendin-3 labelled with ^{111}In for monitoring of BCM following intraperitoneal islet transplantation in a microwell scaffold platform. The targeting characteristics of ^{111}In -labelled exendin-3 were examined in BALB/c mice transplanted with 1,000 islets in microwell scaffolds. Mice were injected with 15 MBq ^{111}In -labelled exendin-3 and single photon emission computed tomography (SPECT) acquisition was performed 1 h post injection, followed by dissection, biodistribution, *ex vivo* SPECT and autoradiography studies. Although the transplants were not visible *in vivo*, the uptake of ^{111}In -exendin-3 could be clearly visualized on *ex vivo* SPECT scans. Histology and autoradiography studies showed vascularized islets with specific uptake of ^{111}In -exendin-3 in β -cell areas. In this study, we provide the proof-of-principle that β -cells mass can be targeted with ^{111}In -exendin-3 after islet transplantation *in vivo*. This method provides a mean to monitor the influence of native and engineered transplantation sites on long-term β -cell survival aiding the development of an optimal transplantation environment for islets of Langerhans.

INTRODUCTION

A promising therapy option for patients with type 1 diabetes is the transplantation of islets of Langerhans from donor organs into the portal circulation (1). The long-term success of this treatment is still disappointing; only ~10% of the recipients are insulin independent five years after transplantation, most likely due to progressive islet loss (2). Although allograft rejection and autoimmune disease recurrence are likely to be involved in the long-term islet destruction (3), there is strong evidence that site-specific factors such as the exposure to high concentrations of immunosuppressants (4) and the instant blood-mediated inflammatory reaction (IBMIR) (5, 6), contribute to early islet loss. This early islet loss has driven the search for alternative transplantation sites. Many extrahepatic sites have been explored, but the ideal site remains to be identified (7, 8). However, to date, only islet function and not the exact β -cell mass can be determined after islet transplantation, whereas longitudinal monitoring of β -cell mass would aid in the identification of a transplantation site that is most beneficial for islet survival and engraftment.

Clinically relevant imaging modalities being explored for non-invasive monitoring of β -cell mass after transplantation are magnetic resonance imaging (MRI), positron emission tomography (PET), and single photon emission computed tomography (SPECT). MRI has the ability to provide high spatial resolution images. However, in order to obtain sufficient contrast between the islets and the surrounding tissue, islets need to be labelled *in vivo* or *ex vivo*. The feasibility of visualizing islets labelled with a paramagnetic compound prior to infusion was previously shown (9–14), however with the risk of iron overload (15). Despite the lower spatial resolution of PET and SPECT compared to MRI, the sensitivity of these modalities is superior to MRI. Early engraftment and post-transplant islet loss have been successfully monitored with PET using [^{18}F]fluorodeoxy-glucose-labelled islets (16–19). Long-term monitoring using this pre-labelling method however is impossible due to the short half-life (108 minutes) of the radioactive tracer and externalization from the islets (20). The development of radioactive labelled tracers that specifically target β -cells *in vivo* would allow serial imaging over time, since these tracers can be injected repeatedly. One of these tracers is exendin, a GLP-1R agonist (21, 22). GLP-1R is abundantly expressed in rat, mouse and human pancreatic β -cells but not in α -, δ - and PP-cells (23). It has been shown that this tracer can be labelled with indium-111 (21), copper-64 (24), or fluor-18 (25), and has been successfully applied to measure β -cell mass in both rodents (21, 24, 25) and humans (21) using SPECT (21) or PET (24, 25).

Recently, we have developed a porous microwell scaffold as a transplant vehicle that restricts islets to a confined environment for extrahepatic islet transplantation (26, 27). The islets retained in the scaffold have been shown to preserve their rounded morphology, undergo revascularization, and are able to reverse diabetes when transplanted extrahepatically in diabetic mice (27). In the current study, we investigated the potential of exendin-3 labelled with indium-111 for determination of BCM following intraperitoneal islet transplantation in

two different microwell scaffold designs. In the future, this method would allow monitoring the effect of different scaffold designs and transplantation sites on β -cell survival.

MATERIALS AND METHODS

Microwell scaffold fabrication

Scaffolds consisted of a thin polymer film patterned with microwells and a porous cap with ~ 40 μm pores. The porous microwell scaffolds were prepared as described previously (27). Briefly, scaffolds were fabricated from 400PEOT30/PBT70 thin polymer films. These films were rendered porous by laser drilling using an Yb:YAG laser source (TruMicro 5050, Trumpf GmbH, Germany) with a fixed pulse duration of 7 ps, a maximum pulse frequency of 400 kHz, and a central wavelength of 1030 nm (IR). Thin polymer films were stretched on a Teflon sample holder to ensure a flat surface for laser processing. Pores with a diameter of 10 μm and an inter-pore spacing of 50 μm were obtained by percussion drilling using a pulse energy (E_p) of 1 μJ and 150 pulses at a pulse-repetition frequency (F_{pr}) of 10 kHz. For the caps, trepanning with a pulse energy of 1 μJ , a pulse-repetition frequency of 10 kHz, 2 iterations, and a speed of 15 mm/s was used to obtain pores with a diameter of 40 μm and an inter-pore spacing of 200 μm .

Subsequently, microwells were introduced into the thin polymer films using microthermoforming as described previously (26). For this, the thin polymer film was heated and pressed into a negative, stainless steel mold (produced by Lightmotif BV, The Netherlands) using polyethylene films as backing material. Molding temperature and pressure were 85°C and 45 kN, respectively.

In this study, two methods were assessed to attach the cap to the microwell-patterned film. For the first method, the cap was sutured (sutured scaffold) to the patterned film as described previously (27), whereas a sealing technique was developed for the second method (sealed scaffold) (Figure 1). The latter method involved two metal plates, both containing a circular hole with a diameter of 1 cm and a groove at one side of the hole. The porous microwell scaffold and cap were placed between the two metal plates and hot-pressed at 130°C for two minutes at 150 kN. Only at the position of the groove, the scaffold and cap were not sealed, forming the inlet of the scaffold.

Islet isolation, scaffold seeding, and implantation

Islets were isolated from eight weeks old female BALB/c mice by enzymatic digestion. Immediately after CO₂ euthanization, a midline abdominal incision was made and the common bile duct was exposed and cannulated. The pancreas was perfused with 2 mL of 0.9 mg/mL collagenase type V (Sigma Aldrich, USA) in RPMI-1640 medium (Invitrogen, USA). The pancreas was dissected and digested at 37°C for 12 minutes. The digestion was stopped by adding complete RPMI medium (RPMI-1640 medium supplemented with 10% fetal calf serum (HyClone, Celbio, USA), 2 mM L-glutamine (Sigma Aldrich, USA), 100 U/ml penicillin and 100 U/ml streptomycin

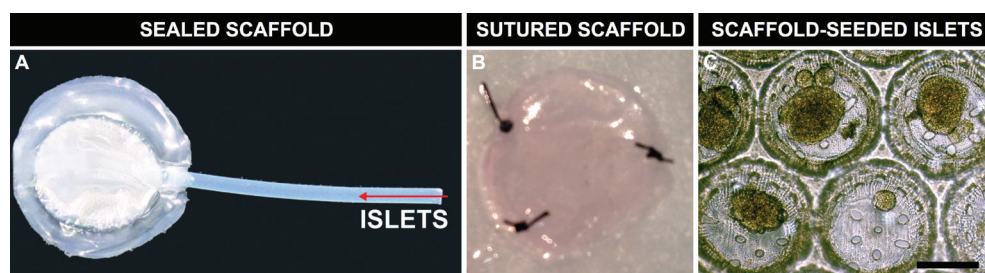


Figure 1: A) Sealed and B) sutured microwell scaffolds. Islets are seeded using polyethylene tubing. C) Light-microscopy image of scaffold-seeded islets. Scalebar: 200 μ m.

(Sigma Aldrich, USA)). The digested tissue was washed twice in complete RPMI medium and filtered through a 500 μ m mesh. Subsequently, the islets were purified on a discontinuous Ficoll gradient (densities 1.108, 1.096, 1.037 g/ml, Cellgro by Mediatech Inc., USA), washed, and cultured overnight in complete RPMI medium.

For scaffold seeding, 1,000 islets were aspirated in complete RPMI medium in polyethylene tubing (PE50, Becton Dickinson, USA) using a Hamilton syringe (Hamilton Company, USA) and gently infused into the scaffold.

As transplant recipients, eight weeks old female BALB/c mice were used. Prior to isoflurane anesthetics (induction 4-5%, maintenance 1.5-2% in O_2 and air), recipient mice were given Carprofen (5 mg/kg s.c., Pfizer Animal Health B.V., Netherlands) for analgesia. The intraperitoneal fat was exposed by a midline, abdominal incision. The scaffold was transplanted between the peritoneum and the intraperitoneal fat and fixated to the peritoneum with one suture. The peritoneum and skin were sutured. Mice were allowed free access to food and water postoperatively and were routinely checked throughout the duration of the study. In total three mice were transplanted; one with an empty scaffold, one with a sutured scaffold, and one with a sealed scaffold.

Radiolabelling

[Lys⁴⁰(DTPA)]exendin-3 (Peptides Specialty Laboratories, Heidelberg, Germany) was radiolabelled as described by Brom *et al* (21). Briefly, 150 MBq ¹¹¹InCl₃ was added to 1 μ g [Lys⁴⁰(DTPA)]exendin-3 dissolved in 0.5 M MES, pH 5.5 (Sigma Aldrich, USA) and incubated for 20 minutes at room temperature. After incubation, EDTA (Sigma Aldrich, USA) and Tween80 (Sigma Aldrich, USA) were added to a final concentration of 5 mM and 0.1%, respectively. The radiochemical purity of ¹¹¹In-exendin-3 was determined by instant thin-layer chromatography (ITLC-SG, Pall Corporation Life Sciences, USA), using 0.1 M NH₄Ac (Sigma Aldrich, USA) in 0.1 M EDTA, pH 5.5.

The reaction mixture was purified by solid-phase extraction using hydrophilic-lipophilic balance (HLB) cartridge (30 mg, Water Oasis, Milford, MA, USA), to eliminate the unlabelled

^{111}In . The cartridge was activated with 1 ml ethanol, washed with 2 ml water and conditioned with 1 ml of 0.5 M MES, pH 5.5. Subsequently the labelling mixture was loaded on the cartridge and washed with 1 ml 0.5 M MES and 2 ml water. ^{111}In -exendin-3 was eluted from the cartridge with 200 μL 100% ethanol. For injection, the purified labelling solution was diluted in 0.5% BSA/PBS to obtain a final ethanol concentration of less than 10%.

SPECT acquisition, reconstruction and biodistribution

Two and four weeks after transplantation mice were injected intravenously in the tail vein with 15 MBq ^{111}In -exendin-3 (peptide dose 0.1 μg (20 pmol) in 200 μl 0.5% BSA/PBS). One hour after injection, mice were anesthetized with isoflurane (induction 4-5%, maintenance 1.5-2% in O_2 and air). Before SPECT/CT acquisition, the bladder was catheterized and rinsed with sterile 0.9% NaCl to remove radioactive urine. Subsequently, SPECT images were acquired using a dedicated small animal SPECT/CT scanner (U-SPECT-II, MILabs, The Netherlands) with a 1.0 mm pinhole general-purpose mouse collimator, 36 bed positions with an acquisition time of 50 minutes. Subsequently CT images were acquired for anatomical information (65 kV, 615 μA , 1 bed position). After the last SPECT/CT acquisition, mice were euthanized by CO_2/O_2 suffocation and the grafts were retrieved and fixed in 1% paraformaldehyde in PBS. The pancreas and other relevant tissues were dissected, weighed and counted in a γ -counter (Wallac 1480-Wizard; Perkin-Elmer, Boston, MA, USA) to determine the distribution of the tracer uptake. The %ID per gram of tissue (%ID/g) was calculated for each tissue. In addition, SPECT images of the dissected islet grafts were acquired with a 1.0 mm pinhole general-purpose rat and mouse collimator, 45 bed positions with an acquisition time of 6 hours. To enable quantification of the SPECT-signal, 7 standards with activities between 5-300 kBq were scanned with the same settings. After SPECT imaging, islet grafts were post-fixed in 4% paraformaldehyde in PBS at 4°C for 4 hours. All SPECT images were reconstructed using the U-SPECT reconstruction software (U-SPECT-Rec, MILabs, The Netherlands) with the following settings: OSEM (1 iteration, 16 subsets, voxel size 0.75 mm^3). A 3-dimensional (3D) volume of interest was drawn around the scaffolds using Inveon Research Workplace software (IAW 4.0; Siemens Preclinical Solutions, Knoxville, USA) to quantify the uptake in the grafts.

Immunohistochemistry

Histological analyses were performed to assess islet morphology, cellular composition, and vascularization. Each scaffold containing the islet graft was completely sectioned in five-micrometer slices. To identify islet-containing regions, sections spaced 50 μm apart were stained for insulin combined with a Masson-Goldner trichrome staining. For this, sections were deparaffinized, and antigen retrieval was performed for 10 minutes at 100 °C in a PT module (DAKO, Denmark) using citrate buffer (pH 6.0). Slides were incubated with rabbit anti-insulin IgG (Santa Cruz Biotechnology, USA, 1:50, 1h) followed by an HRP- conjugated swine-anti-rabbit IgG (DAKO, Denmark, 1:50, 30 min) and developed with 3,3'-diaminobenzidine tetrahydrochloride

(Sigma Aldrich, USA). Subsequently, slides were stained with Masson-Goldner trichrome (Merck Chemicals, Germany, according to manufacturer's protocol). Slides were imaged using a 3DHistech Panoramic 250 Flash II scanner (3DHistech, Hungary).

To assess cellular composition and vascularization, slides were immunostained for insulin, glucagon, and collagen IV. For this, primary antibodies against insulin (guinea pig-anti-insulin, DAKO, Denmark, 1:1,000, 1h, 37°C), glucagon (rabbit-anti-glucagon, Abcam, USA, 1:2000, 1h, 20°C) and collagen IV (Southern Biotech, USA, 1:100, o/n, 4°C) were used. Secondary antibodies were Alexa-647-anti-guinea pig (Invitrogen Life Technologies, UK, 1:500, 1h, 20°C), Alexa-488-goat-anti-rabbit (Invitrogen Life Technologies, UK, 1:500, 1h, 20°C), and Cy3-donkey-anti-goat (Jackson ImmunoResearch, USA, 1:200, 1h, 20°C). DAPI (Invitrogen Life Technologies, UK) was applied as nuclear counterstaining. Sections were examined using a Zeiss

Axioskop microscope (Zeiss, Germany) with a custom designed macro.

Digital autoradiography

Ex vivo digital autoradiography was performed to visualize tracer accumulation. Sections (5 μm), 50 μm apart were exposed to a phosphor imaging plate (Fuji Film BAS-SR 2025, Raytest, Straubenhardt, Germany) for 7 days at room temperature. After 7 days, the imaging plate was developed using a radioluminography laser imager (Fuji Film BAS 1800 II system, Raytest, Germany).

Micro-autoradiography

Ex vivo micro-autoradiography was performed on 5 μm tissue sections. Sections were deparaffinized and dipped in a hypercoat emulsion (Amersham LM-1, GE Healthcare, UK) at 42 °C to create a homogeneous coating on the slide and incubated in the dark. After 3 weeks sections were developed for 3 minutes with D-19 developer (Kodak, USA) and fixed with a 24 % (w/v) sodium thiosulphate solution for 4 minutes. The sections were rinsed with water for 1 minute and stained with Haematoxylin for 30 seconds. After imaging using a 3DHistech Panoramic 250 Flash II scanner (3DHistech, Hungary), slides were immunostained for insulin and glucagon, as described before, and imaged with an Olympus FV1000 Confocal Laser Scanning Microscope (Olympus, Japan).

RESULTS

Radiolabelling

Exendin-3 was labelled with ^{111}In with a specific activity of 700 GBq/ μmol . Chemical purity exceeded 99% after HLB purification.

Biodistribution

The results of the biodistribution two hours after intravenous injection of radiolabelled exendin-3 are summarized in Figure 2. The uptake in the sealed and sutured scaffold was higher compared to the uptake in the empty scaffold (sealed scaffold: 1.5% ID, sutured scaffold: 1.0% ID, empty scaffold: 0.7 %ID). Organs known to express the GLP-1R, such as the pancreas, stomach, duodenum and lungs show high uptake of ^{111}In -exendin-3, which correspond with observations described previously (28). The kidneys show high non-GLP-1R mediated uptake (>70 %ID/g) due to reabsorption and retention of ^{111}In -exendin-3 in the proximal tubules (29).

SPECT imaging

To visualize early engraftment of the islets in the scaffold two and four weeks after transplantation *in vivo* SPECT images were acquired. No SPECT signal in the scaffold could be observed (data not shown).

Four weeks after transplantation scaffolds were dissected, and scanned *ex vivo*. The uptake of ^{111}In -exendin-3 was clearly visualized in both scaffold types (Figure 3). The uptake was >2 times higher for both scaffolds compared to the uptake in the empty control scaffold (sealed scaffold: 189.9 kBq, sutured scaffold: 169.2 kBq, empty scaffold: 83.4 kBq).

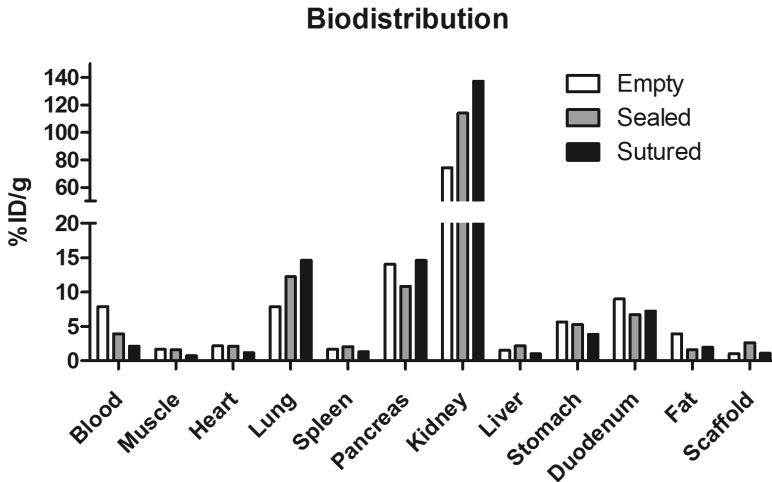


Figure 2: Biodistribution of ^{111}In -labelled exendin-3 in BALB/c mice with an empty scaffold, a sealed scaffold containing 1,000 islets, or a sutured scaffold containing 1,000 islets (expressed as % injected dose/g tissue [%ID/g]). Organs and scaffolds were dissected 2 h p.i.

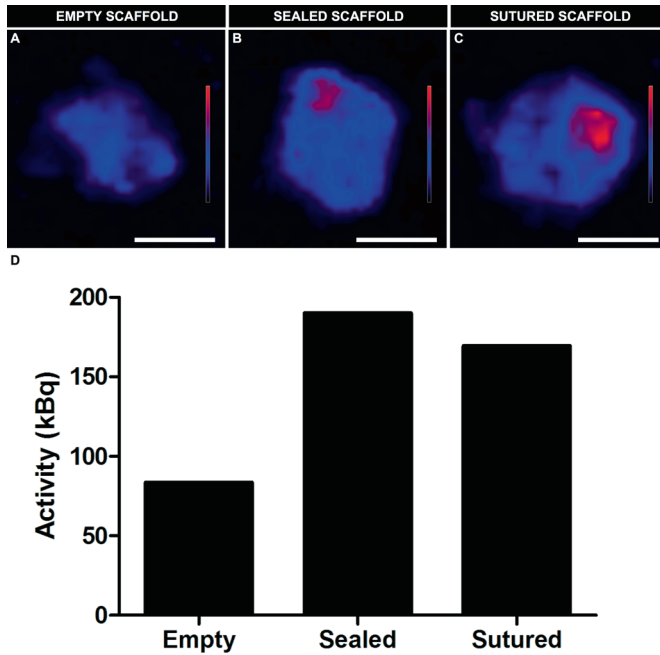


Figure 3: *Ex vivo* SPECT scans of a dissected A) empty scaffold, B) sealed scaffold containing 1,000 islets, and C) sutured scaffold containing 1,000 islets four weeks after implantation. D) ^{111}In -labelled exendin-3 uptake in the scaffolds determined by quantitative analysis of SPECT scans.

Autoradiography and histology

Ex vivo digital autoradiography of 5 μm scaffold sections demonstrated hotspots of ^{111}In -exendin-3 accumulation (Figure 4A-B). Insulin staining on consecutive sections, clearly showed co-localization of these hotspots with scaffold-implanted islets (Figure 4C-D). The insulin-trichrome staining showed strong infiltration of host cells with loose fibrous tissue formation within both scaffold types. However, islets were better retained within the microwells when sutures were used to attach the cap on the microwell patterned film; in the sealed scaffold, infiltrating tissue displaced the islets out of the microwell structure and islets were engrafted between the microwell patterned film and the cap (Figure 4 C-D).

Collagen IV immunohistochemistry, a marker for vascular basal lamina, showed vascular structures within the islets (Figure 4E-F). These vessels were functional as indicated by the presence of red blood cells in the insulin-trichrome staining (Figure 4G-H). Islets were positive for both insulin and glucagon. However, the characteristic core-mantle structure as observed in native rodent islets is disrupted in the scaffold-implanted islets (Figure 4I-J). Detailed evaluation of tracer uptake by micro-autoradiography indicated co-localization of tracer uptake with insulin positive regions and not with glucagon positive regions (Figure 5A-B).

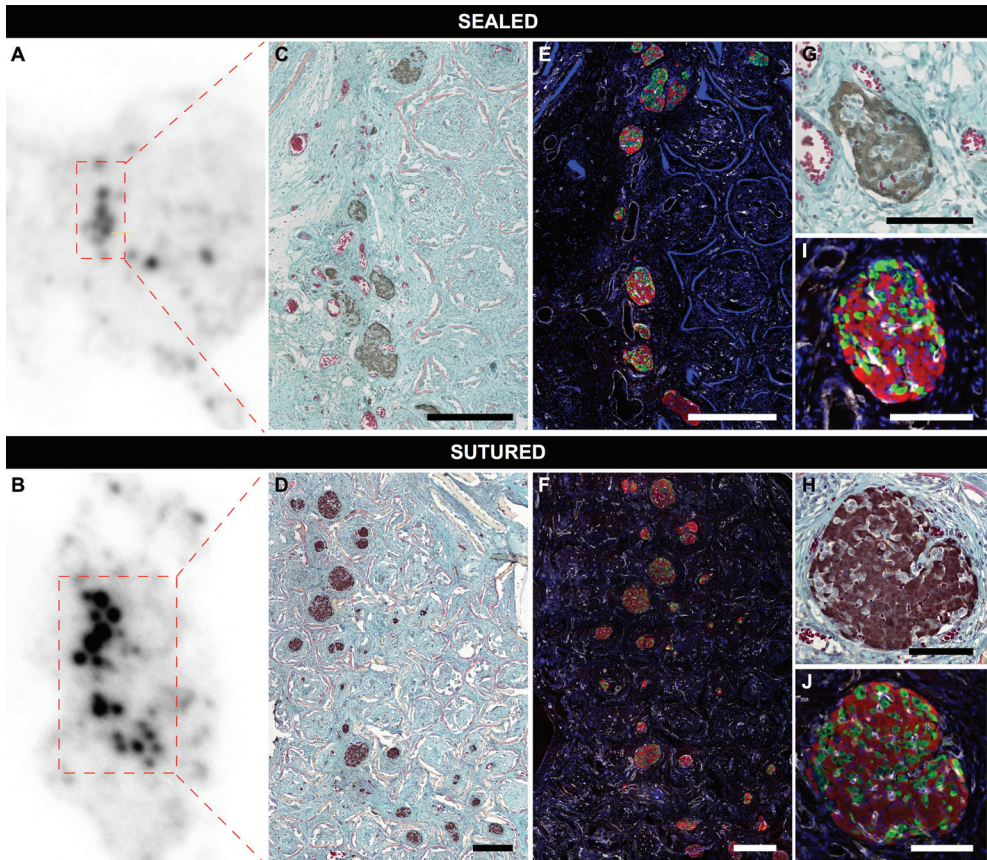


Figure 4: A-B) Macroautoradiography of a A) sealed and B) sutured scaffold containing 1,000 islets indicating the presence of activity within scaffold-implanted islets. Consecutive sections were stained for insulin and Masson's Trichrome (C-D) and insulin (red), glucagon (green) and collagen IV (white) (E-F). (G-J) Enlargements of scaffold-implanted islets indicating the presence of perfused blood vessels and the expression of insulin and glucagon. Scalebars C-F: 400 μm . Scalebars G-J: 100 μm

DISCUSSION

In the current study, we propose a method to non-invasively monitor the β -cell mass *in vivo* after extrahepatic islet transplantation in porous microwell scaffolds using ^{111}In -exendin-3. Two different microwell scaffold designs were monitored; fabricated of a porous microwell film with a cap that is either sutured or sealed to the microwell film. Although islets in both scaffold designs were not visible *in vivo*, the uptake of ^{111}In -exendin-3 could be clearly visualized on *ex vivo* SPECT scans. Histology and autoradiography studies showed vascularized islets with specific uptake of ^{111}In -exendin-3 in β -cell areas. To date, only β -cell function can be determined non-invasively after transplantation. However, this does not provide information about the amount

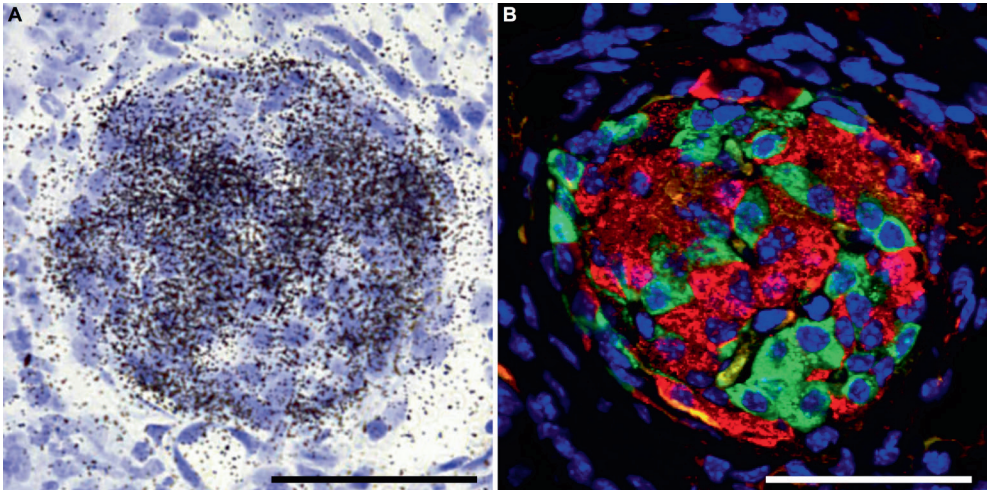


Figure 5: A) Microautoradiography of a scaffold-implanted islet. (B) After microautoradiography the section was stained for insulin and glucagon indicating specific uptake in insulin-positive cells. Scalebars: 100 μ m.

of β -cells present at the time of measurement. Provided that β -cell mass can be determined *in vivo*, this method would enable studying the relation between β -cell function and β -cell mass and aid in identifying factors and transplantation environments that improve long-term graft performance.

Previously, bioluminescent imaging has been used to visualize islets transplanted in biomaterial carriers (30). Although this method is feasible for intravital monitoring of scaffold-implanted islets, the use of bioluminescence hampers the clinical application. Witkowski *et al.* successfully visualized 200 islets transplanted intramuscularly in cyclic-RGDfK-modified alginate hydrogels using ^{11}C labelled dihydrotetrabenazine (DTBZ) (31). DTBZ is a specific ligand for the vesicular monoamine transporter type 2 (VMAT2). However, VMAT2 is expressed on both β - and PP-cells, which makes this tracer unsuitable for absolute quantification of β -cell mass (32). In contrast to VMAT2, GLP-1R is expressed by β -cells but not by α -, δ - and PP-cells (23). Previously, we have shown a linear correlation between pancreatic uptake of ^{111}In -labelled exendin-3 and β -cell mass (21), but not with the alpha cells mass (33), indicating the potential of this tracer for intravital β -cell mass quantification

In this study we show that a clear *ex vivo* SPECT signal can be obtained from 1,000 islets transplanted within both scaffold designs. However, during *in vivo* imaging no SPECT signal could be detected. This is in contrast to unpublished results of Eter *et al.* who show that even a low islet mass of 50 islets can be visualized with this technique after intramuscular transplantation (34). This discrepancy might be explained by a difference in packing density of the islet grafts; inter-islet spacing in the scaffold is ~ 400 μ m whereas intramuscular islet grafts are densely

packed. This results in a lower signal intensity per volume in scaffold-implanted islet grafts. In addition, the height of the scaffold is 350 μm , which is near the lower range of the resolution of the scanner. Therefore, the resulting signal intensity could be close to, or even below the detection limit of the SPECT system. Also the lower target-to-background ratio could explain the absence of SPECT signal, since the scaffolds were transplanted near the stomach and the duodenum, which have a higher uptake compared to the muscle (Figure 2).

Another important factor to consider is the survival of β -cells during the engraftment period in microwell scaffolds. It might be that too many β -cells are lost during engraftment to obtain a sufficient target-to-background ratio for imaging. Previously, we have shown that islets transplanted in the sutured scaffolds become highly vascularized and are able to restore blood glucose levels in diabetic mice (27). However, we did observe an anisotropic vascularization pattern in scaffold-implanted islets with a higher vascular density in the outer shell compared to the inner core and a concomitant reduction in cellular density (27). It is known that β -cells are highly susceptible to hypoxia leading to β -cell death (35). In line with our previous results (27), we observe that the characteristic core-mantle structure of murine islets is disrupted after islet transplantation, which might be an indication of cellular rearrangement after cell-death in the β -cell rich islet core. However, further studies are needed to evaluate whether the absence of *in vivo* SPECT-signal is due to substantial β -cell death or the large inter-islet spacing.

The current study proposes a method to non-invasively monitor β -cell mass within a microwell scaffold platform. This pilot study showed that the tracer is able to target the islets four weeks after transplantation as indicated by a clear tracer uptake in the *ex-vivo* SPECT-scans and autoradiography. Provided that islets can be visualized within microwell scaffolds using ^{111}In -exendin-3, the combined strategy of controlled islet transplantation in a confined environment and SPECT imaging would provide the opportunity to study the effect of different transplantation sites or modifications of the engineered microenvironment on β -cell survival.

REFERENCES

1. Shapiro AM et al. (2006) International trial of the Edmonton protocol for islet transplantation. *N Engl J Med* 355:1318–1330.
2. Ryan EA et al. (2005) Five-year follow-up after clinical islet transplantation. *Diabetes* 54:2060–2069.
3. Abreu JRF, Roep BO (2013) Immune monitoring of islet and pancreas transplant recipients. *Curr Diab Rep* 13:704–12.
4. Desai NM et al. (2003) Elevated portal vein drug levels of sirolimus and tacrolimus in islet transplant recipients: local immunosuppression or islet toxicity? *Transplantation* 76:1623–5.
5. Moberg L et al. (2002) Production of tissue factor by pancreatic islet cells as a trigger of detrimental thrombotic reactions in clinical islet transplantation. 360:11–13.
6. Johansson H et al. (2005) Tissue factor produced by the endocrine cells of the islets of Langerhans is associated with a negative outcome of clinical islet transplantation. *Diabetes* 54:1755–62.
7. Merani S, Toso C, Emamaullee J, Shapiro AM (2008) Optimal implantation site for pancreatic islet transplantation. *Br J Surg* 95:1449–1461.
8. Cantarelli E, Piemonti L (2011) Alternative transplantation sites for pancreatic islet grafts. *Curr Diab Rep* 11:364–74.
9. Jiráková D et al. (2004) MRI of transplanted pancreatic islets. *Magn Reson Med* 52:1228–1233.
10. Joo HT et al. (2006) Imaging islets labeled with magnetic nanoparticles at 1.5 Tesla. *Diabetes* 55:2931–2938.
11. Evgenov N V, Pratt J, Pantazopoulos P, Moore A (2008) Effects of glucose toxicity and islet purity on in vivo magnetic resonance imaging of transplanted pancreatic islets. *Transplantation* 85:1091–1098.
12. Juang JH et al. (2010) Magnetic resonance imaging of transplanted mouse islets labeled with chitosan-coated superparamagnetic iron oxide nanoparticles. *Transplant Proc* 42:2104–2108.
13. Zacharovová K et al. (2012) Processing of superparamagnetic iron contrast agent ferucarbotran in transplanted pancreatic islets. *Contrast Media Mol Imaging* 7:485–493.
14. Malosio ML et al. (2014) MR Imaging Monitoring of Iron Labeled Pancreatic Islets in a Small Series of Patients: Islets Fate in Successful, Unsuccessful and Auto-Transplantation. *Cell Transplant*.
15. Toso C et al. (2008) Clinical magnetic resonance imaging of pancreatic islet grafts after iron nanoparticle labeling. *Am J Transplant* 8:701–6.
16. Toso C et al. (2005) Positron-Emission Tomography Imaging of Early Events after Transplantation of Islets of Langerhans. *Transplantation* 79:353–355.
17. Eich T et al. (2007) Positron emission tomography: a real-time tool to quantify early islet engraftment in a preclinical large animal model. *Transplantation* 84:893–8.
18. Eich, Torsten, Eriksson O (2007) Visualization of Early Engraftment in Clinical Islet Transplantation by Positron-Emission Tomography. *N Engl J Med*.
19. Eriksson O et al. (2009) Positron emission tomography in clinical islet transplantation. *Am J Transplant* 9:2816–24.
20. Medarova Z, Moore A (2008) Non-invasive detection of transplanted pancreatic islets. *Diabetes Obes Metab* 10:88–97.
21. Brom M et al. (2014) Non-invasive quantification of the beta cell mass by SPECT with (111)In-labelled exendin. *Diabetologia*.
22. Nalin L et al. (2014) Positron emission tomography imaging of the glucagon-like peptide-1 receptor in healthy and streptozotocin-induced diabetic pigs. *Eur J Nucl Med Mol Imaging*.

23. Tornehave D, Kristensen P, Rømer J, Knudsen LB, Heller RS (2008) Expression of the GLP-1 receptor in mouse, rat, and human pancreas. *J Histochem Cytochem* 56:841–51.
24. Wu Z et al. (2011) In Vivo Imaging of Transplanted Islets with (64)Cu-DO3A-VS-Cys(40)-Exendin-4 by Targeting GLP-1 Receptor. *Bioconjug Chem* 22:1587–1594.
25. Wu Z et al. (2013) Development and evaluation of 18F-TTCO-Cys40-Exendin-4: a PET probe for imaging transplanted islets. *J Nucl Med* 54:244–51.
26. Buitinga M et al. (2013) *Microwell scaffolds for the extrahepatic transplantation of islets of langerhans.*
27. Buitinga M et al. (2015) *Microwell scaffolds with a defined porosity: a potential platform for extrahepatic islet transplantation. Unpublished data.*
28. Brom, M, Joosten, L, Oyen, W.J.G, Gotthardt, M, Boerman OC (2012) Radiolabelled GLP-1 analogues for in vivo targeting of insulinomas Maarten. *Contrast* 7:160–166.
29. Vegt E et al. (2010) Albumin-derived peptides efficiently reduce renal uptake of radiolabelled peptides. *Eur J Nucl Med Mol Imaging* 37:226–34.
30. Blomeier H et al. (2006) Polymer scaffolds as synthetic microenvironments for extrahepatic islet transplantation. *Transplantation* 82:452–459.
31. Witkowski P et al. (2009) Islet grafting and imaging in a bioengineered intramuscular space. *Transplantation* 88:1065–74.
32. Freeby M, Ichise M, Harris PE (2012) Vesicular monoamine transporter, type 2 (vmat2) expression as it compares to insulin and pancreatic polypeptide in the head, body and tail of the human pancreas. *Islets* 4:393–397.
33. Brom M, Joosten L, Frielink C, Boerman O, Gotthardt M (2015) 111In-exendin Uptake in the Pancreas Correlates With the β -Cell Mass and Not With the α -Cell Mass. *Diabetes* 64:1324–1328.
34. Eter WA et al. (2015) *Quantitative imaging of transplanted beta cells with SPECT using In-111-labeled exendin-3. Unpublished data.*
35. Bloch K, Vennäng J, Lazard D, Vardi P (2012) Different susceptibility of rat pancreatic alpha and beta cells to hypoxia. *Histochem Cell Biol* 137:801–810.

Chapter 6

Conclusions and Outlook



6.1 THE ISLET TRANSPLANTATION DILEMMA

The main objective of the work described in this thesis was to develop bioengineering strategies to improve the outcome of islet transplantation. Maintaining insulin production by the transplantation of pancreatic islets in the liver represents a promising therapeutic strategy to improve glycemic control in patients with type 1 diabetes. However, to date, the restoration of euglycemia is short-lived, requires islets from multiple donors, and necessitates life-long immunosuppressive therapy. In **chapter 1**, we identified multiple barriers to successful islet transplantation, such as delayed and insufficient islet revascularization, the presence of an instant blood-mediated inflammatory reaction, toxicity of immunosuppressive drugs, allograft rejection and autoimmune recurrence. These barriers embody the current dilemma of islet transplantation strategies: should we improve islet revascularization or promote immunoprotection? Pursuing one course of action will typically exacerbate the other, and vice versa, causing any attempt to improve the transplantation outcome to negatively affect islet survival. Immunoprotection has the great advantage of shielding the islets from the auto- and alloimmune reactions (1). However, absolute immunoprotection requires the absence of intra-islet vascularization, which interferes with both functional performance and survival of the islets. A mathematical model developed by Buchwald *et al.*, coupling hormone secretion and nutrient consumption kinetics with diffusive and convective transport, clearly predicts the physiological limitations of alginate-encapsulation regarding the glucose-stimulated insulin release (2), which is consistent with *in vivo* observations, as reviewed in (3). On the other hand, rapid and extensive islet revascularization will limit hypoxic damage, but requires immunosuppression regimens, which are islet-toxic and interfere with insulin secretion, insulin action, impairing islet engraftment, and neogenesis (4). In our opinion, the answer to this conundrum and the future of islet transplantation will likely involve a combinatorial approach of inducing durable immunologic tolerance towards the islet graft while supporting rapid and abundant revascularization. As a step towards the “ultimate islet transplantation strategy”, we have focused on bioengineering strategies to facilitate and stimulate islet vascularization after transplantation in order to overcome some of the barriers associated with intrahepatic islet transplantation.

6.2 BIOENGINEERED CONSTRUCT FOR ISLET TRANSPLANTATION

6.2.1 Conceptual design, *in vivo* performance and their implications

In this thesis we have described the development of a novel scaffold platform to support extrahepatic islet transplantation. The microwell scaffold design is conceptualized to address three central tenets considered essential for islet survival and function: preservation of native islet morphology, maximizing nutrient diffusion, and supporting islet revascularization.

Preservation of native islet morphology – In **chapter 2** we have shown that the microwell structure in conjunction with a polymeric biomaterial with low cell adhering properties is able to preserve islet morphology and function *in vitro*. It has been reported by others that disruption of the islet microanatomy by dispersion (5, 6) as well as spreading due to islet attachment on tissue culture plastic (7) can result in altered insulin secretory responses. The finding that alterations in insulin secretion caused by dispersion can be reversed by reaggregation (5, 6) supports the notion that cell-to-cell coupling and communication within the islet are pivotal for normal insulin secretion (8). Furthermore, *in vitro* islet culture on adherent substrates has demonstrated loss of native islet morphology with proliferating mesenchymal stromal cells migrating out of islets and a gradual loss of insulin staining. Lineage-tracing studies have provided evidence that this loss of insulin staining is associated with de-differentiating beta-cells (9). Besides cell attachment and loss of islet morphology, the aggregation and fusion of multiple islets affects mass transport of nutrients and oxygen. Several studies have shown that an increase in islet size is associated with more abundant apoptosis and necrosis in the central core of the islet (10–12), resulting in decreased *in vivo* performance (11, 12). Previously reported porous sponges designed for islet transplantation can prevent mass fusion to some degree, but these constructs have poor control over islet spacing, distribution and density (13–21) and can still allow islets to aggregate and coalesce. Creating microwells with an appropriate size and distribution makes it possible to sequester and retain islets while limiting islet aggregation and fusion and maintaining islet morphology.

Maximizing nutrient diffusion – The second tenet is maximizing the diffusion capacity of the scaffold for nutrients and oxygen. While native islets are highly vascularized, islet isolation procedures sever vascular connections of islets. Until islets become revascularized, a process initiated several days after transplantation, they are solely dependent on diffusion for nutrients and oxygen (22). Several *in vitro* studies have highlighted the significance of oxygen and nutrients for islet survival and function; mild deprivation already results in central core necrosis (10, 23) and is detrimental to the glucose-stimulated insulin secretion capacity of the islets (24, 25). Therefore, a high degree of porosity is an important hallmark of our scaffold design. In **chapter 2**, we have explored the use of electrospinning to fabricate fibrous porous scaffolds. Electrospinning utilizes an electrostatic field to control the formation and deposition of polymeric fibers, mimicking the fibrillar structure of extracellular matrix (26). To our knowledge, we are the first to apply a 3D structure to porous fibrous sheets using microthermoforming. Although we report an increase in the diffusion capacity, diffusion is hampered due to compression of the fibrous mesh. Possible strategies to increase the porosity and pore size are the use of patterned collectors to avoid pressure assisted microwell formation (27), adaptation of electrospinning parameters such as fiber diameter, or post-electrospinning modifications such as co-electrospinning with a sacrificial polymer and hybrid processes with polymer melt deposition (28). In addition, these fabrication approaches can assist in the creation of multifaceted constructs with, for example, varying degrees of degradation rates to create

gradients of diffusible chemo-attractants for guided vascular ingrowth or producing multiple fiber populations exhibiting different conjugation chemistries to introduce various proteins supporting islet survival and function as well as vascular infiltration.

Supporting islet revascularization – As pore size, porosity, and pore interconnectivity not only dictate the exchange of nutrients, metabolites, and waste products, but also the extent of vascular infiltration and tissue ingrowth, a greater degree of control over pore size and porosity is necessary to meet the third tenet of vascular infiltration. Observations by others have indicated that pore size of an implanted scaffold, as opposed to the scaffold material, influences the vascular density of the capsule that is formed around the implant. These studies report an optimum pore size around 30–40 μm (29–35), motivating us to obtain pores with a maximum diameter of 40 μm . This pore size also guarantees islet retention, since the majority of islets are bigger than 50 μm (36). In **chapter 3**, we have explored three other techniques to introduce well-defined pores in the microwell scaffold platform; 1) particulate leaching using salt crystals; 2) solvent casting on patterned silicon wafers; and 3) laser drilling using an ultra short laser source. As reported in this chapter, the latter method is most flexible and reproducible, with a pore-size range between ~ 10 –40 μm .

In vivo evaluation of islet-seeded laser drilled scaffold has shown that the obtained pores allow vascular infiltration and that islet function could be restored. Six out of eight animals (75%) reverted to stable normoglycemia. However, the mean time to remission was slightly, though not significantly, longer compared to renal subcapsular islet grafts (scaffold: 6.2 ± 3.2 days vs. kidney capsule: 2.2 ± 0.83 days). Histological evaluation four weeks after implantation found a difference in vascularization pattern in scaffold-implanted islets compared to native pancreatic islets, with a higher vascular density in the outer shell of the islets compared to the inner core, whereas renal subcapsular islet grafts showed a more homogeneous vascularization pattern. We hypothesize that the observed vascularization pattern in scaffold-implanted islets is a result of oxygen-gradient dependent cell death and a concomitant reduction in expression of proangiogenic factors, such as VEGF, due to a delay in revascularization. Indeed, we observed a corresponding pattern of decreased cellular density in the islet core, attributed primarily to a significant reduction in beta-cell density. In the immediate post-transplantation period islets are exposed to hypoxia (37). Although hypoxia enhances VEGF-A expression and secretion from islet cells, thereby inducing revascularization, prolonged hypoxic exposure has been shown to result in central core necrosis and cell death (10). This cell loss would translate to a decrease in VEGF-A production in the islet core, reinforcing a superficial revascularization pattern. Lammert *et al.* (38) have shown that inactivation of VEGF-A in pancreatic islets leads to a profound loss of intra-islet capillary density, vascular permeability, and islet function. In particular, when only the VEGF-A production in murine beta-cells is inactivated, the vessel density in the islet core is much lower than around the islet perimeter where VEGF-A is still expressed by non-beta-cells (39). This vascularization pattern is similar to the pattern observed in our scaffold-implanted islets,

which underlines our hypothesis that the observed vascularization pattern might be related to a reduction in VEGF-A expression due to cellular death in the islet core.

Besides hypoxia, also elevated blood glucose levels (40, 41), lipids (42, 43), and inflammatory cytokines (44) can lead to beta-cell dedifferentiation and apoptosis. As we have transplanted islets in diabetic mice, glucotoxicity might have contributed to the observed reduction in beta-cell mass. It has been shown that islet cell apoptosis is increased when islets are transplanted in hyperglycemic mice compared to islet transplantation in insulin-treated mice (45). Davalli *et al.* have also reported that the presence of diabetes has an adverse effect on beta-cell survival in islet transplants, an effect which can be partially prevented by insulin treatment (46). As indicated by the slight delay in curing of scaffold-implanted mice compared to renal subcapsular transplanted mice, prolonged exposure to glucotoxicity might be a contributing factor explaining the difference in beta-cell density observed between both conditions. Future studies should elucidate the effect of insulin treatment during the post-transplantation period on the survival of beta-cells in scaffold-implanted islets. Furthermore, despite the use of a syngeneic transplantation model avoiding immune responses, the influx of macrophages due to the foreign body response and concomitant cytokine release could also have affected the beta-cell mass. Occasionally macrophages and foreign body cells were observed at the polymer surface. Future studies should aim to alleviate these stress-factors to improve beta-cell survival and function of scaffold-implanted islets.

These findings provide directions for future strategies to prevent or limit the abovementioned effects and improve islet function and survival in bioengineered constructs. As we have shown in **chapter 3**, the microwell scaffold platform facilitates detailed histological analysis at a subcellular level to substantiate functional physiological observations. Although histology can provide valuable information regarding the status of the islet graft, this method usually is an end-point measure and is not suitable when translating into clinical practice. Therefore, we have evaluated a method to monitor non-invasively the beta-cell mass with SPECT using a radiolabelled GLP-1 analogue, exendin-3. In the pilot-study described in **chapter 5** we show the uptake of exendin-3 labelled with indium-111 in scaffold-implanted islets. This uptake could be clearly visualized on *ex vivo* SPECT scans, but we were not yet able to detect a signal *in vivo*. However, provided that islets can be visualized within microwell scaffolds using ¹¹¹In-exendin-3, this method could be used to monitor the effect of future strategies aimed to improve beta-cell survival in time. In the next section we discuss some strategies that might have significant impact on islet survival and engraftment during the initial phase after islet transplantation.

6.2.2 Directions towards a more effective bioengineered construct

Tuning the oxygenation – Until transplanted islets become revascularized, they depend solely on diffusion for oxygen and nutrient supply (47). Interesting approaches to improve islet oxygenation during this period are the use of an “*in vivo* gas chamber” or oxygen releasing biomaterials. Barkai *et al.* (48) designed a subcutaneous implantable bioartificial pancreas (BAP)

for islet encapsulation with a 'refuellable' gas chamber. The enhanced oxygen supply facilitated islet survival in the implant at the subcutaneous site in mice and islets were functional during the observed period of 60 days. In response to these promising results, they implanted the device in a patient with type 1 diabetes (49). Persistent graft function over a period of 10 months was demonstrated with regulated insulin secretion and preservation of islet morphology and function without any immunosuppressive therapy. Although normoglycemia was not obtained, the transplanted islet mass was marginal, 2,100 IEQ/kg body weight, and much lower compared to the suggested ~10,000 IEQ/kg body weight that is required to achieve insulin independence after intrahepatic islet transplantation (50, 51). Another interesting approach is the incorporation of fluorinated compounds (52) or peroxides (53) into biomaterials to enable controlled release of oxygen. Pedraza *et al.* have shown that the addition of a PDMS-CaO₂ disk in the culture medium can prevent hypoxia-induced cell death in islets *in vitro* (21). However, the challenge will be to get a sustained release of oxygen for several days. At the very least, incorporating these compounds into the microwell scaffold platform may limit the hypoxia related stress the islets are exposed to in the immediate transplantation period.

Tuning revascularization – As we hypothesize that the observed changes in vascularization pattern and cellular density and composition might be related to a delay in revascularization, strategies to stimulate angiogenesis and vessel infiltration in the scaffold could improve transplant outcome. By using lacZ- (54) or GFP- (55) tagged donor endothelial cells, it has been demonstrated that, after transplantation, functional islet vasculature is chimeric, composed of host and donor endothelial cells. Brissova *et al.* (54) demonstrated that as much as 40% of the endothelial cells in the revascularized graft originates from the donor islets and that a subset of these cells become a functional part of revascularized islet graft. However, the amount of endothelial cells present in the islets largely depends on the *in vitro* culture period prior to transplantation (55). These observations suggest that interventions to activate, amplify, or sustain intraislet endothelial cells before and after transplantation may enhance and accelerate islet revascularization. An example of such interventions is the stimulation of islet endothelial outgrowth *in vitro* in e.g. fibrin matrix as a form of prevascularization (56). Reducing the *in vitro* culture period or stimulating endothelial outgrowth *in vitro* prior to implantation might be viable options to accelerate the reconnection to the vascular system after transplantation.

Another approach would be to introduce proangiogenic factors, such as VEGF-A, PDGF, or bFGF, to stimulate the proliferation, migration, and maturation of endothelial cells into functional vessels. Various studies have evaluated the effect of such growth factors on islet revascularization and reported promising results (20, 57, 58). However, the challenge remains to identify the optimal growth-factor cocktail and to precisely control the timing, dose, and duration of these factors to acquire mature, fully functional vasculature.

Also the co-transplantation of proangiogenic cells has been suggested as a mean to stimulate revascularization. Various cell types have been trialed, such as mature endothelial cells (59), mesenchymal stromal cells (60–64), and endothelial progenitor cells (65–67). Most

of these studies co-infused these cells with islets underneath the kidney capsule (60, 62, 63, 65, 67) or into the liver (61, 66), whereas others have coated islets prior to implantation (59, 64, 68). Both strategies show promising results regarding islet functionality, survival and revascularization. In **chapter 4** we have compared the angiogenic potential of islet coatings with different proangiogenic cell types on islet revascularization at the poorly vascularized, subcutaneous transplantation site. Using a subcutaneous Matrigel plug assay, we demonstrated that composite islets with hMSCs and HUVECs exhibit a higher angiogenic potential compared to uncoated control islets or islets combined with hMSCs or pre-conditioned hMSCs in EGM-2 medium. Although we observed an increasing trend in the percentage of vascularized islets using hMSCs or hMSCs pre-conditioned in EGM-2 medium, these conditions did not show a significant difference in perfused vessel density compared to vascularized uncoated control islets. A factor that might influence the revascularization of coated islets is tissue deformation. Rivron *et al.* have shown that tissue contractility and deformation can modulate the formation of gradients of VEGF and the local overexpression of VEGF-receptor 2 in co-cultures of hMSCs and HUVECs (69). Furthermore, they have demonstrated that star- and triangle-shaped microwells result in anisotropic deformation and tissue compaction, which partially contributed to the formation of vascular patterns. Coating islets in star- or triangle-shaped microwells with hMSCs and HUVECs or even implant these composite islets within star- or triangle-shaped microwell scaffolds might further improve the angiogenic potential of these composite islets. The microwell scaffold platform can be easily adapted by changing the mould to obtain differently shaped microwells (unpublished data, Figure 1).

A disadvantage of islet coating is the increase in islet size and concomitant risk of central core necrosis in the avascular period after transplantation. An alternative option would be to prevascularize the scaffold prior to implantation to accelerate revascularization *in vivo*. Kaufman *et al.* have reported enhanced engraftment and reduced blood glucose levels using prevascularized PLGA/PPLA scaffolds with HUVECs and human foreskin fibroblast cells (70). Future studies should focus on different application methods and clinically relevant pro-angiogenic cell sources to identify the most efficient and effective transplantation strategy.

Tuning the immune response – Although islet transplantation at an extrahepatic, extravascular transplantation site avoids the deleterious effects of the instant blood-mediated inflammatory reaction (IBMIR), islets do encounter immune reactions, such as the foreign body response, and the allo- and recurrent auto-immune responses. These immune responses may be minimized and/or controlled by the use of immunosuppressive drugs, but one of the disadvantages of these agents is that they are toxic for the islets and interfere with insulin secretion, insulin action, and impair islet engraftment, and neogenesis (4). An emerging and promising approach is the induction of antigen-specific tolerance to the transplanted islets, without systemically affecting the immune system. Absolute tolerance necessitates “training” or “modulating” a diverse array of cell types that recognize and respond to the introduced alloantigens, including antigen presenting cells, T-lymphocytes, and B-lymphocytes. Different

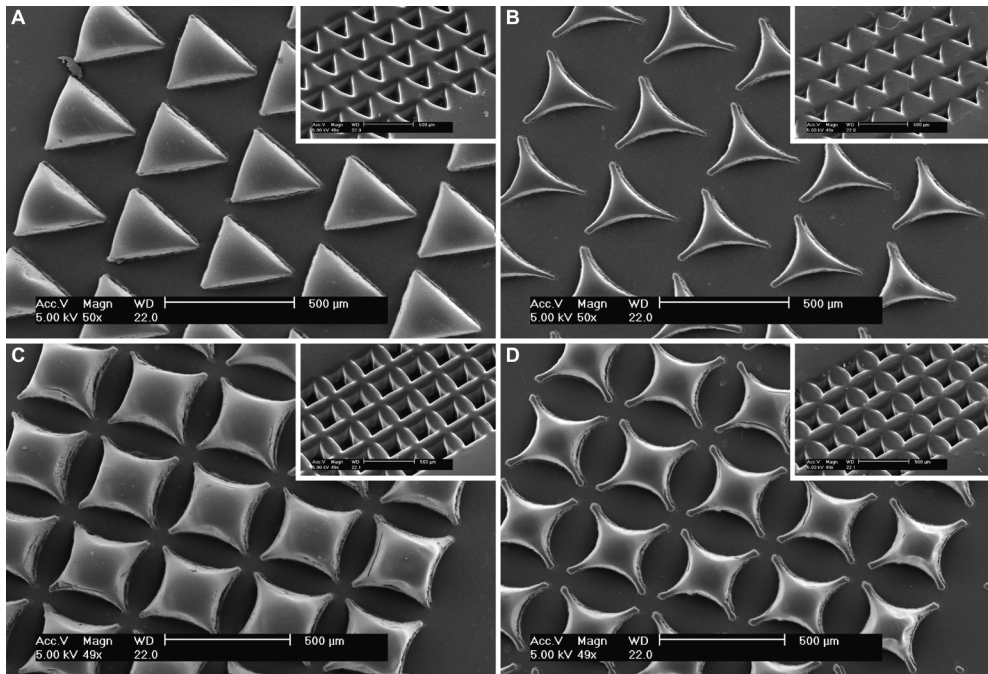


Figure 1: Bottom of triangle- (A-B) and star-shaped (C-D) microwell scaffold fabricated from 4000PEOT30PBT70. Inserts represent the wells. Scalebars: 500 µm. Unpublished data.

approaches have been proposed that may facilitate this objective, such as chemical agents as well as cell-based treatments with hematopoietic stem cells and regulatory immune cell subsets (i.e. T regulatory cells, mesenchymal stromal cells, or dendritic cells) (71).

Another interesting approach is to modulate the foreign body response. The implantation of a scaffold and the associated tissue injury trigger a cascade of inflammatory and wound healing responses and is associated with a robust macrophage response (72). Activated macrophages possess diverse, plastic phenotypes that play an important role in the host inflammatory response and the process of tissue repair and remodeling following injury. Macrophage phenotype has been broadly characterized as the “classically activated” pro-inflammatory M1 macrophages, and the “alternatively activated” M2 macrophages (73). M1 macrophages strongly upregulate inflammatory proteins such as IL-1 β , and TNF α (74), factors associated with beta-cell dedifferentiation and function loss (44), however they also express genes involved in the initiation of angiogenesis, such as VEGF and bFGF (74). M2 macrophages can be subdivided into M2a, b, and c, each with specific cytokine profiles and different functional properties. Overall, the M2 macrophages are involved in processes such as immunoregulation and tissue remodelling (75). By tuning the macrophage polarization profile a more optimal body response might be achieved, shifting from a pro-inflammatory to a pro-regenerative environment.

Importantly though, the balance should not be shifted too far to the M2 phenotype, since both types of macrophages are required for scaffold vascularization (74). One strategy to modulate the macrophage polarization in and around a construct is modifying the scaffold topography; pore size (35) as well as fiber size, fiber alignment and intranodal distance in case of electrospun meshes (76, 77) has been shown to influence macrophage polarization. In order to study the effect of pore size on islet engraftment and revascularization, a higher degree of control over pore size is necessary. All fabrication methods described in this thesis rely on pore formation prior to microthermoforming and due to the stretching involved in microwell formation, the pore size range in the final construct remains large (between 10-40 μm). Future studies should focus on pore formation after microwell formation or alternative fabrication methods to create porous microwell scaffolds, such as direct laser writing by multi-photon polymerization (78). Also the combination of an electrospun microwell scaffold (**chapter 2**) with laser-drilled pores (**chapter 3**) might be an effective strategy to modulate the foreign body response.

Tuning the microenvironment – There is significant evidence that islets are heavily influenced by interactions with their microenvironment; islet interactions with ECM or synthetic matrix materials have been shown to regulate survival (79–82), insulin secretion (79–82), and aid in the preservation of spherical islet morphology (83). Interestingly, islets that retain some of their native ECM have been shown to have markedly reduced apoptosis rates and significantly greater function with respect to glucose stimulated insulin secretion *in vitro* compared to “naked” islets (84).

Daoud *et al.* have studied the effect of different extracellular matrix components on the preservation of human islet morphology and function *in vitro* (85). They have shown that various ECM proteins elicit different islet responses and integrin-mediated behavior. Collagen I, IV and fibronectin were able to induce islet adhesion, in contrast to poor adhesion to laminin, and only fibronectin capable of maintaining islet structural integrity and insulin content distribution while facilitating attachment. Furthermore, although islet phenotype was eventually lost when islets were cultured on collagen I and IV, insulin gene expression was highest for these conditions. However, insulin release was highest when islets were cultured on fibronectin, along with a decrease in SUR1 expression, whereas glucose metabolism, along with GLUT2 and GCK expression, was highest on collagen I and IV surfaces. These results indicate that a combination of different ECM proteins, each with their mode of action, might be necessary to maintain an optimal islet response.

Although the bulk of the islet cells are not in direct contact with the introduced ECM, these matrix components have been shown to improve islet survival and function, both *in vitro* and *in vivo* (17, 18, 79–82, 86, 87). It has been suggested that intra-islet cell–cell communication via paracrine and autocrine signalling as well as Cx36 gap junctions and cell–cell coupling may contribute to these improvements (88). However, further studies are warranted to demonstrate this. An interesting advancement to study the interaction of islets with different materials or ECM protein coatings, is the development of high-throughput screening platforms (89, 90).

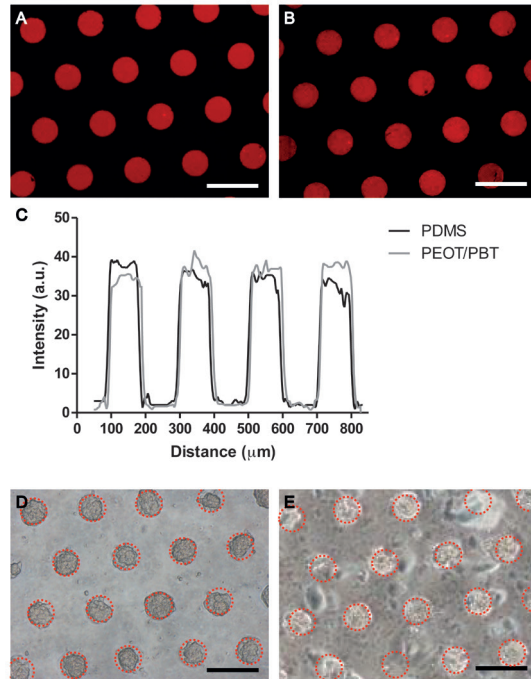


Figure 2. Fabrication of microcontact printed biomaterials for controlled production of uniformly sized aggregates. Fluorescence microscopy image of microcontact printed patterns of rhodamine-labeled fibronectin (100 μm diameter dots and 100 μm spacing) on (A) poly(dimethylsiloxane (PDMS), and (B) PEOT/PBT block copolymer. (C) Intensity profiles showing the intensity of the fluorescent images of microcontact printed polymers in A and B. Scale bars = 200 μm . Uniform INS-1E cell clusters were formed after 7 days of culture on (D) microcontact printed PDMS, and (E) microcontact printed PEOT/PBT copolymer. Adapted from (95)

These platforms allow evaluating integrin-mediated behavior of islets on many different materials and with many combinations of ECM proteins. However, these articles have only described the attachment of dispersed islet cells on different materials and future studies are necessary to also obtain information about attachment and spreading of intact islets. An interesting approach would be to combine these high-throughput platforms with microfluidic systems as described by Easley *et al.* (91) and Dishinger *et al.* (92) to assess islet functionality or the function of different gap-junctions of islets cells cultured on these different biomaterial substrates with or without ECM protein coatings.

In several pilot studies, not part of this thesis, we have explored the feasibility to immobilize ECM proteins on 4000PEOT30PBT70 block copolymer films by microcontact printing (μCP). This technique has been shown to allow tethering of ECM proteins on different substrates, such as silicon oxide (93), and bio-polymers (94). The advantage of this approach is that defined patterns of

proteins can be created to e.g. restrict islet spreading after attachment. As a proof-of-principle, thin PEOT/PBT polymer films were treated with oxygen plasma to create reactive surface groups and were successfully patterned with 100 μm diameter dots of fibronectin using PDMS stamps (Figure 2). Using this technique, both ins1E cell clusters and islets of Langerhans could be immobilized on protein spots while maintaining their rounded morphology and function (95). Since the protein stamping procedure requires a flat surface, the translation of this technique to the 3D surface of the microwell scaffold platform necessitates patterning prior to microwell formation. However, a complicating factor is the required temperature of 85 $^{\circ}\text{C}$ for microwell formation, which causes the proteins to denature. Therefore, we have explored the use of various heat-stable linker molecules, such as *N*-hydroxysuccinimide (NHS) groups and epoxysilane. For this strategy, polymer films were treated with oxygen plasma. To introduce NHS groups, substrates were rinsed in ethanol, dipped in NaOH (1M) to cleave ester bonds and washed in MilliQ before incubating in a 2-(*N*-morpholino)ethanesulfonic acid (MES)(Sigma) buffer (0,1M, pH5) for at least 30 minutes. *N*-(3-Dimethylaminopropyl)-*N'*-ethylcarbodiimide hydrochloride (EDC; Sigma) and *N*-Hydroxysuccinimide (NHS; Sigma) were solved in the MES buffer to create a 50mM EDC/NHS solution. Substrates were incubated in the EDC/NHS solution for 1 hour, and then rinsed with MES buffer and dried under nitrogen flow. To introduce epoxysilane linkers on the polymer surface, substrates were incubated for 24 hours under argon gas in a 1% (v/v) solution of (3-Glycidyloxypropyl)trimethoxysilane (GPTMS; Sigma) in dry hexane. Substrates were then rinsed in hexane, and twice in ethanol before drying under nitrogen flow. PDMS stamps patterned with lines were used to introduce PEG-NH₂ on the treated polymer surface to obtain non-cell-adherent PEG-lines. Subsequently, polymer films were used for microwell formation after which they were incubated in a fibronectin solution to introduce the protein to the remaining available linker molecules. Limited patterning was observed using confocal microscopy when NHS groups were used as a linker molecule (unpublished data, Figure 3). This can be attributed to insufficient or even no carboxylic groups on the surface after treatment; groups that are required for the introduction of NHS groups using 1-ethyl-3-(3-dimethylaminopropyl)-carbodiimide (EDC). Further characterization of the polymer surface should be performed using X-ray photoelectron spectroscopy (XPS) or time-of-flight secondary ion mass spectrometry (ToF-SIMS) to characterize the reactive groups obtained at the polymer surface after surface treatment. In contrast to NHS chemistry, epoxysilane requires the presence of hydroxyl groups. A clear pattern of both PEG (auto-fluorescent green) and fibronectin (DyLight 650 labelled fibronectin, white) could be observed prior to microwell formation (unpublished data, Figure 3). However, after heating the polymer film, the pattern seems less distinct compared to unheated substrates. In **chapter 2** we have shown by atomic force microscopy that heating causes reorganization of the different blocks in the PEOT/PBT polymer films (96). This reorganization might explain the change in the observed pattern. After microwell formation, no PEG lines could be observed due to the stretching of the microwells and no clear fibronectin lines could be detected. Recently, Waterkotte *et al.* published a similar approach to pattern cyclo-olefin polymer films with fibronectin (97). They used poly-

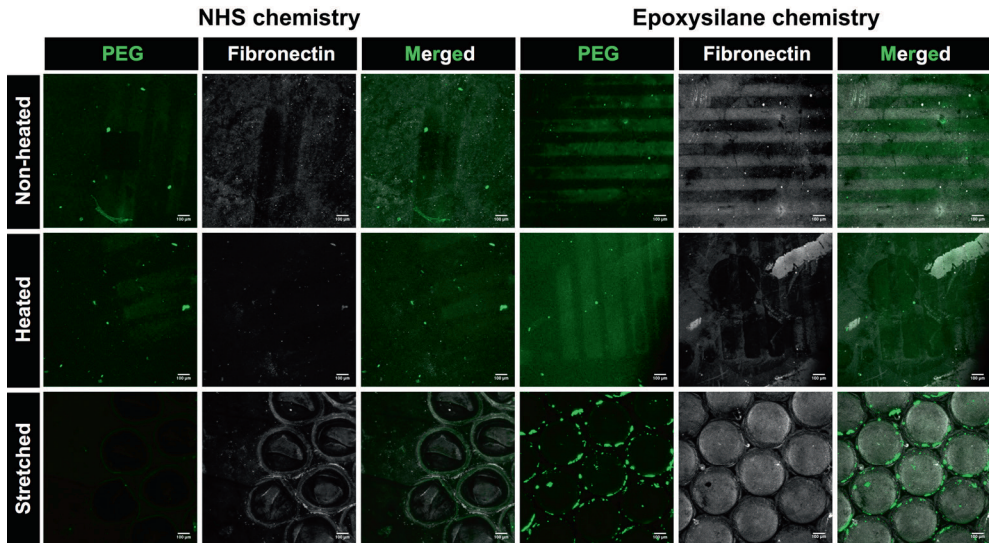


Figure 3. Confocal images of polyactive after functionalization with NHS or epoxy silane chemistry, micro-contact printing with PEG-NH₂ (green), and backfilling with fibronectin (white). Three situations were tested: backfilling directly after micro contact printing, after heating the polymer film, and after microthermoforming. Scalebars: 100 μ m. Unpublished data.

(p-xylylene-4-methyl-2-bromoisobutyrate-co-p-xylylene) and poly(p-xylylene-4-carboxylic acid pentafluorophenolester-co-p-xylylene) as heat-stable linkers. Poly[poly(ethylene glycol) methyl ether methacrylate] was used to react with the bromoisobutyrate-functionalized areas to prevent cell attachment. They report a distinct pattern, even after the introduction of microchannels using microthermoforming. However, the stretching involved to create the microchannels was less compared to the microwell structure described in our study, which could explain the difference in the observed pattern after microthermoforming. Future studies are necessary to optimize the micropatterning in 3D structures with high aspect ratios, such as the microwells. Eventually this method could be applied not only to immobilize islets in the microwells and improve their functionality by restoring the islet-ECM interaction, but also to promote endothelial cell alignment for *in vitro* prevascularization (98, 99) or to direct macrophage polarity towards an M2 phenotype (100).

6.3 REFERENCES

1. Vos P De, Hamel a F, Tatrakiewicz K (2002) Considerations for successful transplantation of encapsulated pancreatic islets. *Diabetologia* 45:159–173.
2. Buchwald P, Cechin SR, Weaver JD, Stabler CL (2015) Experimental evaluation and computational modeling of the effects of encapsulation on the time-profile of glucose-stimulated insulin release of pancreatic islets. *Biomed Eng Online* 14:1–14.
3. De Vos P, Faas MM, Strand B, Calafiore R (2006) Alginate-based microcapsules for immunoisolation of pancreatic islets. *Biomaterials* 27:5603–5617.
4. Shapiro a MJ (2011) State of the art of clinical islet transplantation and novel protocols of immunosuppression. *Curr Diab Rep* 11:345–54.
5. HOPCROFT DW, MASON DR, SCOTT RS (1985) Structure-Function Relationships in Pancreatic Islets: Support for Intraislet Modulation of Insulin Secretion. *Endocrinology* 117:2073–2080.
6. Salomon D, Meda P (1986) Heterogeneity and Contact-dependent Regulation Hormone Secretion by Individual B Cells Direct interactions between neighboring cells are thought to play a role in the normal functioning of several glands [17]. The B cells of the islets of Langerhans rep. 162:507–520.
7. Andersson A (1978) Isolated mouse pancreatic islets in culture: effects of serum and different culture media on the insulin production of the islets. *Diabetologia* 14:397–404.
8. Benninger RKP, Piston DW (2014) Cellular communication and heterogeneity in pancreatic islet insulin secretion dynamics. *Trends Endocrinol Metab* 25:399–406.
9. Weinberg N, Ouziel-yahalom L, Knoller S, Efrat S, Dor Y (2007) Lineage Tracing Evidence for In Vitro Dedifferentiation but Rare Proliferation of Mouse Pancreatic-Cells. 56.
10. Giuliani M et al. (2005) Central necrosis in isolated hypoxic human pancreatic islets: evidence for postisolation ischemia. *Cell Transplant* 14:67–76.
11. Lehmann R et al. (2007) Superiority of small islets in human islet transplantation. *Diabetes* 56:594–603.
12. Macgregor RR, Williams SJ, Tong PY, Kover K, Moore W V (2006) Small rat islets are superior to large islets in vitro function and in transplantation outcomes. 66160:771–779.
13. Dufour JM et al. (2005) Development of an ectopic site for islet transplantation, using biodegradable scaffolds. *Tissue Eng* 11:1323–1331.
14. Salvay DM et al. (2009) Extracellular Matrix Protein-Coated Scaffolds Promote the Reversal of Diabetes After Extrahepatic Islet Transplantation David. *Transplantation* 85:1456–1464.
15. Kheradmand T et al. (2011) Permanent protection of PLG scaffold transplanted allogeneic islet grafts in diabetic mice treated with ECDI-fixed donor splenocyte infusions. *Biomaterials* 32:4517–24.
16. Gibly RF et al. (2011) Extrahepatic islet transplantation with microporous polymer scaffolds in syngeneic mouse and allogeneic porcine models. *Biomaterials* 32:9677–84.
17. Gibly RF, Zhang X, Lowe WL, Shea LD (2013) Porous scaffolds support extrahepatic human islet transplantation, engraftment, and function in mice. *Cell Transplant* 22:811–9.
18. Yap WT et al. (2013) Collagen IV-Modified Scaffolds Improve Islet Survival and Function and Reduce Time to Euglycemia. 19.
19. Blomeier H et al. (2006) Polymer scaffolds as synthetic microenvironments for extrahepatic islet transplantation. *Transplantation* 82:452–459.
20. Brady A-C et al. (2013) Proangiogenic Hydrogels Within Macroporous Scaffolds Enhance Islet Engraftment in an Extrahepatic Site. 19:2544–2552.
21. Pedraza E et al. (2013) Macroporous Three-Dimensional PDMS Scaffolds for Extrahepatic Islet Transplantation. *Cell Transplant* 22:1123–1135.

22. Jansson L, Carlsson P-O (2002) Graft vascular function after transplantation of pancreatic islets. *Diabetologia* 45:749–63.
23. Moritz W et al. (2002) Apoptosis in hypoxic human pancreatic islets correlates with HIF-1 α expression. *FASEB J* 16:745–747.
24. Dionne KE, Colton CK, Yarmush ML (1993) Effect of hypoxia on insulin secretion by isolated rat and canine islets of Langerhans. *Diabetes* 42:12–21.
25. Cantley J, Grey ST, Maxwell PH, Withers DJ (2010) The hypoxia response pathway and β -cell function. 12:159–167.
26. Nisbet DR, Forsythe JS, Shen W, Finkelstein DI, Horne MK (2009) Review paper: a review of the cellular response on electrospun nanofibers for tissue engineering. *J Biomater Appl* 24:7–29.
27. Nedjari S et al. (2014) Electrospun Honeycomb as Nests for Controlled Osteoblast Spatial Organization. *Macromol Biosci* 14:1580–1589.
28. Rnjak-Kovacina J, Weiss AS (2011) Increasing the Pore Size of Electrospun Scaffolds. *Tissue Eng Part B Rev* 17:365–372.
29. Sharkawy a a, Klitzman B, Truskey G a, Reichert WM (1997) Engineering the tissue which encapsulates subcutaneous implants. I. Diffusion properties. *J Biomed Mater Res* 37:401–12.
30. Sharkawy a a, Klitzman B, Truskey G a, Reichert WM (1998) Engineering the tissue which encapsulates subcutaneous implants. II. Plasma-tissue exchange properties. *J Biomed Mater Res* 40:586–97.
31. Sharkawy a a, Klitzman B, Truskey G a, Reichert WM (1998) Engineering the tissue which encapsulates subcutaneous implants. III. Effective tissue response times. *J Biomed Mater Res* 40:598–605.
32. Williams SK, Berman SS, Kleinert LB (1997) Differential healing and neovascularization of ePTFE implants in subcutaneous versus adipose tissue. *J Biomed Mater Res* 35:473–81.
33. Brauker JH et al. (1995) Neovascularization of synthetic membranes directed by membrane microarchitecture. *J Biomed Mater Res* 29:1517–24.
34. Salzmann DL, Kleinert LB, Berman SS, Williams SK (1997) The effects of porosity on endothelialization of ePTFE implanted in subcutaneous and adipose tissue. *J Biomed Mater Res* 34:463–76.
35. Madden LR et al. (2010) Proangiogenic scaffolds as functional templates for cardiac tissue engineering. *Proc Natl Acad Sci U S A* 107:15211–6.
36. Kim A, Miller K, Jo J, Kilimnik G, Wojcik P (2009) Islet architecture: A comparative study. *Islets* 1:129–136.
37. Molnár C et al. (2013) Islet engraftment and revascularization in clinical and experimental transplantation. *Cell Transplant* 22:243–51.
38. Lammert E et al. (2003) Role of VEGF-A in Vascularization of Pancreatic Islets. *Curr Biol* 13:1070–1074.
39. Brissova M et al. (2006) Pancreatic islet production of vascular endothelial growth factor-A is essential for islet vascularization, revascularization, and function. *Diabetes* 55:2974–85.
40. Jonas J-C et al. (1999) Chronic Hyperglycemia Triggers Loss of Pancreatic Cell Differentiation in an Animal Model of Diabetes. *J Biol Chem* 274:14112–14121.
41. Talchai C, Xuan S, Lin H V, Sussel L, Accili D (2012) Pancreatic β cell dedifferentiation as a mechanism of diabetic β cell failure. *Cell* 150:1223–34.
42. Poitout V, Robertson RP (2002) Minireview: Secondary beta-cell failure in type 2 diabetes--a convergence of glucotoxicity and lipotoxicity. *Endocrinology* 143:339–342.
43. De Jesus DF, Kulkarni RN (2014) Epigenetic modifiers of islet function and mass. *Trends Endocrinol Metab* 25:628–636.
44. Darville MI, Eizirik DL (2006) Notch signaling: A mediator of β -cell de-differentiation in diabetes? *Biochem Biophys Res Commun* 339:1063–1068.

45. Kikawa K et al. (2014) Beneficial effect of insulin treatment on islet transplantation outcomes in akita mice. *PLoS One* 9:1–12.
46. Davalli AM et al. (1996) Vulnerability of Islets in the Immediate Posttransplantation Period. 19:1161–1167.
47. Korsgren O et al. (2008) Optimising islet engraftment is critical for successful clinical islet transplantation. *Diabetologia* 51:227–232.
48. Barkai U et al. (2013) Enhanced Oxygen Supply Improves Islet Viability in a New Bioartificial Pancreas. 22:1463–1476.
49. Ludwig B et al. (2013) Transplantation of human islets without immunosuppression. *Proc Natl Acad Sci U S A* 110:1–5.
50. Ichii H, Ricordi C (2009) Current status of islet cell transplantation. *J Hepatobiliary Pancreat Surg* 16:101–112.
51. The CITR Coordinating Center Investigators (2011) The Collaborative Islet Transplant Registry (CITR) 2011 Seventh Annual Report. *US Dep Heal Hum Serv Bethesda, MA, USA*.
52. Seifu DG, Isimjan TT, Mequanint K (2011) Tissue engineering scaffolds containing embedded fluorinated-zeolite oxygen vectors. *Acta Biomater* 7:3670–8.
53. Camci-Unal G, Alemdar N, Annabi N, Khademhosseini A (2013) Oxygen Releasing Biomaterials for Tissue Engineering. *Polym Int* 62:843–848.
54. Brissova M et al. (2004) Intraislet Endothelial Cells Contribute to Revascularization of Transplanted Pancreatic Islets. *Diabetes* 53:1318–1325.
55. Nyqvist D, Köhler M, Wahlstedt H, Berggren PO (2005) Donor islet endothelial cells participate in formation of functional vessels within pancreatic islet grafts. *Diabetes* 54:2287–2293.
56. Linn T et al. (2003) Angiogenic capacity of endothelial cells in islets of Langerhans. *FASEB J* 17:881–883.
57. Cai Q et al. (2012) Enhanced expression of VEGF-A in B cells increases endothelial cell number but impairs islet morphogenesis and B cell proliferation. *Dev Biol* 367:40–54.
58. Phelps E a., Headen DM, Taylor WR, Thulé PM, García AJ (2013) Vasculogenic bio-synthetic hydrogel for enhancement of pancreatic islet engraftment and function in type 1 diabetes. *Biomaterials* 34:4602–4611.
59. Li Y et al. (2013) Combined Strategy of Endothelial Cells Coating, Sertoli Cells Coculture and Infusion Improves Vascularization and Rejection Protection of Islet Graft. *PLoS One* 8.
60. Figliuzzi M et al. (2009) Bone marrow-derived mesenchymal stem cells improve islet graft function in diabetic rats. *Transplant Proc* 41:1797–800.
61. Ito T et al. (2010) Mesenchymal Stem Cell and Islet Co-Transplantation Promotes Graft Revascularization and Function. *Transplantation* 89:1438–1445.
62. Sakata N, Chan NK, Chrisler J, Obenaus A, Hathout E (2010) Bone marrow cell cotransplantation with islets improves their vascularization and function. *Transplantation* 89:686–93.
63. Rackham CL et al. (2011) Co-transplantation of mesenchymal stem cells maintains islet organisation and morphology in mice. *Diabetologia* 54:1127–1135.
64. Cavallari G et al. (2012) Mesenchymal Stem Cells and Islet Co-Transplantation in Diabetic Rats: Improved Islet Graft Revascularization and Function By Human Adipose Tissue-Derived Stem Cells Preconditioned With Natural Molecules. *Cell Transplant* 21:2771–2781.
65. Oh BJ et al. (2013) Co-transplantation of bone marrow-derived endothelial progenitor cells improves revascularization and organization in islet grafts. *Am J Transplant* 13:1429–40.
66. Quaranta P et al. (2014) Co-transplantation of endothelial progenitor cells and pancreatic islets to induce long-lasting normoglycemia in streptozotocin-treated diabetic rats. *PLoS One* 9:e94783.

67. Kang S et al. (2012) Endothelial progenitor cell cotransplantation enhances islet engraftment by rapid revascularization. *Diabetes* 61:866–76.
68. Jung HS et al. (2014) The potential of endothelial colony-forming cells to improve early graft loss after intraportal islet transplantation. *Cell Transplant* 23:273–283.
69. Rivron NC et al. (2012) Tissue deformation spatially modulates VEGF signaling and angiogenesis. *Proc Natl Acad Sci* 109:6886–6891.
70. Kaufman-Francis K, Koffler J, Weinberg N, Dor Y, Levenberg S (2012) Engineered vascular beds provide key signals to pancreatic hormone-producing cells. *PLoS One* 7:e40741.
71. Chhabra P, Brayman KL (2014) Overcoming barriers in clinical islet transplantation: Current limitations and future prospects. *Curr Probl Surg* 51:49–86.
72. Morais JM, Papadimitrakopoulos F, Burgess DJ (2010) Biomaterials/tissue interactions: possible solutions to overcome foreign body response. *AAPS J* 12:188–196.
73. Brown BN et al. (2012) Macrophage phenotype as a predictor of constructive remodeling following the implantation of biologically derived surgical mesh materials. *Acta Biomater* 8:978–987.
74. Spiller KL et al. (2014) The role of macrophage phenotype in vascularization of tissue engineering scaffolds. *Biomaterials* 35:4477–88.
75. Mantovani A et al. (2004) The chemokine system in diverse forms of macrophage activation and polarization. *Trends Immunol* 25:677–686.
76. Garg K, Pullen N a., Oskertizian C a., Ryan JJ, Bowlin GL (2013) Macrophage functional polarization (M1/M2) in response to varying fiber and pore dimensions of electrospun scaffolds. *Biomaterials* 34:4439–4451.
77. Saino E et al. (2011) Effect of electrospun fiber diameter and alignment on macrophage activation and secretion of proinflammatory cytokines and chemokines. *Biomacromolecules* 12:1900–1911.
78. Selimis A, Mironov V, Farsari M (2015) Microelectronic Engineering Direct laser writing : Principles and materials for scaffold 3D printing. *Microelectron Eng* 132:83–89.
79. Lucas-Clerc C, Massart C, Campion JP, Launois B, Nicol M (1993) Long-term culture of human pancreatic islets in an extracellular matrix: Morphological and metabolic effects. *Mol Cell Endocrinol* 94:9–20.
80. Navarro-Alvarez N et al. (2008) Reestablishment of microenvironment is necessary to maintain in vitro and in vivo human islet function. *Cell Transplant* 17:111–119.
81. Wang RN, Rosenberg L (1999) Maintenance of beta-cell function and survival following islet isolation requires re-establishment of the islet – matrix relationship. 181–190.
82. Weber LM, Hayda KN, Anseth KS (2008) Cell-matrix interactions improve beta-cell survival and insulin secretion in three-dimensional culture. *Tissue Eng Part A* 14:1959–1968.
83. Daoud J, Rosenberg L, Tabrizian M (2010) Pancreatic islet culture and preservation strategies: advances, challenges, and future outlook. *Cell Transplant* 19:1523–35.
84. Thomas FT et al. (1999) Anoikis, extracellular matrix, and apoptosis factors in isolated cell transplantation. *Surgery* 126:299–304.
85. Daoud J, Petropavlovskaja M, Rosenberg L, Tabrizian M (2010) The effect of extracellular matrix components on the preservation of human islet function in vitro. *Biomaterials* 31:1676–82.
86. Daoud JT et al. (2011) Long-term in vitro human pancreatic islet culture using three-dimensional microfabricated scaffolds. *Biomaterials* 32:1536–1542.
87. Salvay DM et al. (2008) Extracellular matrix protein-coated scaffolds promote the reversal of diabetes after extrahepatic islet transplantation. *Transplantation* 85:1456–1464.
88. Bavamian S et al. (2007) Islet-cell-to-cell communication as basis for normal insulin secretion. *Diabetes Obes Metab* 9 Suppl 2:118–32.

89. Mei, Y., Hollister-Lock, J., Bogatyrev, S.R., Cho, S., Weir, G.C., Langer, R., Anderson DG (2012) A High Throughput Microarray System of Polymer Surfaces for the Manipulation of Primary Pancreatic Islet Cells. *Biomaterials* 31:8989–8995.
90. Williams, S.J., Wang, Q., MacGregor, R.R., Siahaan, T.J., Stehno-Bittel, L, Berkland C (2012) Adhesion of Pancreatic Beta Cells to Biopolymer Films. *Biopolymers* 91:676–685.
91. Easley CJ, Rocheleau J V, Head WS, Piston DW (2009) Quantitative Measurement of Zinc Secretion from Pancreatic Islets with High Temporal Resolution Using Droplet-Based Microfluidics. *Anal Chem* 81:9086–9095.
92. Dishinger JF, Reid KR, Kennedy RT (2009) Quantitative Monitoring of Insulin Secretion from Microfluidic Chip. 81:3119–3127.
93. Mendelsohn AD, Bernards D a., Lowe RD, Desai T a. (2010) Patterning of mono- and multilayered pancreatic beta-cell clusters. *Langmuir* 26:9943–9949.
94. Altomare L, Riehle M, Gadegaard N, Tanzi M, Farè S (2010) Microcontact printing of fibronectin on a biodegradable polymeric surface for skeletal muscle cell orientation. *Int J Artif Organs* 33:535–543.
95. Hilderink J (2013) Beating diabetes: Strategies to improve pancreatic islet transplantation. Dissertation (University of Twente).
96. Buitinga M et al. (2013) *Microwell scaffolds for the extrahepatic transplantation of islets of langerhans*.
97. Waterkotte B et al. (2014) Biofunctional micropatterning of thermoformed 3d substrates. *Adv Funct Mater* 24:442–450.
98. Co CC, Wang Y, Ho C (2005) Biocompatible Micropatterning of Two Different Cell Types Biocompatible Micropatterning of Two Different Cell Types. 127:1598–1599.
99. Moon JJ, Hahn MS, Kim I, Nsiah B a, West JL (2008) Micropatterning of Poly(Ethylene Glycol) Diacrylate Hydrogels with Biomolecules to Regulate and Guide Endothelial Morphogenesis. *Adv Tissue Eng Angiogenesis* 14:157–163.
100. McWhorter FY, Wang T, Nguyen P, Chung T, Liu WF (2013) Modulation of macrophage phenotype by cell shape. *Proc Natl Acad Sci U S A* 110:17253–8.

Summary

Pancreatic islet transplantation has come a long way since the first successful clinical case study in 1990 describing insulin independence after intraportal islet infusion. Although nowadays replacement of insulin production by intrahepatic islet transplantation represents a promising therapeutic strategy for patients with type 1 diabetes experiencing labile glycemic control, the restoration of euglycemia is short-lived, requires islets from multiple donors, and necessitates life-long immunosuppressive therapy. The barriers that limit the success of islet transplantation, and the advances to overcome these barriers, are reviewed in **chapter 1**. These barriers and advances set the motivation for the work described in this thesis.

To improve islet transplantation outcome, we propose different bioengineering strategies. In **chapter 2 and 3** we describe the development and characterization of a microwell scaffold platform for extrahepatic islet transplantation. The advantages of the proposed design are that it (1) prevents islet attachment, spreading, and aggregation by the confinement of individual islets in separate microwells preserving the rounded islet morphology; (2) is mechanically stable to protect islets against physical stresses; and (3) has an open structure permitting fast vascular ingrowth. In **chapter 2** the concept of the microwell design is introduced using thin biomaterial films and electrospun meshes. We have shown that human islets cultured in this platform for seven days exhibit an insulin secretion profile and insulin content comparable to those of free-floating control islets. To stimulate vascular ingrowth after *in vivo* transplantation, **chapter 3** explores three different fabrication methods to introduce pores in the microwell scaffold platform: particulate leaching, solvent casting on pillared wafers, and laser drilling. Methods were evaluated for pore size and geometry, reproducibility and flexibility, and the form and stability of the final construct. Transplantation studies in the epididymal fat elucidate the potential of this porous scaffold platform to restore blood glucose levels in a diabetic mouse model and facilitate islet engraftment. Although we demonstrate that the microwell scaffold makes the epididymal fat a viable option for islet transplantation, with performance that is approaching the gold standard, we do observe a significant decrease in beta-cell density and a changed vascularization pattern compared with native pancreatic islets, which, we hypothesize, are indications for delayed revascularization. Therefore, we explore in **chapter 4** the potential of composite islets with different proangiogenic cell types as a bioengineering approach to improve islet revascularization after transplantation. Here, we demonstrate that composite islets with hMSCs and HUVECs exhibit a higher *in vivo* angiogenic potential compared with uncoated islets or islets combined with hMSCs or pre-conditioned hMSCs in EGM-2 medium. In **chapter 5**, we propose a method to monitor non-invasively beta-cell mass after islet transplantation. For this, we describe the use of radiolabelled exendin-3, a GLP-1 analogue that targets the GLP-1R, which is specifically expressed in pancreatic β -cells but not in α -, δ - and PP-cells. In a pilot-

study, we demonstrate that the uptake of ^{111}In -exendin-3 in scaffold-implanted islets could be clearly visualized on *ex vivo* SPECT scans, with histology and autoradiography studies showing vascularized islets with specific uptake of ^{111}In -exendin-3 in β -cell regions. However, we were not yet able to detect uptake *in vivo*. Provided that β -cell mass can be determined after islet transplantation *in vivo*, this presents a viable method to monitor the influence of native and engineered transplantation sites on long-term β -cell survival aiding the development of an optimal transplantation environment for islets of Langerhans.

Nederlandse samenvatting

De transplantatie van eilandjes van Langerhans heeft een lange weg afgelegd sinds de eerste succesvolle klinische casus studie in 1990 waarin beschreven werd dat insulineonafhankelijkheid en euglykemie verkregen kon worden na infusie van eilandjes in de poortader naar de lever. Hoewel tegenwoordig de transplantatie van eilandjes van Langerhans een veelbelovende therapie is voor patiënten met type 1 diabetes die een sterk fluctuerende bloedsuikerspiegel hebben, is de verkregen euglykemie van korte duur. Bovendien vereist deze therapie eilandjes van meerdere donororganen, en moet de patiënt levenslang immunosuppressiva innemen. In hoofdstuk 1 zijn de factoren besproken die het succes van de transplantatie van eilandjes van Langerhans belemmeren. Deze factoren vormen de motivatie voor het werk dat beschreven is in deze thesis.

Om de uitkomst van de transplantatie van eilandjes van Langerhans te verbeteren, stellen wij in deze thesis verschillende bioengineering strategieën voor. In hoofdstuk 2 en 3 beschrijven we de ontwikkeling en karakterisering van een scaffold platform bedoeld voor de transplantatie van eilandjes buiten de lever. Het voorgestelde ontwerp heeft een aantal voordelen: (1) het voorkomt de hechting van eilandjes aan het scaffold-materiaal; (2) het verschaft mechanische stabiliteit aan het transplantaat; en (3) het heeft een open structuur waardoor ingroei van bloedvaten snel kan plaatsvinden. In hoofdstuk 2 introduceren wij het concept van dit voorgestelde scaffold platform waarbij scaffolds worden gemaakt van zowel polymeerfilms als van fibreuze polymeermatten vervaardigd middels electrospinnen. Tevens laten wij hier zien dat humane eilandjes minimaal zeven dagen kunnen overleven wanneer deze *in vitro* worden gekweekt in het scaffold platform. Het insuline secretieprofiel na glucosestimulatie en het insulinegehalte van eilandjes gekweekt in dit scaffold platform is vergelijkbaar met die van controle-eilanden.

In hoofdstuk 3 vergelijken wij drie verschillende methoden om poriën te creëren in het scaffold platform om zo de ingroei van bloedvaten na implantatie te bevorderen. De drie methoden zijn: het perforeren van polymeerfilms met behulp van zoutkristallen, het vervaardigen van poreuze polymeerfilms door een polymeeroplossing te gieten op een wafer met kleine pilaren, en het vervaardigen van poreuze polymeerfilms met behulp van een laser. De verschillende methoden worden met elkaar vergeleken op basis van poriegrootte en geometrie, reproduceerbaarheid en flexibiliteit, en de vorm en stabiliteit van het uiteindelijke construct. Transplantatiestudies in het epididymaal vet van diabete muizen laten zien dat eilandjes getransplanteerd in het poreuze scaffold platform in staat zijn om de bloedsuikerspiegel te herstellen. Ondanks het feit dat het scaffold platform een haalbare strategie lijkt om eilandjes buiten de lever te kunnen transplanteren, tonen wij aan dat de beta-cel dichtheid na transplantatie is afgenomen in vergelijking met controle eilandjes in de pancreas. Ook het patroon van de bloedvaten in de getransplanteerde eilandjes is anders, wat een aanwijzing kan

zijn voor vertraagde of inadequate revascularisatie. Daarom onderzoeken wij in hoofdstuk 4 een strategie om de revascularisatie van eilandjes na transplantatie te kunnen verbeteren waarbij we de eilandjes coaten met verschillende pro-angiogene celtypen. In dit hoofdstuk laten wij zien dat wanneer eilandjes gecoat worden met een combinatie van humane mesenchymale stamcellen (hMSCs) en met HUVECs, de vascularisatie van de eilandjes verbetert ten opzichte van ongecoate eilandjes of eilandjes die gecoat zijn met hMSCs alleen of met hMSCs die gepreconditioneerd zijn met EGM-2 medium.

In hoofdstuk 5 testen wij een niet-invasieve methode om de beta-cel massa te bepalen na eilandjestransplantatie in het scaffold platform waarbij gebruik gemaakt wordt van radioactief gelabeld exendin. Exendin is een GLP-1 analoog dat bindt aan de GLP-1R, een receptor die specifiek tot expressie komt in beta-cellen. In de pilot-studie beschreven in dit hoofdstuk, laten wij zien dat de beta-cellen in de getransplanteerde eilandjes het radioactief gelabelde exendin opnemen. Helaas waren wij alleen in staat om deze opname *ex vivo* te detecteren met behulp van SPECT. Wanneer wij echter in staat zouden zijn om op een dergelijke manier de beta-cel massa *in vivo* te kunnen bepalen, zou dit een goede methode zijn om overleving van beta-cellen na transplantatie te monitoren en zo het effect van verschillende scaffold platforms op de overleving van beta-cellen te testen. Deze techniek zou kunnen helpen om de optimale transplantatie-omgeving voor eilandjes van Langerhans te bepalen.

List of publications

Peer-reviewed articles

Buitinga, M., Truckenmüller, R.K., Engelse, M.A., Moroni, L., Hoopen, H.W.M. ten, Blitterswijk, C.A. van, Koning, E.J.P. de, Apeldoorn, A.A. van, Karperien, H.B.J. (2013). Microwell Scaffolds for the Extrahepatic Transplantation of Islets of Langerhans. *PLOS one*, 8(5), e64772-e64782.

Buitinga, M.*, Janeczek Portalska, K.*, Hanegraaf, M.A.J., Cornelissen, D.J., Plass, J.R.M., Hanegraaf, M.A.J., Carlotti, F, Koning, E.J.P. de, Engelse, M.A., Blitterswijk, C.A. van, Karperien, H.B.J, Apeldoorn, A.A. van, Boer, J. de. Composite islets with proangiogenic support cells to improve islet revascularization at the subcutaneous transplantation site. *Submitted*.

Buitinga, M., Koning, E.J.P. de, Karperien, H.B.J, Apeldoorn, A.A. van. Barriers in clinical islet transplantation: current limitations and future prospects. *In preparation*.

Buitinga, M., Assen, F.P.A., Hanegraaf, M.A.J., Wieringa, P.A., Hilderink, J., Moroni, L., Truckenmüller, R.K., Blitterswijk, C.A. van, Römer G.W., Carlotti, F., Koning, E.J.P. de, Karperien, H.B.J, Apeldoorn, A.A. van. Microwell scaffolds with a defined porosity: a potential platform for extrahepatic islet transplantation. *In preparation*.

Buitinga, M.*, Kroon, I van der*, Brom, M, Truckenmüller, R.K., Blitterswijk, C.A. van, Römer G.W, Karperien, H.B.J, Gotthardt, M., Apeldoorn, A.A. van. Non-invasive monitoring of β -cell mass in a porous microwell scaffold platform by ^{111}In -exendin-3 SPECT imaging: a pilot study. *In preparation*.

Abstracts selected for oral presentation

TERMIS World Congress, Vienna, Austria, 2012. **Buitinga, M.** Janeczek-Portalska, K. K. Hilderink, J. de Koning, E. J. Engelse, M. A. van Blitterswijk, C. Karperien, M. de Boer, J. and van Apeldoorn, A. A. Coating Islets of Langerhans with cells improves sprout formation in vitro.

4th Joint ESAO-IFAO Congress, Porto, Portugal, 2011. **Buitinga, M.** de Koning, E. J. P. Engelse, M. A. Truckenmuller, R. Moroni, L. van Blitterswijk, C. A. Karperien, M. van Apeldoorn, A. A., Microwell scaffolds for extrahepatic islets of Langerhans transplantation in type 1 diabetes.

TERMIS European Congress, Granada, Spain, 2011. **M. Buitinga**, E.J.P. de Koning, M.A.Engelse, C.J.M.Loomans, R.Truckenmüller, L.Moroni, C.A. van Blitterswijk, A.A. van Apeldoorn, M.Karperien. Microwell scaffolds for extrahepatic islets of Langerhans transplantation in type 1 diabetes.

Bootcongres, Dutch transplantation Society, 2011. **M.Buitinga**, E.J.P. de Koning, M.A.Engelse, C.J.M.Loomans, R.Truckenmüller, L.Moroni, C.A. van Blitterswijk, A.A. van Apeldoorn, M.Karperien. Microwell scaffolds for extrahepatic islets of Langerhans transplantation in type 1 diabetes.

The Netherlands Society for Biomaterials and Tissue Engineering annual meeting, Lunteren, The Netherlands, 2010. **M.Buitinga**, E.J.P. de Koning, M.A.Engelse, C.J.M.Loomans, R.Truckenmüller, L.Moroni, C.A. van Blitterswijk, A.A. van Apeldoorn, M.Karperien. Microwell scaffolds for extrahepatic islets of Langerhans transplantation in type 1 diabetes.

Annual meeting of the Dutch Association for Diabetes Research (NVDO), Oosterbeek, The Netherlands, 2009. **Buitinga M.**, Loomans C.J.M., Engelse M.A., van Blitterswijk C.A., Rabelink T.J., Karperien M., de Koning E.J.P., van Apeldoorn, A.A. Fabrication of microchip scaffolds as alternative transplantation site for beta-cell transplantation in type 1 diabetes.

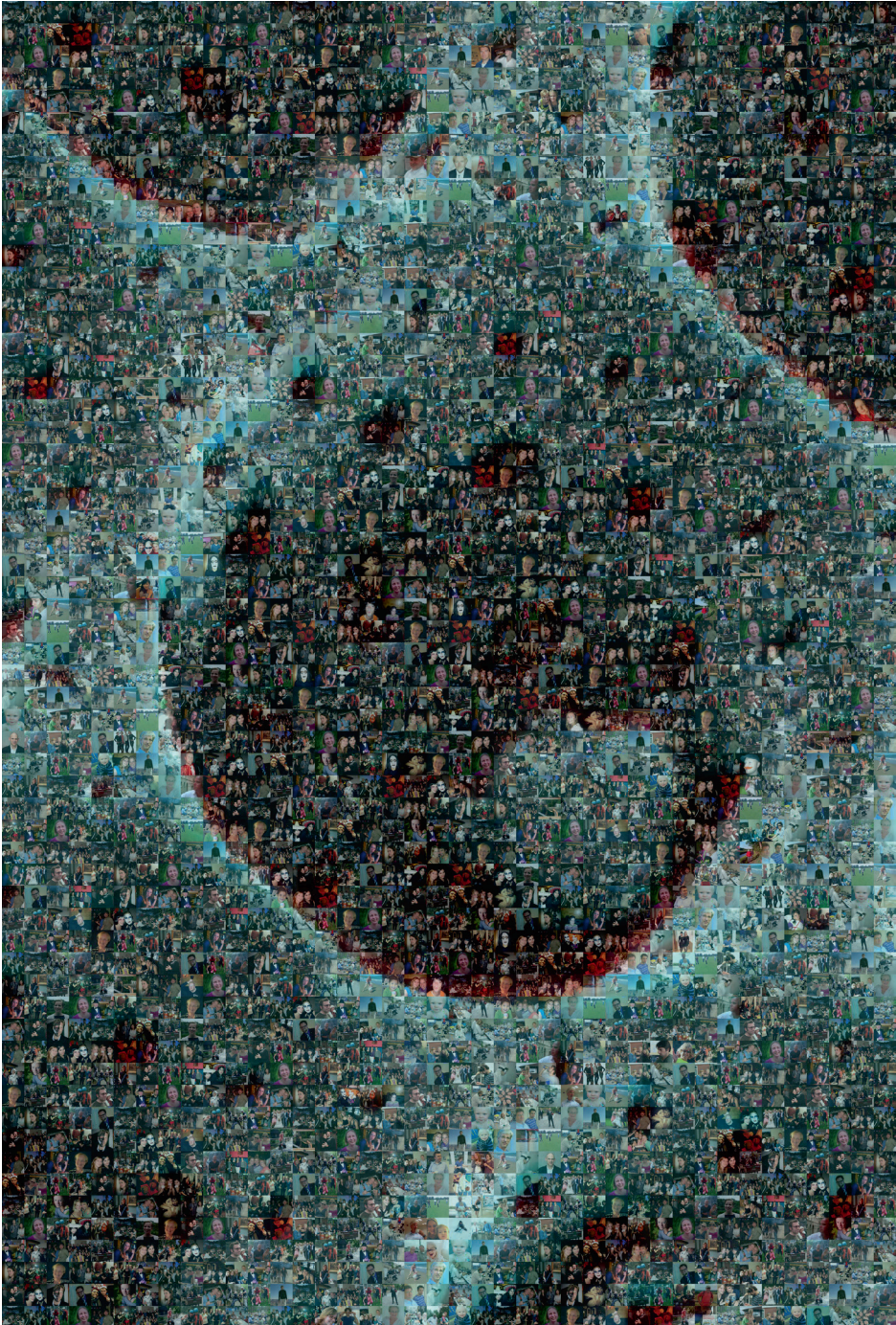
TERMIS World Congress, Seoul, Korea, 2009. **Buitinga M.**, Loomans C.J.M., Engelse M.A., Karperien M., de Koning E.J.P. van Apeldoorn A.A., van Blitterswijk C.A. Nano-Engineered Microchips for Extrahepatic Islet of Langerhans Transplantation.

Abstracts selected for poster presentation

The Netherlands Society for Biomaterials and Tissue Engineering annual meeting 2012, Bilthoven, The Netherlands; for this poster I received the poster award. **M. Buitinga**, F.P. Assen, R.Truckenmüller, M.A.Engelse, L.Moroni, E.J.P. de Koning, M.Karperien, A.A. van Apeldoorn. Microwell scaffold platform for islet of Langerhans transplantation.

Advanced Functional Biomaterials for Medicine, Enschede, The Netherlands, 2011. **Buitinga, M.** de Koning, E. J. P. Engelse, M. A. Truckenmuller, R. Moroni, L. van Blitterswijk, C. A. Karperien, M. van Apeldoorn, A. A., Microwell scaffolds for extrahepatic islets of Langerhans transplantation in type 1 diabetes.

Acknowledgements



Curriculum Vitae

Mijke Buitinga was born in Hengelo (OV), The Netherlands, on March 9th, 1985. In 2003, she received her high school diploma at the Bataafse Kamp in Hengelo (OV). In the same year, she started with the study Technical Medicine at the University of Twente in Enschede, The Netherlands. Six years later, she obtained her master's degree in Regenerative Medicine. During her graduation internship she started a research line in bioengineering strategies for type 1 diabetes, which she continued during her PhD, starting in December 2009 under the supervision of Prof. Dr. Clemens van Blitterswijk, Prof. Dr. Marcel Karperien, and Dr. Aart van Apeldoorn. During her PhD, she closely collaborated with the laboratories of Prof. Dr. Eelco de Koning, Leiden University Medical Center, The Netherlands, and Prof. Dr. Gotthardt, Radboud University Medical Center, Nijmegen, The Netherlands. Since April 2014, Mijke continues her scientific work as a Postdoctoral Fellow in beta-cell imaging at the department of Radiology and Nuclear Medicine at the Radboud University Medical Center in Nijmegen, The Netherlands, under the supervision of Prof. Dr. Gotthardt.

